ISSN 0042-8469
e-ISSN 2217-4753
УДК 623 + 355/359

Вол. 71, бр. 2
2023

НАУЧНИ ЧАСОПИС МИНИСТАРСТВА ОДБРАНЕ И ВОЈСКЕ СРБИЈЕ

ВОЈНОТЕХНИЧКИ ГЛАСНИК

ВТГ.МО.УПР.СРБ

www.vtg.mod.gov.rs

ВОЈНОТЕХНИЧКИ ГЛАСНИК
2 2023

ISSN 0042-8469
e-ISSN 2217-4753
УДК 623 + 355/359

Том 71, № 2
2023

НАУЧНЫЙ ЖУРНАЛ МИНИСТЕРСТВА ОБОРОНЫ
И ВООРУЖЕННЫХ СИЛ РЕСПУБЛИКИ СЕРБИЯ

ВОЕННО-ТЕХНИЧЕСКИЙ ВЕСТНИК

ВОЕННО-ТЕХНИЧЕСКИЙ ВЕСТНИК
2 2023

ВТГ.МО.УПР.СРБ
www.vtg.mod.gov.rs

ISSN 0042-8469
e-ISSN 2217-4753
UDC 623 + 355/359

Vol. 71, Issue 2
2023

MILITARY TECHNICAL COURIER

2 2023

SCIENTIFIC JOURNAL OF THE MINISTRY OF DEFENCE AND THE SERBIAN ARMED FORCES

MILITARY TECHNICAL COURIER

ВТГ.МО.УПР.СРБ

www.vtg.mod.gov.rs

ISSN 0042-8469
e-ISSN 2217-4753
UDC 623 + 355/359

НАУЧНИ ЧАСОПИС МИНИСТАРСТВА ОДБРАНЕ И ВОЈСКЕ СРБИЈЕ

ВОЈНОТЕХНИЧКИ ГЛАСНИК

ВОЛУМЕН 71 • БРОЈ 2 • АПРИЛ – ЈУН 2023.

NAUČNI ČASOPIS MINISTARSTVA ODBRANE I VOJSKE SRBIJE

VOJNOTEHNIČKI GLASNIK

VOLUMEN 71 • BROJ 2 • APRIL – JUN 2023.

втг.мо.упр.срб
www.vtg.mod.gov.rs
COBISS.SR-ID 4423938
DOI: 10.5937/VojnotehnickiGlasnik

ISSN 0042-8469
e-ISSN 2217-4753
UDC 623 + 355/359

НАУЧНЫЙ ЖУРНАЛ МИНИСТЕРСТВА ОБОРОНЫ И ВООРУЖЁННЫХ СИЛ РЕСПУБЛИКИ СЕРБИЯ

ВОЕННО-ТЕХНИЧЕСКИЙ ВЕСТНИК

ТОМ 71 • НОМЕР ВЫПУСКА 2 • АПРЕЛЬ-ИЮНЬ 2023.

SCIENTIFIC JOURNAL OF THE MINISTRY OF DEFENCE AND SERBIAN ARMED FORCES

MILITARY TECHNICAL COURIER

VOLUME 71 • ISSUE 2 • APRIL-JUNE 2023

ВТГ.МО.УПР.СРБ
www.vtg.mod.gov.rs
COBISS.SR-ID 4423938
DOI: 10.5937/VojnotehnickiGlasnik

ВЛАСНИЦИ:
Министарство одбране и Војска Србије

ИЗДАВАЧ:
Универзитет одбране у Београду, Војна академија

СОБСТВЕННИКИ: Министерство обороны и Вооружённые силы Республики Сербия

ИЗДАТЕЛЬСТВО: Университет обороны в г. Белград, Военная академия

С А Д Р Ж А Ј

С О Д Е Р Ж А Н И Е

C O N T E N T S

ОРИГИНАЛНИ НАУЧНИ РАДОВИ
ОРИГИНАЛЬНЫЕ НАУЧНЫЕ СТАТЬИ
ORIGINAL SCIENTIFIC PAPERS

Classification and analysis of the MNIST dataset using PCA and SVM algorithms

Mokhaled N. A. Al-Hamadani

University of Debrecen, Doctoral School of Informatics,
Department of Data Science and Visualization, Debrecen, Hungary;
Northern Technical University, Technical Institute/Alhawija,
Department of Electronic Techniques, Adan, Kirkuk, Republic of Iraq,
e-mail: mokhaled_hwj@ntu.edu.iq,
ORCID iD: https://orcid.org/0000-0002-7042-3178

DOI: 10.5937/vojtehg71-42689; https://doi.org/10.5937/vojtehg71-42689

FIELD: mathematics, computer sciences, IT
ARTICLE TYPE: original scientific paper

Abstract

Introduction/purpose: The utilization of machine learning methods has become indispensable in analyzing large-scale, complex data in contemporary data-driven environments, with a diverse range of applications from optimizing business operations to advancing scientific research. Despite the potential for insight and innovation presented by these voluminous datasets, they pose significant challenges in areas such as data quality and structure, necessitating the implementation of effective management strategies. Machine learning techniques have emerged as essential tools in identifying and mitigating these challenges and developing viable solutions to address them. The MNIST dataset represents a prominent example of a widely-used dataset in this field, renowned for its expansive collection of handwritten numerical digits, and frequently employed in tasks such as classification and analysis, as demonstrated in the present study.

Methods: This study employed the MNIST dataset to investigate various statistical techniques, including the Principal Components Analysis (PCA) algorithm implemented using the Python programming language. Additionally, Support Vector Machine (SVM) models were applied to both linear and non-linear classification problems to assess the accuracy of the model.

Results: The results of the present study indicate that while the PCA technique is effective for dimensionality reduction, it may not be as effective for visualization purposes. Moreover, the findings demonstrate that both

linear and non-linear SVM models were capable of effectively classifying the dataset.

Conclusion: The findings of the study demonstrate that SVM can serve as an efficacious technique for addressing classification problems.

Keywords: statistical analysis, machine learning, SVM, PCA, classification.

Introduction

Classification and data analysis are central to the discipline of machine learning, as they enable the effective comprehension of data (Suthaharan, 2014; Wang et al, 2019; Subasi, 2020; Ahmed et al, 2022). In this study, statistical methods were utilized to gain a deeper understanding of the data. Two machine learning techniques, namely the Support Vector Machine (SVM) and the Principal Components Analysis (PCA), were employed on the MNIST dataset, the largest collection of handwritten digit images used for classification problems (LeCun, 2023). The MNIST dataset consists of 70,000 handwritten digits, divided into 60,000 training images and 10,000 testing images (Al-Hamadani, 2015). Simple statistical techniques were applied to the MNIST dataset to improve the knowledge about the data. The PCA, an unsupervised machine learning technique, was utilized for visualization purposes, utilizing two principal components for plotting (Abdi & Williams, 2010). The SVM, a supervised machine learning technique, was utilized in linear and nonlinear models to classify the MNIST dataset into classes (Suthaharan, 2016).

The paper is organized as follows: Section 2 provides an overview of the dataset, programming language, and statistical techniques employed. In Section 3, the PCA algorithm utilized for visualization is explained, as well as the determination of the number of principal components for dimensionality reduction. The SVM linear and nonlinear models are discussed in Section 4. Finally, conclusions and future work are presented in Section 5.

Research method

Dataset

The MNIST (Modified National Institute of Standards and Technology) dataset is the largest and most well-known handwritten digits dataset for recognition and classification problems in machine learning (LeCun et al, 1995). This dataset has been taken from Yann LeCun website (LeCun, 2023). The MNIST dataset consists of 70,000 images of handwritten digits,

each labeled with a number from 0 to 9. These images were collected by the National Institute of Standards and Technology (NIST) and split into two parts (Nielsen, 2019). The first part includes 60,000 images which were provided by 250 individuals, including employees of the US Census Bureau and high school students. These images were normalized and centered in (28 *28) = 784 gray scale pixels per image. Each pixel is represented by a value between 0 and 255, with 0 being black, 255 being white, and any value in between representing a shade of gray. The second part of the MNIST dataset includes 10,000 images for testing, which were also provided by 250 different individuals to properly evaluate the performance of the algorithms trained on the dataset.

Program

Python has gained widespread popularity among data scientists due to its simplicity and ease of use in coding (Hao & Ho, 2019). Python is a widely-used programming language that supports various programming styles such as object-oriented, functional, and imperative programming (Raschka et al, 2020). Nowadays, most of machine learning complex problems, or AI in general, are being solved by using Python. Python can be written and developed using various Integrated Development Environments (IDEs), including PyCharm and Google Colab. For this paper, we have used both IDEs for building models over the MNIST dataset.

Visualizing and analyzing the MNIST dataset

To better understand the MNIST dataset, we need to analyze and visualize it. We started by examining the training and testing parts of the dataset to see if the data is balanced in terms of understanding the number of classes and their attributes. Also, we checked the dimensionality of each part of the dataset. Additionally, we plotted some samples from the training dataset to visualize the digits included in the MNIST dataset. Furthermore, we used the describe () method to calculate some statistical data such as mean, standard deviation, and percentile of the numerical values in the data frame. Table 1 shows the dimensionality of the training and testing dataset.

In Table 2, we have computed various statistical measures. One of them is the standard deviation which indicates how spread out the data in a dataset is from the mean.

The mean is the average of a set of numbers and can be found by adding all the numbers together and dividing by the number of values. In

the table, the mean of the 10 classes (ranging from class 0 to class 9) is 4.45.

Additionally, the minimum and maximum values in each column are shown in Table 2.

Lastly, we have calculated the quantiles which divide the dataset into groups containing an equal number of data points.

Table 1 – Dimensionality of the MNIST training and testing dataset
Таблица 1 – Размерность набора данных для обучения и тестирования MNIST
Табела 1 – Димензионалност скупа података за увежбавање и тестирање МНИСТ

No.	Dataset	Dimensions (Shape)
1	Training Data	(60000, 784)
2	Training Labels	(60000, 1)
3	Testing Data	(10000, 784)
4	Testing Labels	(10000, 1)

Table 2 – Statistical distribution of the MNIST training dataset
Таблица 2 – Статистическое распределение набора данных для обучения MNIST
Табела 2 – Статистичка расподела скупа података за увежбавање МНИСТ

index	Label	Pixel0	pixel1	Pixel2	Pixel3	Pixel4	Pixel5	Pixel6	Pixel7
count	60000.0	60000.0	60000.0	60000.0	60000.0	60000.0	60000.0	60000.0	60000.0
mean	4.4539333333333335	0.0	0.0	0.0	0.0	0.0	0.0	0.0	0.0
std	2.8892704373739795	0.0	0.0	0.0	0.0	0.0	0.0	0.0	0.0
min	0.0	0.0	0.0	0.0	0.0	0.0	0.0	0.0	0.0
25%	2.0	0.0	0.0	0.0	0.0	0.0	0.0	0.0	0.0
50%	4.0	0.0	0.0	0.0	0.0	0.0	0.0	0.0	0.0
75%	7.0	0.0	0.0	0.0	0.0	0.0	0.0	0.0	0.0
max	9.0	0.0	0.0	0.0	0.0	0.0	0.0	0.0	0.0

To continue with the visualization part, we have checked the number of observations for each class in the MNIST dataset by plotting randomly some samples from the dataset, as the following:

MNIST training dataset

It contains 60,000 images of handwritten digits (ranging from 0 to 9). Figure 1 shows the ratio of the training set. At the same time, Table 3 shows the number of the observations with the corresponding digits.

We observed that the training set is balanced because each class has 6,000 images approximately.

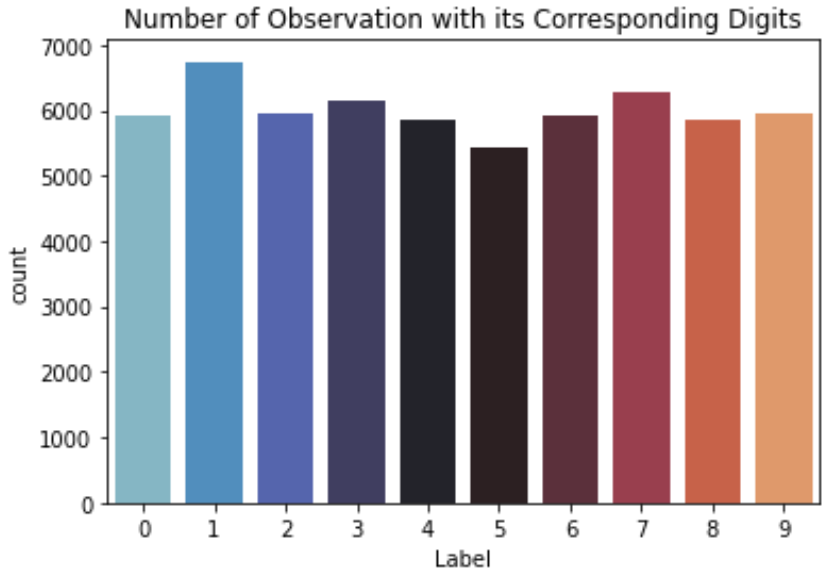

Figure 1 – Number of observations for each digit-training set
Рис. 1 – Количество распознаваний по каждой цифре в учебном наборе
Слика 1 – Број опсервација за сваку цифру у сету за увежбавање

Table 3 – Number of observations in the MNIST training set
Таблица 3 – Количество распознований в обучающей выборке MNIST
Табела 3 – Број опсервација у сету за увежбавање МНИСТ

MNIST Training Dataset Classes	Number of Observations
0	5923
1	6742
2	5958
3	6131
4	5842
5	5420
6	5918
7	6265
8	5851
9	5949

MNIST testing dataset

It contains 10,000 images of handwritten digits (ranging from 0 to 9). Figure 2 shows the ratio of the training set. At the same time, Table 4 shows the number of the observations with the corresponding digits. We observed that the training set is balanced because each class has 1,000 images approximately.

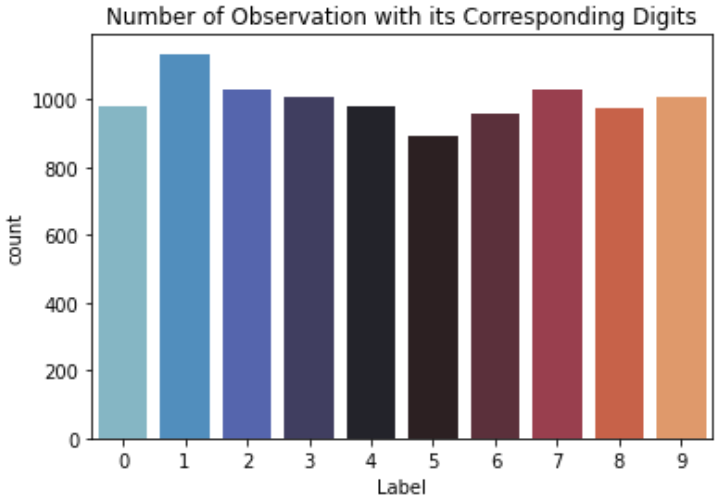

Figure 2 – Number of observations for each digit-testing set
Рис. 2 – Количество распознаваний по каждой цифре в тестовом наборе
Слика 2 – Број опсервација за сваку цифру у сету за тестирање

Table 4 – Number of observations in the MNIST testing set
Таблица 4 – Количество распознаваний в тестовом наборе MNIST
Табела 4 – Број опсервација у сету за тестирање МНИСТ

MNIST Training Dataset Classes	Number of Observations
0	980
1	1135
2	1032
3	1010
4	982
5	892
6	958
7	1028
8	974
9	1009

Samples plotting from the MNIST dataset

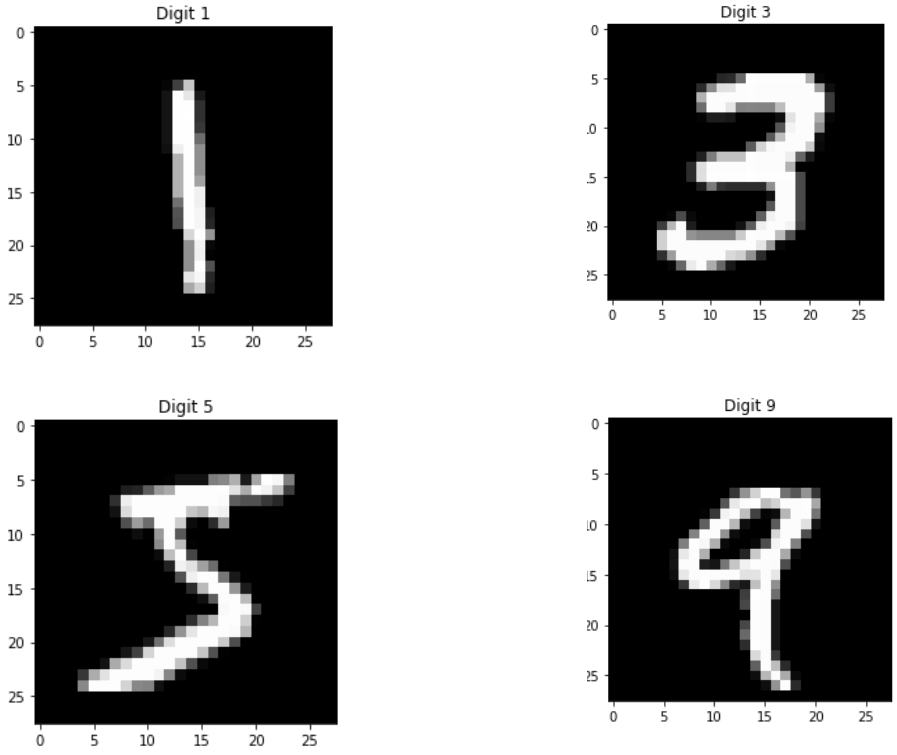

Figure 3 – Plotting samples from the MNIST dataset
Рис. 3 – Формирование выборок из набора данных MNIST
Слика 3 – Узорци добијени плотовањем за скуп података МНИСТ

Principal Components Analysis (PCA)

The PCA is unsupervised machine learning and statistical technique that is used to examine relationships between multiple variables in a dataset (Abdi & Williams, 2010). It aims to extract important information from the data by finding a new set of variables, known as principal components. These variables can describe the data more efficiently. These principal components are orthogonal (uncorrelated) and are ranked by their ability to explain the variance in the data. The PCA relies on the decomposition of positive semi-definite matrices using eigenvalues and eigenvectors, as well as the decomposition of rectangular matrices using singular values and singular vectors (Mishra et al, 2017). Therefore, the PCA is a statistical technique used for dimensionality reduction and

visualization of high-dimensional datasets such as, in our case, the MNIST dataset. Since each digit in the MNIST dataset consists of 784 features (dimensions) or pixels, the PCA reduces this number into a smaller number of dimensions while keeping as much of the variance in the data. This method is useful in terms of reducing the computational cost of training machine learning techniques, reducing the problem of overfitting in the data, and making the data easy for plotting in 2D or 3D plots.

To determine the principal components of a dataset, the PCA performs the following steps as shown in Figure 4:

Figure 4 – PCA processing flowchart
Рис. 4 – Блок-схема обработки PCA
Слика 4 –Ток процесирања ПЦА

Standardization

This step is known as standardization and is often referred to as a preprocessing step. Standardization involves transforming the data so that each variable has a mean of zero and a standard deviation of one. This helps to ensure that all of the variables are on a similar scale and have similar variances, which can improve the accuracy of the PCA analysis. Standardization can be done as follows:

$$S = \frac{Variable\ values - mean}{Standard\ deviation}$$

We have used the whole MNIST training dataset which contains 60,000 handwritten digits. For this purpose, we used this method (**standardized_data = StandardScaler().fit_transform(data)).**

Covariance matrix computation

A covariance matrix is a square matrix that shows the correlation between any two or more elements (attributes) in a multidimensional dataset.

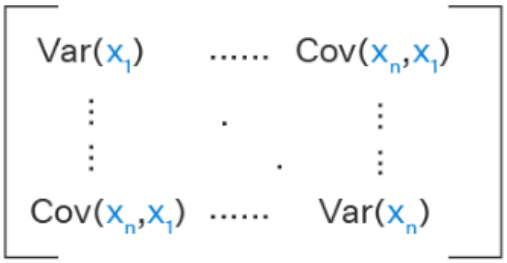

The correlation between the attributes can be either positive covariance or negative covariance. Positive covariance means that increasing the value of one variable is associated with an increase in the value of some other variable and vice versa. Negative covariance means that increasing the value of one variable is associated with a decrease in the value of some other variable. Therefore, we calculate the covariance matrix which is equal to (A^T * A) using this method **(covar_matrix = np.matmul(sample_data.T , sample_data)).**

Eigenvectors and eigenvalues

Eigenvectors and eigenvalues are mathematical concepts that are used in linear algebra, and they are closely related to the diagonalization of matrices. Given a square matrix A, an eigenvector of A is a non-zero vector v such that $Av = \lambda v$, where λ is a scalar value known as the eigenvalue associated with the eigenvector v. The eigenvectors of a matrix are often used to represent the "directions" of the maximum variance in a dataset and are used as the principal components. Therefore, finding the eigenvector with the highest eigenvalue is the principal component of the dataset. To project the data onto a 2D space, we can find the top two eigenvalues and the corresponding eigenvectors, and use these to transform the data.

Feature vector

Feature vectors are constructed by selecting the top eigenvectors from the covariance matrix of the original dataset (Manshor et al, 2011). The eigenvectors are determined by calculating the eigenvalues and eigenvectors of the covariance matrix, which capture the most important features or variations of the data. These eigenvectors are then sorted by eigenvalues in a descending order to determine which ones represent the most important features. The final feature vector can be in this form:

$$v = (eig_1, eig_2, eig_3, ..., eig_n)$$

Plotting

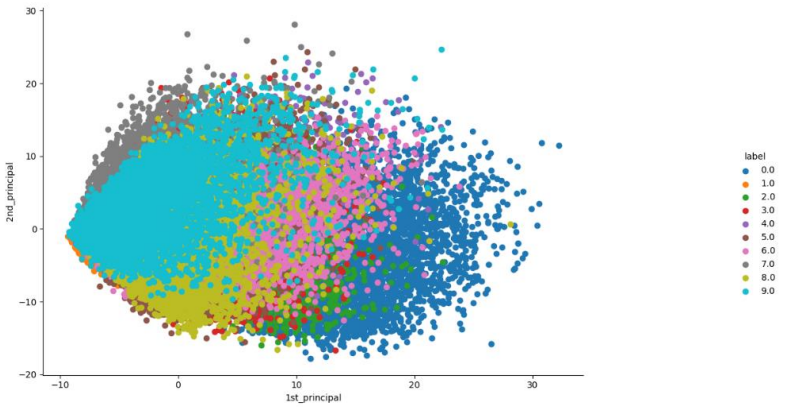

Figure 5 – 2D data points visualization
Рис. 5 –Визуализация точек 2D данных
Слика 5 – Визуализација тачака 2Д података

The overlapping of classes in Figure 5 suggests that the PCA is not the most effective method for visualizing high-dimensional data, as it is unable to clearly distinguish between different classes. In such cases, it may be more effective to use other visualization techniques such as t-SNE, UMAP or non-linear dimensionality reduction techniques, which are more effective in visualizing high-dimensional datasets.

To determine the number of principal components that we keep for the purpose of visualization in our work, we take into consideration what we really want from the PCA in order to deduce the right value of the number of components. We applied the following methods:

1. Since we use the PCA for the purpose of visualization, we need to select 2 or 3 principal components in order to plot them as 2D or 3D. Therefore, we convert high dimensional data into 2-dimensional data to visualize it in a 2D plot. This is shown in Figure 5.

2. We can create a scree plot which is the visual representation of eigenvalues that define the magnitude of eigenvectors (principal components). Figure 6-A shows the explained variance ratio for each component. Figure 6-B shows the eigenvalues for each component on the y-axis and the number of components on the x-axis. By these two plots, we can determine the number of principal components we have to keep.

Note: We used the PCA for visualization only in this paper.

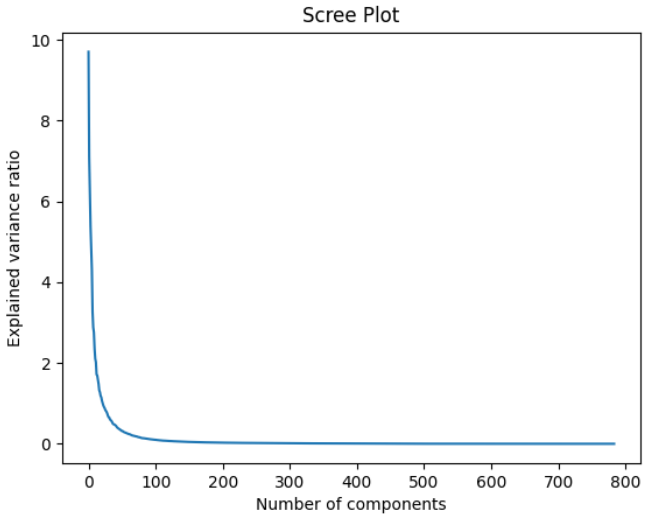

Figure 6a – Scree plot of the explained variance ratio for each component
Рис. 6а – График осыпи объясненной дисперсии ро каждому компоненту
Слика 6а – Scree plot објашњене варијансе за сваку компоненту

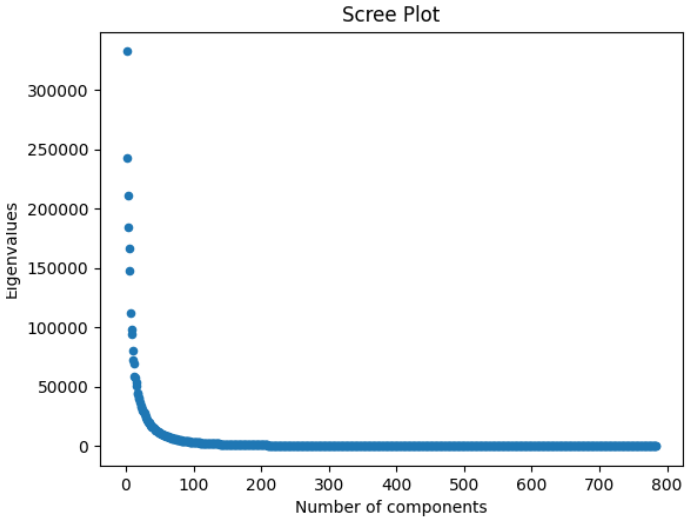

Figure 6b – Scree plot of the eigenvalues for each component
Рис. 6б – График осыпи собственных значений каждого компонента
Слика 6б – Scree plot сопствених вредности за сваку компоненту

Dimensionality reduction

We applied the Principal Component Analysis (PCA) for dimensionality reduction. As shown in Figure 7, the first 300 components explain almost 90% of the variance in the data. Based on this, we can reduce the dimensions of the dataset by selecting only the most important components, which will preserve a high level of variance while also significantly reducing the complexity of the data. This can be useful for tasks such as classification or clustering, where a high-dimensional dataset may be more difficult to work with.

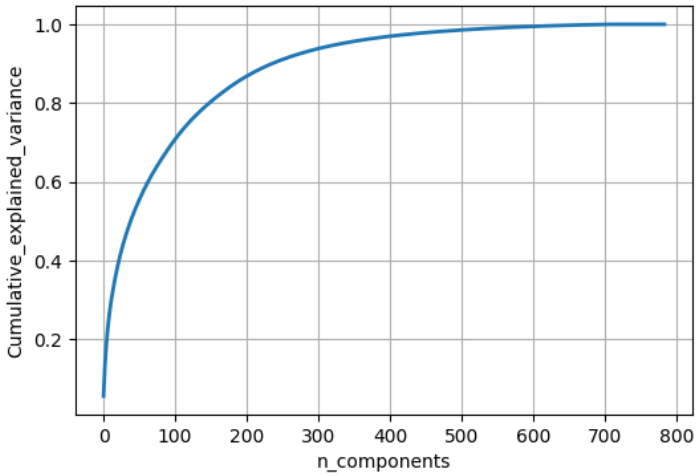

Figure 7 – Cumulative sum of variance with the components
Рис. 7 – Совокупная сумма дисперсии с компонентами
Слика 7 – Кумулативни збир варијансе са компонентама

Classifier

Support Vector Machine (SVM)

The Support Vector Machine is a well-known supervised machine learning technique that can be applied to solve big data classification and regression problems (Suthaharan, 2016). The SVM is relatively robust to overfitting that occurs in other machine learning algorithms, especially when using a nonlinear kernel (Guenther & Schonlau, 2016). There are two main types of SVM models which are linear and nonlinear (Saputra et al, 2022). The SVM is called linear when data classes can be separated by a linear line or a hyperplane using the simple mathematical model $y = wx + b$ where y is the response (dependent) variable, x is the

predictor (independent) variable, w is the estimated slope, and b is the estimated intercept. The optimal hyperplane can be selected by finding the hyperplane with the maximum margin which is the distance between the nearest data points of different classes. This is in case the problem can be solved by a linear hyperplane. If a problem cannot be solved linearly, then the data can be separated into different classes using a linear boundary in a transformed space called the feature space. This case is called the nonlinear SVM which uses the mathematical model $y = w\emptyset(x) + b$ where the $\emptyset$ is the kernel function (Suthaharan, 2016).

Since the SVM is a binary classification method,it is used to support classification for two classes. In our case, we used the SVM algorithm for multiclass classification. In multiclass classification, the SVM approach mainly involves splitting the dataset into several binary classification sub-datasets and then fitting a separate binary classifier for each one. There are two different types of multiclass classification for this SVM approach which are one versus one (OvO) and one versus the rest or all (OvR).

The OvO method is splitting the Multiclass dataset the data into Multiple binary classification problems. This approach splits the dataset into one dataset for each class versus every other class. The formula for calculating the number of binary datasets is: (Num_Classes * (Num_Classes – 1)) / 2. For the MNIST dataset is (10 *(10-1)/2)=45 binary classification problems.

The OvR method is also splitting the multiclass dataset into multiple binary classification problems. This approach trains a binary SVM classifier for each class, where the class is treated as a positive class and all other classes are combined into a single negative class. For example, class No (0) versus all the other classes combined as one class.

In this paper, we used the SVC (Support Vector Classification) method which implements the “one-versus-one” approach for multi-class classification.

For our MNIST dataset, we build linear and nonlinear SVM models to check the accuracy of these models. For the linear SVM model, we build it with its default hyperparameters to check the accuracy using the confusion matrix. The confusion matrix provides a decision that has been collected in training and testing which contains the actual labels with the predicted ones (Saputra et al, 2022). Accuracy can be calculated based on this equation:

$$Accuracy = \frac{TP + TN}{(Tp + TN + FP + FN)}$$

where true positive (TP) refers to the data that has been correctly classified as positive, true negative (TN) refers to the data that has been correctly

classified as negative while false positive (FP) refers to the data that has been incorrectly classified as positive and false negative (FN) refers to the data that has been incorrectly classified as negative.

We build the nonlinear SVM with its randomly chosen hyperparameters using the RBF kernel (Specifying the kernel type since it has several types such as “linear”, RBF, which is the radial basis function, “poly”, which is polynomial kernel function, “Sigmoid”) and it is used to take the data as an input and transform it into a required form of processing data. We used the RBF kernel because it is a commonly used kernel function due to its ability to perform well in classification tasks, as well as due to its flexibility since it does not require prior information about the dataset to be used effectively. When C=1, it is the regularization parameter which controls the trade-off between maximizing the margin and minimizing the training error in the model. When the value of the regularization parameter C is large, the model prioritizes correctly classifying all training points over having a larger margin. On the other hand, when C is small, the model will prioritize having a larger margin, even if it leads to misclassifying more training points. Both models have been built using sklearn.svm.SVC from scikit-learn (Scikit-learn, 2023). Table 5 shows the accuracy of linear and nonlinear SVM models.

Table 5 – Accuracy of linear and nonlinear SVM models
Таблица 5 –Точность линейных и нелинейных SVM-моделей
Табела 5 – Прецизност линеарних и нелинеарних СВМ модела

SVM Model	Accuracy
Linear SVM	91 %
Nonlinear SVM	94 %

Conclusion

In recent years, understanding and analyzing datasets have been a major challenge in the field of machine learning. To address this issue, we used the MNIST dataset which is the largest collection of handwritten digits. We applied various statistical techniques, including the PCA, to analyze the dataset. While the PCA was effective for dimensionality reduction, it was not as effective for visualization. In addition, we used both linear and nonlinear SVM models to classify the dataset. These models achieved accuracies of 91% and 94%, respectively. For future endeavors, utilizing the PCA and the SVM together can enhance the efficiency and accuracy of the classifier. The PCA will perform dimensionality reduction

by transforming features into a set of principal components, thus reducing the number of features in the dataset. Subsequently, training the SVM on this reduced dataset will result in quicker training times and improved performance.

References

Abdi, H. & Williams, L.J. 2010. Principal component analysis. *WIREs (Wiley Interdisciplinary Reviews*), 2(4), pp.433-459. Available at: https://doi.org/10.1002/wics.101.

Ahmed, A.H., Al-Hamadani, M.N.A. & Abdulrahman Satam, I. 2022. Prediction of COVID-19 disease severity using machine learning techniques. *Bulletin of Electrical Engineering and Informatics*, 11(2), pp.1069-1074. Available at: https://doi.org/10.11591/eei.v11i2.3272.

Al-Hamadani, M.N.A. 2015. *Evaluation of the Performance of Deep Learning Techniques Over Tampered Dataset*. Master thesis. Greensboro, North Carolina, USA: The University of North Carolina, Faculty of The Graduate School [online]. Available at: https://www.proquest.com/openview/769d2aa550c12fcf40655405e8df7689/1?pq-origsite=gscholar&cbl=18750 [Accessed: 05 February 2023].

Guenther, N. & Schonlau, M. 2016. Support Vector Machines. *The Stata Journal*, 16(4), pp.917-937. Available at: https://doi.org/10.1177/1536867X1601600407.

Hao, J. & Ho, T.K. 2019. Machine Learning Made Easy: A Review of Scikit-learn Package in Python Programming Language. *Journal of Educational and Behavioral Statistics*, 44(3), pp.348-361. Available at: https://doi.org/10.3102/1076998619832248.

LeCun, Y. 2023. *MNIST dataset* [online]. Available: https://yann.lecun.com/exdb/mnist/.

LeCun, Y., Jackel, L., Bottou, L., Brunot, A., Cortes, C., Denker, J., Drucker, H., Guyon, I., Muller, U., Sackinger, E., Simard, P. & Vapnik, V. 1995. Comparison of learning algorithms for handwritten digit recognition. In: *Fogelman, F. & Gallinari, P. (Eds.) International Conference on Artificial Neural Networks (ICANN'95),* Paris, pp. 53-60, October 9-13.

Manshor, N., Halin, A.A., Rajeswari, M. & Ramachandram, D. 2011. Feature selection via dimensionality reduction for object class recognition. In: *2011 2nd International Conference on Instrumentation, Communications, Information Technology, and Biomedical Engineering*, Bandung, Indonesia, pp.223-227, November 08-09. Available at: https://doi.org/10.1109/ICICI-BME.2011.6108645.

Mishra, S.P., Sarkar, U., Taraphder, S., Datta, S., Swain, D.P., Saikhom, R., Panda, S. & Laishram, M. 2017. Multivariate Statistical Data Analysis-Principal Component Analysis (PCA). *International Journal of Livestock Research*, 7(5), pp.60-78.

Nielsen, M. 2019. *Neural Networks and Deep Learning* [online]. Available at: http://neuralnetworksanddeeplearning.com/ [Accessed: 05 February 2023].

Raschka, S., Patterson, J. & Nolet, C. 2020. Machine Learning in Python: Main Developments and Technology Trends in Data Science, Machine Learning, and Artificial Intelligence. *Information*, 11(4), art.number:193. Availiable at: https://doi.org/10.3390/info11040193.

Saputra, D., Dharmawan, W.S. & Irmayani, W. 2022. Performance Comparison of the SVM and SVM-PSO Algorithms for Heart Disease Prediction. *International Journal of Advances in Data and Information Systems*, 3(2), pp.74-86. Available at: https://doi.org/10.25008/ijadis.v3i2.1243.

-Scikit-learn. 2023. *sklearn.svm.SVC* [online]. Available: https://scikit-learn.org/stable/modules/generated/sklearn.svm.SVC.html [Accessed: 05 February 2023].

Subasi, A. 2020. *Practical Machine Learning for Data Analysis Using Python.* London, United Kingdom: Elsevier, Academic Press. ISBN: 978-0-12-821379-7.

Suthaharan, S. 2014. Big data classification: problems and challenges in network intrusion prediction with machine learning. *ACM SIGMETRICS Performance Evaluation Review,* 41(4), pp.70-73. Available at: https://doi.org/10.1145/2627534.2627557.

Suthaharan, S. 2016. Support Vector Machine. In: *Machine Learning Models and Algorithms for Big Data Classification. Integrated Series in Information Systems*, 36. Boston, MA: Springer. Available at: https://doi.org/10.1007/978-1-4899-7641-3_9.

Wang, P., Li, Y. & Reddy, C.K. 2019. Machine Learning for Survival Analysis: A Survey. *ACM Computing Surveys*, 51(6), art.number:110, pp.1-36. Available at: https://doi.org/10.1145/3214306.

Классификация и анализ набора данных MNIST с использованием алгоритмов PCA и SVM

Мохалед Н.А. Аль-Хамадани

Дебреценский университет, Докторская школа информатики,
факультет науки о данных и визуализации, г. Дебрецен, Венгрия;
Северный технический университет, Технический институт/Аль-Хавиджа,
департамент электронных технологий, Адан, Киркук, Республика Ирак

РУБРИКА ГРНТИ: 27.41.23 Машинные, графические и другие методы вычислительной математики,
50.35.37 Программирование гибридных ЭВМ и ВК
ВИД СТАТЬИ: оригинальная научная статья

Резюме:

Введение/цель: В современном мире использование методов машинного обучения стало незаменимым при анализе крупномасштабных и сложных данных. Данные методы широко применяются в различных областях: от оптимизации бизнес-операций до продвижения научных исследований. Несмотря на то что такие большие наборы данных открывают возможности для

глубокого понимания и инноваций, они также представляют серьезную проблему в таких областях, как качество и структура данных, которые требуют применения эффективных стратегий управления. Методы машинного обучения стали ключевыми инструментами в выявлении и смягчении вышеописанных проблем, а также в разработке соответствующих решений. Набор данных MNIST представляет собой яркий пример широко используемого набора данных в этой области, отличающегося огромной коллекцией рукописных цифр. Данный набор часто используется в таких задачах, как классификация и анализ, о чем свидетельствует настоящее исследование.

Методы: В данном исследовании использовался набор данных MNIST для изучения различных статистических методов, включая алгоритм анализа основных компонентов (PCA), с помощью скриптового языка программирования Python. Также применялись модели опорных векторов (SVM) для оценки точности модели в задачах линейной и нелинейной классификации.

Результаты: Результаты настоящего исследования показывают, что хотя метод PCA эффективен для уменьшения размерности, он может оказаться не столь эффективным для целей визуализации. Более того, полученные результаты показали, что линейные, так же как и нелинейные SVM-модели эффективно классифицируют набор данных.
Выводы: Результаты исследования показали, что SVM явдяется эффективным методом для решения проблем классификации.

Ключевые слова: статистический анализ, машинное обучение, SVM, PCA, классификация.

Класификција и анализа скупа података МНИСТ помоћу алгоритама ПЦА и СВМ

Мокхалед Н.А. Ал-Хамадани

Универзитет у Дебрецину, Докторске студије информатике,
Одсек за науку и визуализацију података, Дебрецин, Мађарска;
Северни технички универзитет, Технички институт/Алхавија,
Одељење за електронске технике, Адан, Киркук, Република Ирак

ОБЛАСТ: математика, рачунарске науке, информационе технологије
КАТЕГОРИЈА (ТИП) ЧЛАНКА: оригинални научни рад

Сажетак:

Увод/циљ: Методи машинског учења постали су незаменљиви у анализи сложених података великог обима у савременим окружењима заснованим на подацима. Примењују се у најразличитијим областима, од оптимизације пословних процеса до сложених научних истраживања. Упркос томе што овакви обимни

скупови података нуде могућности дубинског сагледавања, као и иновација, они представљају и велики изазов у областима као што су квалитет и структура података, што захтева примену ефикасних стратегија управљања. Технике машинског учења су се показале као суштински важни алати за идентификацију и смањивање тих изазова, као и за развијање могућих решења. Скуп података МНИСТ представља изразит пример широко коришћених сетова података у овој области, познат по својој великој колекцији руком писаних цифара, и често је употребљаван за класификације и анализе, као што је то показано у овој студији.

Методе: Скуп података МНИСТ коришћен је за испитивање различитих статистичких поступака, укључујући алгоритам анализе главних компоненти (Principal Components Analysis (PCA – ПЦА)) уз помоћ програмског језика Пајтон. Такође, примењени су модели метода потпорних вектора (Support Vector Machine (SVM – СВМ)) за процењивање тачности модела у линеарним и нелинеарним класификационим проблемима.

Резултати: Показано је да, иако техника ПЦА јесте ефикасна у редуковању димензионалности, она није толико ефикасна за визуализацију. Штавише, налази показују да су и линерани и нелинеарни модели СВМ успели да ефикасно класификују скуп података.

Закључак: Резултати студије показују да СВМ може да буде ефикасна техника за решавање проблема класификације.

Кључне речи: статистичка анализа, машинско учење, СВМ, ПЦА, класификација.

Paper received on / Дата получения работы / Датум пријема чланка: 08.02.2023.
Manuscript corrections submitted on / Дата получения исправленной версии работы / Датум достављања исправки рукописа: 26.03.2023.
Paper accepted for publishing on / Дата окончательного согласования работы / Датум коначног прихватања чланка за објављивање: 28.03.2023.

A new solution for solving a multi-objective integer programming problem with probabilistic multi - objective optimization

Maosheng Zheng[a], *Jie* Yu[b]

[a] Northwest University, School of Chemical Engineering,
Xi'an, People's Republic of China,
e-mail: mszhengok@aliyun.com, **corresponding author**,
ORCID iD: https://orcid.org/0000-0003-3361-4060

[b] Northwest University, School of Life Science,
Xi'an, People's Republic of China,
e-mail: yujie@nwu.edu.cn,
ORCID iD: https://orcid.org/0000-0001-6606-5462

DOI: 10.5937/vojtehg71-41556; https://doi.org/10.5937/vojtehg71-41556

FIELD: mathematics, computer science
ARTICLE TYPE: original scientific paper

Abstract:

Introduction/purpose: In this paper, a new solution for solving a multi-objective integer programming problem with probabilistic multi – objective optimization is formulated. Furthermore, discretization by means of the good lattice point and sequential optimization are employed for a successive simplifying treatment and deep optimization.

Methods: In probabilistic multi – objective optimization, a new concept of preferable probability has been introduced to describe the preference degree of each performance utility of a candidate; each performance utility of a candidate contributes a partial preferable probability and the product of all partial preferable probabilities deduces the total preferable probability of a candidate; the total preferable probability thus transfers a multi-objective problem into a single-objective one. Discretization by means of the good lattice point is employed to conduct discrete sampling for a continuous objective function and sequential optimization is used to perform deep optimization. At first, the requirements of integers in the treatment could be given up so as to simply conduct above procedures. Finally, the optimal solutions of the input variables must be rounded to the nearest integers.

Results: This new scheme is used to deal with two production problems, i.e., maximizing profit while minimizing pollution and determining a purchasing plan for spending as little money as possible while getting as large amount of raw materials as possible. Promising results are obtained for the above two problems from the viewpoint of the probability theory for simultaneous optimization of multiple objectives.

Conclusion: This method properly considers simultaneous optimization of multiple objectives in multi-objective integer programming, which naturally reflects the essence of multi-objective programming, and opens a new way of solving multi-objective problems.

Key words: multi-objective optimization, integer programming problem, preferable probability, discrete sampling, sequential optimization.

Introduction

Multi-objective programming (GP) is an important branch of optimization theory. It is a mathematical method developed to solve multi-objective decision-making problems based on linear and nonlinear programmings. Since 1960s, it has been gradually developed and matured. It is widely used in economic management and planning, human resource management, government management, optimization of large - scale projects and other important areas.

The idea of multi-objective programming originated from the study of the utility theory in economics in 1776. In 1896, economist Pareto first put forward the multi-objective programming problem in the study of economic balance, and gave a simple idea which was later called the Pareto optimal solution. In 1947, von Neumann and Morgenster mentioned the multi-objective programming problem in their game theory work, which attracted more attention to this problem. In 1951, Koopmans put forward the multi-objective optimization problem in the analysis of production and sales activities, and first formed the concept of the Pareto optimal solution. In the same year, Kuhn and Tucker gave the concept of the Pareto optimal solution of the vector extremum problem from the angle of mathematical programming. The necessary and sufficient conditions for the existence of this solution are also studied. Debreu's discussion on evaluation balance in 1954 and Harwicz's research on multi-objective optimization in topological vector space in 1958 laid the foundation for the establishment of this discipline. In 1968, Johnsen published the first monograph on the multi-objective decision-making model. Until 1970s-1980s, the basic theory of multi-objective programming was finally established through the efforts of many scholars, making it a new branch of applied mathematics (Huang et al, 2017; Liu, 2014; Ying, 1988).

Up to now, there are the following general methods to solve multi-objective programming: one is to transfer multiple objectives into a single objective that is easier to solve, such as the main objective method, the linear weighting method, the ideal point method, etc.; the other method is called the hierarchical sequence method, i.e. a sequence is given

according to the importance of the target, and the next target optimal solution is searched in the previous target optimal solution set every time until a common optimal solution is obtained; the third one is the main target method, which takes one $f_1(x)$ as the main target, and the other *P-1* as the non-main target. At this time, it is hoped that the main target will reach the maximum value, and other targets will meet certain conditions; the fourth one is the linear weighting method, which sets a series of weight coefficients ω_j for objective functions $f_j(x)$, and thus a new evaluation function $U(x) = \sum_{i=1}^{p} \omega_j \cdot f_{j(x)}$ is obtained by linear weighted summation, which makes the multi-objective problem become a single-objective problem. However, under the condition that the dimensions of the target are different, normalization is needed. For a multi-objective linear programming problem, decision makers hope to achieve these goals in turn under these constraints by minimizing the total deviation from the target value, which is the problem to be solved by goal programming (Huang et al, 2017; Liu, 2014; Ying, 1988).

In practical engineering systems, such as many nonlinear, multi-variable, multi-constraint and multi-objective optimization problems in power systems, the existing mathematical methods have limited ability to optimize these problems, and the solutions obtained are not satisfactory.

The above discussion shows that normalization and the introduction of subjective factors in the previous methods are indispensable processes in their "additive" algorithm, and the final result depends to a great extent on the normalization method adopted after the targets with different attributes are converted into "single" targets (Zheng et al, 2021). Different normalization methods may lead to completely different results. In addition, in some algorithms, the beneficial performance index and the unbeneficial performance index are treated unequally.

From the point of view of the set theory, the "additive" algorithm in the previous methods for multi-objective optimization corresponds to the form of "union". Therefore, the above algorithm can only be regarded as a semi-quantitative method in a sense.

Recently, a probabilistic multi - objective optimization (PMOO) method has been proposed to solve the inherent problems of subjective factors of the previous methods of multi - objective optimization (Zheng et al, 2021; Zheng et al, 2022a; Zheng et al, 2022b). A brand - new concept of preferable probability is put forward to reflect the preference degree of performance indicators in project management optimization. PMOO aims to deal with multi-objective simultaneous optimization from the perspective of the probability theory. In the new methodology of PMOO, the performance utility indicators of all candidates are preliminarily divided into

the beneficial category and the unbeneficial category according to their roles and preferences in optimization; each performance utility index of the candidate quantitatively contributes to a partial preferable probability; the product of all partial preferable probabilities deduces the total preferable probability of a candidate; the total preferable probability thus transfers a multi-objective problem into a single-objective one. In the evaluation, the total preferable probability of a candidate is the unique and decisive index of the candidate.

In this article, by using probabilistic multi - objective optimization and the good lattice point to conduct discrete sampling and sequential optimization for successive deep optimization, a reasonable method of multi - objective programming is formulated, and the application details of this method are illustrated with two examples.

Solution for solving an integer programming problem by means of probabilistic multi - objective optimization

In this section, probabilistic multi - objective optimization, good lattice point (GLP) discretization and sequential optimization are organically combined, which establishes a rational method for solving a multi-objective programming problem. The probabilistic multi - objective optimization method is used to transfer a multi - objective optimization problem into a single - objective optimization one from the perspective of the probability theory; the discretization of GLP provides an effective discrete sampling to simplify mathematical processing, which is especially important for dealing with multi - objective programming problems with continuous objective functions; and sequential optimization is used for successive deep optimization.

The systematic implementation is demonstrated in the subsections A) and B).

A) A method based on the perspective of probabilistic multi - objective optimization

From the perspective of probabilistic multi - objective optimization, the whole event with multi - objective simultaneous optimization corresponds to the product of all single objectives (events). For multi - objective programming problems, each objective can be analogically seen as a single event (Zheng et al, 2021; Zheng et al, 2022a; Zheng et al, 2022b). All performance utility indexes of the candidate are preliminarily divided into two categories: beneficial and unbeneficial, according to their role and preference of a candidate in optimization, respectively.

Specifically, the assessment of the preferable probability P_{ij} of both beneficial indicators and unbeneficial indicators can be carried out according to the evaluation procedure in Figure 1 (Zheng et al, 2021; Zheng et al, 2022a; Zheng et al, 2022b).

B) Discrete sampling by means of the good lattice point and successive sequential optimization

In multi - objective programming problems, the objective function is usually continuous. In order to simplify mathematical processing, the discrete sampling by means of the good lattice point (GLP) can be used. As described in literature (Hua & Wang, 1981; Fang & Wang, 1994; Fang et al, 2018), the methods of good lattice point and uniform experimental design (UED) make discrete sampling possible and practical. The GLP method and UED are based on the number theory, and it can obtain an effective approximate value for a definite integral or an extreme value problem with a limited number of sampling points (Hua & Wang, 1981; Fang & Wang, 1994; Fang et al, 2018). Such a limited number of sampling points is uniformly distributed in the super space with low discrepancy. The characteristic of the uniform point set makes its convergence speed much faster than that of the Monte Carlo sampling method (Hua & Wang, 1981; Fang & Wang, 1994; Fang et al, 2018), so it is considered as an efficient approximation named quasi-Monte Carlo method. In order to use this uniformly distributed point set appropriately, Professor Fang specially developed uniform design and uniform design tables (Fang, 1994; Fang et al, 2018).

As to the successive sequential optimization of multi - objective optimization problems, a sequential optimization algorithm (SNTO) can be employed for deep optimization (Zheng et al, 2022c; Zheng et al, 2023).

Moreover, by combining probabilistic multi - objective optimization, discrete sampling, and sequential optimization, the multi - objective programming problem can be solved rationally.

At first, the requirements of integers could be given up so as to simply conduct the above procedures. Finally, the optimum solutions of the input variables must be rounded to the nearest integers, which must be withstanding the constraint conditions as well.

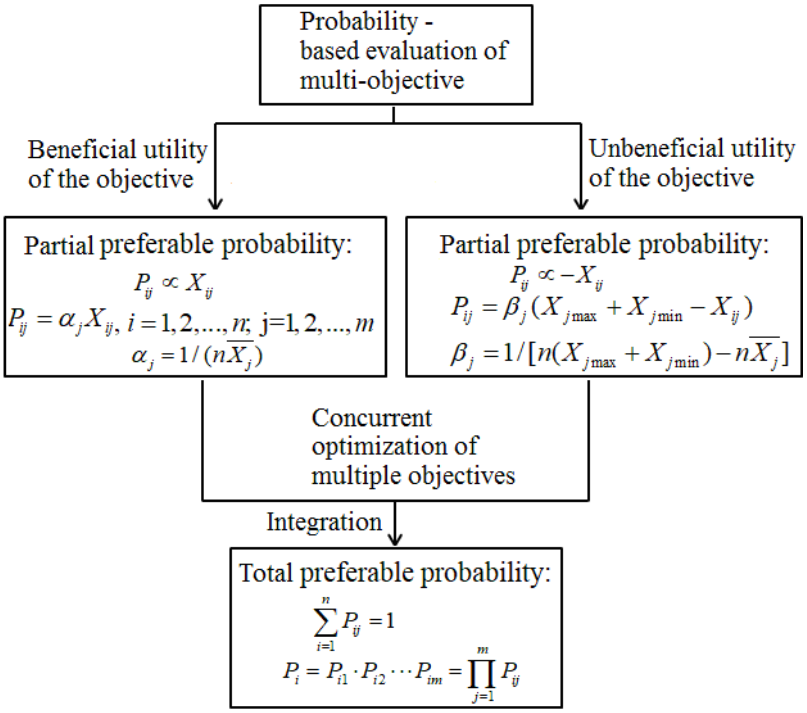

Figure 1 – Evaluation procedure of the PMOO method
Рис. 1 – Процедура оценки метода PMOO
Слика 1 – Поступак евалуације метода PMOO

Applications

In this section, two examples are employed to illustrate the use of the above methods in solving multi - objective integer programming problems.

I) An integer programming problem that maximizes profits and minimizes pollution

A factory plans to produce two products, *PV cell 1* and *PV cell 2*. During production, it causes certain polluting gas release into the air (Huang et al, 2017). So, in the production plan, the goals are to get maximum profit with minimum pollution at the same time. Profit, unit pollution of each product, mechanical ability, manpower resource and resource limits are shown in Table 1 (Huang et al, 2017). Therefore, the problem is how to organise production which maximizes profits and causes the least pollution.

Table 1 – Resource consumption, profit and pollution of each product
Таблица 1 – Потребление ресурсов, прибыль и загрязнение каждого продукта
Табела 1 – Потрошња ресурса, профит и загађивање сваког производа

Content	Product		Limit unit
	Cell 1	*Cell 2*	
Resource exhaust unit per product	1	5	72
Mechanical ability exhaust per product	0.5	0.25	8
Manpower resource exhaust per product	0.2	0.2	4
Profit per product (¥RMB)	1	3	
Pollution unit per product	1.5	1	

Solution

Assuming that the output of the products *Cell 1* and *Cell 2* is x_1 and x_2, respectively, the mathematical model and the constraint conditions of this problem are as follows,

Max $f_1(x) = x_1 + 3x_2$,
Min $f_2(x) = 1.5x_1 + x_2$,

s. t. $0.5x_1 + 0.25x_2 \leq 8$ (Mechanical ability),
$0.2x_1 + 0.2x_2 \leq 4$ (Manpower resource),
$x_1 + 5x_2 \leq 72$ (Resource limit), and
$x_1, x_2 > 0$.

Because there are two input variables x_1 and x_2 in this problem, at least 17 evenly distributed sampling points are needed for the discretization in the working domain according to literature (Zheng et al, 2022c). Here, we try to use the uniform design table $U^*_{24}(24^9)$ to implement the discretization (Fang, 1994; Fang et al, 2018), and the results are shown in Table 2. As it can be seen from Table 2, five sampling points were excluded due to the limitation of the constraint conditions, and the remaining 19 sampling points were within the working area, which meets the basic requirement of at least 17 uniformly distributed sampling points within the working zone.

Additionally, in this problem, the objective function $f_1(x)$ is a beneficial indicator while the objective function $f_2(x)$ is an unbeneficial indicator. Table 3 shows the evaluation results of the partial preferable probabilities P_{f1} and P_{f2} of the objective functions $f_1(x)$ and $f_2(x)$ at the corresponding discrete sampling point, respectively; P_t represents the total/overall preferable probabilities of each sampling point.

As it can be seen from Table 3, sampling point No 2 shows the maximum value of the total preferable probability. Therefore, around sampling point No 2 of Table 2, sequential uniform design is adopted for successive deep optimization.

Table 2 – Evaluation results of discrete sampling with $U^*_{24}(24^9)$

Таблица 2 – Результаты оценки дискретной выборки с $U^*_{24}(24^9)$

Табела 2 – Резултати евалуације дискретног узорковања са $U^*_{24}(24^9)$

No	Input variable		Objective		Note
	x1	x2	f_1	f_2	
1	0.3333	6.3	19.2333	6.8	
2	**1**	**12.9**	**39.7**	**14.4**	
3	1.6667	4.5	15.1667	7	
4	2.3333	11.1	35.6333	14.6	
5	3	2.7	11.1	7.2	
6	3.6667	9.3	31.5667	14.8	
7	4.3333	0.9	7.0333	7.4	
8	5	7.5	27.5	15	
9	5.6667	14.1			Excl.
10	6.3333	5.7	23.4333	15.2	
11	7	12.3	43.9	22.8	
12	7.6667	3.9	19.3667	15.4	
13	8.3333	10.5	39.8333	23	
14	9	2.1	15.3	15.6	
15	9.6667	8.7	35.7667	23.2	
16	10.3333	0.3	11.2333	15.8	
17	11	6.9	31.7	23.4	
18	11.6667	13.5			Excl.
19	12.3333	5.1	27.6333	23.6	
20	13	11.7			Excl.
21	13.6667	3.3	23.5667	23.8	
22	14.3333	9.9			Excl.
23	15	1.5	19.5	24	
24	15.6667	8.1			Excl.

Table 3 – Evaluation results of discrete PMOO using $U^*_{24}(24^9)$
Таблица 3 – Результаты оценки дискретного PMOO с помощью $U^*_{24}(24^9)$
Табела 3 – Резултати евалуације дискретне PMOO помоћу $U^*_{24}(24^9)$

No	Preferable probability		
	Partial		Total
	P_{f1}	P_{f2}	$P_t \times 10^3$
1	0.0402	0.0877	3.5268
2	**0.0830**	**0.0601**	**4.9936**
3	0.0317	0.0870	2.7581
4	0.0745	0.0594	4.4280
5	0.0232	0.0862	2.0018
6	0.0660	0.0587	3.8749
7	0.0147	0.0855	1.2577
8	0.0575	0.0580	3.3340
10	0.0490	0.0572	2.8055
11	0.0918	0.0297	2.7277
12	0.0405	0.0565	2.2892
13	0.0833	0.0290	2.4146
14	0.0320	0.0558	1.7854
15	0.0748	0.0283	2.1139
16	0.0235	0.0551	1.2938
17	0.0663	0.0275	1.8255
19	0.0578	0.0268	1.5494
21	0.0493	0.0261	1.2857
23	0.0408	0.0254	1.0343

Table 4 shows the evaluation results of the successive deep optimization using sequential uniform optimization, in which $c(t)$ = (Max $P_t^{(i-1)}$ – Max $P_t^{(i)}$)/Max $P_t^{(i-1)}$ represents the relative error of the maximum total preferable probability of the i-th sequential step. If we assume that the pre-assignment of $c^{(t)}$ = 2%, the successive deep optimization can be terminated in step 3. At this time, the final optimal results of this multi-objective programming optimization problem are $f_{1Opt.}$ = 42.7625 ¥RMB, $f_{2Opt.}$ = 14.4 unit, while the instant input variables of the successive deep optimization in step 3 are x_1 = 0.125 and x_2 = 14.2125, respectively. Since this is an integer programming problem, the solution for x_1 and x_2 must be rounded to the nearest integers, so the values of x_1 and x_2 are 0 and 14, respectively, and the optimal values of objective functions are thus $f_{1Opt.}$ = 42 ¥RMB yuan and $f_{2Opt.}$ = 14 unit, individually. This result is much better

than that given by Huang with a linear weighting algorithm (Huang et al, 2017).

Table 4 – Evaluation results of sequential optimization with $U^*_{24}(24^9)$ discrete sampling
Таблица 4 – Результаты оценки последовательной оптимизации с дискретной выборкой $U^*_{24}(24^9)$
Табела 4 – Резултати евалуације секвенцијалне оптимизације помоћу дискретног узорковања $U^*_{24}(24^9)$

Step	Range	Instant input variable		Optimal objective		Max $P_t \times 10^3$	$c^{(t)}$
		x_1^*	x_2^*	$f_{1\text{Opt.}}$	$f_{2\text{Opt.}}$		
0	[0, 16] x [0, 14.4]	1	12.9	39.7	14.4	4.9936	
1	[0,8] x [7.2, 14.4]	0.5	13.65	41.45	14.4	4.4152	
2	[0, 4] x [10.8, 14.4]	0.25	14.025	42.325	14.4	4.2855	0.0294
3	[0, 2] x [12.6, 14.4]	0.125	14.2125	42.7625	14.4	4.2034	0.0191

II) Purchasing raw material for production

A factory needs to purchase certain raw material for production. There are two kinds of raw materials in the market, *A* and *B*, with unit prices of 2 ¥RMB yuan / kg and 1.5 ¥RMB yuan /kg, respectively. It is required that the total cost now should not exceed 300 ¥RMB yuan, and the raw material *A* should not be less than 60 kg. How to determine the best purchasing plan, spend the least money and purchase the largest amount of raw materials? The smallest weight unit is 1 kg.

Assuming that the two raw materials, *A* and *B*, are purchased in x_1 and x_2 kg, respectively, then the total cost is:

$f_1(x) = 2x_1 + 1.5x_2$;

The total amount of the purchased raw materials is:

$f_2(x) = x_1 + x_2$.

Then the goal of our solution is to spend the least money to buy the most raw materials, i.e. to minimize $f_1(x)$ while maximizing $f_2(x)$.

At the same time, it is necessary to meet the requirements that the total cost should not exceed 300 ¥RMB yuan, and the raw materials *A* should not be less than 60 kg, so the constraint conditions are as follows:

$2x_1 + 1.5x_2 \leq 300$;

$x_1 \geq 60$, $x_2 \geq 0$.

Solution

Based on the above analysis, the following optimal mathematical model is given:

$Min\ f_1(x) = 2x_1 + 1.5x_2$;

Max $f_2(x) = x_1 + x_2$;

s. t.

$2x_1 + 1.5x_2 \leq 300$;

$x_1 \geq 60$, $x_2 \geq 0$.

Because this problem has two input variables x_1 and x_2, similarly, at least 17 evenly distributed sampling points in the working domain are needed (Zheng et al, 2022c; Zheng et al, 2023). Here, we try to use the uniform test table $U_{37}(37^{12})$ conduct the discrete sampling (Fang, 1994; Fang et al, 2018), and the results are shown in Table 5. It can be seen from Table 5 that, due to the limitation of the constraint conditions, 18 sampling points are excluded, and, luckily, 19 sampling points are within the scope of the constraint conditions, which meets the requirement of at least 17 uniformly distributed sampling points within the scope of s. t. condition. In this problem, the objective function $f_1(x)$ is the unbeneficial indicator, and $f_2(x)$ is the beneficial indicator.

Table 6 shows the evaluation results of the partial preferable probabilities of the functions f_1 and f_2 at the discrete sampling points, P_{f1} and P_{f2}, respectively; P_t represents the total/overall preferable probability of each sampling point. As it can be seen from Table 6, sampling point No 2 shows the maximum value of the total preferable probability. Therefore, around the 2nd sampling point in Table 6, sequential optimization is adopted for successive deep optimization. Table 7 shows the evaluation results of the sequential optimization using the uniform design table $U_{37}(37^{12})$. Similarly, if a pre-specified value of 0.7% is set for $c^{(t)}$, then the deep optimization can be terminated in step 3. At this point, the final optimal results of this multi-objective programming optimization problem are $f_{1Opt.}$ = 298.7635 ¥RMB yuan and $f_{2Opt.}$ = 179.0270 kg, while the instant input variables of the successive deep optimization at step 3 are x_1 = 60.4460 kg and x_2 = 118.5810 kg. Similarly, since this is an integer programming problem, the solution for x_1 and x_2 must be rounded to the nearest integers, so the values of x_1 and x_2 are 60 kg and 119 kg, respectively, and the optimal values of objective functions are thus $f_{1Opt.}$ = 298.5 ¥RMB and $f_{2Opt.}$ = 179 kg, individually.

Table 5 – Results of discretization with $U_{37}(37^{12})$
Таблица 5 – Результаты дискретизации с $U_{37}(37^{12})$
Табела 5 – Резултати дискретизације са $U_{37}(37^{12})$

No	Input variable		Objective		Note
	x_1	x_2	f_1	f_2	
1	61.2162	53.5135	202.7027	114.7297	
2	**63.6487**	**108.6490**	**290.2703**	**172.2970**	
3	66.0811	43.7838	197.8378	109.8649	
4	68.5135	98.9189	285.4054	167.4324	
5	70.9459	34.0541	192.9730	105	
6	73.3784	89.1892	280.5405	162.5676	
7	75.8108	24.3243	188.1081	100.1351	
8	78.2432	79.4595	275.6757	157.7027	
9	80.6757	14.5946	183.2432	95.2703	
10	83.1081	69.7297	270.8108	152.8378	
11	85.5405	4.8649	178.3784	90.4054	
12	87.9730	60	265.9459	147.9730	
13	90.4054	115.1351			Excl.
14	92.8378	50.2703	261.0811	143.1081	
15	95.2703	105.4054			Excl.
16	97.7027	40.5405	256.2162	138.2432	
17	100.1351	95.6757			Excl.
18	102.5676	30.8108	251.3514	133.3784	
19	105	85.9460			Excl.
20	107.4324	21.0811	246.4865	128.5135	
21	109.8649	76.2162			Excl.
22	112.2973	11.3514	241.6216	123.6486	
23	114.7297	66.4865			Excl.
24	117.1622	1.6216	236.7568	118.7838	
25	119.5946	56.7568			Excl.
26	122.0270	111.8919			Excl.
27	124.4595	47.0270			Excl.
28	126.8919	102.1622			Excl.
29	129.3243	37.2973			Excl.
30	131.7568	92.4324			Excl.
31	134.1892	27.5676			Excl.
32	136.6216	82.7027			Excl.
33	139.0541	17.8378			Excl.
34	141.4865	72.9730			Excl.
35	143.9189	8.1081	300	152.027	
36	146.3514	63.2432			Excl.
37	148.7838	118.3784			Excl.

Table 6 – Evaluation results of PMOO discrete sampling with $U_{37}(37^{12})$
Таблица 6 – Результаты оценки дискретной выборки PMOO с $U_{37}(37^{12})$
Табела 6 – Резултати евалуације дискретног узорковања PMOO са $U_{37}(37^{12})$

No	Preferable probability		
	Partial		Total
	P_{f1}	P_{f2}	$P_t \times 10^3$
1	0.0615	0.0456	2.8059
2	**0.0420**	**0.0685**	**2.8754**
3	0.0626	0.0437	2.7344
4	0.0430	0.0666	2.8664
5	0.0637	0.0418	2.6586
6	0.0441	0.0647	2.8533
7	0.0647	0.0398	2.5787
8	0.0452	0.0627	2.8360
9	0.0658	0.0379	2.4945
10	0.0463	0.0608	2.8145
11	0.0669	0.0360	2.4061
12	0.0474	0.0589	2.7887
14	0.0485	0.0569	2.7588
16	0.0495	0.0550	2.7247
18	0.0506	0.0531	2.6864
20	0.0517	0.0511	2.6439
22	0.0528	0.0492	2.5971
24	0.0539	0.0473	2.5462
35	0.0398	0.0605	2.4058

Table 7 – Evaluation results of sequential optimization with $U_{37}(37^{12})$ discrete sampling
Таблица 7 – Результаты оценки последовательной оптимизации с дискретной выборкой $U_{37}(37^{12})$
Табела 7 – Резултати евалуације секвенцијалне оптимизације помоћу дискретног узорковања $U_{37}(37^{12})$

Step	Range	Instant input variable		Objective		Max $P_t \times 10^3$	$c^{(t)}$
		x_1^*	x_2^*	$f_{1\text{Opt.}}$	$f_{2\text{Opt.}}$		
0	[60, 150] × [0, 120]	63.6487	108.6490	290.2703	172.2970	2.8754	
1	[60, 105]× [60, 120]	61.8243	114.3240	295.1351	176.1490	2.8481	0.0095
2	[60, 82]× [90, 120]	60.8919	117.1620	297.5270	178.0540	2.8102	0.0133
3	[60, 71] × [105, 120]	60.4460	118.5810	298.7635	179.0270	2.7909	0.0069

Discussion

When solving multi - objective programming problems, the approaches employed in the previous work of other methods include the linear weighting method (Zheng et al, 2022c), i.e. the "additive" algorithm, which transfers multi – objective problems into single objective ones. However, from the perspective of the probability theory, this essentially means a "union", and some methods even take several objectives as constraint conditions to solve multi-objective programming problems (Zheng et al, 2022c), which is not realized to the intrinsic meaning of multi - objective programming problems, while probabilistic multi-objective optimization tries to deal with simultaneous optimization of multiple objectives from the perspective of the probability theory, which is a rational method of multi - objective optimization (Zheng et al, 2022c). Therefore, the results obtained by other methods cannot be compared with the results of probabilistic multi - objective optimization.

Conclusion

By using the combination of probabilistic multi - objective optimization, discrete sampling by means of the good lattice points, and successive sequential optimization to solve the multi - objective integer programming problem, we establish a reasonable scheme for solving the multi - objective programming problem. This method properly considers simultaneous optimization of many objectives in the problem, which rationally reflects the essence of simultaneous optimization of multiple objectives, and opens a new approach to the relevant problem.

References

Fang, K.-T. 1994. *Uniform Design vs. Uniform Design Table.* Beijing, China: Science Press (in Chinese). ISBN: 7-03-004290-5 [online]. Available at: https://book.ixueshu.com/book/91793a0541929c0e41e4b4d7d021b3f0318947a18e7f9386.html [Accessed: 01 December 2022].

Fang, K.-T. & Wang, Y. 1994. *Number-theoretic Methods in Statistics.* London, UK: Chapman & Hall/CRC. ISBN: 978-0412465208.

Fang, K.-T., Liu, M.-Q., Qin, H. & Zhou, Y.-D. 2018. *Theory and Application of Uniform Experimental Designs.* Singapore: Springer. Available at: https://doi.org/10.1007/978-981-13-2041-5.

Huang, Q., Lv, X., Li, X. & Wang, C. 2017. *Modern Optimum Theory and Method*. Science Press, Beijing (in Chinese). ISBN: 978-7-03-053961-8/O·6977.31.

Hua, L.-K. & Wang, Y. 1981. *Applications of Number Theory to Numerical Analysis*. Berlin, Heidelberg: Springer. Available at: https://doi.org/10.1007/978-3-642-67829-5.

Liu, S. 2014. *Theoretical Method and Application of Multi-objective Programming.* Shanghai, China: Shanghai Jiaotong University Press (in Chinese). ISBN: 978-7-313-10574-5/O.

Ying J. 1988. *Multi – objective Progamming.* Beijing, China: People's Educational Press (in Chinese). ISBN: 978-7-107-10086-6/G·456.

Zheng, M., Teng, H. & Wang, Y. 2023. Hybrids of Uniform Test and Sequential Uniform Designs with "Intersection" Method for Multi- objective Optimization. *Tehnički glasnik,* 17(1), pp.94-97. Available at: https://doi.org/10.31803/TG-20211130132744.

Zheng, M., Teng, H., Yu, J., Cui, Y. & Wang Y. 2022c. *Probability-Based Multi-objective Optimization for Material Selection.* Singapore: Springer. Available at: https://doi.org/10.1007/978-981-19-3351-6.

Zheng, M., Wang, Y. & Teng, H. 2021. A New "Intersection" Method for Multi-Objective Optimization in Material Selection. *Tehnički glasnik,* 15(4), pp.562-568. Available at: https://doi.org/10.31803/tg-20210901142449.

Zheng, M., Wang, Y. & Teng, H. 2022a. A novel method based on probability theory for simultaneous optimization of multi-object orthogonal test design in material engineering. *Kovove Materialy,* 60(1), pp.45-53. Available at: https://doi.org/10.31577/km.2022.1.45.

Zheng, M., Wang, Y. & Teng, H. 2022b. A novel approach based on probability theory for material selection. *Materialwissenschaft und Werkstofftechnik,* 53(6), pp.666-674. Available at: https://doi.org/10.1002/mawe.202100226.

Новое решение для многоцелевых задач целочисленного программирования с помощью вероятностной многоцелевой оптимизации

Маошенг Чжэн[а], *Джи* Йю[б]

Северо-западный политехнический университет,
г. Сиань, Народная Республика Китай

[а] факультет химической инженерии, **корреспондент**

[б] факультет естественных наук

РУБРИКА ГРНТИ: 27.47.00 Математическая кибернетика,
27.47.19 Исследование операций
ВИД СТАТЬИ: оригинальная научная статья

Резюме:

Введение/цель: В данной статье представлено новое решение для многоцелевых задач целочисленного программирования с помощью вероятностной многоцелевой оптимизации. Кроме того, в целях сукцессивного упрощения обработки и глубокой оптимизации

используются дискретизация с помощью соответствующих узлов решетки и последовательная оптимизация.

Методы: В вероятностную многоцелевую оптимизацию введена новая концепция предпочтительной вероятности для описания степени предпочтения полезности каждого кандидата. Каждая полезность характеристик кандидата вносит частичную предпочтительную вероятность, а произведение всех частичных предпочтительных вероятностей составляет общую предпочтительную вероятность кандидата. Таким образом, общая предпочтительная вероятность переводит многоцелевую проблему в одноцелевую. Дискретизация по методу узлов идеальной решетки применяется для дискретной выборки, а последовательная оптимизация — для глубокой оптимизации. Также в целях упрощения данной процедуры можно отказаться от целочисленных требований. В конце процедуры оптимальные решения введенных переменных необходимо округлить до ближайшего целого числа.

Результаты: Данный подход используется для решения двух производственных задач, а именно: максимизации прибыли при минимизации загрязнения и составления плана закупок как можно большего количества сырья при наименьших затратах. С помощью теории вероятностей вышеуказанные задачи показали многообещающие результаты одновременной оптимизации нескольких целей.

Выводы: Данное решение учитывает одновременную оптимизацию нескольких целей при многокритериальном целочисленном программировании, что, естественно, отражает суть многокритериального программирования и тем самым открывает новые возможности к решению многокритериальных задач.

Ключевые слова: многоцелевая оптимизация, задача целочисленного программирования, предпочтительная вероятность, дискретная выборка, последовательная оптимизация.

Ново решење проблема вишекритеријумског целобројног програмирања помоћу вишекритеријумске оптимизације засноване на вероватноћи

Маошенг Џенг[а], *Ђаи* Ју[б]

Универзитет Северозапад, Сијан, Народна Република Кина

[а] Факултет хемијског инжењерства, **аутор за преписку**

[б] Факултет природних наука

ОБЛАСТ: математика, рачунарске науке
КАТЕГОРИЈА (ТИП) ЧЛАНКА: оригинални научни рад

Сажетак:

Увод/циљ: У раду се формулише ново решење проблема вишекритеријумског целобројног програмирања помоћу пробабилистичке вишекритеријумске оптимизације. Такође, користи се дискретизација помоћу добрих тачака решетке, као и секвенцијална оптимизација ради сукцесивног поједностављивања и дубинске оптимизације.

Методе: У пробабилистичку вишекритеријумску оптимизацију уведен је нови концепт пожељне вероватноће како би се описао степен пожељности сваке појединачне корисности перформансе неког кандидата. Свака појединачна корисност перформансе кандидата доприноси парцијалној пожељној вероватноћи, а производ свих тих вероватноћа чини укупну пожељну вероватноћу кандидата. На тај начин укупна пожељна вероватноћа преводи вишекритеријумски проблем у једнокритеријумски. Дискретизацијом помоћу метода добрих тачака решетке врши се дискретно узорковање за континуалну функцију циља, а секвенцијалном оптимизацијом дубинска оптимизација. Такође, може се одустати од захтева целих бројева ради поједностављивања наведеног поступка. На крају се оптимална решења унетих варијабли морају заокружити на најближи цели број.

Резултати: Овај приступ се користи за решавање два проблема у производњи: за максимизацију прихода уз најмање могуће загађење и за креирање плана за набавку највеће количине репроматеријала по најмањој цени. Обећавајући резултати су добијени за два наведена проблема помоћу теорије вероватноће за истовремену оптимизацију више циљева.

Закључак: Ово решење узима у обзир истовремену оптимизацију више циљева при вишекритеријумском целобројном програмирању, што природно одсликава суштину вишекритеријумског програмирања и тиме отвара нове путеве ка решавању вишекритеријумских проблема.

Кључне речи: вишекритеријумска оптимизација, проблем целобројног програмирања, пожељна вероватноћа, дискретно узорковање, секвенцијална оптимизација.

Paper received on / Дата получения работы / Датум пријема чланка: 04.12.2022.
Manuscript corrections submitted on / Дата получения исправленной версии работы / Датум достављања исправки рукописа: 23.03.2023.
Paper accepted for publishing on / Дата окончательного согласования работы / Датум коначног прихватања чланка за објављивање: 25.03.2023.

Application of Cube IQ software and multicriteria optimization models for the selection of vehicles for the transport of goods in the Serbian Armed Forces

Ivana D. Đuričić

Serbian Armed Forces, Directorate for Logistics,
Central Logistics Base, First Warehouse Battalion,
Gornji Milanovac, Republic of Serbia,
e-mail: ivanadjuricic5@gmail.com,
ORCID iD: https://orcid.org/0000-0002-1961-0672

DOI: 10.5937/vojtehg71-42298; https://doi.org/10.5937/vojtehg71-42298

FIELD: mathematics, transport, logistics
ARTICLE TYPE: original scientific paper

Abstract:

Introduction/purpose: An adequate selection of vehicles used for the transport of goods is a very important factor that affects the economical and rational use of vehicle fleets, as well as the quality and efficiency of carrying out transport activities in the Serbian Armed Forces. The goal of this work is to design a model that should be of help to the traffic service authorities to select the vehicle that is best for the performance of the assigned transport task based on the defined criteria.

Methods: This paper therefore proposes a model for the selection of vehicles for the transport of goods using a fuzzy logic system, as a type of artificial intelligence system. In order to solve the problem of choosing a vehicle for the transport of goods, five criteria are defined in the work based on a survey of the commanders of the transport lines, which represent the input values in the fuzzy logic system.The vehicle is selected based on five criteria. The input variables are represented by three membership functions, while the output variable is defined by five membership functions. All the rules in the fuzzy logic system are determined using the rule premise weight aggregation method (ATPP), which enables the formation of a rule base based on experience. By applying this method and based on the number of input variables and the number of their membership functions, a base of 243 rules was defined. The values of the weighting coefficients of the membership functions were determined using the LMAW method. A user "interface" program was created for the developed fuzzy logic system, which enables the practical application of this model.

Results: The model was tested on the example of choosing the optimal vehicle for goods transported to the IVP "Pasuljanske livade" in 2020. The selection of the optimal means of transport was made among the transport

motor vehicles that are most used in the Serbian Army, namely: TAM 150 T11, FAP 2026 and FAP 1118. After packing all three vehicles with these goods in Cube IQ and after performing calculation and evaluation of individual vehicles in the user "interface" program, the values of the output variable for each vehicle were obtained. The obtained values for each vehicle were ranked and the optimal vehicle for the transport of defined goods was shown to be the FAP 1118.

Conclusion: The significance of this study is that it is among the first ones to demonstrate the application of a model based on artificial intelligence that solves the problem of vehicle selection for the transportation of movable assets. The study provides considerable opportunity for further research.

Key words: fuzzy logic, fuzzy set, ATPP, LMAW, cube IQ, Matlab.

Introduction

Economical use of means of transport in peacetime is of great importance for the defense system of the Republic of Serbia. Transport motor vehicles with different usage characteristics are the basis of unit mobility. That is why it is important to choose the one that will best meet the set requirements from the large number of different types of motor vehicles that can be used to transport goods. A large number of different types of means of transport means that for every transport it is necessary to choose a motor vehicle that will perform a particular task best and most easily. Proper evaluation and selection of the right vehicle ensure the conditions for the efficient execution of the tasks set before the units of the Serbian Armed Forces. Taking into account the above, the choice of the optimal vehicle is of great importance for economical, successful and safe transport of units. In order to determine the optimal vehicle for the transport of goods for carrying out an assigned transport task, a choice must be made between the motor vehicles used in the Serbian Armed Forces. In order to facilitate the work of the traffic service authorities when choosing the optimal vehicle for the transport of goods, a model based on artificial intelligence is presented in the paper, in order to help solving that problem. Until now, the Serbian Army has not developed such a model that solves the problem of vehicle selection based on artificial intelligence.

Based on a survey of transport line commanders, several criteria were defined to represent the input variables in the fuzzy logic system, namely: number of transport vehicles, capacity utilization, motor vehicle reliability, fuel consumption per 100 km, and suitability for transport manipulative work. This is followed by the fuzzy system modeling through five stages: problem analysis, definition of linguistic variables, selection of membership functions, formation of the rule base, and selection of inference and

defuzzification methods. For the developed fuzzy logic system, the user "interface" of the program for the selection of vehicles for the transport of goods was created in the Matlab 2017a program package.

The presented model was tested on the example of choosing the optimal vehicle for goods that were transported to the IVP "Pasuljanske livade" in 2020 for the needs of the Military Academy. The selection of the optimal means of transport was made from among the transport motor vehicles that are used the most in the Serbian Armed Forces, and these are TAM 150, FAP 2026, and FAP 1118. After packing the off-road vehicle TAM 150 with these goods in Cube IQ, we read the data from the software on how many motor vehicles we need to transport that type of goods and use the carrying capacity per vehicle. In order to unify the load capacity and obtain only one value, the arithmetic mean of all obtained values of the load capacity utilization of those vehicles was taken. In the same way, the packaging and obtaining the data necessary for the input variables in the fuzzy logic system is carried out for the off-road vehicles FAP 2026 and FAP 1118. The input value of fuel consumption per 100 km is obtained from the technical instructions for the mentioned motor vehicles, while the reliability of a motor vehicle and its suitability for transport manipulative work are obtained on the basis of the processed data from the survey of the commanders of the transport lines.

The defined input values are entered into the created user program and by starting the fuzzy system, the output variables are obtained, that is, the preference for the vehicle is obtained in the form of a numerical value and a linguistic descriptor. Based on the obtained values for each vehicle, a ranking was performed and the optimal vehicle for the transport of defined goods is the one with the highest preference value.

The paper consists of five parts. In the second part, the means of transport most commonly used in the army are mentioned. The third part presents the description and the method of designing the fuzzy logic system, as well as the display and the method of creating a user "interface" program for the selection of vehicles for transporting goods. Then the application of Cube IQ is defined. The fourth part deals with the data used when testing the modeled fuzzy system, a presentation of the use of Cube IQ and the method of obtaining the necessary parameters. Finally, concluding remarks with further research proposals are given.

Means of transport in the Serbian Army

In accordance with the Rulebook on the use of military vehicles in the Ministry of Defense and the Serbian Armed Forces, "a military vehicle is

any combat and non-combat vehicle and any other vehicle that is registered under special regulations of the Ministry of Defense, as well as any other properly marked vehicle while performing material obligations in use in the units and institutions of the Ministry of Defense and the Serbian Army". According to this Rulebook, military vehicles are divided into:

- Non-combat motor vehicles of general purpose;
- Non-combat special purpose motor vehicles;
- Trailers;
- Combat vehicles;
- Engineering machines powered by liquid fuels;
- Special purpose vessels;
- Means of internal transport; and
- Other vehicles.

A general-purpose non-combat motor vehicle is a vehicle that, in accordance with its construction, devices and equipment, is intended for transporting people and cargo, for performing certain works, as well as for towing a trailer, while non-combat special-purpose vehicles represent vehicles that, by design, devices and assemblies, are intended and adapted for special purposes. Off-road non-combat vehicles, depending on their purpose and technical characteristics, can be divided into (Starčević, 2020):

- All-terrain vehicles for transporting people; and
- All-terrain vehicles for towing and transport.

The basic purpose of all-terrain vehicles for towing and transport in the Serbian Army is the transportation of people and cargo, towing tools and attachments, as well as the application for special superstructures of the cabin type. Constructive solutions of all-terrain vehicles allow the transportation of 12 to 20 people, while the carrying capacity of the vehicle ranges from 1.5 to 20 tons. All-terrain vehicles for towing and transport were mainly created on the basis of commercial vehicles, where the basic assemblies were modified to a greater or lesser extent for military use. Drive formulas for these vehicles are 4x2, 4x4, 6x6 and 8x8, depending on the total weight and load capacity of the vehicle. In the units of the Serbian Army, the following are mostly used: TAM 150, FAP 2026 and FAP 1118.

Off-road vehicle TAM 150 B/BV

The off-road vehicle TAM 150 T11 is a multi-purpose vehicle with all-wheel drive. This vehicle has great maneuverability and is designed so

that it can be used in different weather, adverse road and terrain conditions. It is produced in variants:

– TAM 150 T11 BV – with winch; and
– TAM 150 T11 B – without winch.

The off-road vehicle TAM 150 T11 is intended for the transportation of personnel (18 + 2 persons), transport of loads up to 5t useful load on roads and up to 3t useful load off-road. Also, it can be used for towing tools, trailers, as well as for superstructures. This model of the off-road vehicle is in use in all units and institutions of the Serbian Armed Forces and its average age is over 30 years. Maintenance is difficult due to the lack of adequate spare parts, and therefore the degree of reliability of using the vehicle when performing daily tasks is reduced.

Figure 1 – All-terrain vehicle TAM 150 T11
Рис. 1 – Крупнотоннажный грузовой автомобиль TAM 150 T11
Слика 1 – Теренско возило TAM 150 T11

The dimensions of the off-road vehicle TAM 150 T11 are 6550mm x 2275mm x 2890mm, fuel consumption is 24 - 30 l/100km, while the dimensions of the cargo box are 4170mm x 2120mm x 1560mm (500mm) (Starčević, 2020).

Off-road vehicle FAP 2026

The all-terrain vehicle FAP 2026 is a domestically produced multi-purpose vehicle intended for driving on impassable terrain, transporting

people (20 + 2 persons) with complete equipment, transporting material assets up to 10t useful load capacity on roads and up to 6t useful load capacity off-road, as well as for towing tools. Its dimensions are 7720mm x 2490mm x 3100mm, cargo box dimensions 4530mm x 2020mm x 1600mm (470mm), while fuel consumption is 33 l/100km (Starčević, 2020).

Figure 2 – All-terrain vehicle FAP 2026
Рис. 2 – Крупнотоннажный грузовой автомобиль ФАП 2026
Слика 2 – Теренско возило ФАП 2026

This model of all-terrain vehicle is used in the artillery and logistics units of the Serbian Army. The average age of the vehicle is over 20 years and the maintenance of these vehicles is regular due to the fact that the vehicle was produced in the Republic of Serbia and that the units of the Serbian Armed Forces have trained personnel and the necessary spare parts. It follows that the vehicles have an appropriate degree of reliability of use in the execution of everyday tasks.

Off-road vehicle FAP 1118

The all-terrain vehicle for towing and transport FAP 1118 was introduced to the Serbian Armed Forces in 2010 after successful development and final tests, and has been serially produced since 2012. This vehicle model was developed by a domestic manufacturer with the aim of renewing the vehicle fleet in the units of the Serbian Armed Forces and replacing the TAM 110 and TAM 150 vehicles. Its main purpose is to

transport people with complete equipment (20 people), transport cargo up to 4t payload, tow tools and connecting devices, as well as application for special superstructures of the cabin type. The dimensions of the all-terrain vehicle FAP 1118 are: 6414mm x 2500mm x 3310mm, and the cargo box dimensions are 4000mm x 2440mm x 1720mm (550mm). Fuel consumption per 100km is 17-30l.

Figure 3 – All-terrain vehicle FAP 1118
Рис. 3 – Крупнотоннажный грузовой автомобиль ФАП 1118
Слика 3 – Теренско возило ФАП 1118

In the units of the Serbian Armed Forces, this vehicle is the newest and youngest all-terrain vehicle for towing and transport and is in use in the largest number of units and institutions of the Serbian Armed Forces, with a focus on logistics units. Vehicle maintenance is regular due to the fact that the vehicle is manufactured in the Republic of Serbia and that the units have trained personnel and the necessary spare parts, and therefore the vehicles have an appropriate level of reliability when performing daily tasks (Starčević, 2020).

Criteria for choosing a vehicle for transporting goods

The analysis came to the conclusion that there is no software based on artificial intelligence that is used for the selection of vehicles for the transport of goods in the Serbian Army. As a result of the research, the

paper proposed a decision-making model, based on artificial intelligence, for the selection of vehicles for the transport of goods in the Serbian Armed Forces, and developed software for its practical application. For the selection of criteria for creating this model, the commanders of transport lines were surveyed. Based on the obtained data, the criteria for the selection of vehicles for the transport of goods were defined, which represent the input variables in the software. The criteria and their description are presented in the table.

Table 1 – Defined criteria for the selection of vehicles for the transport of goods in the Serbian Army
Таблица 1 – Определенные критерии выбора транспортных средств для перевозки грузов в сербской армии
Табела 1 – Дефинисани критеријуми за избор возила за транспорт робе у Војсци Србије

	Criterion	Description
1.	Number of means of transport	Required number of means of transport for transporting goods.
2.	Capacity utilization	The coefficient of static utilization of the vehicle's carrying capacity represents the ratio of the amount transported and the amount of cargo that could be transported, if the vehicle's carrying capacity were fully used while driving with the load.
3.	Motor vehicle reliability	The ability of the vehicle to carry out transport work, keeping its exploitation indicators at a given level during a certain time (mileage traveled) in given conditions of exploitation.
4.	Fuel consumption per 100 km	The amount of fuel used per 100 km of travel.
5.	Suitability for transport and manipulative work	Adaptation of the vehicle to loading and unloading processes, i.e., to enable loading or unloading with the least expenditure of time and labor, as well as optimal conditions for the goods.

A model for optimizing the choice of vehicles when transporting goods in the Serbian Armed Forces

The scheme of the model for optimizing the choice of vehicles when transporting goods in the Serbian Army is shown in Figure 4. In the first phase, after analyzing the problem, when modeling the fuzzy logic system,

linguistic values are defined as well as the choice of membership functions, which allows us to form a rule base, and then select the inference and defuzzification method.

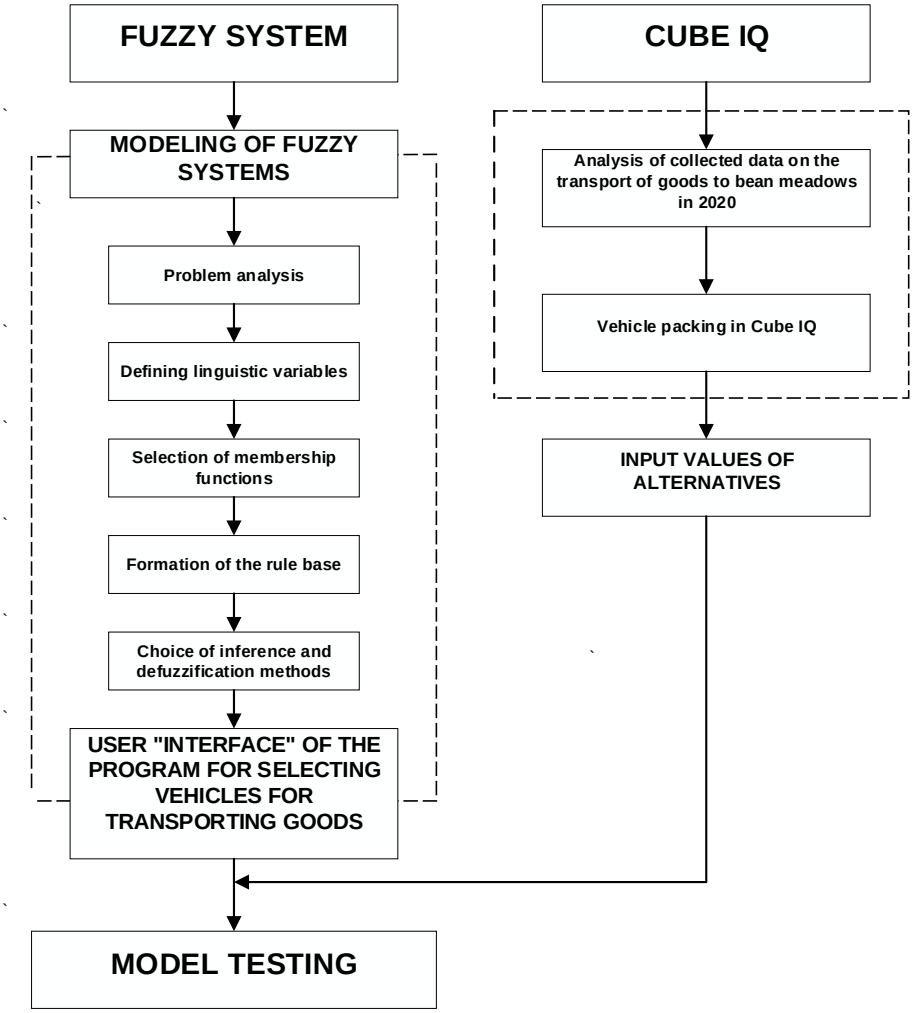

Figure 4 – Scheme of the model for the optimization of vehicle selection
Рис. 4 – Схема модели оптимизации выбора транспортных средств
Слика 4 – Шема модела за оптимизацију избора возила

After the completion of the first phase, in the next step, the user "interface" of the program is created, which allows us to apply this model in practice. In the second phase, by applying the Cube IQ software, based on the analysis of the collected data, the vehicle is packed, which allows

us to define the input values of the alternatives that are inserted into the user form which performs model testing.

FUZZY systems

Artificial intelligence is defined as the branch of computer science that deals with the creation of computer programs capable of exhibiting "intelligent" behavior, one that is typically considered a uniquely human quality (Luger et al, 1994). The term "artificial intelligence" is widely used as the name of the branch of computer science that studies the ways in which computers can be made "smarter" (Raphael, 1976). Artificial intelligence as a scientific discipline deals with the method of automating intelligent behavior. It is based on learning from experimental data, learning from different patterns and transferring human knowledge to analytical models. The goal of this scientific discipline is the development and application of algorithms that will enable the computer to perform tasks in the way that the human brain performs them. Artificial intelligence methods are widely applied in all areas of solving engineering problems through (Zuber & Ličen, 2011):

- Expert systems - systems based on knowledge bases;
- Fuzzy logic systems - based on the transfer of human knowledge (experience) into the working system;
- Artificial neural networks - there are mathematical models behind the learning process; and
- Hybrid artificial intelligence systems – computer systems that integrate different intelligent techniques.

Words such as: vague, undefined, vague, imprecise, blurred, ambiguous, hazy could be replaced by one word - fuzzy. The founder of fuzzy logic is considered to be a professor of computer science at the University of California, Berkeley, whose name is Lofty Zadeh (Zadeh, 1975a; 1975b; 1975c). He laid the foundations of this science in 1965, and according to him, fuzzy logic can have two different meanings (Zadeh, 1965):

- In a broader sense, fuzzy logic is a synonym for the theory of fuzzy sets, and it refers to objects with unclear boundaries whose membership is measured by a certain degree; and
- In a narrower sense, fuzzy logic is a logical system that is an extension of classical logic.

The basis of his theory is that descriptions should be imprecise, which he shows by the principle of incompatibility, where he claims that by increasing the impreciseness of the statement, with which we describe the phenomenon, we increase its importance. A historically important element in the development and application of fuzzy logic is the first practical application, i.e. the first fuzzy regulator for controlling a steam engine, which was constructed by Mamandi and Assilian in 1974. In the 1990s, the market saw many products whose operation was based on the application of fuzzy logic. Today, it is a clear fact that fuzzy systems can be successfully applied in many areas: traffic management, stock exchange business, medical diagnostics, financial management, etc.

A set of elements with the same properties is called a classic discrete set and each element of a discrete set belongs to that set 100%, i.e. with a membership degree of 1 on a scale from 0 to 1. While fuzzy logic is based on the theory of fuzzy sets where the basic elements for representation and processing are imprecise, it represents an extension and generalization of a discrete set, that is, it represents a set of elements with similar characteristics where the membership of the elements can be any real number in the interval [0-1] (Zadeh, 1975a; 1975b; 1975c). The basic difference between these two types of sets is that classic sets always have a unique membership function, while fuzzy sets can be described with many different membership functions. A fuzzy set (A) can be defined as a set of ordered pairs.

$$\mathrm{A} = \{(x, \mu_A(\mathrm{x}))|\mathrm{x} \in \mathrm{X}\ , 0 \leq \mu_A(\mathrm{x}) \leq 1\ \} \qquad (1)$$

X is the universal set or set of considerations on which the fuzzy set A is defined, and μA (h) is the membership function of the element (h) of the set A (Puška et al, 2023). Each fuzzy set is completely and uniquely determined by its membership function. An element of a fuzzy set is every element in a confidence interval with a certain degree of membership, while the membership function is chosen based on the experience gained.

The confidence interval for each fuzzy variable is determined by the designer based on experience, observation or measurement. A confidence interval that is within the physical limits of the variable is most often adopted. A standardized value is adopted or an abstract confidence interval is defined (Božanić & Pamučar, 2014).

One of the features of fuzzy logic is that it is based on natural language where linguistic objects are words and not numbers. Linguistic expressions represent the connection between the numerical

representation of information in a computer and the human way of thinking (Tešić et al, 2022).

So input and output variables can have different linguistic names which are displayed with descriptive names. The transformation of linguistic expressions into the form of a mathematical representation is made possible by the theory of fuzzy sets. In order to define linguistic variables more precisely, they should also have linguistic values, such as: "very little", "small", "medium", "large", "very large". These values can also be assigned a numerical representation for the purpose of easier and shorter marking.

Fuzzy relations are a natural extension of the concept of fuzzy sets and are used to represent relationships between elements that hold to a certain degree. In binary relations, two elements can either satisfy or not satisfy the relation, while in non-binary relations, the strength of the relation is expressed by expressions that express gradualness (Ćirović et al, 2014). In fuzzy relations, elements can have a higher or lower degree of belonging, which is expressed as a number from the interval [0,1].

Fuzzy proposition is a structure of the form "h is A", where the variable h and the set A are compared, that is, it determines the degree of belonging of the variable h to the fuzzy set A. Where variable h can be 0 or 1 or fuzzy 0.75. The combination of propositions and conjunctions creates a fuzzy rule that can be presented in the following form:

IF x is A

THEN y is B

Where x and y represent linguistic variables, and A and B linguistic values described by fuzzy sets with the confidence intervals X and Y. The conjunctions AND, OR, NOT, IF - THEN are used to connect propositions, which are quantified through T and S norms. The fuzzy rule describes a cause-and-effect relationship between input and output variables, while from the aspect of automation it represents a combination of sensor information and control actions.

Models based on fuzzy logic consist of "If - Then" rules that are connected by "Else" expressions. The first part of the If rule represents the input state, and the fuzzy proposition represents the premise, while the second part of the Then rule represents the output state, and the fuzzy proposition in this part represents the conclusion. A set of rules in which the solution to a problem is described in words is a rule base or expert rules. The rules are written in a convenient order for easier understanding and are connected by the conjunction Or (Else), which is often not stated (Pamučar, 2010).

In the relation, the input variables are most often represented by a number, while the output values are also obtained in numerical notation. Since the fuzzy system is described verbally (qualitatively) through production rules, it is necessary to convert (fuzzify) numerical values using fuzzy logical operations. After that, the mechanism of approximate reasoning (inference) processes them in the fuzzy system through three phases: aggregation, activation and accumulation (Pamučar et al, 2014).

The first step in solving a problem in fuzzy systems is fuzzification. It is a process that converts each numeric input into a membership degree. There is a degree of membership for each linguistic variable that applies to a particular physical quantity (Bozanić et al, 2019).

Aggregation is the stage in which the process of associating a certain value of the membership function with a measured numerical value is carried out, that is, it is determined with what degree of confidence some input numerical value belongs to a given fuzzy set. It is equivalent to phasing if there is only one input.

Activation is an inference made in the Then part of the rule and represents a deduction of the conclusion. The minimum and the algebraic product are used as the activation operator, as the most common methods of direct reasoning - Mamdani's method. In this type of reasoning, only true premises are taken into account. By applying this method, fuzzy sets are both input and output; this is important because another method is often used - the Takagi-Sugeno-Kang method. The difference between these two methods is in the structure of fuzzy rules, that is, in the conclusion, instead of a fuzzy set, there is a linear function of input and output.

Accumulation consists of activating the conclusion, which is accumulated by addition. The maximum or algebraic sum is used as an accumulation operator.

Defuzzification means converting the resulting fuzzy set into a real number. During mathematical defuzzification, information is reduced, because different values of the linguistic variable can be mapped into the same defuzzified real number. Therefore, it is necessary to be very careful when choosing a defuzzification method, because there is no method that is optimal for everyone. Also, one of the big problems is adjusting the fuzzy rule parameters in order to get the desired output. The adjustment methods are different and depend on the type of problem, because it is impossible to define a general methodology by which it is possible to perform the adjustment (Badi & Abdulshahed, 2021).

Models based on fuzzy logic generally require more iterations. In the first step, a set of rules and corresponding membership functions are defined, and then correction of individual rules and/or membership

functions is performed, if necessary based on the observed results. Then the model is tested again.

Modeling fuzzy logic system

Based on the described system, the foundations were created to model the given system of interdependence of input criteria as a complex fuzzy system for the selection of vehicles for transporting goods. The final solution is reached through several stages, which in general modeling represent system design, optimization and application. All those stages in the fuzzy system can be specifically defined as:

- Problem analysis;
- Defining linguistic values;
- Selection of affiliation functions;
- Formation of the rule base;
- Choice of inference and defuzzification methods; and
- Application of fuzzy model.

Problem analysis

When modeling a fuzzy logic system, a detailed analysis of the problem is performed in order to determine the number of variables and their interdependence. If the problem is complex, the system is divided into several smaller subsystems, the goal and purpose of each subsystem is determined, and then the ways of connecting them and the priorities among them are defined.

Defining linguistic values

Linguistic variables, as already explained, take values from spoken language or are artificially synthesized. They are represented by fuzzy sets. It is thought that the designed fuzzy system, for the selection of vehicles for transporting goods, consists of five input linguistic variables:

- Number of means of transport;
- Utilization of carrying capacity;
- Reliability of the motor vehicle;
- Fuel consumption per 100 km;
- Suitability for transport and manipulative work;

and one output linguistic variable Vehicle Preference. The table shows the interval of linguistic variables that was used when designing the fuzzy system.

Table 2 – Interval of the input and output linguistic variables
Таблица 2 – Интервал входных и выходных лингвистических переменных
Табела 2 – Интервал улазних и излазних лингвистичких променљивих

Input linguistic variables	Interval	
	from	to
Number of means of transport	1	8
Capacity utilization	0	1
Motor vehicle reliability	0	10
Fuel consumption per 100 km	0	40
Suitability for transport and manipulative work	0	10
Output linguistic variable	Interval	
	from	to
Vehicle preference	0	1

After defining and determining the interval of linguistic variables, it is necessary to determine the number and type of membership functions for all input and output variables. Setting up the system complicates a larger number of membership functions, and, cosequently, a larger number of rules, so it is recommended to start with reducing the number of membership functions in accordance with the nature of the variable (Krstić, 2006). This reduction must not be done if there is a change in the quality of the variable. Therefore, it is defined that in the model each input variable has three membership functions, while the output variable has five membership functions. The linguistic values of all input variables are: Small, Medium, Large, while the output linguistic values are: Very Small, Small, Medium, Large and Very Large.

Since it is a decision support system, a large number of linguistic variables was not needed. With three linguistic values, a satisfactory gradualness in changing the output values was achieved, which maximized the number of rules to 243, which is within the range that an expert can control.

Selection of membership functions

The choice of membership functions and their range is an important stage when modeling a fuzzy logical system. In the fuzzy system, Gaussian curves were used, since they describe the input and output variables well and enable optimal sensitivity of the system (Vesković et al, 2020). Figure 5 shows the membership functions of the input linguistic variables, while Figure 6 shows the membership function of the output variable.

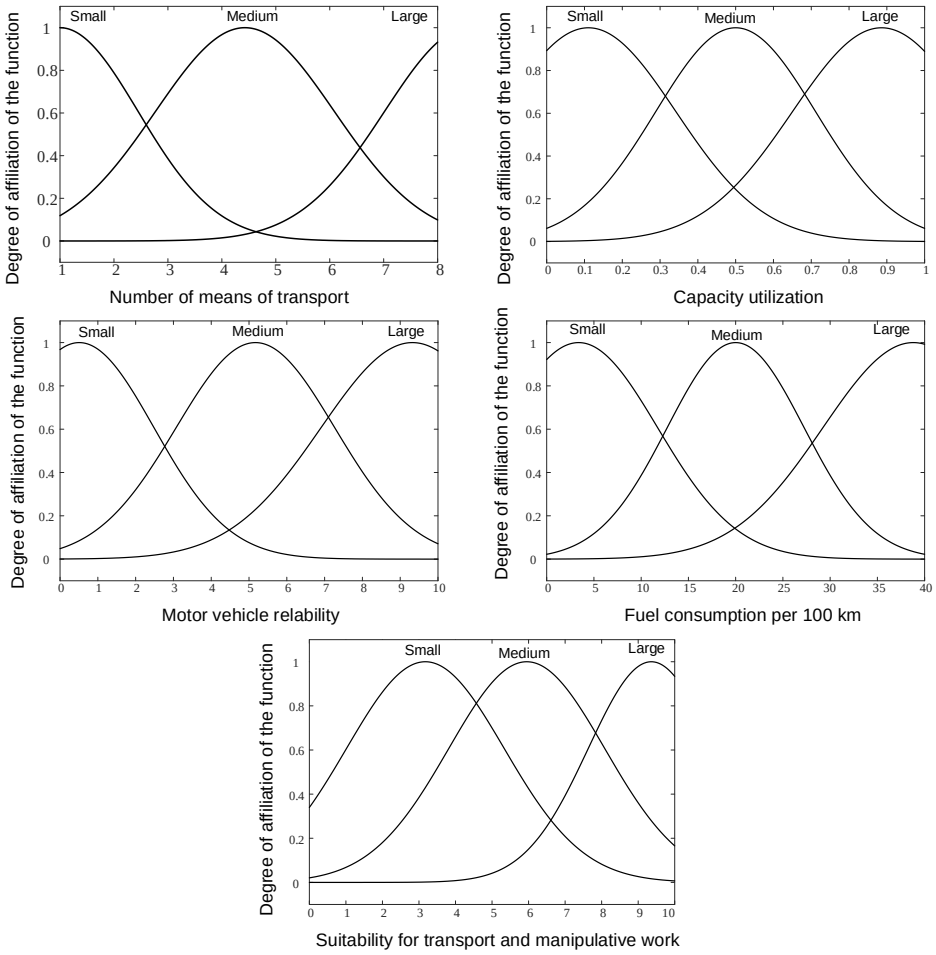

Figure 5 – Membership functions of the input linguistic variables
Рис. 5 – Функции принадлежности входных лингвистических переменных
Слика 5 – Функције припадности улазних лингвистичких променљивих

The values of membership functions of input and output variables are shown in Table 3, where the first number in the interval represents the left and right distribution of the Gaussian curve along the abscissa, and the second number represents the value in which the Gaussian curve has a value of 1 on the abscissa axis.

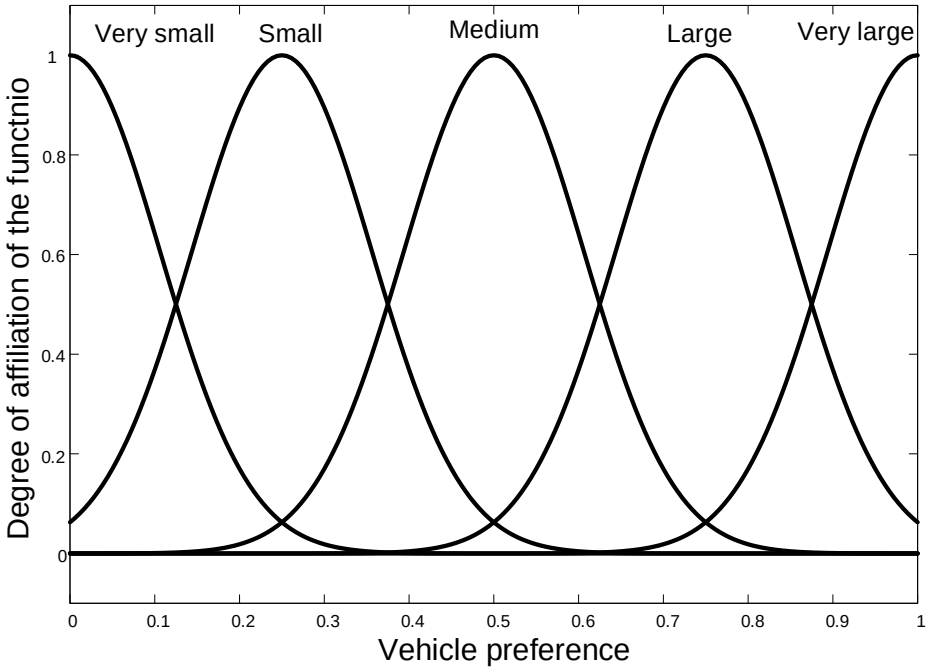

Figure 6 – Membership functions of the output variable
Рис. 6 – Функции принадлежности выходной переменной
Слика 6 – Функције припадности излазне променљиве

Table 3 – Values of the membership functions of the input variables
Таблица 3 – Значения функций принадлежности входных переменных
Табела 3 – Вредности функција припадности улазних променљивих

Membership function/ Input value	Small	Medium	Large
Number of means of transport	[1.45 , 1]	[1.66 , 4.428]	[1.58 , 8.59]
Capacity utilization	[0.232 , 0.1104]	[0.2119 , 0.5]	[0.236 , 0.8859]
Motor vehicle reliability	[1.98 , 0.5074]	[2.1 , 5.169]	[2.42 , 9.3]
Fuel consumption per 100 km	[8.37 , 3.38]	[7.254 , 20]	[9.575 , 38.8]
Suitability for transport and manipulative work	[2.16 , 3.174]	[2.136 , 5.95]	[1.728 , 9.36]

Formation of the rule base

The rule base is composed of a certain number of rules, expressed in spoken or artificial language words, which represent the expert's knowledge. A big problem with complex systems is that there is no standard and systematic method for transforming engineering knowledge or experience into fuzzy rules. As already mentioned, there is also no general procedure for choosing the optimal number of rules, since many factors influence such a decision.

At the beginning, for each combination of the input linguistic variable, the expert suggests the corresponding output value. As already mentioned, the system consists of five input linguistic variables (n=5) with three linguistic values each (M=3) that can be combined in a database with a total of M^n=3^5=243 rules. In the paper, to determine the rules of the fuzzy logical system, the "Method of Aggregation of Rule Premise Weights" (ATPP) was used. The ATPP method for determining the rule base consists of six steps (Ćirović & Pamučar, 2013):

- Determination of the weight coefficients of the input variables;
- Determination of the type (type) and function numbers of the input - output variables;
- Determination of the weighting coefficients of the membership functions of the input variables;
- Generation of the initial (incomplete) rule base with the maximum number of combinations of input - output pairs;
- Generating a "complete" rule base by assigning appropriate conclusions $(y_i^{(r)})$to premises ($x_i^{(j)}$); and
- Optimization of rules.

At the beginning, the weighting coefficients of the relevance functions ($w_{x_i}^{(j)}$) of the input variables are determined, usually based on the subjective assessment of the expert who models the fuzzy logic system. In addition, the weight coefficients of the membership function can be determined by group decision-making or aggregation of expert decisions (Kiptum et al, 2022).

The distribution of weight coefficients can be even or uneven, but it should reflect reality as much as possible. In the specific case, it was defined with the help of the LMAW method based on a questionnaire. An overview of the LMAW method is given in (Pamučar et al, 2021). The value of the weight coefficients is given in Table 4.

Table 4 – Weighting coefficients of criteria
Таблица4 – Весовые коэффициенты критериев
Табела 4 – Тежински коефицијенти критеријума

Criterion	Weight coefficient of criteria	$w_{x_i}^{(1)}$	$w_{x_i}^{(2)}$	$w_{x_i}^{(3)}$
K1 (number of means of transport)	0.229	0.229	0.114	0.05
K2 (capacity utilization)	0.207	0.05	0.103	0.207
K3 (motor vehicle reliability)	0.247	0.06	0.123	0.247
K4 (fuel consumption per 100 km)	0.178	0.178	0.11	0.04
K5 (suitability for transport and manipulative work)	0.138	0.03	0.09	0.138

An initial "incomplete" rule base is then generated with the maximum number of combinations that can combine the membership functions. The initial base of rules contains only premises (the "If" part of the rule), that is, combinations of all membership functions of the input variables of the fuzzy logic system ($x_i^{(j)}$). The initial "incomplete" rule base (R) is displayed in a matrix form as:

$$R = \begin{array}{c} \\ R_1 \\ R_2 \\ \vdots \\ R_c \end{array} \begin{array}{c} \begin{array}{cccc} X_1 & X_2 & \dots & X_n \end{array} \\ \begin{pmatrix} x_1^{(1)} & x_2^{(1)} & \dots & x_n^{(1)} \\ x_1^{(2)} & x_2^{(1)} & \dots & x_n^{(2)} \\ \vdots & \vdots & \dots & \vdots \\ x_1^{(m)} & x_2^{(m)} & \dots & x_n^{(m)} \end{pmatrix} \end{array} \quad (2)$$

where $x_1^{(p)}, \dots, x_n^{(q)}$ is the membership function of the input variables $X_1,\dots, X_n$.

Then the matrix R' is constructed in which the combinations of input pairs are replaced by the weight coefficients ($w_{x_i}^{(j)}$).

$$R' = \begin{pmatrix} w_{x_1}^{(1)} & w_{x_2}^{(1)} & w_{x_3}^{(1)} & \dots & w_{x_n}^{(1)} \\ w_{x_1}^{(2)} & w_{x_1}^{(2)} & w_{x_3}^{(2)} & \dots & w_{x_n}^{(2)} \\ w_{x_1}^{(3)} & w_{x_2}^{(3)} & w_{x_3}^{(3)} & \dots & w_{x_n}^{(3)} \\ \dots & \dots & \dots & \dots & \dots \\ w_{x_1}^{(m)} & w_{x_2}^{(m)} & w_{x_3}^{(m)} & \dots & w_{x_n}^{(m)} \end{pmatrix} \quad (3)$$

After forming the matrix R', the elements of the matrix are summed up by rows:

$$w_j = \sum_{j=1}^{n} w_{x_i}^{(j)}\, y^+, y^+ \in [y^-, y^+] \,\& \quad (4)$$

where y^+ represents the upper limit of the confidence interval $[y^-, y^+]$ of the output variable Y. Then it is necessary to determine the degree of the membership of the real number w_j to the membership function $y^{(r)}$ of the output variable Y.

$$y^{(r)} = \max(w_y \cap \mu_{y^{(r)}}) \quad (5)$$

in order to generate the rule base, it is necessary at the beginning that each pair of the membership function ($x_i^{(i)}$) of the input variables (X_i) is associated with the corresponding membership function $(y^{(r)})$ of the output variable (Y). That is why redundant rules are eliminated in order not to burden the system, especially when there are several rules that have similar or the same combinations of the membership functions of input/output variables. When this happens, the rule that has the largest sum of the weight coefficients of the membership functions contained in the rule is left, namely:

$$R = \max \sum w_{x_R}^{(i)} \ , i = 1,2, \dots, n \quad (6)$$

If we define that:

- A - number of means of transport
- B - capacity utilization;
- C - motor vehicle reliability;
- D - fuel consumption per 100 km;
- E - suitability for transport and manipulative work; and
- F – vehicle preference;

then an example rule reads:

IF (A is Small) **AND** (B is Small) **AND** (C is Medium) **AND** (D is Small) **AND** (E is Large) **THEN** (F is Very Small).

By entering numerical values into the fuzzy system, different values of the input variables are set and the value of the output variable Preference according to the vehicle is controlled.

Choice of inference and defuzzification method

The most frequently used methods in direct inference are MIN-MAX and PROD-SUM (Mamdani method). At the beginning of this phase, the MIN-MAX method was used and it is used when it is not important to manage the entire confidence interval of the output variable. In a large number of system simulations, this method proved unsuitable. One of the

basic requirements was to achieve a satisfactory level of system sensitivity, which cannot be achieved using this method. The desired shape could not be obtained with the settings, and even if it was achieved, it would only be valid for certain values of the input variables. By changing the parameters, the surface would appear even less acceptable, and therefore the system would be even less sensitive (Milošević et al, 2021). Therefore, the method of direct inference was used - PROD-SUM as the best one offered by the Matlab program package.

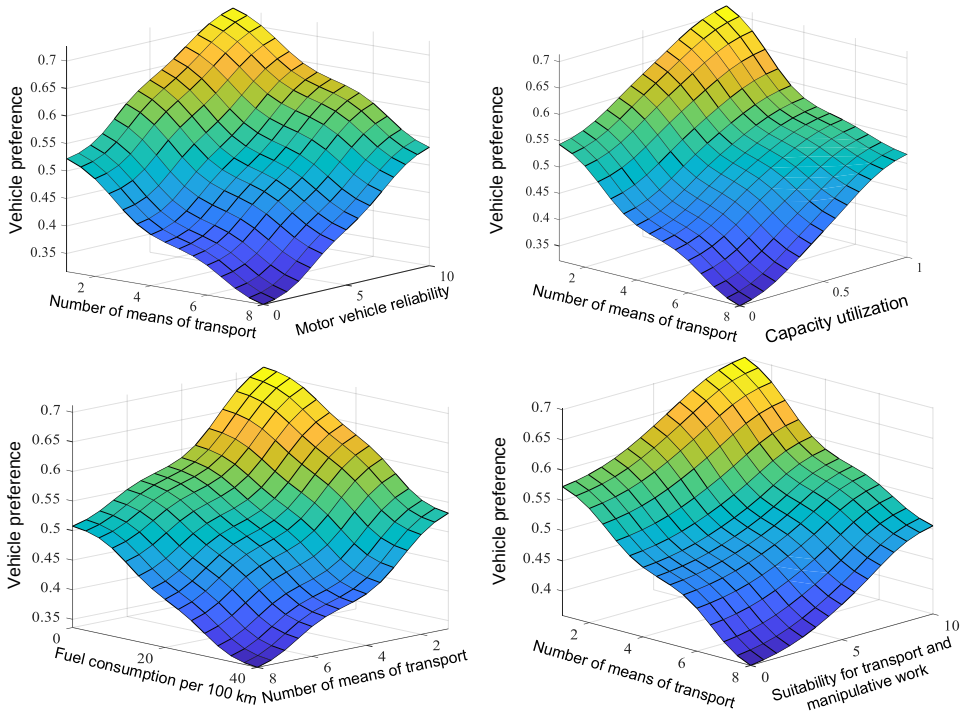

Figure 7 – Interdependence of the solution and two input variables by the PROD-SUM method

Рис. 7 – Взаимозависимость решения и двух входных переменных при применении метода PROD-SUM

Слика 7 – Међузависност решења и две улазне променљиве применом методе ПРОД-СУМ

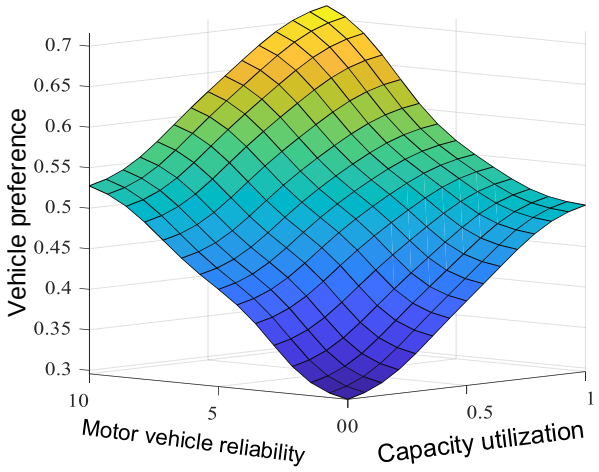

Figure 8 – Interdependence of the solution and two input variables by the PROD-SUM method
Рис. 8 – Взаимозависимость решения и двух входных переменных при применении метода PROD-SUM
Слика 8 – Међузависност решења и две улазне променљиве применом методе ПРОД-СУМ

The difference between the MIN-MAX and PROD-SUM methods is that in the activation phase of the fuzzy rule according to the MIN-MAX method, cutting is performed, in fact only the activated parts of the fuzzy sets are taken into account, and with the PROD-SUM method, scaling is performed - proportionally reduction. Activation of the conclusion by the MAX method accumulates the union of two phase sets, while the accumulation contours by the SUM method are obtained as an algebraic sum. At the beginning of the inference process, the values of the input variables are phased. During the fuzzification process, the membership functions defined for the input variables are applied to the actual value of the input variable to determine the degree of membership for the premise of each of the rules in the database. After this, the expert system performs an analysis in accordance with the previously defined limits, which represent the membership functions of individual variables. Each linguistic variable consists of multiple fuzzy sets and the goal of fuzzification is to determine which fuzzy set "belongs" to each input variable and to represent that membership with a numerical value located in the interval [0,1]. After phasing the input variables, those values are analyzed and compared with the sets of premise values from the rule base. In order for

all conditions to be satisfied, a smaller value is taken, i.e. the intersection of fuzzy sets, due to the use of the operator "and" between the elements. Then the obtained value is transferred to the fuzzy set which represents the conclusion.

User "interface" of the program for selecting vehicles for transporting goods

For the developed fuzzy logic system, the user "interface" of the program for the selection of vehicles for the transport of goods was created in the Matlab 2017a program package. By entering "T" in the command line of the program package, the home page of the user program for the selection of vehicles for the transport of goods in the Serbian Armed Forces is launched.

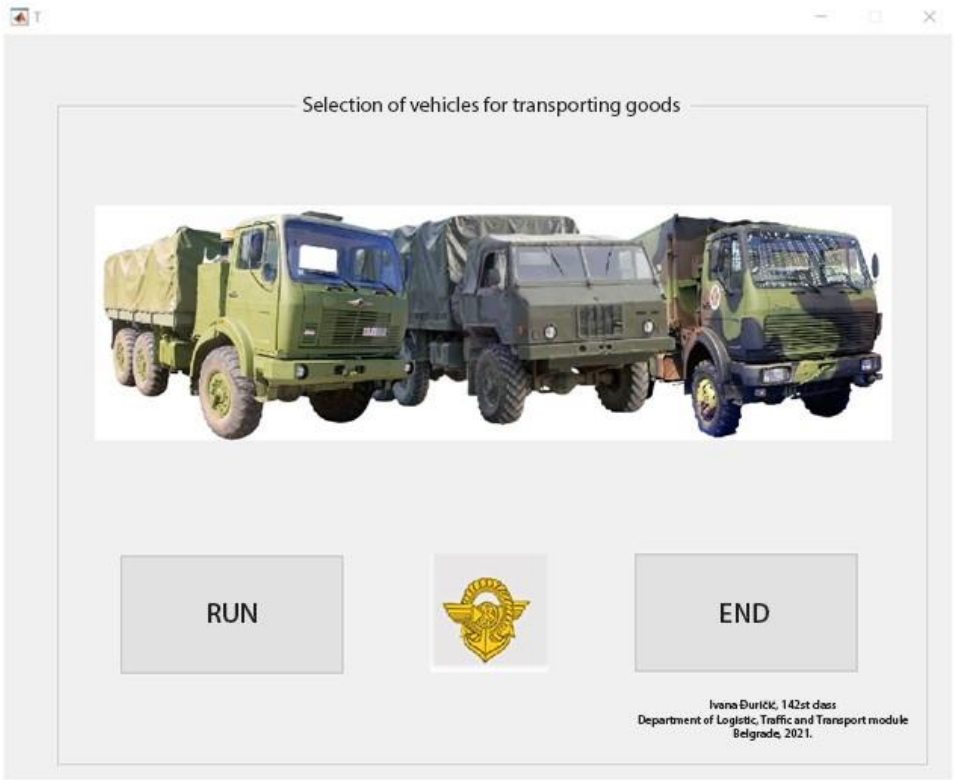

Figure 9 – Home page of the user form
Рис. 9 – Главная страница пользовательской формы
Слика 9 – Почетна страна корисничке форме

Pressing the "RUN" button opens the fuzzy logic model. In the "Entry to fuzzy system" part of the user form, the user enters the desired values in the empty field below the defined criteria, while the interval values are below the empty field.

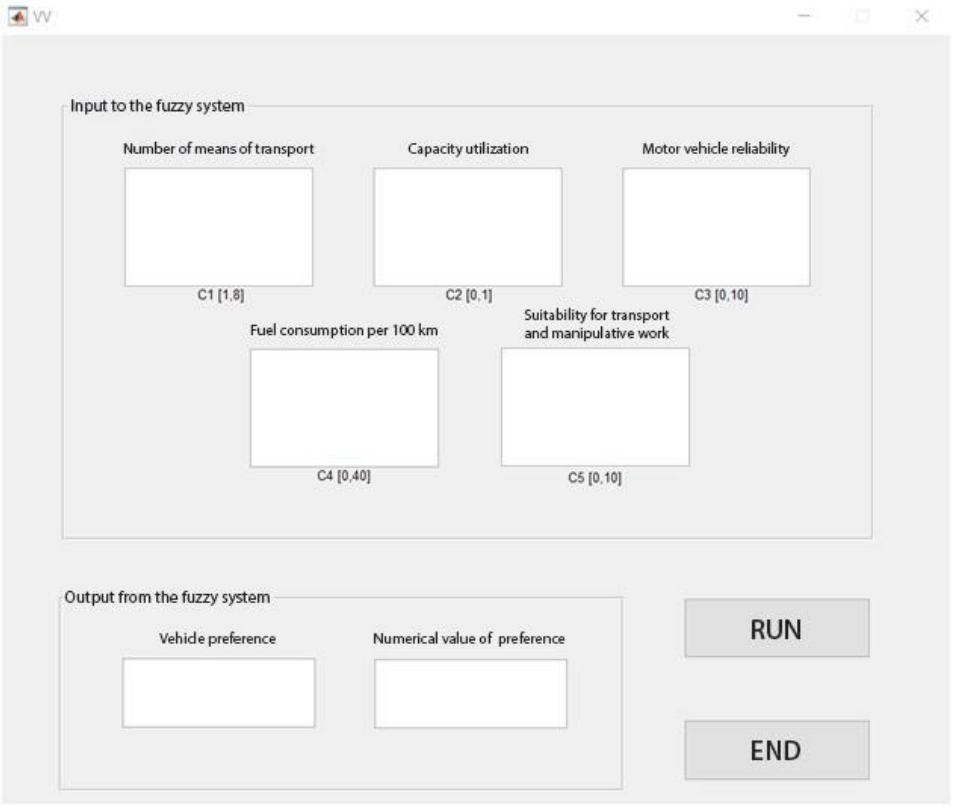

Figure 10 – A model for entering input values into the system and displaying output values from the fuzzy logic system.
Рис. 10 – Модель ввода входных значений в систему и отображения выходных значений из системы нечеткой логики.
Слика 10 – Модел за уношење улазних вредности у систем и приказ излазних вредности из fuzzy логичког система

Upon completion of identification, the user closes the user form by pressing the "END" button, after which the program returns him to the initial page of the user interface for vehicle selection, and closing the interface is also done by pressing the "END" button.

Cube IQ

Cube IQ is software designed for optimal packing of containers, trucks, pallets, crates and boxes. This software is unique in that, in addition to regular shaped containers, it can also pack irregularly shaped containers, such as air containers (ULD - Unit Load Device). It can also determine the position of the center of gravity, pack loads in the form of rolls, and optimize multiple containers/trucks at the same time. The great advantage of this software is that there is no limit to the number of trucks during optimization, as well as the possibility of obtaining certain parameters (capacity utilization coefficient, volume utilization coefficient) when packing vehicles with goods of different sizes. How to use Cube IQ software is covered in (MagicLogic Optimization Inc, 2004)

The work uses Cube IQ software for packing off-road vehicles TAM 150, FAP 2026, and FAP 1118. From the software, we get data on the number of vehicles and utilization of payload and use these values for input variables in the fuzzy logic system. In the next chapter, the application of Cube IQ, as well as the designed fuzzy system, will be described.

Model testing

Practical application is a logical phase in the life cycle of the model. The model should be applied and, if necessary, certain corrections, changes, and improvements should be made again, which is relatively easy in the fuzzy system (Pamučar at al, 2016). The confidence intervals of the input variables as well as the output variables can be changed and adapted to the circumstances in which the program will be used. The interval [0,1] was taken for the confidence interval of the output variable Preference towards the vehicle.

To test the described model, data were used on the goods transported in 2020 to the Intervidov Polygon (IVP) of "Pasuljanske livade" for the needs of the Military Academy. For the transport of these goods, the vehicle optimal for the task is selected using the designed fuzzy logic system. During the selection process, three vehicle types used in the Serbian Armed Forces, already mentioned in the paper, were considered. The input values for Number of transport means and Capacity utilization are obtained from Cube IQ, Fuel consumption per 100 km is obtained from the technical manual for the mentioned motor vehicles, while Motor vehicle reliability and Suitability for transport manipulative work are obtained based on the data processed from the survey.

Data analysis

Data were collected on dangerous goods transported to the IVP "Pasuljanske livade" in 2020 for the needs of the Military Academy. These data represent the input values to Cube IQ software, after which the vehicle to be packed is selected. At the same time, how this software works is shown and data are obtained to be used when testing the fuzzy system, i.e. for the selection of vehicles that would be optimal to use when transporting dangerous goods to the IVP "Pasuljanske livade" in 2020.

Table 5 – Data on goods transported in 2020 at the IVP "Pasuljanske livade"
Таблица 5 – Данные о товарах, перевезенных в 2020 году на ИВП "Пасулянске ливаде"
Табела 5 – Подаци о роби која је транспортована 2020. године на ИВП „Пасуљанске ливаде"

IVP "Pasuljanske livade" 2020. years	Box dimensions			Carrying capacity of the crate (kg)	Amount of crates transported
	l (m)	b (m)	h (m)		
Bullet 12, 7mm regular grain M09	0.37	0.33	0.21	34	11
Bullet 5.56 mm with ordinary grain M03 and MČ P-1800	0.555	0.315	0.14	28.5	60
Bullet 7.62mm, T.Z. M30 MCH P-1200	0.5	0.3	0.18	38	40
Bullet 7.62mm for PKT, ordinary grain M908, ch.ch (s), R	0.44	0.29	0.2	40	40
Bullet 7.9mm, UNIV.Z.MČ.PB-900 for sniper rifle	0.44	0.36	0.22	45	15
RBR 64 mm M80 -Zolja-	0.965	0.32	0.27	25	1
Bullet 7.62mm marking grain T-46	0.48	0.35	0.16	26	27
Bullet 12.7mm MC BZT (S) P288 DSKM	0.5	0.315	0.2	48	1
Signal bullet 26mm	0.49	0.33	0.39	48	9
Mine 120mm LTF	0.71	0.35	0.22	43	1
Bullet 152mm TFP	0.95	0.46	0.24	95	169
Mine 82mm M74	0.55	0.52	0.27	46	4
Capsule No. 8	0.44	0.21	0.03	20	1
Caps ek 40-69	0.38	0.3	0.29	18	1
Detonating stick, PVC insulated	0.78	0.24	0.24	22	1
Slow-burning stick	0.61	0.3	0.33	22	1
Bullet TM-200 B.G.	0.57	0.25	0.19	27	1

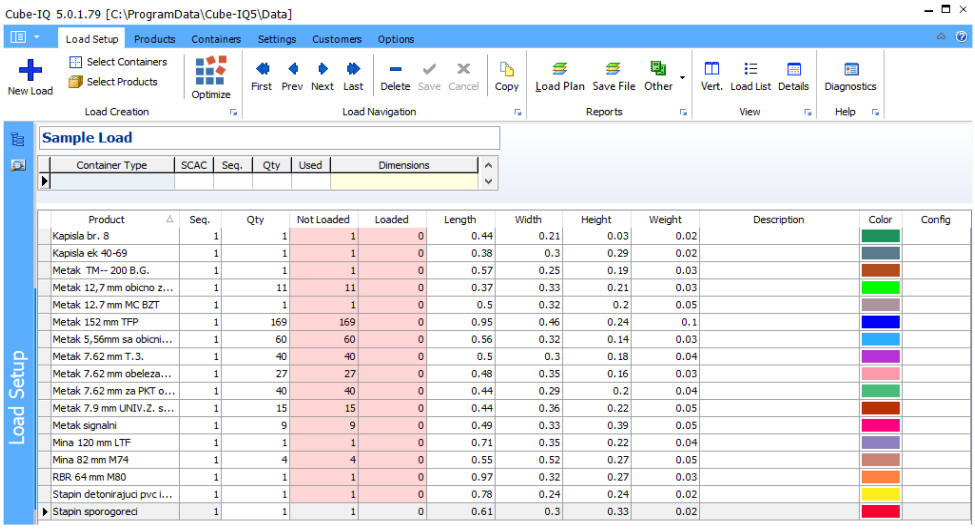

Figure 11 – Entry of goods input into Cube IQ
Рис. 11 – Ввод товарных данных в Cube IQ
Слика 11 – Унос улазних података о роби у Cube IQ

Before selecting a vehicle, it is necessary to enter the basic vehicle data into the software and these data are shown in Table 6, while Figure 12 shows how the data entry in Cube IQ looks like.

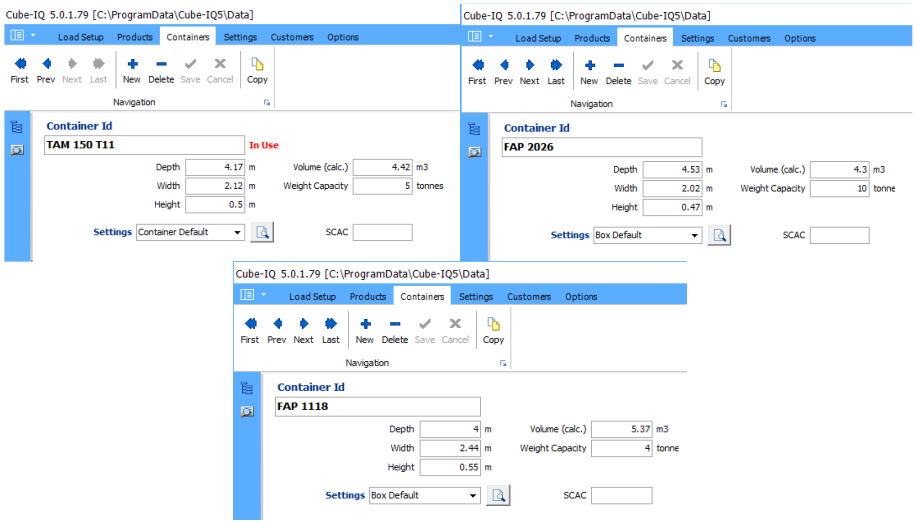

Figure 12 – Entering vehicle data into Cube IQ
Рис. 12 – Ввод данных о транспортых средствах в Cube IQ
Слика 12 – Унос података о возилима у Cube IQ

Table 6 – Basic data about vehicles that are entered into Cube IQ

Таблица 6 – Основные данные о транспортных средствах, которые вводятся в Cube IQ

Табела 6 – Основни подаци о возилима који се уносе у Cube IQ

Off-road vehicle	Dimensions of the cargo box of the vehicle			Vehicle load capacity (t)
	L (m)	B (m)	H (m)	
TAM 150 T11	4.17	2.12	0.5	5
FAP 2026	4.53	2.02	0.47	10
FAP 1118	4	2.44	0.55	4

Vehicle packing

After entering all the necessary data, the packing of the off-road vehicle TAM 150 T11 was carried out, by selecting the vehicle from the database and by calling the "Optimize" option, the packing of the vehicle begins, while at the end the packing plan of the vehicle is obtained.

Figure 13 shows the entire process in Cube IQ.

Once the vehicle packing plan has been obtained, the required data are read. Thus, 6 TAM 150 T11 all-terrain vehicles are needed for the transport of goods, while the capacity utilization is shown per vehicle. In order to unify it and obtain only one value, the arithmetic mean of all obtained values of the load capacity utilization of those vehicles was taken.

$$\bar{\gamma} = \frac{\sum_{i=0}^{n} \gamma_i}{n} \tag{7}$$

In the same way, the packaging and obtaining the data, necessary for the input variables in the fuzzy logic system, are carried out for the off-road vehicles FAP 2026 and FAP 1118. So, 7 FAP 2026 vehicles and 6 FAP 1118 vehicles are needed.

Table 7 shows utilization of carrying capacity by vehicles, as well as the final value obtained on the basis of formula (7).

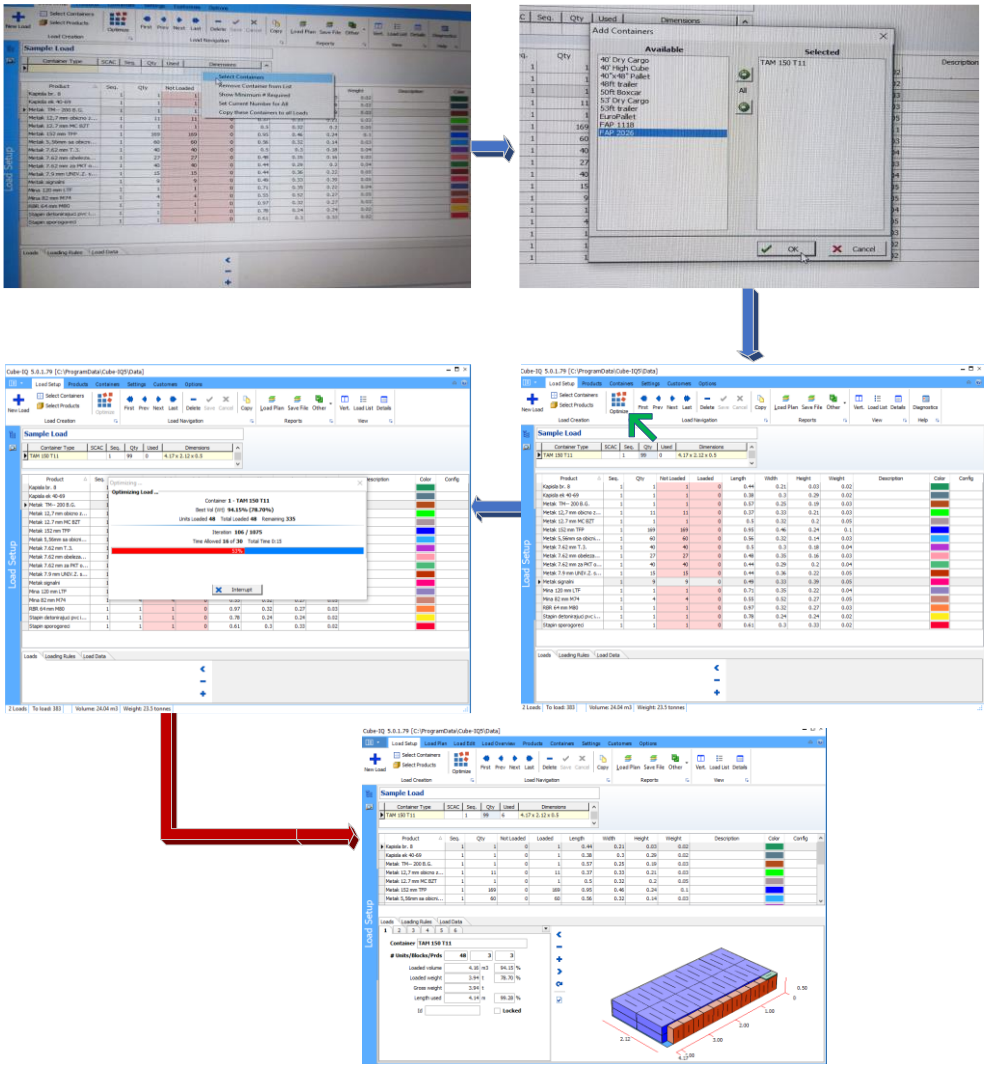

Figure 13 – Procedures for selecting a vehicle and packing it in Cube IQ

Рис. 13 – Процедуры выбора транспортного средства и его погрузки в Cube IQ

Слика 13 – Поступци приликом избора возила и његовог паковања у Cube IQ

Table 7 – Utilization of the vehicle's carrying capacity
Таблица 7 – Использование грузоподъемности транспортного средства
Табела 7 – Искоришћење носивости возила

		Off-road vehicle		
		TAM 150 T11	FAP 2026	FAP 1118
	Number of means of transport (n)	6	7	6
Capacity utilization	Vehicle 1 (γ_1)	0.787	0.4313	0.9985
	Vehicle 2 (γ_2)	0.7508	0.44	0.9985
	Vehicle 3 (γ_3)	0.7508	0.361	0.999
	Vehicle 4 (γ_4)	0.7508	0.361	0.999
	Vehicle 5 (γ_5)	0.9396	0.361	0.999
	Vehicle 6 (γ_6)	0.7224	0.3647	0.8815
	Vehicle 7 (γ_7)	/	0.317	/
	Final value of payload utilization ($\bar{\gamma}$)	0.78	0.38	0.98

Table 8 summarizes the defined values of the input variables in the fuzzy logic system for each vehicle and these parameters are entered into the user program.

Table 8 – Values of the input variables in the fuzzy system
Таблица 8 – Значения входных переменных в нечеткой системе
Табела 8 – Вредности улазних променљивих у fuzzy систему

	Number of means of transport	Capacity utilization	Motor vehicle reliability	Fuel consumption per 100 km	Suitability for transport and manipulative work
TAM 150 T11	6	0.78	6	24	7
ФАП 2026	7	0.38	8	33	8
ФАП 1118	6	0.98	9	23.5	9

After entering the values into the user program and starting the fuzzy system, the output values shown in Figure 14 are obtained, after which they are entered in Table 9.

Figure 14 – Display of the output values from the fuzzy system
Рис. 14 – Отображение выходных значений из нечеткой системы
Слика 14 – Приказ излазних вредности из fuzzy система

Table 9 – Output values from the fuzzy system - Vehicle preference
Таблица 9 – Выходные значения из нечеткой системы - Предпочтение транспортного средства
Табела 9 – Излазне вредности из fuzzy система – преференција према возилу

VEHICLES	VEHICLE PREFERENCE	
	Preference	The numeric value of the preference
TAM 150 T11	Medium preference	0.57
FAP 2026	Medium preference	0.48
FAP 1118	Large preference	0.71

Based on the results obtained, the optimal vehicle for carrying out the transportation of goods to the IVP "Pasuljanske livade" is FAP 1118. The vehicle ranking can be shown as FAP 1118 > TAM 150 T11 > FAP 2026.

Conclusion

In the life and work of the units, there are daily needs to transport large quantities of various goods. For the execution of these tasks, military vehicle fleets are used, mainly for transport on shorter distances, while for longer distances, the vehicles of transport organizations are used most often. In this regard, more and more attention is being paid to the economical, that is, rational use of the vehicle fleet. One of such methods is centralized transport, which has not yet been fully implemented in the Serbian Army. This paper presents a proposal for choosing the optimal motor vehicle for the transport of mobile assets in the Serbian Army, all with the aim of facilitating the work of the traffic service authorities in planning the transport of mobile assets.

The selection of vehicles for the transport of movable assets was carried out using a fuzzy logic system, which belongs to the group of models based on artificial intelligence.

There are a large number of different types of motor vehicles in the Serbian Army, and it is not easy to define which type of vehicle is optimal for the delivery of mobile assets. Each unit and institution of the Ministry of Defense and the Armed Forces has a different organizational and formation structure, and therefore different needs related to support.

The basis for solving the problem of choosing a vehicle for transporting goods is the correct definition of the criteria and their relative importance. By surveying the commanders of transport lines, five criteria were defined in this paper, which represent the input values of the fuzzy logic system. The selected criteria are: number of means of transport, capacity utilization, motor vehicle reliability, fuel consumption per 100 km and suitability for transport manipulative work. To date, no motor vehicle has been made that can satisfy all criteria simultaneously in their optimal sizes, but overall, based on all these criteria, the most favorable should be selected with the help of a fuzzy system. The output variable is represented as vehicle preference.

The input variables are represented by three membership functions, while the output variable is defined by five membership functions. For the membership functions of the input and output variables, Gaussian bell functions were used, due to the requirement that there is a certain degree of sensitivity of the system. All the rules in the fuzzy logic system are

determined by applying the rule premise weight aggregation method (ATPP), which enables the formation of a rule base based on experience. By applying this method and based on the number of input variables and the number of their membership functions, a base of 243 rules was defined. The values of the weighting coefficients of the membership functions were determined using the LMAW method. In order to increase the sensitivity of the system as an inference method, the PROD-SUM method was used.

The presented model was tested on the example of choosing the optimal vehicle for the goods transported to the IVP "Pasuljanske livade" in 2020. The selection of the optimal means of transport was made between the transport motor vehicles that are most used in the Serbian Army, namely: TAM 150 T11, FAP 2026 and FAP 1118.

After packing all three vehicles with these goods in Cube IQ, the values of the input parameters for the fuzzy logic system were obtained, for the criteria of the number of means of transport and the utilization of carrying capacity. After the calculation and evaluation of the individual vehicles, the values of the output variable of the fuzzy logic system were obtained in the user "interface" program, that is, the preference for the vehicle was obtained, in the form of a numerical value and a linguistic descriptor. The obtained values for each vehicle were ranked and the optimal vehicle for the transport of defined goods was shown to be the FAP 1118.

The significance of this work is that it is among the first ones to demonstrate the application of a model based on artificial intelligence that solves the problem of vehicle selection for the transportation of movable assets. The work provides great opportunities for further research.

In this sense, further research is needed to establish the criteria that are crucial for the transport of goods in the army. Next, one should determine the intervals that the input variables will cover and properly divide them into the required number of parameters. In this way, the number of criteria and the interval values of the input variables would be adapted to a real situation and this model could be included in the daily work of the traffic service authorities.

References

Badi, I. & Abdulshahed, A. 2021. Sustainability performance measurement for Libyan Iron and Steel Company using Rough AHP. *Journal of Decision Analytics and Intelligent Computing*, 1(1), pp.22-34. Available at: https://doi.org/10.31181/jdaic1001202222b.

Bozanic, D., Tešić, D. & Kočić, J. 2019. Multi-criteria FUCOM – Fuzzy MABAC model for the selection of location for construction of single-span bailey bridge. *Decision Making: Applications in Management and Engineering*, 2(1), pp.132-146 [online]. Available at: https://dmame.rabek.org/index.php/dmame/article/view/32 [Accessed: 20 March 2021].

Božanić, D. & Pamučar, D. 2014. Making of fuzzy logic system rules base for decision making support by aggregation of weights of rules premises. *Tehnika*, 69(1), pp.129-138 (in Serbian). Available at: https://doi.org/10.5937/tehnika1401129B.

Ćirović, G. & Pamučar, D. 2013. Decision support model for prioritizing railway level crossings for safety improvements: Application of the adaptive neuro-fuzzy system. *Expert Systems with Applications*, 40(6), pp.2208-2223. Available at: https://doi.org/10.1016/j.eswa.2012.10.041.

Ćirović, G., Pamučar, D. & Božanić, D. 2014. Green logistic vehicle routing problem: Routing light delivery vehicles in urban areas using a neuro-fuzzy model. *Expert Systems with Applications*, 41(9), pp.4245-4258. Available at: https://doi.org/10.1016/j.eswa.2014.01.005.

Kiptum, C.K., Bouraima, M.B., Stević, Ž., Okemwa, S., Birech, S. & Qiu, Y. J. 2022. Sustainable strategies for the successful operation of the bike-sharing system using an ordinal priority approach*. Journal of Engineering Management and Systems Engineering*, 1(2), pp.43-50. Available at: https://doi.org/10.56578/jemse010201.

Krstić, B.V. 2006. Strategy's motor vehicle maintenance. *Poljoprivredna tehnika*, 31(1), pp.55-65 [online]. Available at: https://scindeks.ceon.rs/article.aspx?artid=0554-55870601055K&lang=en (in Serbian) [Accessed: 15 January 2023].

Luger, G.F., Johnson, P., Stern, C., Newman, J.E. & Yeo, R. 1994. Cognitive science: The science of intelligent systems. Cambridge, MA, USA: Academic Press. ISBN: 9780124595705.

-MagicLogic Optimization Inc. 2004. *Cube-IQ release 3.0 user guide*. Vancouver, Canada: MagicLogic Optimization Inc.

Milošević, T., Pamučar, D. & Chatterjee, P. 2021. Model for selecting a route for the transport of hazardous materials using a fuzzy logic system. *Vojnotehnički glasnik/Military Technical Courier*, 69(2), pp.355-390. Available at: https://doi.org/10.5937/vojtehg69-29629.

Pamučar, D. 2010. Using fuzzy logic and neural networks during a decision making process in transport. *Vojnotehnički glasnik/Military Technical Courier*, 58(3), pp.125-145 (in Serbian). Available at: https://doi.org/10.5937/vojtehg1003125P.

Pamučar, D., Vasin, Lj., Atanasković, P. & Miličić, M. 2016. Planning the City Logistics Terminal Location by Applying the Green -Median Model and Type-2 Neurofuzzy Network. *Computational Intelligence and Neuroscience*, 2016(art.ID:6972818). Available at: https://doi.org/10.1155/2016/6972818.

Pamučar, D., Žižović, M., Biswas, S. & Božanić, D. 2021, Anew logarithm methodology of additive weights (LMAW) for multi-criteria decision-making: Application in logistics. *Facta Universitatis, series: Mechanical Engineering*, 19(3), pp.361-380. Available at: https://doi.org/10.22190/FUME210214031P.

Puška, A., Štilić, A., & Stojanović, I. 2023. Approach for multi-criteria ranking of Balkan countries based on the index of economic freedom. *Journal of Decision Analytics and Intelligent Computing*, 3(1), pp.1-14. https://doi.org/10.31181/jdaic10017022023p.

Raphael, B. 1976. *The Thinking Computer: Mind Inside Matter*. New York, USA: W.H. Freeman and Company. ISBN-13: 978-0716707233.

Starčević, M. 2020. *Model of selection of transport vehicles used by military units engaged in multinational operations*. Ph.D. thesis. Belgrade, Serbia: University of Belgrade, Faculty of Transport and Traffic Engineering (in Serbian) [online]. Available at: https://nardus.mpn.gov.rs/handle/123456789/20483?locale-attribute=en [Accessed: 10 January 2023].

Tešić, D.Z., Božanić, D.I., Pamučar, D.S. & Din, J. 2022. DIBR - Fuzzy MARCOS model for selecting a location for a heavy mechanized bridge. Vojnotehnički glasnik/Military Technical Courier, 70(2), pp.314-339. Available at: https://doi.org/10.5937/vojtehg70-35944.

Vesković, S., Milinković, S., Abramović, B. & Ljubaj, I. 2020. Determining criteria significance in selecting reach stackers by applying the fuzzy PIPRECIA method. *Operational Research in Engineering Sciences: Theory and Applications*, 3(1), pp.72-88 [online]. Available at: https://oresta.org/menu-script/index.php/oresta/article/view/69/69 [Accessed: 10 January 2023].

Zadeh, L.A. 1965. Fuzzy sets. *Information and Control*, 8(3), pp.338-353. Available at: https://doi.org/10.1016/S0019-9958(65)90241-X.

Zadeh, L A. 1975a. The concept of a linguistic variable and its application to approximate reasoning I. *Information Sciences*, 8(3), pp.199-249. Available at: https://doi.org/10.1016/0020-0255(75)90036-5.

Zadeh, L.A. 1975c. The concept of a linguistic variable and its application to approximate reasoning III. *Information Sciences*, 9(1), pp.43-80. Available at: https://doi.org/10.1016/0020-0255(75)90017-1.

Zadeh, L.A. 1975b. The concept of a linguistic variable and its application to approximate reasoning II. *Information Sciences*, 8(4), pp.301-357. Available at: https://doi.org/10.1016/0020-0255(75)90046-8.

Zuber, N. & Ličen, H. 2011. Possibilities of applying artificial intelligence methods for automated analysis of vibration. *Tehnička dijagnostika*, 10(2), pp.9-16 [online]. Available at: https://scindeks.ceon.rs/article.aspx?artid=1451-19751102009Z&lang=en (in Serbian) [Accessed: 10 January 2023].

Применение программного обеспечения Cube Iq и многокритериальной модели оптимизации при выборе транспортных средств для перевозки грузов в Вооруженных силах Республики Сербия

Ивана Д. Джуричич

Вооруженные силы Республики Сербия, Управление тылового обеспечения, центральная база тылового обеспечения, Первый складской батальон, г. Горни Милановац, Республика Сербия

РУБРИКА ГРНТИ: 27.47.19 Исследование операций,
28.17.31 Моделирование процессов управления,
73.47.12 Организация управления и автоматизированные системы управления транспортом,
81.88.00 Материально-техническое снабжение. Логистика

ВИД СТАТЬИ: оригинальная научная статья

Резюме:

Введение/цель: Правильный выбор транспортных средств, используемых для перевозки грузов, является важным фактором, влияющим на экономичное и рациональное использование автопарков, а также на качество и эффективность осуществления транспортной деятельности в Вооруженных силах Республики Сербия. Целью данной статьи является разработка модели на основании определенных критериев, которая поможет органам транспортной службы выбрать наиболее подходящее транспортное средство для выполнения поставленной транспортной задачи.

Методы: В данной статье предлагается модель выбора транспортных средств для перевозки грузов с использованием системы нечеткой логики как разновидности системы искусственного интеллекта. Для того чтобы решить проблему выбора транспортного средства для перевозки грузов, в статье на основе опроса командиров транспортных взводов были определены пять критериев, которые представляют входные значения в системе нечеткой логики. Транспортное средство выбирается на основе пяти критериев. Входные переменные представлены тремя функциями принадлежности, в то время как выходная переменная определяется пятью функциями принадлежности. Все правила в системе нечеткой логики определяются с помощью метода агрегирования подусловий в нечетких правилах, который позволяет сформировать базу правил на основании опыта. Благодаря данному методу, а также количеству входных переменных и функций принадлежности к ним, была определена

база из 243 правил. Значения весовых коэффициентов функций принадлежности были определены с помощью метода LMAW. Для разработанной системы нечеткой логики была создана программа пользовательского интерфейса, которая позволяет применять эту модель на практике.

Результаты: Модель была протестирована на примере выбора оптимального транспортного средства для перевозки грузов на ИВП "Пасулянске ливаде" в 2020 году. Выбор оптимального транспортного средства был сделан на основании транспортных средств, которые наиболее часто используются в сербской армии, а именно: TAM 150 T11, FAP 2026 и FAP 1118. После погрузки грузов во все три вида транспортных средств в Cube IQ и после выполнения расчета и оценки отдельных транспортных средств в пользовательской "интерфейс" программе были получены значения выходной переменной по каждому транспортному средству. На основании ранжирования полученных значений всех видов транспортных средств выявлено, что оптимальным транспортным средством для перевозки определенных грузов является FAP 1118.

Выводы: Значимость данного исследования заключается в том, что оно одним из первых продемонстрировало применение модели, основанной на искусственном интеллекте, которая решает проблему выбора транспортного средства для перевозки движимого имущества. Данная статья может оказаться весьма полезной в дальнейших исследованиях.

Ключевые слова: нечеткая логика, нечеткое множество, ATPP, LMAW, cube IQ, Matlab.

Примена Cube Iq софтвера и модела вишекритеријумске оптимизације за избор возила за транспорт робе у Војсци Србије

Ивана Д. Ђуричић

Војска Србије, Управа за логистику, Централна логистичка база,
Први складишни батаљон, Горњи Милановац, Република Србија

ОБЛАСТ: математика, саобраћај, логистика
ВРСТА ЧЛАНКА: оргинални научни рад

Сажетак:

Увод/циљ: Адекватан избор возила који се користи за транспорт робе је веома важан фактор. Он утиче на економичну и рационалну употребу возног парка, као и на квалитет и ефикасност обављања транспортне делатности у Војсци Србије. Пројекат овог модела може да помогне органима саобраћајне службе да, на основу

дефинисаних критеријума, одаберу возило које је најбоље за извршење постављеног транспортног задатка.

Методе: Предлаже се модел за избор возила за транспорт робе применом fuzzy логичког система, као једне врсте система вештачке интелигенције. За решавање проблема избора возила за транспорт робе дефинисано је пет критеријума, на основу анкетирања командира транспортних водова, који представљају улазне вредности у fuzzy логички систем. Улазне променљиве представљене су са по три функције припадности, док је излазна променљива дефинисана са пет функција припадности. Сва правила у fuzzy логичком систему одређена су применом методе агрегације тежине премиса правила (АТПП), која омогућава формирање базе првила на основу искуства. Применом ове методе, као и на основу броја улазних променљивих и броја њихових функција припадности, дефинисана је база од 243 правила. Вредности тежинских коефицијената функција припадности одређене су применом LMAW методе. За развијени fuzzy логички систем израђен је кориснички „интерфејс" програм који омогућава практичну примену овог модела.

Резултати: Модел је тестиран на примеру избора оптималног возила за робу која је транспортована на ИВП „Пасуљанске ливаде" 2020. године. Избор оптималног транспортног средстава вршен је између транспортних моторних возила која се највише користе у Војсци Србије, а то су: ТАМ 150 Т11, ФАП 2026 И ФАП 1118. Након паковања сва три возила овом робом у Cube IQ и извршеном прорачуну и евалуацији појединачног возила у корисничком „интерфејс" програму добијене су вредности излазне променљиве за свако возило. Те вредности за свако возило су рангиране, па се показало да је оптимално возило за транспорт дефинисане робе ФАП 1118.

Закључак: Овај рад један је од првих који доказује примену модела заснованог на вештачкој интелигенцији који решава проблем избора возила за транспорт покретних средстава. Такође, рад пружа велике могућности за даља истраживања.

Кључне речи: fuzzy логика, fuzzy скуп, АТПП, LMAW, Cube IQ, Matlab.

Paper received on / Дата получения работы / Датум пријема чланка: 18.01.2023.
Manuscript corrections submitted on / Дата получения исправленной версии работы / Датум достављања исправки рукописа: 25.03.2023.
Paper accepted for publishing on / Дата окончательного согласования работы / Датум коначног прихватања чланка за објављивање: 25.03.2023.

Security of wireless keyboards: threats, vulnerabilities and countermeasures

Siniša V. Jovanović[a], *Danijela* D. Protić[b], *Vladimir* D. Antić[c], *Milena* M. Grdović[d], *Dejan* A. Bajić[e]

Serbian Armed Forces, General Staff, Telecommunications and Information Security Directorate (J-6), Centre for Applied Mathematics and Electronics, Belgrade, Republic of Serbia

[a] e-mail: sinisa.jovanovic711@gmail.com, ORCID iD: https://orcid.org/0009-0002-6088-9553

[b] e-mail: danijelaprotic318@gmail.com, **corresponding author**, ORCID iD: https://orcid.org/0000-0003-0827-2863

[c] e-mail: vladimirantic2013@gmail.com, ORCID iD: https://orcid.org/0000-0001-9843-0743

[d] e-mail: milena.grdovic@gmail.com, ORCID iD: https://orcid.org/0000-0003-4310-7935

[e] e-mail: strelacyu@yahoo.com, ORCID iD: https://orcid.org/0009-0007-5283-4110

DOI: 10.5937/vojtehg71-43239; https://doi.org/10.5937/vojtehg71-43239

FIELD: computer sciences, electronics, telecommunications, mechanical engineering

ARTICLE TYPE: original scientific paper

Abstract:

Introduction/purpose: This paper provides an overview of research on computer system vulnerabilities caused by compromised electromagnetic radiation by wireless keyboards. Wireless devices that use event-triggered communication have been shown to have critical privacy issues due to the inherent leakage associated with radio frequency emissions. Wireless connectivity technology is a source of signal emanation that must be protected in terms of performance and security.

Methods: Wireless device vulnerabilities and side-channel attacks are observed, along with electromagnetic emission of radio waves.

Results: The findings highlight a specific wireless keyboard's security and encryption flaws. The results of penetration testing reveal vulnerabilities of targeted wireless keyboards in terms of outdated firmware, encryption, wireless reliability, and connection strength.

Conclusion: Wireless keyboards have security flaws that disrupt radio communication, giving a malicious user complete access to the computer to which the keyboard is connected. An attacker can steal sensitive data by observing how the system works using compromised electromagnetic emissions.

Key words: wireless keyboard, radio frequency, electromagnetic emission, software defined radio.

Introduction

Manipulation and compromise of wireless devices are not new concepts. Wireless devices that use event-triggered communication have been shown to have critical privacy issues due to the inherent leakage associated with radio frequency (RF) emissions (Oligeri et al, 2020, pp.231-241). Wireless keyboards allow users to move keyboards to a more comfortable or visually pleasing position, resulting in a mess-free workspace. These keyboards, on the other hand, are not typically selected or used with security in mind, and a surprising number of wireless keyboards affected by multiple vulnerabilities can allow malicious users to completely compromise the computers to which these devices are connected.

This paper advances the attack frontier by reviewing inexpensive, easy-to-implement, efficient, and effective attacks capable of detecting typing on a wireless keyboard. Such attacks are particularly harmful because they succeed even when an eavesdropping antenna is several meters away from the target keyboard, regardless of the encryption scheme, communication protocol, radio noise, or physical obstacles. We also discuss attacks on wireless capabilities, such as wireless access points, routers, mice, and keyboards. However, it is critical to understand that of all wireless risks, not just those associated with network connectivity must be considered (Sheimo, 2021). In terms of performance and security, wireless connectivity technology is also a source of signal emanation and must be protected (Logitech, 2023). Furthermore, we offer some recommendations for mitigating attacks.

This paper is organized as follows. Wireless keyboard layouts and standards are covered in the second chapter. The third chapter discusses wireless security, vulnerabilities, and threats. The fourth chapter is about penetration testing. The final chapter concludes the paper.

Computer keyboards

The computer keyboard is a primary component needed while working on desktops. There are various types of keyboards available in the market, and choosing the best one is dependent on the user's requirements. Selecting a layout such as QWERTY, QWERTZ or

AZERTY can influence the decision on what type of keyboard should be used for a specific purpose.

Computer keyboard layout

A keyboard is a type of input, a peripheral device that allows users to enter text into another electronic device and communicate with a computer in the simplest way possible. It is made up of a number of buttons that generate numbers, symbols, letters, and special keys. The design of the keyboard is inspired by typewriter keyboards, and the arrangement of numbers and letters on the keyboard aids in typing speed. Table 1 shows the most commonly used keyboard layouts.

Table 1 – Keyboard layouts (WebNots, 2022)
Таблица 1 – Раскладка клавиатуры (WebNots, 2022)
Табела 1 – Тастатура (WebNots, 2022)

Keyboard layouts	Description
Ergonomic	Designed to reduce wrist and arm pain. Curvy to accommodate palms and provide a comfortable experience.
Flexible	Foldable and portable. Made of rubber-like material resistant to water and dust. Bluetooth keyboards with a connector. Require a hard surface to be placed on and typed on.
Mechanical	Designed for heavier usage. Keys are placed on spring-activated switches. An electric circuit sends signals to the computer based on the pressed keys. Produces more noise than rubber membrane keyboards, but they reduce the possibility of accidentally pressing a different key.
Membrane	Keys tightly packed and occasionally protected by a transparent membrane. Lightweight and resistant to dust. Error-prone nature when typing.
Multimedia	Include multimedia keys for play, pause rewind, forward, and volume adjustments. May be useful if the user frequently watches videos or listens to music. The keyboard replaces the controls on a computer's video/audio player apps. Some may include gaming controls.
Projection	Come with a default onscreen or touchscreen monitors. Eliminates need for a physical keyboard. Lack physical components in the layout section. Necessitates use of a small handheld device connected to the computer via Bluetooth or USB cable. When turned on, the device displays a laser projection of the keyboard layout.
Wireless	Connect to computers via Bluetooth or USB RF. To use it, customer should insert a small connector into the USB port and turn on Bluetooth

Keyboard standards

The keyboard is primarily used to enter the alphabet, numbers, commands, and other data into a computer (see Table 2). It has over 100

keys (see Figure 1) (Chauhan, 2020). Most keyboards today use one of three different physical layouts by the (1) worldwide International Standard Organization/International Electrotechnical Commission ISO/IEC 9995-2 standard, (2) American National Standard Institute ANSI-INCITS 154-1988 standard, and (3) Japanese Industrial Standard (JIS) X 6002-1980 (ANSI webstore, 1999).

Table 2 – Key type description (Chauhan, 2020)
Таблица 2 – Описание клавиш (Chauhan, 2020)
Табела 2 – Опис мастера (Chauhan, 2020)

Keyboard keys	Description
Navigation	Turn the page up and down (arrows, Home, End, Insert, Delete, Page Up, Page Down)
Function	Used to perform specific tasks (F1-F12)
Control	Mostly used in combination with other keys to perform specific tasks (Ctrl, Alt, Windows key, Esc)
Typing	Alphanumeric keys, symbols and punctuation marks
Numeric	Equal to calculator keys, at the right side of the keyboard
Special	Used to perform special functions related to the computer system (Shift, Enter, Alt, Ctrl, Esc)

Figure 1 – Keyboard keys (Chauhan, 2020)
Рис. 1 – Клавиши (Chauhan, 2020)
Слика 1 – Тастери (Chauhan, 2020)

Figure 2 shows physical division and a reference grid defined by ISO/IEC 9995 standard series. The sections are further subdivided into zones as follows:

- alphanumeric section:
  - alphanumeric zone (green),
  - function zone (blue),

- numeric section:
  - numeric (dark red),
  - function (lighter red),
- editing/function section:
  - cursor keys (darker grey),
  - editing function zone (lighter grey).

Figure 2 – ISO/IEC keyboard (ISO, 2009)
Рис. 2 – Клавиши ISO/IEC (ISO, 2009)
Слика 2 –Тастатура ISO/IEC (ISO, 2009)

Each key can be identified using the reference grid by a unique combination of a letter (indicating the row) and a two-digit sequence (indicating the column). The labelling rules allow for function keys to be arranged in rows other than above the alphanumeric section (thus, an AT keyboard is compliant with the standard):

• Columns containing editing/function keys should be numbered from 60 onwards if they are placed beyond a right numeric section, or from 80 onwards if they are placed left of the alphanumeric section.

• Rows above the alphanumeric section should be labelled beginning with K, and rows below the space key should be labelled beginning with Z.

• The grid can be angled or squared.

The characters that can be entered using the keys in the alphanumeric section are organized in levels. Level 1 contains lower-case letters, while Level 2 contains capital letters (e.g. unshifted/shifted). There are no rules governing the distribution of non-letter characters, while digits are most commonly found in Level 1. The standard allows for a third level (characters are selected by the means of an AltGr key). If the three-level organization of the keyboard is insufficient to accommodate all characters to be contained in a specific layout, “groups” may be defined as a higher hierarchical unit than levels. The Japanese keyboard layout, as well as the Canadian Quebec layout and the German T2

layout, are common examples of layouts that allow characters from different scripts to be input (ISO/IEC 9995-1, 2009).

ANSI-INCITS 154-1988 standard describes the layout of the 48 keyboard basic keys as well as the upper- and lower-case characters that can appear on the keys (ANSI webstore, 1999). In recognition of the various graphic character requirements of each application, the character assignments are divided into five application areas.

The Japanese Industrial Standard specifies the layout of a keyboard used for information processing with both hands that implements the JIS X 0201 7-bit alphanumeric-katakana code (JSAJIS, 2018). This standard specifies the relative positions of keys on a keyboard but does not specify key spacing, keyboard inclination, keytop and space bare shapes, or else. This standard makes no mention of character representation on keytops.

Keyboard prevalence

The QWERTY keyboard is widely used in the Americas and parts of Europe. In German-speaking countries, the QWERTZ keyboard, also known as the Swiss keyboard, is used, whereas in France and Belgium, the AZERTY keyboard is standard. American keyboards used to be alphabetically organized. This layout, while logical, presented some technical challenges. Some of the most commonly used keys were placed near one another, their mechanisms too close next to each other. As a result, the letters and the QWERTY keyboard had to be rearranged. Because the most commonly used characters vary from language to language, a slightly different layout was chosen in certain non-English-speaking areas. German speakers adopted the QWERTZ keyboard because the letter Z is more common than the letter Y. New keys have also been added in several countries. For example, the keys needed to enter French accents were added to the traditional English QWERTY layout. QWERTY was retained in Spain and Latin America, but with the addition of Ñ, a commonly used character in Spanish.

Wireless keyboard security

Because wireless signals travel through the air and can be intercepted and read by a skilled attacker, wireless devices are almost always a security risk. The wireless link is usually encrypted with an encryption algorithm such as the Advanced Encryption Standard - AES (NIST, 2001), which is widely used to protect the majority of wireless keyboards. However, using a Software Defined Radio (SDR), for

example, encrypted signals can be recorded. Wireless Universal Serial Bus (USB) dongles are also at risk. Unencrypted input can still be sent to the dongle and used to access the attached computer and send signals while the keyboard is connected to the dongle in an encrypted session (Weiss, 2023).

Wireless communication

Wireless communications are globally regulated, but certain bands are reserved for unlicensed users. The industrial, scientific, and medical (ISM) bands which range from 2.4 GHz to 2.5 GHz and are defined as such by the International Telecommunication Union Radio Regulation are one example. Wireless keyboards also use the ISM band (Tomsic, 2022). Analog RFs are used to transmit digital data using various modulation techniques such as frequency shift keying (FSK). Because the use of two distinct discrete frequencies allows for the transmission of either zero or one, binary data can be transmitted over an analogue channel. The digital data transmitted by a radio transceiver will have limitations on how frequently a new symbol can be sent, which will affect the data rate. To convey the correct data, a transmitter and a receiver must use the same data rate and be synchronized. A protocol must be used to structure the data transmitted between devices. The protocol stack typically defines a logical link frame as a preamble (a series of bits) to allow the receiver's clock to be synchronized with that of the transmitter, a destination address, and data. Some protocols make use of other fields, and the exact protocol specifications vary greatly between manufacturers and devices (Pohl & Noack, 2019). Because software-defined radios are devices in which many radio components are replaced with software variations of them, it is possible to control the radio flexibly through software and adapt it to a wide range of applications and scenarios. This, however, makes it useful in debugging and research situations where the system under investigation by a malicious user is not completely known (Sadiku & Akujuobi, 2004, pp.14-15).

Wireless keyboard security vulnerabilities, threats, and countermeasures

Every wireless device has weaknesses that malicious users can take advantage of. The top ten sources of vulnerability, as identified by Bastille Networks in 2020 and presented by de Jesus Rugeles Uribe in 2022, include, among other things, wireless peripherals that are open to Keystroke injection attacks on keyboards without data encryption. A

hacked wireless keyboard could reveal sensitive information because of the wireless keyboard flaws such as:

- Flaws in encryption: the signal travels unprotected through the air and is easily intercepted.
- Firmware flaws: even if a wireless keyboard is encrypted, firmware bugs can be used to read the wireless signal.
- Keylogger: a type of spyware that records every keystroke and sends the stolen information back to the attackers.
- Keysniffer: a set of security flaws affecting non-Bluetooth wireless keyboards from eight different vendors (Anger, EagleTec, General Electric, Hewlett-Packard, Insignia, Kensington, Radio Shack and Toshiba) since they use unencrypted radio communication protocols enabling an attacker to eavesdrop on all the keystroke typed (Bastille Networks Internet Security, 2023).
- A compromised access point: cybercriminals can install rogue access points in public places with the intent of stealing data from unsuspecting users who connect to them.

To help in the prevention of wireless keyboard attacks, the connections must be as secure as possible. The first step is to ensure that the firmware of the keyboard is up to date and that the connections it establishes are encrypted. Bluetooth devices should also use the Secure Connection only mode, which is compliant with the Federal Information Processing Standard (FIPS) developed by the National Institute of Standards and Technology (NIST). Furthermore, an anti-rollback feature for security-based device firmware upgrades should be considered for keyboards that connect via a USB dongle. This prevents critical security patches from being unintentionally removed while still allowing non-security-related updates to be rolled back. Third, the encryption algorithms, such as AES which is the most known symmetric algorithm today, should be used (FIPS, 2001). When two devices connect, a key is generated and shared between them. The key is then used by the devices to encrypt and decrypt the data they transmit and receive (Griskenas, 2023).

Side channel attacks over USB connection

The most common standard used to connect wired peripheral devices to a main host and transmit data is the USB standard. The standard has evolved over the years, going from version 1.1 to the most recent version 4.0, which supports a transmission rate of up to 40 Gbps (Liu et al, 2021). Different plugs, transmission speeds, and power

delivery capacities define each standard. The ability to power or recharge standalone devices is just one example of the new features that could be integrated thanks to the evolution of the USB standard over time. As a result, the USB standard is now used for a variety of purposes, expanding the range of peripheral devices that are mutually compatible, while also exposing brand-new vulnerabilities. Malicious users today take advantage of the default trust on USB ports to extract sensitive data from wireless devices. Despite efforts by security experts and manufacturers to detect and block threats to a wireless keyboard, an even more subversive approach to compromising user privacy relies on a USB side-channel attack (Liu et al, 2021).

According to Barthe et al (2018, pp.328-343), side-channel attacks are typically physical intrusions in which malicious parties steal protected and confidential data by observing how the system operates physically. To defeat a cryptographic system, these attacks use specific factors like electromagnetic (EM) radiation, timing, and power consumption (Mangard et al, 2007). The goal of every side-channel attack is to exploit an unintentional emission (Sayakkara et al, 2018; Grdović et al, 2022, pp.836-855). This problem is also related to Compromising EM radiation (CER), which is primarily associated with devices protected by some of the cryptographic methods (Markagić, 2018, pp.143-153). In general, attacks on user information can be either passive or active, with the former having no effect on the sender, the receiver, or the data transmitted over a communication channel, and the latter involving a malicious user engaging in an attack and affecting one of these. Side-channel attacks are a type of passive attack that involves “listening” to devices, equipment and transmission to monitor communication between two (or more) parties while leaving no traces. As a result of these factors, users are frequently unaware of the attack.

A malicious user can passively and covertly record everything typed on the wireless keyboard from several meters away using an antenna, a wireless dongle, and a few lines of software code in a side-channel attack to USB. It is a difficult-to-prevent attack that almost no one sees coming. Due to several flaws, low-cost wireless keyboards enable a malicious user to listen in from afar. Though not all wireless keyboards are created equal, and many are not vulnerable to eavesdropping, there is a simple solution to the problems caused by malicious attacks on the wireless keyboard - make use of a wired keyboard (Whittaker, 2016).

Electromagnetic emission and electromagnetic signal acquisition

Electromagnetic compatibility (EMC) is a property of electric equipment that allows it to operate as expected in the presence of other electric/electronic equipment while not interfering with it (ETSI, 2023). EMC is focused on the analysis of EM interferences of RF interferences in electric devices, to reduce the unintentional generation, propagation, and reception of EM energy. Unwanted emissions can be categorized into two groups: conductive coupling and radiative coupling. Through transmit interferences through the system, conductive coupling requires physical support (such as wires). Radiative coupling, on the other hand, occurs when an internal circuit component acts as an antenna and transmits unwanted EM waves. EMC also distinguishes two types of EM emissions based on the type of radiation source: differential mode (generated by loops) and common mode (the result of internal voltage drops) (Vuagnoux & Pasini, 2009). There are several standards, two of which are specifically related to RF, telecommunication network equipment, radio equipment and services, EN 300 386 V16.1, EN 301 489-1 V1.9.2 (ETSI, 2011; ETSI, 2012).

There are two techniques for detecting compromising EM radiation. Standard techniques include using a spectral analyser to detect signal carriers (compromised emanation is composed of peaks) or a wide-band receiver tuned to a specific frequency (scanning a receiver's entire frequency range of the receiver to demodulate the signal based on its amplitude or frequency modulation). Unfortunately, some direct and indirect EM emanations may go undetected using standard techniques, especially if the signal contains irregular peaks or erratic frequency carriers. Indeed, spectral analysers rely heavily on static carrier signals. Similarly, the scanning process of wide-band receivers is not instantaneous and takes a long time to cover the entire frequency range. Demodulation may also conceal some intriguing compromising emanations (Vuagnoux & Pasini, 2009). Novel approaches detect compromising EM emanation by directly collecting raw signals from the antenna and processing the entire captured EM spectrum, which is extremely useful for detecting EM emanations from the keyboards (both wired and wireless).

Software defined radio

SDR is a dynamic radio transmitter and/or receiver, capable of changing operational characteristics, setting or changing RF operating

parameters such as frequency range, modulation type, output power, and coding rate, allowing a single hardware platform to be adapted to be a transmitter or a receiver under different technologies, based on software configuration for any type of signal through software or firmware functions (Natase et al, 2018; Chamran et al, 2019; Molina-Tenorio et al, 2021; de Jesus Rugeles Uribe, 2022). In SDR, software modules execute in real-time on microprocessor platforms. The main operational characteristics of the system can be modified or changed while running, allowing SDR to be easily reconfigured to perform different functions (Garcia Reis et al, 2012). As a result of this, as well as due to relatively low-cost technology, SDR platforms are now frequently used for side-channel attacks.

An ideal SDR has very little hardware at the RF front end, consisting of only an antenna and a very fast sampler capable of capturing and digitizing wideband radio signals. However, relatively long coverage distances may be achieved only by employing amplifiers before both analogue-to-digital and digital-to-analogue conversion (ADC/DAC) stages (see Figure 3). LNA, PA, FPGA, and DSP are acronyms for Low-Noise Amplifier, Power-Amplifier, Fast Programmable Gate Array, and Digital Signal Processor, respectively (Stewart et al, 2015; Duarte et al, 2019, p.1490).

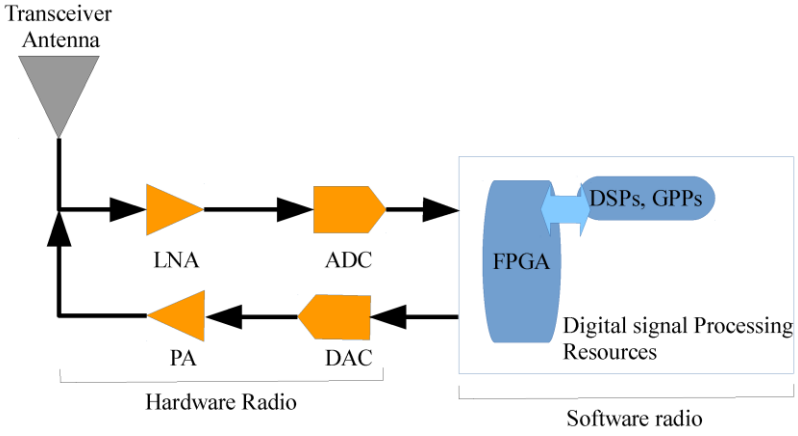

Figure 3 – Software defined radio (Duarte et al, 2019)
Рис. 3 – Программно-определяемое радио (Duarte et al, 2019)
Слика 3 – Софтверски дефинисани радио (Duarte et al, 2019)

Rugeles Uribe et al (2022) compare 19 commercially available SDR platforms in terms of ADC/DAC, Tx/Rx, Fmin-Fmax, Max RF Bandwidth, signal processing platforms (MATLAB, Labview), and GNU radio (free

open-source toolkit available for low-cost external RF hardware to create SDRs). The following devices are classified as low-cost hardware: FUNCube, RTL, RSPduo, AirSpy, HackRF, BladeRF, LimeRF, and Pluto. These SDR platforms, together with open-source software and signal processing platforms, have enabled the global advancement of SDR technology. At the same time, the possibility of side-channel attacks increased exponentially. As a result, SDR is now opening up entirely new pathways for penetration testing and security research even though EMC standards and regulations address emerging threats from side-channel attacks. When considering the EMC requirements of devices, the International Organization for Standardization (ISO) advisory notice K.841 states that information leakage from EMC must be considered (ITU, 2014).

Penetration testing

Liu et al (2021) presented the findings of a survey on vulnerabilities and side-channel attacks related to, among other things, wireless devices and the EM emission of radio waves. The results show vulnerabilities of the targeted wireless keyboard in terms of keystrokes as targeted information. Vuganoux and Pasini (2009) conducted a comprehensive study on this type of attack, testing its feasibility on various keyboard technologies, including wireless. The authors specifically rate the Matrix Scan Technique (MST) as the most effective method for keystroke interference over a USB cable. The authors propose three countermeasures against side-channel attacks: (1) shielded cables and wired keyboards to reduce EM emanations (effective but costly), (2) signal-shielded areas (low cost, effective, but valid only within a certain range), and (3) encrypted USB communication (improves communication security but encryption can be cracked). In similar circumstances, a brief study by Sim et al. (2016, pp.518-520) aims to infer keystrokes from wired keyboards solely through signal processing.

Wireless keyboards, on the other hand, have many advantages, but they also have some critical flaws that allow malicious users to take complete control of connected devices. Throughout the years, numerous test methods have been developed and implemented to identify vulnerabilities and improve the security of wireless keyboards.

Goodin (2019) shows that keystrokes can be recorded, replayed and injected into Fujitsu wireless model. Researchers from the penetration-testing firm SySS created a proof-of-concept attack that takes advantage of the insecure design. They were able to send commands to vulnerable

Fujitsu keyboard set LX901 receiver dongles within the range using a small hardware device. The researchers were able to send input that was automatically routed to the connected computer. The distance was about 10 meters.

Gatlan (2019) discovered in 2018 four novel vulnerabilities of the Logitech Unifying USB receivers that allow users to connect wireless keyboards to the same computer via a 2.4 GHz radio connection. The flaws are caused by Logitech's outdated firmware that allowed physical access to the target computer to exploit the bugs and launch keystroke injection attacks, record keystrokes, and take control of the compromised system. Logitech fixed two of them with patches in 2019.

Logitech introduced Logi Bolt, a new standard for secure, robust wireless connections in terms of both security and encryption, in 2022 (Logitech, 2022). Logi Bolt is the next-generation wireless connectivity protocol that ensures compatibility with multiple operating systems while also improving security, wireless reliability, and connection strength. It reduces the risk of cyber-attacks while also addressing the growing security concerns brought on by more mobile workforce. The Logi Bolt provides security through encryption using Elliptic Curve Diffie-Hellman P-256 and AES-128.

Wadell (2016) discusses wireless keyboards that are vulnerable to KeySniffer, all of which are low-end, inexpensive models. Anker, EagleTec, General Electric, Hewlett-Packard, Insignia, Kensington, Radio Shack and Toshiba are among the companies affected (Bastille Networks Internet Security, 2023). Note that, although Bastille Networks has tested these products, the results should not be interpreted as an exhaustive list of all vulnerable keyboards.

Deeg and Klostermeier (2019) present security concerns about wireless keyboards that use 2.4GHz radio communication that they have collected over two years. They began opening keyboards, identifying chips, reading documentation, locating testing points, and analysing data communication with a logic analyser. Then they used SDR (HackRF one), a wireless development platform (Ubertooth One), research firmware (Crazy Radio PA) and GNU radio to record and analyze radio communication to identify used transceivers and communication protocols, among other things. The findings on two Fujitsu wireless keyboard sets (LX901 and LX390) and Cherry B.Unilimited 3.0 (all of which include wireless keyboards and mice) reveal the following flaws: no protection against Replay attacks, no encryption of sensitive data (KeyStroke sniffing attack), and insufficient verification of data authenticity (KeyStroke injection attack).

Tomsic (2022) describes seven steps of penetration testing: (1) pre-engagement (communication with the client about the scope, approvals, and terms), (2) information gathering (post scanning and gathering open source intelligence), (3) threat modelling (threat a plan how to attack targeting system, based on gathered information), (4) vulnerability analysis (developed threat model is used to discover vulnerabilities if any), (5) exploitation (attacking vulnerabilities), (6) post-exploitation (determining the actual impact of the exploit), and (7) reporting (the findings of the penetration test). He used HackRF SDR connected to the computer via high-speed USB 2.0 to conduct the research. Following the SDR analysis, a Crazy Radio PA was used to capture and send data. Furthermore, 10 wireless keyboards from nine different manufacturers (Clas Ohlson, Corsair, Deltaco, Exibel, Siglo, Logitech, Plexgear, Rapoo, and Razer) were subjected to penetration testing. Penetration testing revealed that the majority of protocols contained flaws that allowed for keystroke injection or key sniffing. Eight of the keyboards were found to have previously unknown vulnerabilities that could give an attacker complete control of the computer to which the keyboard was connected. Furthermore, only one of the keyboards promised any type of encryption.

Conclusion

Wireless keyboards have security flaws that disrupt radio communication, giving a malicious user complete access to the computer to which the keyboard is connected. Because malicious users can easily either passively or actively attack the sender, the receiver, or the data transmitted over a communication channel, secure connections and secure communications are required to aid in the prevention of wireless keyboard attacks. Side-channel attacks are physical intrusions in which the attacker steals sensitive data by observing how the system works using compromised electromagnetic emissions. The results of penetration testing presented in this article reveal vulnerabilities of the targeted wireless keyboard in terms of outdated firmware, encryption, wireless reliability, and connection strength.

References

-ANSI webstore. 1999. *ANSI INCTIS 154-1998 (R1999). Office machines and supplies – Alphanumeric machines – Keyboard arrangement (Formerly ANSI X3. 154-1988 (R1999))* [online]. Available: https://webstore.ansi.org/standards/incits/ansiincits1541988r1999 [Accessed: 05 January 2023].

Barthe, G., Gregorie, B. & Laporte, V. 2018. Secure Compilation of Side Channel Countermeasures: The Case of Cryptographic “Constant-Time”. In: *2018 IEEE 31st Computer Security Foundations Symposium (CSF)*, Oxford, UK, pp.328-343, July 09-12. https://doi.org/10.1109/CSF.2018.00031.

-Bastille Networks Internet Security. 2023. *KeySniffer affected devices* [online]. Available at: https://keysniffer.net/affected-devices [Accessed: 05 January 2023].

Chamran, M.K., Yau, K.-L.A., Noor, R.M.D. & Wong, R. 2019. A Distributed Testbed for 5G Scenarios: An Experimental Study. *Sensors*, 20(1), art.number:18. Available at: https://doi.org/10.3390/s20010018.

Chauhan, P. 2020. What is keyboard? & Types of keyboard. *RKR Knowledge,* 12 May [online]. Available at: https://rkrknowledge.com/what-is-keyboard-types-of-keyboard/ [Accessed: 05 January 2023].

de Jesus Rugeles Uribe, J., Guillen, E.P. & Cardoso. L.S. 2022. A technical review of wireless security for the internet of things: Software defined radio perspective. *Journal of King Saud University – Computer and Information Sciences*, 34(7), pp.4122-4134. Available at: https://doi.org/10.1016/j.jksuci.2021.04.003.

Deeg, M. & Klostermeier, G. 2019. New tales of wireless input devices. *SlideShare* [online]. Available at: https://www.slideshare.net/proidea_conferences/new-tales-of-wireless-input-devices-matthias-deeg-gerhard-klostermeier [Accessed: 05 January 2023].

Duarte, L., Gomes, R., Riberio, C. & Caldeirinha, R.F.S. 2019. A Software-Defined-Radio for future wireless communication systems at 60 GHz. *Electronics*, 8(12), art.number:1490. Available at: https://doi.org/10.3390/electronics8121490.

-ETSI. 2011. *Final draft EN 301 489-1 V1.9.2. (2011-04) Electromagnetic compatibility and Radio spectrum Matters (ERM); Electromagnetic Compatibility (EMC) standard for radio equipment and services; Part 1: Common technical requirements* [online]. Available at: https://www.etsi.org/deliver/etsi_en/301400_301499/30148901/01.09.01_40/en_30148901v010901o.pdf [Accessed: 05 January 2023].

-ETSI. 2012. *ETSI EN 300 386 V16.1. (2012-09) Electromagnetic compatibility and Radio spectrum Matters (ERM); Telecommunication network equipment; ElectroMagnetic Compatibility (EMC) requirements* [online]. Available at: https://www.etsi.org/deliver/etsi_en/300300_300399/300386/01.06.01_60/en_300386v010601p.pdf [Accessed: 05 January 2023].

-ETSI. 2023. *Electro Magnetic Compatibility* [online]. Available at: https://www.etsi.org/technologies/emc [Accessed: 05 January 2023].

Garcia Reis, A.L., Barros, A.F., Gusso Lenzi, K., Pedroso Meloni, L.G. & Barbin, S.E. 2012. Introduction to the Software-defined Radio Approach. *IEEE Latin America Transactions,* 10(1), pp.1156-1161. Available at: https://doi.org/10.1109/TLA.2012.6142453.

Gatlan, S. 2019. Logitec unifying receivers vulnerable to key injection attacks. *Bleeping Computer* [online]. Available at: https://www.bleepingcomputer.com/news/security/logitech-unifying-receivers-vulnerable-to-key-injection-attacks/ [Accessed: 05 January 2023].

Goodin, D. 2019. How a wireless keyboard lets hackers take full control of connected computers. *arsTECHNICA* [online]. Available at: https://arstechnica.com/information-technology/2019/03/how-a-wireless-keyboard-lets-hackers-take-full-control-of-connected-computers/ [Accessed: 05 January 2023].

Grdović, M.M, Protić, D.D, Antic, V.D. & Jovanovic, B.Ž. 2022. Electromagnetic information leakage from the computer monitor. *Vojnotehnički glasnik/Military Technical Courier*, 70(4), pp.836-855. Available at: https://doi.org/10.5937/vojtehg70-38930.

Griskenas, S. 2023. What is wireless keyboard security? Everything you need to know. *Nord VPN* [online]. Available at: https://nordvpn.com/blog/what-is-wireless-keyboard-security/ [Accessed: 05 January 2023].

-ISO. 2009. *ISO/IEC 9995-1:2009. Information technology – Keyboard layouts for text and office systems – Part 1: General principles governing keyboard layouts* [online]. Available at: https://www.iso.org/standard/51645.html [Accessed: 05 January 2023].

-ITU. 2014. *K.84: Test methods and guide against information leaks through unintentional electromagnetic emission* [online]. Available at: https://www.itu.int/rec/T-REC-K.84/en [Accessed: 05 January 2023].

-JSAJIS. 2018. *JIS X 6002:1980 English Edition Keyboard layout for information processing using the JIS 7 bit coded character set* [online]. Available at: http://www.jsajis.org/index.php?main_page=product_info&cPath=4&products_id=16459 [Accessed: 05 January 2023].

Liu, H., Spolaor, R., Turrin, F., Bonafede, C. & Conti, M. 2021. USB powered devices: A survey of side-channel threats and countermeasures. *High-Confidence Computing,* 1(1), art.ID:100007. Available at: https://doi.org/10.1016/j.hcc.2021.100007.

-Logitech. 2022. *Logi Bolt Secure, robust wireless connections*. Logitech [online]. Available at: https://www.logitech.com/content/dam/logitech/en/business/pdf/logi-bolt-white-paper.pdf [Accessed: 05 January 2023].

-Logitech. 2023. *Setting a new standard in wireless peripheral security. Today's work-from-anywhere workplace demands enhanced protection*. Logitech [online]. Available at: https://www.logitech.com/en-us/business/resources/wireless-peripheral-security.html [Accessed: 05 January 2023].

Mangard, S., Oswald, E. & Popp, T. 2007. *Power Analysis Attacks: Revealing the Secrets of Smart Cards*. New York, NY: Springer. Available at: https://doi.org/10.1007/978-0-387-38162-6.

Markagić, M.S. 2018. Compromising electromagnetic radiation–challenges, threats and protection. *Vojnotehnički glasnik/Military Technical Courier,* 66(1), pp.143-153. Available at: https://doi.org/10.5937/vojtehg66-8691.

Molina-Tenorio, Y., Prieto-Guerrero, A. & Aguilar-Gonzales, R. 2021. Real-Time Implementation of Multiband Spectrum Sensing Using SDR Technology. *Sensors,* 21(10), art.number:3506. Available at: https://doi.org/10.3390/s21103506.

-NIST National Institute of Standards and Technology. 2001. *Advanced Encryption Standard (AES). Federal Information Processing Standards*. NIST National Institute of Standards and Technology, NIST Technical Series Publications*.* Available at: https://doi.org/10.6028/NIST.FIPS.197.

Oligeri, G., Sciancalepore, S., Raponi, S. & Di Pietro, R. 2020. BrokenStrokes: on the (in)security of wireless keyboards. In: *WiSec '20: Proceedings of the 13th ACM Conference on Security and Privacy in Wireless and Mobile Networks*, Linc, Austria, pp.231-241, July 08-10. Available at: https://doi.org/10.1145/3395351.3399351.

Pohl, J. & Noack, A. 2019. Automatic Wireless Protocol Reverse Engineering. In: *Proceedings of 13th USENIX Workshop on Offensive Technologies* (WOOT 19), Santa Clara, CA: USENIX Association, August [online]. Available at: https://www.usenix.org/conference/woot19/presentation/pohl [Accessed: 05 January 2023].

Sadiku, M.N.O. & Akujuobi, C.M. 2004. Software-defined radio: a brief overview. *IEEE Potentials*, 23(4), pp.14-15. Available at: https://doi.org/10.1109/MP.2004.1343223.

Sayakkara, A., Le-Khac, N.-A. & Scanlon, M. 2018. Accuracy Enhancement of Electromagnetic Side-Channel Attacks on Computer Monitors. In: *ARES 2018: Proceedings of the 13th International Conference on Availability, Reliability and Security*, Hamburg, Germany, August 27-30. Available at: https://doi.org/10.1145/3230833.3234690.

Sheimo, M. 2021. Ahhh! My mouse and keyboard were hacked! *Sikich*, 23 June [online]. Available at: https://www.sikich.com/insight/ahhh-my-mouse-and-keyboard-were-hacked/ [Accessed: 05 January 2023].

Sim, D.-J., Lee, H.S., Yook, J.-G. & Sim, K. 2016. Measurements and analysis of the compromising electromagnetic emanations from USB keyboard. In: *2016 Asia-Pacific International Symposium on Electromagnetic Compatibility (APEMC)*, Shenzhen, pp.518-520, May 17-21. Available at: https://doi.org/10.1109/APEMC.2016.7522785.

Stewart, R.W., Barlee, K.W., Atkinson, D.S.W. & Crockett, L.H. 2015. *Software Defined Radio Using MATLAB & Simulink and the RTL-SDR.* Glasgow, UK: Strathclyde Academic Media. ISBN: 978-0-9929787-2-3.

Tomsic, N. 2022. *Penetration testing wireless keyboards. Are your devices vulnerable? Degree Project in Computer Science and Technology.* Stockholm, Sweden: KTH Royal Institute of Technology [online]. Available at:

https://www.diva-portal.org/smash/record.jsf?dswid=-5484&pid=diva2%3A1701492 [Accessed: 05 January 2023].

Vuagnoux, M. & Pasini, S. 2009. Compromising Electromagnetic Emanations of Wired and Wireless Keyboards. *USENIX* [online]. Available at: https://www.usenix.org/legacy/events/sec09/tech/full_papers/vuagnoux.pdf [Accessed: 05 January 2023].

Wadell, K. 2016. Hackers Can Spy on Wireless Keyboards From Hundreds of Feet Away: There's a gaping security hole in eight popular models. *The Atlantic*, 26 July [online]. Available at: https://www.theatlantic.com/technology/archive/2016/07/hackers-can-spy-on-wireless-keyboards-from-hundreds-of-feet-away/492962/ [Accessed: 05 January 2023].

-WebNots. 2022. What are Different Types of Computer Keyboards? *WebNots*, 15 August [online]. Available at: https://www.webnots.com/what-are-different-types-of-computer-keyboards/ [Accessed: 05 January 2023].

Weiss, B. 2023. Can Your Wireless Keyboard Be Hacked? *WyzGuys Cybersecurity* [online]. Available at: https://wyzguyscybersecurity.com/can-your-wireless-keyboard-be-hacked/ [Accessed: 05 January 2023].

Whittaker, Z. 2016. Flaws in wireless keyboards let hackers snoop on everything you type. *ZD Net*, 26 July [online]. Available at: https://www.zdnet.com/article/millions-of-wireless-keyboards-at-risk-of-spying-by-hackers-in-new-attack/ [Accessed: 05 January 2023].

Безопасность беспроводных клавиатур: угрозы, уязвимость и меры противодействия

Синиша В. Йованович, *Даниела* Д. Протич, **корессподент**,
Владимир Д. Антич, *Милена* М. Грдович, *Деян* А. Баич

Вооруженные силы Республики Сербия, Генеральный штаб,
Управление информатики и телекоммуникаций (J-6),
Центр прикладной математики и электроники,
г. Белград, Республика Сербия

РУБРИКА ГРНТИ: 20.23.25 Информационные системы с базами знаний,
30.03.17 Физические проблемы механики,
30.19.17 Оболочки,
47.01.11 Современное состояние и перспективы развития,
47.43.21 Влияние различных факторов среды на распространение радиоволн,
47.53.35 Электростатические системы записи и воспроизведения сигналов

ВИД СТАТЬИ: оригинальная научная статья

Резюме:

Введение/цель: В данной статье представлен обзор исследований уязвимости компьютерных систем, вызванных побочным электромагнитным излучением беспроводных клавиатур. Было показано, что беспроводные устройства, использующие связь, инициируемую триггерами, сталкиваются с серьезными проблемами конфиденциальности вследствие утечки, связанной с радиочастотным излучением. Технология беспроводной связи является источником излучения сигнала, который необходимо защищать с точки зрения производительности и безопасности.

Методы: Наблюдаются уязвимости беспроводных устройств и атаки по сторонним каналам, а также электромагнитное излучение радиоволн.

Результаты: В результате исследования выявлены недостатки безопасности и шифрования конкретных беспроводных клавиатур. Результаты тестирования на проникновение показали уязвимость беспроводной клавиатуры, связанной с устаревшим встроенным программным обеспечением, шифрованием и надежностью беспроводной связи.

Выводы: Недостатки безопасности беспроводных клавиатур приводят к нарушению радиосвязи, предоставляя злоумышленникам полный доступ к компьютеру, к которому подключена клавиатура. Таким образом, благодаря наблюдению за работой системы, у злоумышленников появляется возможность украсть конфиденциальные данные, используя побочное электромагнитное излучение.

Ключевые слова: беспроводная клавиатура, радиочастота, электромагнитное излучение, программно-определяемое радио.

Безбедност бежичних тастатура: претње, рањивости и мере заштите

Синиша В. Јовановић*, Данијела* Д. Протић*,* **аутор за преписку**, *Владимир* Д. Антић*, Милена* М. Грдовић*, Дејан* Д. Бајић

Војска Србије, Генералштаб, Управа за телекомуникације и информатику (J-6), Центар за примењену математику и електронику, Београд, Република Србија

ОБЛАСТ: рачунарске науке, електроника, телекомуникације, информационе технологије, машинство
КАТЕГОРИЈА (ТИП) ЧЛАНКА: оригинални научни рад

Сажетак:

Увод/циљ: Рањивост рачунарских система узрокована је компромитујућим електромагнетским зрачењем са бежичних тастатура. Показано је да бежични уређаји који користе комуникацију базирану на тригерима имају проблеме који се односе на приватност, што је узроковано електромагнетским отицањем повезаним са емисијом радио-таласа. Технологија бежичних веза извор је еманације сигнала који мора бити заштићен у погледу перформанси и безбедности.

Методе: Уочавају се рањивости бежичних уређаја и напади на бочне канале, упоредо са електромагнетском емисијом радио-сигнала.

Резултати: Указано је на грешке у безбедности и енкрипцији за одређене бежичне тастатуре. Резултати пенетрационих тестова откривају рањивости циљане бежичне тастатуре у погледу застарелог фирмвера, енкрипције и поузданости бежичне мреже.

Закључак: Бежичне тастатуре имају безбедоносне пропусте који омогућују ометање радио-комуникације, дајући злонамерном кориснику потпун приступ рачунару на који је тастатура повезана. Стога он може да украде осетљиве податке посматрајући рад система и користећи електромагнетску емисију.

Кључне речи: бежична тастатура, радио-фреквенције, електромагнетска емисија, софтверски дефинисани радио.

Paper received on / Дата получения работы / Датум пријема чланка: 06.01.2023.
Manuscript corrections submitted on / Дата получения исправленной версии работы / Датум достављања исправки рукописа: 24.03.2023.
Paper accepted for publishing on / Дата окончательного согласования работы / Датум коначног прихватања чланка за објављивање: 26.03.2023.

Mathematical modeling and simulation of a rectangular pulse transceiver operating in the discrete-time domain

Stevan M. Berber
The University of Auckland,
Department of Electrical, Computer and Software Engineering,
Auckland, New Zealand,
e-mail: s.berber@auckland.ac.nz,
ORCID ID: https://orcid.org/0000-0002-2432-3088

DOI: 10.5937/vojtehg71-43043; https://doi.org/10.5937/vojtehg71-43043

FIELD: electrical engineering, telecommunications
ARTICLE TYPE: original scientific paper

Abstract:

Introduction/purpose: The paper presents the theory and design issues of a discrete-time communication system used for discrete-time pulse transmission with and without filtering. Signals are analyzed in both the time domain and the frequency domain.

Methods: The system is theoretically analyzed using block schematics expressed in terms of mathematic operators and the system simulation is performed to confirm the theoretical findings.

Results: Discrete-time signals are presented in the time domain and the frequency domain as well as confirmed by a simulation designed in Matlab.

Conclusion: The results of the paper contribute to the theoretical modeling and design of modern discrete communication systems.

Keywords: discrete communication system, system design, discrete pulse transceiver, filtering, correlation receiver.

Introduction

Most of the analyses of modern telecommunication systems are based on the presentation of signals in the continuous-time domain, i.e., as continuous functions of time. Consequently, these systems are known under the name of digital communications systems (Haykin, 2001; Proakis, 2001). However, signals of modern communication systems are represented by discrete-time functions and are known under the name of discrete communication systems (Rice, 2009; Berber, 2021; Abramowitz & Stegun, 1972).

This paper aims to present the theoretical base of a discrete communication system assuming that the modulating signal is a

rectangular discrete-time pulse. The content of the paper will include the issues of mathematical modeling and design of a discrete communication system that includes a transmitter, a transmission channel, and a receiver. The signals processed in the system will be presented in the discrete-time domain represented by functions of the discrete-time variable. The system operating in the continuous time domain is named *the digital system*, while the system operating in the discrete-time domain is named *the discrete system* (Miao, 2007; Benvenuto et al, 2007).

Modern designs of transmitters and receivers in a communication system are based on digital technology, primarily on FPGA and DSP platforms. These technologies are in extensive use replacing the analog technologies that are used to implement signal processing functions inside both the baseband and intermediate frequency transceiver blocks. These trends in the design of communication systems became possible due to advances in the theory of discrete-time signal processing, and particularly by the development of the mathematical theory of discrete-time deterministic and stochastic processes (Manolakis et al, 2005; Berber, 2009).

In this paper, all signals inside the transmitter and receiver blocks are analyzed in both the discrete-time domain and the frequency domain. Two different structures of the receiver are analyzed; the first with a low-pass filter and the second with a correlator receiver. To understand the consequences of signal filtering, the transceiver is separately analyzed for the case when a filter is used to reduce the spectrum of the modulating signal, and, consequently, to limit the bandwidth of the modulated signal. The presented system structures are expressed in terms of mathematical operators and their operations are explained using exact mathematical expressions. The designed system is simulated to confirm the theoretical model (Quyen et al, 2015; Ingle & Proakis, 2012).

The related powers and energies of the related signals are precisely calculated for an ideal transmission of signals in the noiseless channel and their filtering. These calculations allowed a clear understanding of the transceiver operation and possible losses in signal power caused by signal processing in the transmitter and receiver blocks.

The theory of discrete-time communication systems is of vital importance for researchers, practicing engineers, and designers of communications devices because the design of these devices is impossible without a deep understanding of the theoretical principles and concepts related to their operation in the discrete-time domain (Rice, 2009; Berber, 2021). Modern communication devices, like wireless and cable modems, TV modems, consumer entertainment systems, and satellite

modems are based on the use of digital processing technology and the principles of the discrete-time signal processing theory.

Discrete-time communication system structure and operation

A discrete-time communication system, including the basic operation of signals, is presented in Figure 1. The system is composed of a transmitter, a band-pass noise generator, and two types of receivers. The first receiver will demodulate the received band-pass (BP) signal using a low-pass filter (LPF). The second receiver will use a correlator to demodulate the received discrete pulse and generate binary zero (0) or binary one (1) at the output. These two receivers will be separately analyzed. In the case of the system simulation, a band-pass noise generator should be used to generate BP discrete-time noise that will be added to the modulated discrete-time signal. The BP noise generation and application for the system investigation is a separate topic.

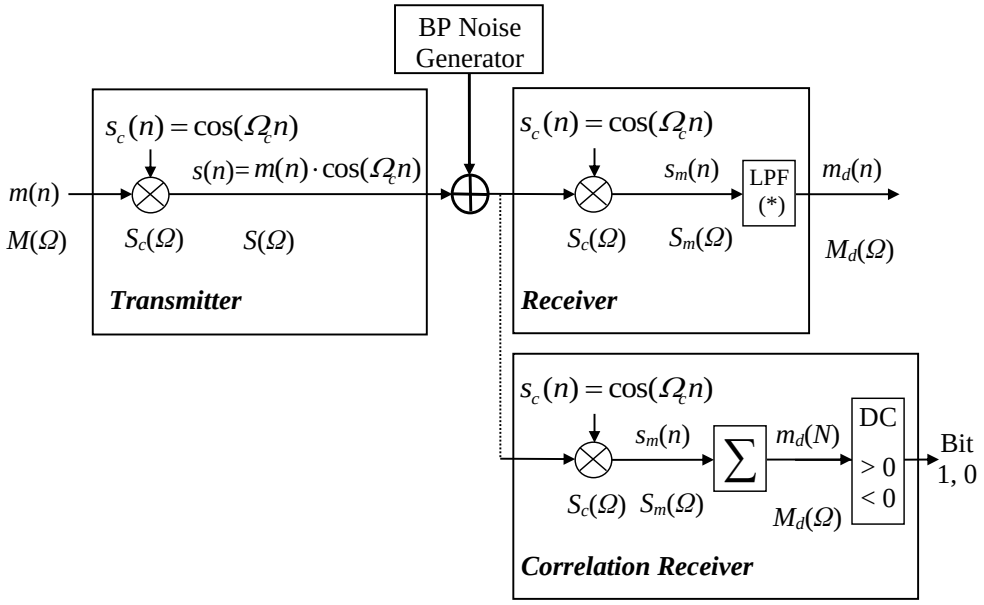

Figure 1 − Discrete communication system
Рис. 1 – Дискретная система связи
Слика 1 – Дискретни телекомуникациони систем

Transmitter operation

Suppose the output of the transmitter is a product of a modulating discrete-time (dt) rectangular pulse *m*(*n*) and the discrete-time carrier $s_c(n) = \cos \Omega_c n$ resulting in a dt modulated signal *s*(*n*), expressed in this form

$$s(n) = m(n) \cos \Omega_c n \,, \tag{1}$$

as shown in Figure 1. We are to find the expression in the time domain and in the frequency domain of the modulated signal and all signals involved in signal processing, assuming that the dt rectangular pulse is of an amplitude *A* and a duration *N* while the frequency of the carrier is Ωc.

The rectangular pulse in the time domain and the frequency domain. The graphs of the dt rectangular pulse in the discrete-time domain are presented in Figure 2. The rectangular pulse in the time domain can be expressed in terms of Koronecker's delta function as a convolution of the signal and the delta functions, i.e.,

$$m(n) = \begin{Bmatrix} A & 0 \le n \le N-1 \\ 0 & otherwise \end{Bmatrix} = \sum_{k=-\infty}^{\infty} m(k)\delta(n\text{-}k) = \sum_{k=0}^{N-1} m(k)\delta(n\text{-}k) \tag{2}$$

for its amplitude *A* = 2 and duration *N* = 8 as shown in Figure 2. The pulse values are defined for each whole number *n* and have no values in the intervals between neighboring numbers. We can say that the signal does not exist in these intervals. The intervals are used to process the discrete signal values.

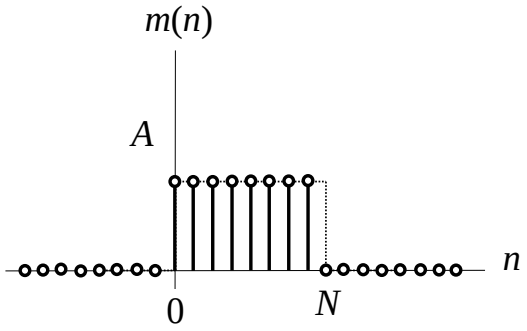

Figure 2 − Discrete-time modulating signal for N = 8 and A = 2.
Рис. 2 – Модулирующий сигнал с дискретным временем для N = 8 и A = 2
Слика 2 – Модулишући сигнал дискретног времена за N = 8 и A = 2

To find the amplitude and magnitude spectral densities of the pulse, we need to find the discrete-time Fourier transform (DTFT) of the modulating signal which is a discrete-time rectangular pulse. Based on the property of Kronecker's delta function, the DTFT of the dt pulse that has *A* values in the interval from 0 to (*N*-1) can be expressed in the following form (Berber, 2021)

$$M(\Omega)=\sum_{n=-\infty}^{\infty}m(n)e^{-j\Omega n}=\sum_{n=-\infty}^{\infty}\sum_{k=0}^{N-1}m(k)\delta(n\text{-}k)e^{-j\Omega n}$$
$$=\sum_{k=0}^{N-1}m(k)\sum_{n=-\infty}^{\infty}\delta(n\text{-}k)e^{-j\Omega n}=\sum_{k=0}^{N-1}Ae^{-j\Omega k}\underset{k=n}{=}\sum_{n=0}^{n=(N-1)}Ae^{-j\Omega n}. \quad (3)$$

Then, the amplitude spectral density can be calculated as

$$M(\Omega)=\sum_{k=0}^{N-1}Ae^{-j\Omega k}\underset{k=n}{=}\sum_{n=0}^{n=(N-1)}Ae^{-j\Omega n}=A\frac{1-e^{-j\Omega N}}{1-e^{-j\Omega}}=Ae^{-j\Omega(N-1)/2}\frac{\sin\Omega N/2)}{\sin\Omega/2}$$
$$=\begin{Bmatrix} AN & \Omega=\pm 2k\pi, k=0,1,2,3,... \\ Ae^{-j\Omega(N-1)/2}\dfrac{\sin\Omega N/2)}{\sin\Omega/2} & otherwise \end{Bmatrix}. \quad (4)$$

Having the amplitude spectral density, we can calculate the magnitude spectral density expressed as

$$|M(\Omega)|=\begin{Bmatrix} AN & \Omega=\pm 2k\pi, k=0,1,2,3,... \\ A\left|\dfrac{\sin\Omega N/2)}{\sin\Omega/2}\right| & otherwise \end{Bmatrix}, \quad (5)$$

and the phase spectral density is expressed as

$$\arg M(\Omega)=-\frac{\Omega}{2}(N-1)+\arg\frac{\sin(\Omega N/2)}{\sin(\Omega/2)}, \quad (6)$$

which are presented in Figure 3 for the case of $N = 8$ and A = 2. Note that the amplitude value of $M(\Omega)$ for $\Omega = 0$ is equal to *AN*, which can be easily obtained by calculating this value from the defining expression for the DTFT. The magnitude spectral density $M(\Omega)$ is a periodic function with a period of 2π. The zeros crossings in this function occur for the condition $\sin(\Omega_0 N/2)=0$, i.e., for $\Omega_0 N/2 = k\pi$, $k = 1, 2, \ldots, N\text{-}1$. For $N = 8$, we may have $\Omega_0 = \pm 2k\pi/N = \pm k\pi/4$, and $k = 1, 2, \ldots, N\text{-}1$. The phase discontinuities of π radians occur at the same frequencies.

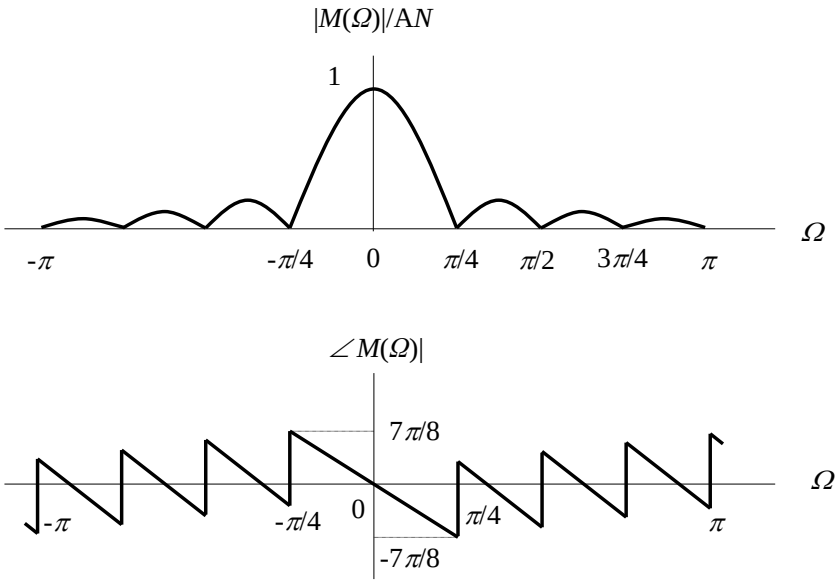

Figure 3 − Magnitude and phase spectral densities of the modulating signal
Рис. 3 – Спектральная плотность колебаний и фазы модулирующего сигнала
Слика 3 – Спектрална густина магнитуде и фазе модулишућег сигнала

The power and energy of the pulse can be calculated in the time domain and in the frequency domain. In the time domain, the power is

$$P_m = \frac{1}{N}\sum_{n=0}^{N-1} m^2(n) = \frac{1}{8}\sum_{n=0}^{n=7} A^2 = A^2, \quad (7)$$

and the related energy is calculated as

$$E_m = P_m \cdot N = \sum_{n=0}^{N-1} m^2(n) = \sum_{n=0}^{n=7} A^2 = 8A^2. \quad (8)$$

The modulating signal m(n) is an energy signal. Therefore, its energy spectral density can be calculated as

$$E_m(\Omega) = \left|M\left(\Omega\right)\right|^2 = A^2\left|\frac{\sin \Omega N/2)}{\sin \Omega/2}\right|^2. \quad (9)$$

This function can be calculated as the DTFT of its autocorrelation function (Berber, 2019). The energy is the integral of the energy spectral density calculated as (Integral calculator, 2023)

$$E_m = \frac{1}{2\pi}\int_{-\pi}^{\pi} E_m(\Omega)\,d\Omega = \frac{A^2}{2\pi}\int_{-\pi}^{\pi}\left|\frac{\sin 4\Omega)}{\sin \Omega/2}\right|^2 d\Omega = \frac{A^2}{2\pi}16\pi = 8A^2. \quad (10)$$

and the power of the pulse is

$$P_m = \frac{E_m}{N} = A^2. \quad (11)$$

The energy inside the first arcade (Figure 3) can be calculated as

$$E_{m1} = \frac{A^2}{2\pi}\int_{-\pi/4}^{\pi/4}\left|\frac{\sin 4\Omega)}{\sin \Omega/2}\right|^2 d\Omega = \frac{A^2}{2\pi}45.64495506949089, \quad (12)$$

and the energy inside both the first and second arcades is

$$E_{m1-2} = \frac{A^2}{2\pi}\int_{-\pi/2}^{\pi/2}\left|\frac{\sin 4\Omega)}{\sin \Omega/2}\right|^2 d\Omega = \frac{A^2}{2\pi}48.29464599062311, \quad (13)$$

which corresponds to 90.81% and 96.08% of the total signal energy, respectively. Therefore, if we are filtering the first arcade of the signal, we will use only 90.81% of the signal power.

Discrete-time carrier in the time domain and the frequency domain. Suppose the discrete-time carrier has a unit amplitude, i.e., it is expressed as $s_c(n) = \cos\Omega_c n$. Suppose the carrier has only N_c = 4 samples per oscillation. Therefore, we can calculate its frequency $\Omega_c = 2\pi f_c / f_s = 2\pi / N_c = \pi/2$, and express it in the discrete-time domain as

$$s_c(n) = \cos\Omega_c n = \cos 2\pi n / N_c = \cos \pi n/2, \quad (14)$$

which is shown in the graphical form in Figure 4. The carrier in the frequency domain can be directly found for any N_c simply applying Euler's formula on the time domain signal as

$$s_c(n) = \frac{1}{2}[e^{j\Omega_c n} + e^{-j\Omega_c n}] = \frac{1}{2}[e^{j2\pi n/N_c} + e^{-j2\pi n/N_c}] = \frac{1}{2}[e^{j2\pi n/N_c} + e^{j2\pi n(N_c-1)/N_c}].$$

For the case analyzed N_c = 4 and $\Omega_c = \pi/2$, we may express the carrier in the time domain as

$$s_c(n) = \frac{1}{2}[e^{j\pi n/2} + e^{j\pi n 3/2}], \quad (15)$$

and in the frequency domain as

$$S_c(\Omega) = \sum_{k=\pm 1}\frac{2\pi}{2}\delta(\Omega + k\cdot\Omega_c) = \pi\delta(\Omega+\Omega_c) + \pi\delta(\Omega-\Omega_c). \quad (16)$$

Because this signal is a periodic function of the continuous frequency Ω with a period of 2π, it can be represented by a periodic stream of Dirac's delta functions (Papoulis & Pillai, 2002), as presented in Figure 4.

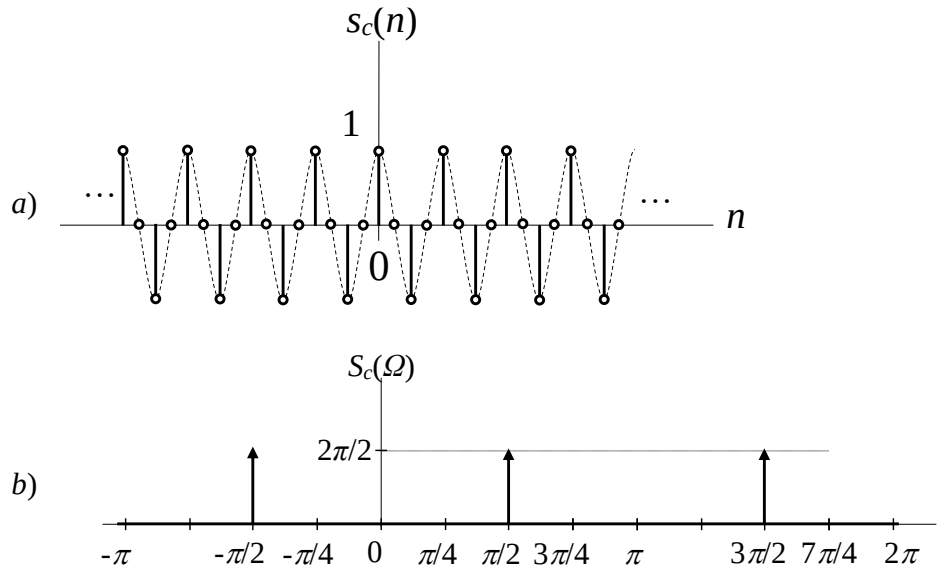

Figure 4 − a) Waveshape of the carrier, b) related amplitude spectral density
Рис. 4 – а) Форма несущей волны, b) относительная спектральная плотность колебаний
Слика 4 – а) Таласни облик носиоца, б) односна спектрална густина амплитуде

Based on (14), the power of the carrier can be calculated in the time domain as

$$P_c = \frac{1}{4}\sum_{n=0}^{n=3}\cos^2(\pi n/2) = \frac{1}{4}\sum_{n=0}^{n=3}\frac{1}{2}(1+\cos\pi n) = \frac{1}{4}\sum_{n=0}^{n=3}\frac{1}{2} = \frac{1}{2}. \qquad (17)$$

The carrier is a power signal (Cavicchi, 2000; Berber, 2021). Therefore, its average power is to be calculated in an infinite interval, according to this expression

$$P_c = \lim_{a\to\infty}\frac{1}{2a}\sum_{n=-a}^{a}\cos^2(\Omega_c n) = \lim_{a\to\infty}\frac{1}{2a}\sum_{n=-a}^{a}\frac{1}{2}(1+\cos\pi n) = \lim_{a\to\infty}\frac{1}{2a}\frac{2a}{2} = \frac{1}{2}, \qquad (18)$$

resulting in the same value as in (17). Because the carrier is a power signal, its energy is expected to be infinite. We can confirm that by calculating the energy of the signal in the frequency domain as

$$E_c = \frac{1}{2\pi}\int_{-\infty}^{\infty} |S_c^2(\Omega)|\, d\Omega = \frac{1}{2\pi}\int_{-\infty}^{\infty}\left(\sum_{k=\pm 1}\frac{2\pi}{2}\delta(\Omega + k\Omega_c)\right)^2 d\Omega$$

$$= \frac{\pi}{2}\int_{-\infty}^{\infty}\left(\delta^2(\Omega+\Omega_c) + 2\delta(\Omega+\Omega_c)\delta(\Omega-\Omega_c) + \delta^2(\Omega-\Omega_c)\right)d\Omega \quad , (19)$$

$$= \frac{\pi}{2}\int_{-\infty}^{\infty}\delta(\Omega+\Omega_c)\delta(\Omega+\Omega_c)d\Omega + 0 + \frac{\pi}{2}\int_{-\infty}^{\infty}\delta(\Omega-\Omega_c)\delta(\Omega-\Omega_c)d\Omega$$

$$= \frac{\pi}{2}(\delta(-\Omega_c+\Omega_c) + \delta(\Omega_c-\Omega_c)) = \pi\delta(0) = \infty$$

because the integral of the product of the two delta functions is zero and the integral of the delta function squared can be considered infinity. The infinite energy value can be confirmed by its calculation in the time domain as

$$E_c = \lim_{a\to\infty}\sum_{n=-a}^{a}\cos^2(\Omega_c n) = \lim_{a\to\infty}\sum_{n=-a}^{a}\frac{1}{2}(1+\cos\pi n) = \lim_{a\to\infty}\frac{2a}{2} = \infty \,. \quad (20)$$

Modulated signal in the time domain and the frequency domain

Plot the graphs of all signals in the frequency domain assuming that the number of samples of the rectangular pulse is N = 8 and there are two oscillations of the carrier inside the pulse, i.e., one oscillation of the carrier is represented by N_c =4 samples. The rectangular pulse in the discrete-time domain has already been expressed by (2). With a precise definition of the modulating signal $m(n)$ in the time domain, the modulated signal can be expressed in terms of Kronecker delta functions as

$$s(n) = m(n)\cos\Omega_c n = \cos\Omega_c n\sum_{k=0}^{N-1} m(k)\delta(n\text{-}k) = \sum_{k=0}^{N-1} m(k)\delta(n\text{-}k)\cos\Omega_c n \quad , (21)$$

$$= A\sum_{k=0}^{N-1}\delta(n\text{-}k)\cos\Omega_c n$$

and graphically presented as in Figure 5. We may get the amplitude spectral density of that signal as the convolution of the modulating signal and the carrier in the frequency domain (Berber, 2021), which will give the modulated signal as

$$S(\Omega) = M(\Omega) * S_c(\Omega) = \frac{1}{2\pi}\int_{-\infty}^{\infty} M(\lambda)\cdot S_c(\Omega-\lambda)d\lambda =$$

$$= \frac{1}{2\pi}\int_{-\infty}^{\infty} M(\lambda)\cdot\frac{2\pi}{2}\delta(\Omega+\Omega_c-\lambda)d\lambda + \frac{1}{2\pi}\int_{-\infty}^{\infty} M(\lambda)\cdot\frac{2\pi}{2}\delta(\Omega-\Omega_c-\lambda)d\lambda \cdot \quad (22)$$

$$= \frac{1}{2}M(\Omega+\Omega_c) + \frac{1}{2}M(\Omega-\Omega_c)$$

Based on the expression for the amplitude spectral density of $m(n)$ (5), the required frequency-shifted components in (22) can be expressed as

$$\frac{1}{2}M\left(\Omega\pm\Omega_c\right) = \frac{A}{2}e^{-j(\Omega-\Omega_c)(N-1)/2}\frac{\sin\left(\Omega\pm\Omega_c\right)N/2)}{\sin\left(\Omega\pm\Omega_c\right)/2}$$

$$= \begin{cases} AN/2 & \Omega\pm\Omega_c = \pm 2k\pi, k = 0, 1, 2, 3, \ldots \\ \dfrac{A}{2}e^{-j(\Omega\pm\Omega_c)(N-1)/2}\dfrac{\sin\left(\Omega\pm\Omega_c\right)N/2)}{\sin\left(\Omega\pm\Omega_c\right)/2} & otherwise \end{cases} \cdot \quad (23)$$

The magnitude spectral density of the modulated signal is presented in Figure 5.

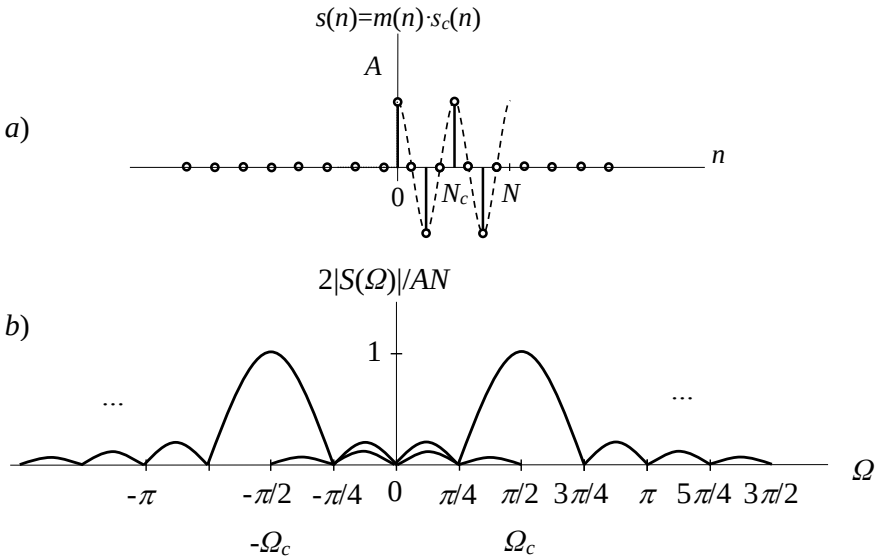

Figure 5 − a) Discrete-time waveshape, and b) magnitude spectral density of the modulated signal

Рис. 5 – а) Форма волны с дискретным временем и b) спектральная плотность модулированного сигнала по величине

Слика 5 – а) Таласни облик у дискретном времену, б) спектрална густина магнитуде модулисаног сигнала

Berber, S., Mathematical modeling and simulation of a rectangular pulse transceiver operating in the discrete-time domain, pp.316-344

The magnitude spectrum is a periodic function with a period of 2π. The two-sided spectrum of the signal can be investigated inside the bandwidth around the carrier frequency of $\pi/2$. We can calculate the signal energy and power in the time domain

$$E_s = P_s \cdot N = \sum_{n=0}^{N-1} s^2(n) = \sum_{n=0}^{n=7} s^2(n) = 4A^2 \tag{24}$$

and the power is

$$P_s = E_s / N = 4A^2 / 8 = A^2 / 2 . \tag{25}$$

The energy calculated in the frequency domain confirms calculations in the time domain, i.e.,

$$\begin{aligned} E_s &= \frac{1}{2\pi}\int_{-\pi}^{\pi} |S(\Omega)|^2 \, d\Omega = \frac{1}{2\pi}\int_{-\pi}^{\pi} |\frac{1}{2}[M(\Omega-\Omega_c)+M(\Omega+\Omega_c)]|^2 \, d\Omega \\ &= \frac{1}{\pi}\frac{A^2}{4}\int_{-\pi}^{\pi} |M(\Omega-\Omega_c)|^2 \, d\Omega = \frac{A^2}{4\pi}\int_{-\pi}^{\pi} |\frac{\sin(\Omega \pm \Omega_c)8/2)}{\sin(\Omega \pm \Omega_c)/2}|^2 \, d\Omega = \frac{A^2}{4\pi}16\pi = 4A^2 \end{aligned} \tag{26}$$

The modulated signal is an energy signal having finite energy. The power calculated in the signal interval is finite.

However, if the average power is calculated in the infinite interval, it would be of zero value which complies with the definition of the power signals.

Simulation of the transmitter operation

We performed a simulation of the transmitter presented in Figure 1 (Ingle & Proakis, 2012).

The signals are generated in the time domain and the frequency domain.

The modulating signal and the carrier obtained by simulation in the time domain and the frequency domain are presented in Figure 6.

They are equivalent to the signals obtained by calculations and presented in Figures 3 and 4, respectively.

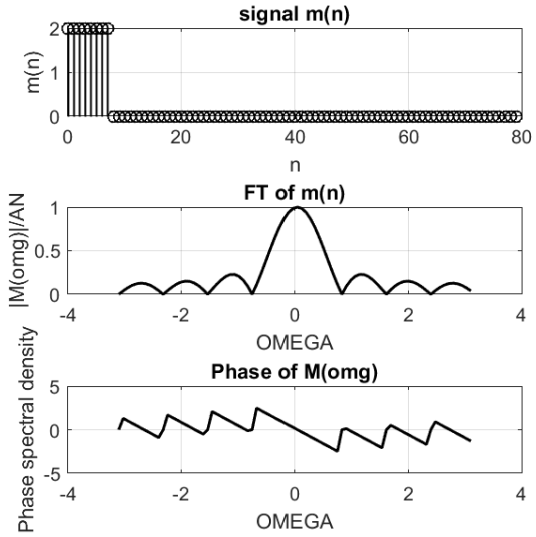

a)

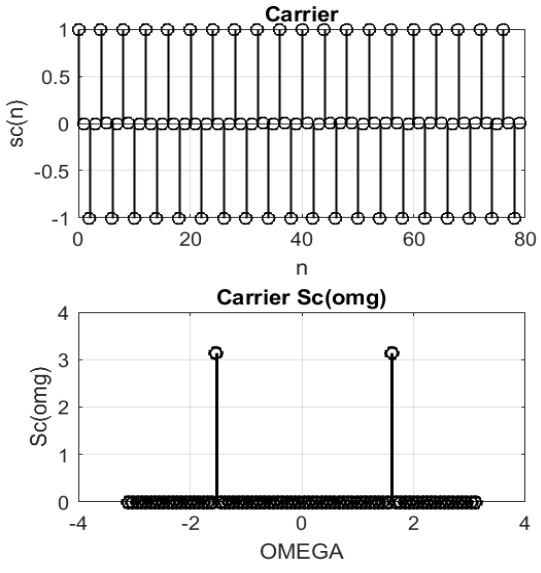

b)

Figure 6 − Magnitude and phase spectra: a) the modulating signal, b) the carrier
Рис. 6 – Амплитудный и фазовый спектры: а) модулирующего сигнала, b) несущей волны
Слика 6 – Спектри магнитуде и фазе: а) модулишући сигнал, б) носилац

A simulated modulated signal in the time domain and the frequency domain is presented in Figure 7. The presentations are equivalent to the graphs obtained by calculations and shown in Figure 5.

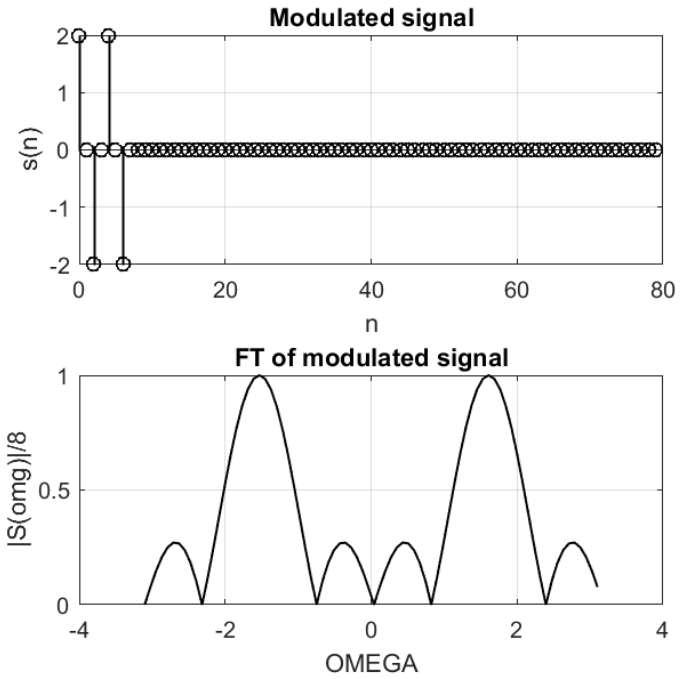

Figure 7 − Magnitude spectral density of the modulated signal in the time domain and in the frequency domain
Рис. 7 – Спектральная плотность колебаний модулированного сигнала во временной и частотной областях
Слика 7 – Спектрална густина магнитуде модулисаног сигнала у временској и фреквенцијској домени

Receiver operation with the implementation of a low-pass filter

The demodulation of the discrete modulate signal results in the discovery of a modulating signal that is in the form of a rectangular pulse. The procedure of demodulation takes place inside the receiver as presented in Figure 1. We will first analyze the case when a low-pass filter is used to demodulate the modulated signal. We use a coherent receiver in this case. Firstly, the received signal is multiplied by the carrier to get the multiplied signal

$$s_m(n) = m(n)\cos^2 \Omega_c n = \left\{ \begin{array}{ll} \frac{1}{2} A(1+\cos 2\Omega_c n) & 0 \le n \le N-1 \\ 0 & otherwise \end{array} \right\}. \quad (27)$$

The wave shape of this signal is shown in Figure 8. The signal is represented by 4 discrete amplitude *A* values. The dashed graph notifies what the shape of the corresponding continuous-time signal would look like. The DC component of the signal having amplitude A/2 is also presented in Figure 8. The double frequency term of the discrete time signal is $\cos 2\Omega_c n = \cos 4\pi n / N_c = \cos 4\pi n / 4 = \cos \pi n$.

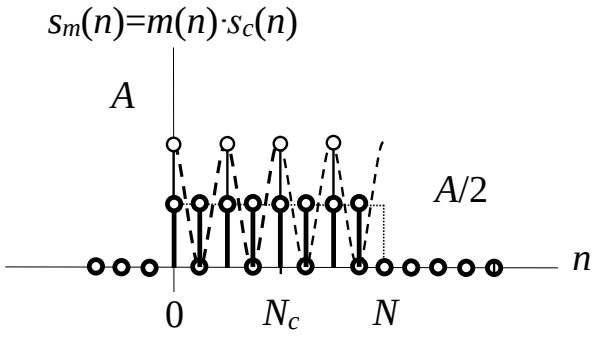

Figure 8 − The output of the signal multiplier
Рис. 8 – Выходной сигнал умножителя сигнала
Слика 8 – Излаз множача сигнала

The DTFT of this signal gives its amplitude spectral density of the form

$$\begin{aligned} S_m(\Omega) &= \frac{1}{2} FT\left\{m(n)(1+\cos 2\Omega_c n)\right\} = \frac{1}{2} FT\left\{m(n) + m(n)\cos 2\Omega_c n\right\} \\ &= \frac{1}{2} M(\Omega) + \frac{1}{4}[M(\Omega - 2\Omega_c) + M(\Omega + 2\Omega_c)] \end{aligned}, \quad (28)$$

where the amplitude spectral density of the low-frequency part is

$$\frac{1}{2} M(\Omega) = \left\{ \begin{array}{ll} AN/2 & \Omega = \pm 2k\pi, k = 0, 1, 2, 3, \ldots \\ \frac{A}{2} e^{-j\Omega(N-1)/2} \frac{\sin \Omega N/2)}{\sin \Omega/2} & otherwise \end{array} \right\}. \quad (29)$$

Berber, S., Mathematical modeling and simulation of a rectangular pulse transceiver operating in the discrete-time domain, pp.316-344

The amplitude spectral density of the LF signal part is shown in Figure 9. This spectrum has the same waveshape as the spectrum of the modulating signal in Figure 3, but all of its amplitudes are two times smaller due to the processing inside the demodulator.

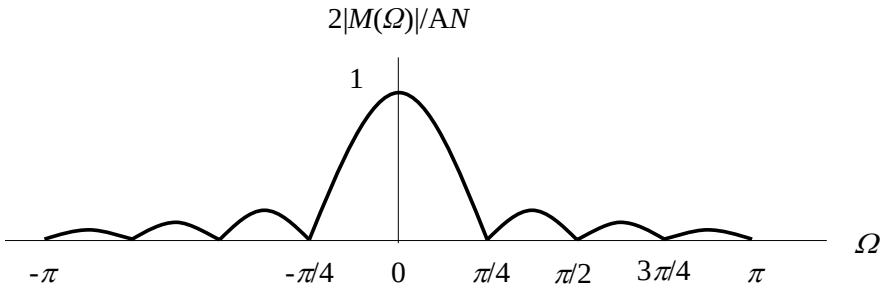

Figure 9 − Magnitude spectral density of the demodulated pulse
Рис. 9 – Амплитудная спектральная плотность демодулированного импульса
Слика 9 – Спектрална густина магнитуде демодулисаног пулса

Also, the shifted components of the signal are

$$\frac{1}{4}M\left(\Omega \pm 2\Omega_c\right) = \frac{A}{4}e^{-j(\Omega \pm 2\Omega_c)(N-1)/2}\frac{\sin\left(\Omega \pm 2\Omega_c\right)N/2)}{\sin\left(\Omega \pm 2\Omega_c\right)/2}$$

$$= \begin{cases} AN/4 & \Omega \pm 2\Omega_c = \pm 2k\pi, k = 0, 1, 2, 3, \ldots \\ \dfrac{A}{4}e^{-j(\Omega \pm 2\Omega_c)(N-1)/2}\dfrac{\sin\left(\Omega \pm 2\Omega_c\right)N/2)}{\sin\left(\Omega \pm 2\Omega_c\right)/2} & \text{otherwise} \end{cases}, \quad (30)$$

and the spectrum of the signal at the output of the multiplier is presented in Figure 10.

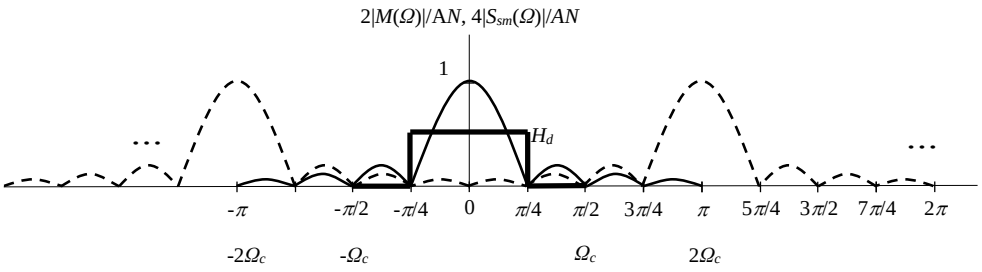

Figure 10 − The spectrum of the signal at the output of the multiplier
Рис. 10 – Спектр сигнала на выходе умножителя
Слика 10 – Спектар сигнала на излазу множача

The power and energy of the demodulated signal can be calculated in both the time domain and the frequency domain. With expression (27), the energy calculated in the time domain can be calculated as

$$E_{sm} = \sum_{n=0}^{n=7} (\frac{1}{2} A(1+\cos 2\Omega_c n))^2 = \sum_{n=0}^{n=7} \frac{1}{4} A^2 + \frac{1}{4} \sum_{n=0}^{n=7} A^2 (\frac{1}{2} + \frac{1}{2} \cos 4\Omega_c n)$$
$$= \sum_{n=0}^{n=7} \frac{1}{4} A^2 + \frac{1}{8} \sum_{n=0}^{n=7} A^2 = 3A^2 \quad (31)$$

and the power is

$$P_{sm} = \frac{E_{sm}}{N} = \frac{3A^2}{8}. \quad (32)$$

Using the magnitude spectral density (28), we can find the energy spectral density. Then, the energy is calculated as the integral value of the energy spectral density, i.e.,

$$E_{sm} = \frac{1}{2\pi} \int_{-\pi}^{\pi} |\frac{1}{2} M(\Omega_c) + \frac{1}{4} M(\Omega - 2\Omega_c) + \frac{1}{4} M(\Omega + 2\Omega_c)|^2 \, d\Omega$$
$$= \left(2 + \frac{1}{4} 4 \right) A^2 = 3A^2 \quad , \quad (33)$$

which also confirms the value of the signal power expressed in (32).

LPF operation in time and frequency domain. If the LP filter with the cut-off frequency $\Omega_F = \pi/4$ and the gain H_d is used to eliminate the HF components at the double carrier frequency, as shown in Figure 10, the demodulated pulse at the output of the LPF, as shown in Figure 1, can be obtained and expressed in the frequency domain as

$$M_d(\Omega) = S_m(\Omega) H_d(\Omega) \approx \begin{cases} H_d \cdot M(\Omega)/2 & |\Omega| \le \Omega_F = \pi/4 \\ 0 & \text{otherwise} \end{cases}. \quad (34)$$

We also assume that the double carrier frequency components in the LP filter bandwidth are negligibly small. We intend to find the signal at the output of the LPF in the time domain. For that purpose, we can perform a convolution of the LPF input signal and the impulse response of the filter. Therefore, we need to calculate first the impulse response of the filter $h(n)$. The LPF here is considered an LTI system. Then, the impulse response of the filter is the DTFT of the filter impulse response, i.e.,

Berber, S., Mathematical modeling and simulation of a rectangular pulse transceiver operating in the discrete-time domain, pp.316-344

$$h(n)=\frac{1}{2\pi}\int_{-\pi}^{\pi}H_d(\Omega)e^{+j\Omega n}d\Omega=\frac{1}{2\pi}\int_{-\Omega_F}^{\Omega_F}H_d e^{+j\Omega n}d\Omega=\frac{H_d\Omega_F}{\pi}\text{sinc}\Omega_F n$$
$$\underset{\Omega_F=\pi/4}{=}\frac{H_d}{4}\text{sinc}\pi n/4 \quad , \quad (35)$$

for the assumed cut-off frequency of the LP filter of $\Omega_F = \pi/4$, as shown in Figure 10. The zero crossings are calculated as: $\sin(\pi n/2)=0$, $(\pi n/2)=k\pi$, and $n=2k$. The demodulated pulse in the time domain can be obtained as the convolution of the input signal $s_m(n)$ and the impulse response h(n), i.e.,

$$m_d(n)=\sum_{l=-\infty}^{l=\infty}h(n-l)s_m(l)=\sum_{l=-\infty}^{l=\infty}s_m(n-l)h(l)=\sum_{l=n-(N-1)}^{l=n}s_m(n-l)h(l)\,. \quad (36)$$

The procedure of doing the convolution is presented in Figure 11. For a fixed position of the demodulated signal on the *n*-axis, the time-inverted impulse response is shifted from minus infinity to plus infinity, and the corresponding products are added for every n value, as notified in Figure 11.

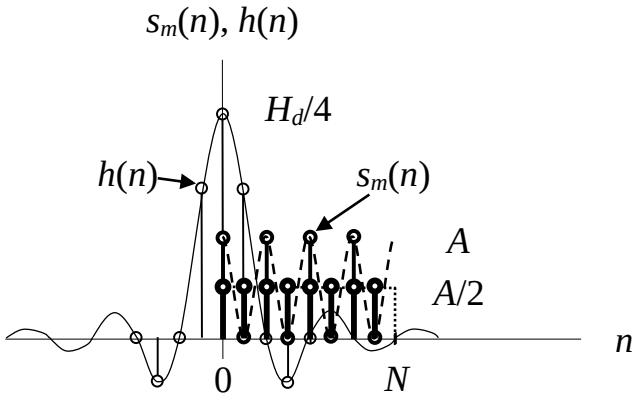

Figure 11 − Convolution of the signals
Рис. 11 – Свертка сигналов
Слика 11 – Конволуција сигнала

The energy of the received rectangular pulse is expressed as (34),

$$E_{md}(\Omega)=\left|M(\Omega)\right|^2=\left|H_d\cdot M(\Omega)/2\right|^2=\frac{H_d^2}{4}\left|M(\Omega)\right|^2=\frac{H_d^2}{4}A^2\left|\frac{\sin\Omega N/2)}{\sin\Omega/2}\right|^2. \quad (37)$$

The energy is the integral of the energy spectral density calculated as

$$E_{md} = \frac{1}{2\pi}\int_{-\pi}^{\pi} E_{md}(\Omega)\,d\Omega = \frac{H_d^2}{4}\frac{A^2}{2\pi}\int_{-\pi}^{\pi}\left|\frac{\sin 4\Omega)}{\sin \Omega/2}\right|^2 d\Omega = \frac{H_d^2}{4}E_m = 2H_d^2A^2 \text{ , (38)}$$

and the power of the pulse is

$$P_{md} = \frac{E_{md}}{N} = \frac{H_d^2}{4}\frac{E_m}{N} = \frac{H_d^2}{4}P_m \text{ .} \qquad (39)$$

Comparing relation (39) with expression (11), we can see that the power of the modulating signal at the transmitter side is attenuated $H_d^2/4$ times. If we assume that the filter is defined by Hd = 1, the power will be attenuated 4 times, or 6.02 dB as it can be seen from this simple calculation.

$$a = 10\log_{10}(P_{md}/P_m) = 10\log_{10}(4/H_d^2) = 10\log_{10}4 = 6.02 \text{ dB.} \qquad (40)$$

In a real system, we will have additional attenuation of the signal due to the propagation and the influence of noise and fading, which will further complicate the procedures of signal processing inside both the transmitter and the receiver.

Simulation of the receiver

We performed a simulation of the receiver presented in Figure 1.

The signals are generated in the time domain and the frequency domain. The demodulated signal obtained by simulation in the time domain and the frequency domain is presented in Figure 12.

The waveshapes of this signal are equivalent to the signals obtained by calculations and presented in Figure 8 and Figure 10.

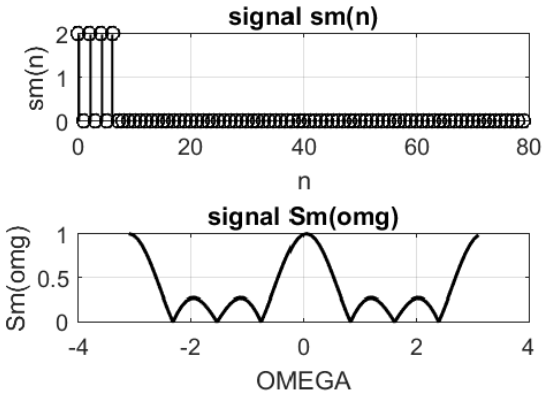

a)

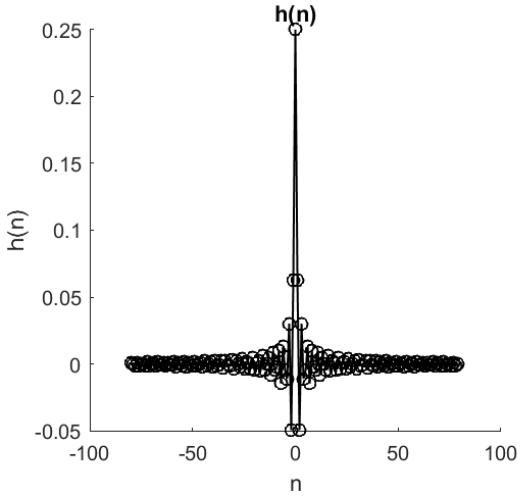

b)

Figure 12 − a) The demodulated signal, b) the impulse response of the LP filter for N = 8, $\Omega_F = \pi / 4$ and $H_d = 1$

Рис. 12 – а) Демодулированный сигнал, b) импульсная характеристика LP-фильтра для N = 8, $\Omega_F = \pi / 4$ и $H_d = 1$

Слика 12 – а) Демодулисани сигнал, б) импулсни одзив нископропусног филтера за N = 8, $\Omega_F = \pi / 4$ и $H_d = 1$

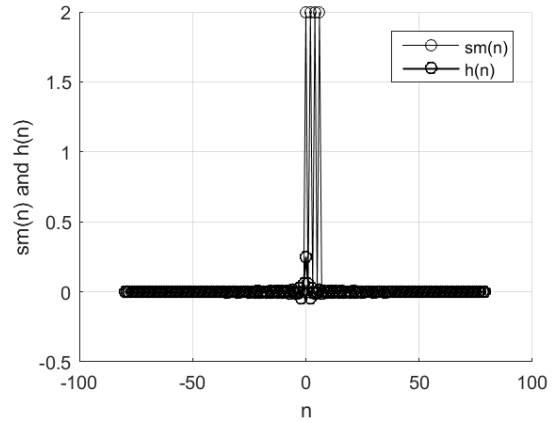

a)

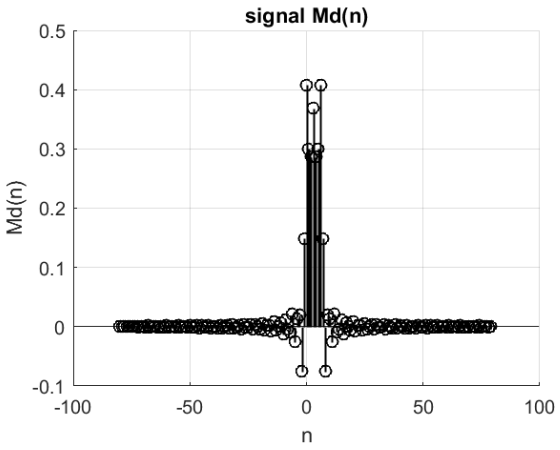

b)

Figure 13 − a) Convolution procedure of the demodulated signal and the impulse response, b) the output signal obtained by convolution
Рис. 13 – а) Процедура свертки демодулированного сигнала и импульсного отклика, b) выходной сигнал, полученный путем свертки
Слика 13 – а) Поступак конволуције демодулисаног сигнала и импулсног одзива, б) излазни сигнал након конволуције

The impulse response of the LP filter is presented in Figure 12b). The procedure of the correlation is presented in Figure 13a) while the waveshape of the LP filter output is presented in Figure 13b).

Correlation receiver implementation and operation

As we have seen, the demodulation of the discrete modulated signal using the LPF results in the discovery of the modulating signal that is in a form of a rectangular pulse. Based on the sign of the pulse received, the Decision Circuit decides on the binary value of the transmitted signal. For the positive pulse, it is said that 1 was transmitted and for the negative pulse, it is said that 0 was transmitted.

For the same structure of the transmitter, the procedure of demodulation takes place inside the correlation receiver as presented in Figure 1 (lower block on the right). The received signal is first multiplied by the carrier to get the signal sm(n) as in (27). This signal in the frequency domain is given by expression (28). The wave shape of this signal is shown in Figure 8. The samples of the signal are accumulated inside the correlator adder to get

$$m_d(N) = \sum_{n=0}^{N-1} s_m(n) = \sum_{n=0}^{N-1} \frac{1}{2} A(1+\cos 2\Omega_c n) = \sum_{n=0}^{N-1} \frac{1}{2} A + \sum_{n=0}^{N-1} \cos 2\Omega_c n = \frac{1}{2} AN \ . \quad (41)$$

The Decision Circuit decides on the $m_d(N)$ value and generates, at its output, 1 or 0 according to this decision rule

$$DC_{out} = \begin{cases} 1 & m_d(N) \geq 0 \\ 0 & m_d(N) < 0 \end{cases}. \quad (42)$$

If we send a stream of bits 1 and 0 (by changing the sense of the amplitude A inside $m(n)$) at the transmitter side, the receiver will generate the same stream at its output. Each bit will be generated at the time instants $i \cdot N$, where i is a set of natural numbers and N is the number of samplers in each discrete pulse $m(n)$. This is the case when noise is not present in the channel, i.e., the channel is noiseless. Therefore, in the system with a noiseless channel, the decision will always be correct in the Decision Circuit. Namely, if a positive pulse is transferred, meaning that the amplitude A is positive, the product (41) will be positive and the Decision Circuit will generate bit 1 (one) at the output. If a negative pulse is transmitted, the product (41) will be negative and the Decision Circuit will generate bit 0 (zero) at the output. We design transceiver blocks and use the noiseless channel to investigate the operation of the transceiver blocks only. When we are sure the blocks are operating properly, we add the channel simulator to investigate the properties of the whole system in real conditions. In the presence of noise, the sign of the product (41) can be changed due to the noise level and the wrong decision can be made.

Discrete communication system for the transmission of a filtered pulse

To reduce interference between communication systems, we can use filtering inside the transmitter. That filtering limits the spectrum of the transmitted signal. We will analyze the case when the modulating signal is filtered by an LPF and then transmitted through the transmitter circuits and received by the receiver circuits in the same way as explained in the previous sections. The block scheme of the transmitter with the LP filter is presented in Figure 14.

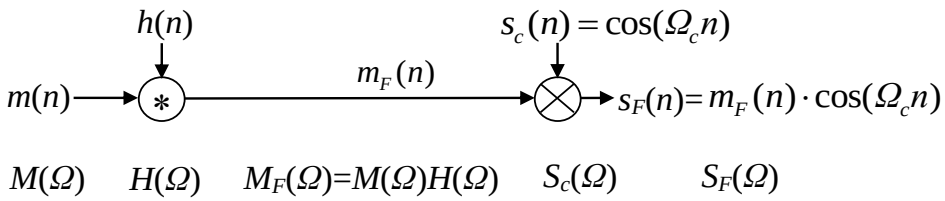

Figure 14 − Discrete-filtered pulse modulator
Рис. 14 – Импульсный модулятор с дискретной фильтрацией
Слика 14 – Модулатор дискретног и филтрираног пулса

At the input of the transmitter, there is a discrete rectangular pulse as in the previously analyzed transmitter. The pulse is already presented in the time domain and the frequency domain in the previous sections. At the output of the transmitter, there is the modulated signal $s_F(n)$ that corresponds to the modulated signal $s(n)$ in Figure 1.

The LP Filter operation. To limit the bandwidth of the signal, we will use an LPF of the gain H, which will filter out the first two arcades of the rectangular pulse defined by the cut-off frequency Ω_F, as shown in Figure 15. In this case, we will limit the power of the filtered pulse to 96.08 % of the pulse total power as calculated in (13). The filter transfer characteristic in the frequency domain is defined as

$$H(\Omega) = \begin{cases} H & |\Omega| \le \Omega_F = \pi/2 \\ 0 & \text{otherwise} \end{cases}. \qquad (43)$$

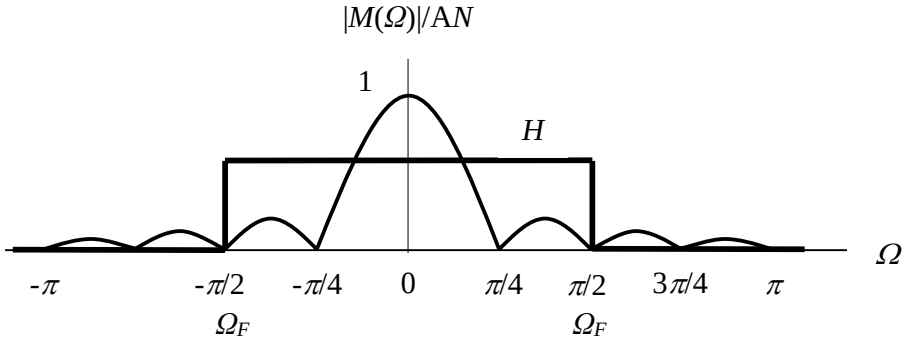

Figure 15 − Spectra of the rectangular pulse and the impulse response of the LP filter
Рис. 15 – Спектры прямоугольного импульса и импульсная характеристика LP-фильтра
Слика 15 – Спектар правоугаоног пулса и импулсног одзива нископропусног филтера

LPF output signal. The output of the filter is a bandlimited signal having the spectrum defined as

$$M_F(\Omega) = M(\Omega) \cdot H(\Omega) = \begin{cases} ANH & \Omega = 0 \\ AHe^{-j\Omega(N-1)/2} \dfrac{\sin \Omega N/2)}{\sin \Omega/2} & |\Omega| \le \Omega_F \end{cases}, \quad (44)$$

as presented in Figure 15 between the cut-off frequencies $-\Omega_F$ and $+\Omega_F$.

*Analysis of the filter operation in the time domain and the frequency domain***.** The filtering process is presented in the frequency domain as the multiplication of the amplitude spectral densities of the input signal *m*(*n*) and the impulse response *h*(*n*). This multiplication in the frequency domain corresponds to the convolution of the signals in the time domain.

Therefore, the filter output signal in the time domain $m_F(n)$ is the convolution of the filter impulse response *h*(*n*), which is the sinc function obtained as the discrete-time inverse Fourier transform (DTIFT) of the spectrum *H*(*Ω*), and the input signal *m*(*n*). The impulse response of the LP filter is calculated as

$$h(n)=\frac{1}{2\pi}\int_{-\pi}^{\pi}H(\Omega)e^{+j\Omega n}d\Omega=\frac{1}{2\pi}\int_{-\Omega_F}^{\Omega_F}He^{+j\Omega n}d\Omega=\frac{H}{2\pi}\frac{e^{+j\Omega n}}{jn}\Bigg|_{-\Omega_F}^{\Omega_F}$$

$$=\frac{H}{\pi n}\frac{e^{+j\Omega_F n}-e^{-j\Omega_F n}}{2j}=\frac{H\Omega_F}{\pi n\Omega_F}\sin\Omega_F n=\frac{H\Omega_F}{\pi}\operatorname{sinc}\Omega_F n \quad , (45)$$

$$\underset{\Omega_F=\pi/2}{=}\frac{H}{2}\operatorname{sinc}\pi n/2$$

having the zero crossings calculated as: $\sin(\pi n/2)=0,\ (\pi n/2)=k\pi,\ n=2k$, as shown in Figure 16.

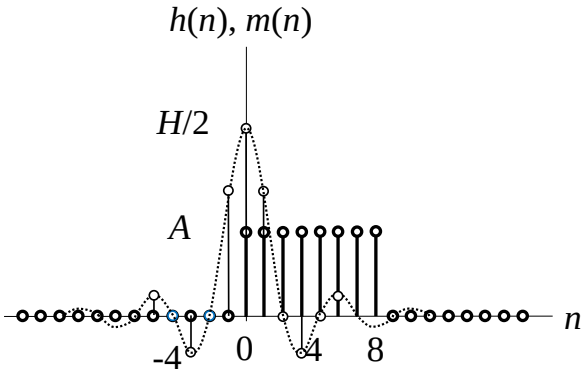

Figure 16 − Impulse response and the output of the ideal LP filter
Рис. 16 – Импульсная характеристика и выходной сигнал идеального LP-фильтра
Слика 16 – Импулсни одзив и излаз идеалног нископропусног филтера

The energy of the impulse response in the time domain can be calculated as

$$E_h=\sum_{n=-\infty}^{\infty}h^2(n)=\sum_{n=-\infty}^{\infty}\left[\frac{H}{2}\operatorname{sinc}\pi n/2\right]^2 \quad , \qquad (46)$$

and in the frequency domain

$$E_H=\frac{1}{2\pi}\int_{-\pi}^{\pi}\left|H(\Omega)\right|^2 d\Omega=\frac{H^2}{2\pi}\int_{-\pi/2}^{\pi/2}d\Omega=\frac{H^2}{2}. \qquad (47)$$

Berber, S., Mathematical modeling and simulation of a rectangular pulse transceiver operating in the discrete-time domain, pp.316-344

The filtered signal in the time domain is the convolution of the rectangular pulse *m*(*n*) and the impulse response *h*(*n*), i.e.,

$$m_F(n) = \sum_{l=-\infty}^{l=\infty} m(n-l)h(l) = \sum_{l=-\infty}^{l=\infty} h(n-l)m(l). \quad (48)$$

This convolution can be calculated if the values of the *sinc* function are calculated and represented by a series of numbers (sufficiently long) and then convolved with the values of *m*(*n*) represented by a finite series of ones. Since the discrete-time Fourier transform of the filtered signal is

$$M_F(\Omega) = \left\{ \begin{array}{cc} ANH & \Omega = 0 \\ AHe^{-j\Omega(N-1)/2} \dfrac{\sin \Omega N/2)}{\sin \Omega/2} & |\Omega| \le \Omega_F \end{array} \right\}, \quad (49)$$

the energy of the signal can be very accurately calculated as it has been already done in (13), i.e.,

$$E_{MF} \approx \frac{1}{2\pi} \int_{-\pi}^{\pi} \left| M_F(\Omega) \right|^2 d\Omega = \frac{A^2}{2\pi} \int_{-\pi/2}^{\pi/2} \left\| \frac{\sin \Omega N/2)}{\sin \Omega/2} \right\|^2 d\Omega = \frac{2}{\pi} 48.295 . \quad (50)$$

Having in mind that the carrier is expressed as $s_c(n) = \cos \Omega_c n$ and that it has 4 samples per oscillation, the spectrum of the modulated signal is a shifted version of the spectrum of the filtered rectangular pulse, i.e.,

$$\begin{aligned} S_F(\Omega) &= FT\{m_F(n)\cos \Omega_c n\} = \frac{1}{2} FT\left\{ m_F(n)(e^{j\Omega_c n} + e^{-j\Omega_c n}) \right\} \\ &= \frac{1}{2}[M_F(\Omega - \Omega_c) + M_F(\Omega + \Omega_c)] \end{aligned} \quad (51)$$

where

$$\frac{1}{2} M_F\left(\Omega - \Omega_c\right) = \left\{ \begin{array}{cc} ANH/2 & \left(\Omega - \Omega_c\right) = 0 \\ \dfrac{AH}{2} e^{-j(\Omega - \Omega_c)(N-1)/2} \dfrac{\sin\left(\Omega - \Omega_c\right) N/2}{\sin\left(\Omega - \Omega_c\right)/2} & |\Omega - \Omega_c| \le \Omega_F \end{array} \right\}, \quad (52)$$

and

$$\frac{1}{2} M_F\left(\Omega + \Omega_c\right) = \left\{ \begin{array}{cc} ANH/2 & \left(\Omega + \Omega_c\right) = 0 \\ \dfrac{AH}{2} e^{-j(\Omega + \Omega)(N-1)/2} \dfrac{\sin\left(\Omega + \Omega\right) N/2}{\sin\left(\Omega + \Omega\right)/2} & |\Omega + \Omega_c| \le \Omega_F \end{array} \right\}, \quad (53)$$

which is presented in Figure 17.

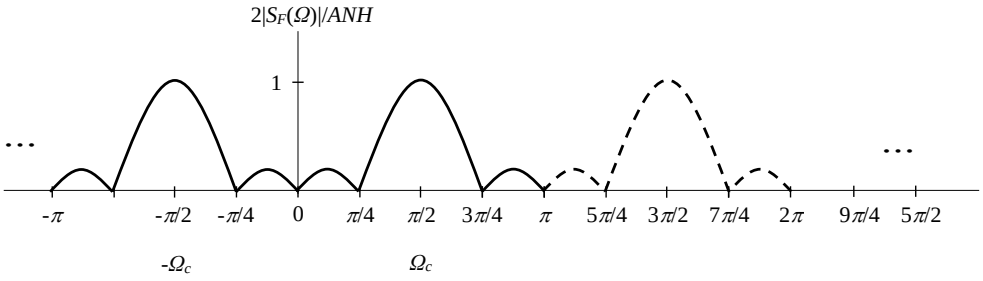

Figure 17 − Magnitude spectral density of the modulated filtered pulse
Рис. 17 – Спектральная плотность модулированного отфильтрованного импульса
Слика 17 – Спектрална густина магнитуде филтрираног модулисаног пулса

The spectrum of the modulated pulse, as a function of the angular frequency, is shown in Figure 17. The filtered modulated pulse in the time domain is a product of the filtered pulse and the carrier, i.e.,

$$s_F(n) = s_c(n) \cdot m_F(n) = \cos \pi n / 2 \cdot \sum_{l=-\infty}^{l=\infty} h(n-l)m(l) \qquad (54)$$

This is the modulated signal which has a limited bandwidth. This signal is transmitted through the channel and processed in the receiver as presented in the previous sections.

Conclusions

This paper presented a theoretical model and the simulation results of a discrete-time communication system. The block schematic of the system's transmitter and receiver is presented in the form of mathematical operators and all input-output signals are presented in both the time domain and the frequency domain. The powers and energies of the signals are calculated and the attenuation of the signals is analyzed.

Two types of transmitters are synthesized: one with an ideal rectangular discrete time pulse and one with a filtered rectangular pulse. It is shown that the application of a filter inside the transmitter reduces the modulating signal spectrum thus causing the reduction of the modulated signal bandwidth. Furthermore, two receivers are analyzed: a receiver that uses a low-pass filter for demodulation and a receiver that uses a correlator for received signal demodulation. All theoretical results are confirmed by simulations.

References

Abramowitz, M. & Stegun, I.A. 1972. *Handbook of Mathematical Functions with Formulas, Graphs, and Mathematical Tables.* Washington, D.C.: United States Department Of Commerce, National Bureau of Standards, Applied Mathematics Series – 55 [online]. Available at: https://personal.math.ubc.ca/~cbm/aands/frameindex.htm [Accessed: 20 January 2023].

Benvenuto, N., Corvaja, R., Erseghe, T. & Laurenti, N. 2007. *Communication Systems, Fundamentals and Design Methods*. Hoboken, NJ, USA: John Wiley & Sons, Inc. ISBN-13: 978-0470018224.

Berber, S. 2009. *Deterministic and Stochastic Signal Processing: Continuous and Discrete-time Signals.* VDM Verlag Dr. Müller. ISBN-13: 978-3639111880.

Berber, S. 2019. Discrete time domain analysis of chaos-based wireless communication systems with imperfect sequence synchronization. *Signal Processing*, 154, pp.198-206. Available at: https://doi.org/10.1016/j.sigpro.2018.09.010.

Berber, S. 2021. *Discrete Communication Systems*. Oxford, UK: Oxford University Press. ISBN-13: 978-0198860792.

Cavicchi, T.J. 2000. *Digital Signal Processing, Solutions Manual.* Hoboken, NJ, USA: John Wiley & Sons, Inc. [Accessed: 20 January 2023].

Haykin, S. 2001. *Digital Communication Systems, 4th edition.* Hoboken, NJ, USA: John Wiley & Sons, Inc. ISBN: 0-471-17869-1.

Ingle, V.K. & Proakis, J.G. 2012. *Digital signal processing using MATLAB, 3rd edition.* Stamford, CNT, USA: Cengage Learning. ISBN-13: 978-1-111-42737-5.

-Integral calculator. 2023. *Calculate integrals online − with steps and graphing!* [online]. Available at: https://www.integral-calculator.com [Accessed: 20 January 2023].

Manolakis, D.G., Ingle, V.K. & Kogan, S.M. 2005. *Statistical and Adaptive Signal Processing: Spectral Estimation, Signal Modeling, Adaptive Filtering and Array Processing, Illustrated edition*. Norwood, MA, USA: Artech House. ISBN-13: 978-1580536103.

Miao, G.J. 2007. *Signal Processing in Digital Communications*. Norwood, MA, USA: Artech House. ISBN 13: 978-1-58053-667-7.

Papoulis, A. & Pillai, S.U. 2002. *Probability, Random Variables, and Stochastic Processes, 4th edition.* McGraw-Hill Europe. ISBN-13: 978-0071226615.

Proakis, J.G. 2001. *Digital Communications, 4th edition.* McGraw Hill Higher Education. ISBN-13: 978-0071181839.

Quyen, N.X., Yem, V.V. & Duong, T.Q. 2015. Design and analysis of a spread-spectrum communication system with chaos-based variation of both phase-coded carrier and spreading factor. *IET Communications,* 9(12), pp.1466-1473. Available at: https://doi.org/10.1049/iet-com.2014.0907.

Rice M. 2009. *Digital Communications: A Discrete-time Approach*, *1st edition*. London, UK: Pearson Prentice Hall. ISBN-13: 978-0130304971.

Математическое моделирование и имитация передатчика прямоугольных импульсов в дискретом времени

Стеван М. Бербер

Университет Окленда,
Кафедра электротехники, вычислительной техники и программного обеспечения, г. Окленд, Новая Зеландия

РУБРИКА ГРНТИ: 50.07.03 Теория и моделирование вычислительных сред, систем, комплексов и сетей
ВИД СТАТЬИ: оригинальная научная статья

Резюме:

Введение/цель: В данной статье обсуждаются вопросы теории и разработки системы связи в дискретном времени, используемой для передачи импульсов дискретного времени с фильтрацией и без нее. Сигналы анализируются как во временной, так и в частотной областях.

Методы: Система теоретически проанализирована на основе блок-схемы, которая была представлена в виде математических операторов, по которым выполнено моделирование системы для подтверждения теоретических выводов.

Результаты: Сигналы дискретного времени представлены во временной и частотной областях, и подтверждены методом имитационного моделирования, разработанного в Matlab.

Выводы: Результаты данного исследования вносят вклад в теоретическое моделирование и разработку современных дискретных систем связи.

Ключевые слова: дискретная система связи, разработка системы, передатчик дискретных импульсов, фильтрация, корреляционный приемник.

Математичко моделовање и симулација примопредајника правоугаоних импулса за рад у дискретном времену

Стеван М. Бербер

Универзитет у Окланду,
Катедра за електротехнику, рачунарску и софтверску технику,
Окланд, Нови Зеланд

ОБЛАСТ: телекомуникације
КАТЕГОРИЈА (ТИП) ЧЛАНКА: оригинални научни рад

Сажетак:

Увод/циљ: У раду су приказани теорија и дизајн телекомуникационог сустема који ради у дискретном времену. Он се користи за пренос

Berber, S., Mathematical modeling and simulation of a rectangular pulse transceiver operating in the discrete-time domain, pp.316-344

филтрираног и нефилтрираног дискретног пулса. Сигнали су анализирани у временском и фреквенцијском домену.

Методе: Систем је теоријски анализиран на основу блок-шеме која је приказана у форми математичких оператора, према којој је извршена и симулација система како би се потврдили теоријски налази.

Резултати: Сигнали дискретног времена презентирани су у временском и фреквенцијском домену и потврђени симулацијом у Матлабу.

Закључак: Резултати овог рада доприносе теоријском моделовању и дизајну модерних дискретних комуникационих система.

Кључне речи: дискретни комуникациони систем, дизајн система, примопредајник дискретног пулса, филтрирање, корелациони пријемник.

Paper received on / Дата получения работы / Датум пријема чланка: 24.01.2023.
Manuscript corrections submitted on / Дата получения исправленной версии работы / Датум достављања исправки рукописа: 25.03.2023.
Paper accepted for publishing on / Дата окончательного согласования работы / Датум коначног прихватања чланка за објављивање: 27.03.2023.

Maximum electric field estimation in the vicinity of 5G base stations before their start-up

Aleksandar V. Lebl[a], *Djuradj* Budimir[b]

[a] IRITEL a.d., Department for Radiocommunications, Belgrade, Republic of Serbia,
e-mail: lebl@iritel.com, **corresponding author**,
ORCID iD: https://orcid.org/0000-0001-6544-6618

[b] University of Westminster, London, United Kingdom,
e-mail: d.budimir@westminster.ac.uk,
ORCID iD: https://orcid.org/0000-0002-7502-9129

DOI: 10.5937/vojtehg71-42426; https://doi.org/10.5937/vojtehg71-42426

FIELD: telecommunications
ARTICLE TYPE: original scientific paper

Abstract:

Introduction/purpose: This paper presents initial development of the procedure for electric field estimation in the vicinity of 5G base stations.

Methods: The procedure allows determination of future radiation levels before traffic is established over applied antenna systems on the basis of measured values of electric field levels caused by the signal forming Synchronization Signal Block. It is possible to perform necessary calculations for a very accurate estimation even if some important parameters of the radiation characteristics (such as the frequency span between the frequency carriers on the radio interface) are not a priori known. In this way, communication with mobile system operators before measurement is significantly simplified because operators do not need to know system technical details.

Results: The developed formula for electric field estimation is verified comparing the calculated values by its implementation to the practical results obtained by intensive measurements on a great number of 5G base stations in a highly developed country. The formula gives a pessimistic result, i.e. a higher electric field level than it is obtained by all such performed measurements.

Conclusion: This estimation allows mobile system operators to predict whether the electromagnetic field around base stations could be dangerous for human health when systems come to full operation while considering national and international recommendations dealing with radiation levels.

Key words: 5G electric field estimation, base station, Synchronization Signal Block, traffic beam, frequency subcarriers.

Introduction

Today mobile telephony becomes an unavoidable part of everyday life. It is hard to imagine everyday life and communication between people without mobile phones. People are exposed to electromagnetic radiation of mobile telephony base stations even when they do not use mobile phones. The number of mobile telephony base stations (BS) which are responsible for this radiation is constantly increasing. The final result of this increase is a growth of harmful effects of the electromagnetic radiation produced on all living beings (people). There is a consensus in science about some effects (first of all, when considering thermal effects) while the other, often much dangerous effects, are still in an investigation phase. This is a reason why electromagnetic field measurement according to international recommendations is often a research subject in the whole world. It is important to predict electromagnetic field levels before traffic is established, especially in the case of 5G systems implementation.

After this short introduction, Section II is a survey of the state of the art when considering already realized measurements for all system generations from 2G to 5G. This section also includes contributions and practical results in the same field which are the direct knowledge base for the presented investigation. Section III presents the procedure for determining the electric field in 5G systems. A formula for the electric field estimation which is developed in the Section III is then verified according to practical independent measurement results presented in the Section IV. Finally, the conclusions are in Section V.

State of the art

Measurements on different generations of mobile systems are numerous and the contributions presented in this paper are only a small part of them. It is important to notice that such measurements have been defined and realized in Serbia for a long time (Ilić et al, 2002). The main concept of frequency selective measurement based on the application of a spectrum analyzer which allows access to all existing frequency channels for measurements is presented in (Ilić et al, 2002). The same measurement principle is used also in (Hamid et al, 2003) where the results obtained by collecting data about GSM base stations radiation using directional and isotropic antennas are mutually compared. In other words, these two measurements are performed on the basis of an analysis based on a spectrum analyzer and a meter with a measuring probe. The results presented in (González & Infante Moreira, 2018) are

based on a specific limited set of measurements on two traffic channels of the GSM system at 850MHz and 1900MHz which allowed estimation of total radiation levels for complete GSM systems using statistical analysis on the basis of the measured mean value and the standard deviation of the electromagnetic field deviation.

Broadband measurements of base station electromagnetic radiation are applied besides frequency selective measurements (Bieńkowski et al, 2015). Broadband measurements are more rarely applied than frequency selective measurements, but the obtained measurement results are less exposed to the risk of statistical uncertainty. The authors in (Kurmaz et al, 2018) have developed a calculation model to estimate the total electric field on the basis of six frequency bands with the highest level with the accuracy of at least 95% to avoid broadband measurements.

Statistical uncertainty of the obtained results by frequency selective measurements is manifested both in the sense of space where a measurement is performed and in the sense of measurement time. Such investigations are the subject of analysis in (Watanabe & Hamada, 2017). It has been proven that measurement results, when considering spatial uncertainty for W-CDMA and LTE systems, do not depend on the surroundings (urban or rural) or the analyzed frequency band. The spatial uncertainty depending on the height from the ground level where a measurement is performed is also analyzed in (Watanabe & Hamada, 2017). When considering time uncertainty, it is shown that a measurement in shorter time intervals of only 10s does not significantly degrade the accuracy of the results comparing to a measurement in time intervals of 6 minutes according to international requests and this is very important to speed up the measurement procedure. Estimation of measurement uncertainty is also the subject of analysis in (Koprivica, 2016).

The coexistence of different mobile system generations at one location is typical nowadays; nevertheless, their base stations are on the same pillar or are placed at a short distance from each other (not greater than 20m). The main directives to realise measurements in such a case are emphasized in (Telecommunication Engineering Centre, 2021) when considering the coexistence of 2G, 3G and 4G systems. Additionally, discussions about malicious effects of new 5G systems on human health are very frequent today. However, the results of the measurements in (Ofcom, 2020) prove that levels of electromagnetic fields in the vicinity of 5G base stations are significantly lower than when considering previous generation systems and, also, that these levels for 5G are lower than it is allowed according to the international recommendations. A

comprehensive analysis in (Huang et al, 2022) further illustrates that there are sites which have even lower levels of electric fields, magnetic fields or power density after 5G system installation than before. The explanation may be that users of mobile systems of generations lower than 5G have switched to 5G systems where radiation is lower. The authors of (Huang et al, 2022) conclude that it is not sufficient to assume that 5G is a health hazard without epidemiological findings. When combining the results from (Huang et al, 2022) and the conclusion from (Şahín et al, 2013) that the safety distance from a base station is only 10m, we can conclude that radiation caused by base station operation is dangerous only in a high proximity to the base station which is further improved by the fact that radiation antennas are usually at the height greater than 10m thus decreasing the radius of health risk at the ground level.

Development of calculation methods to estimate electric field levels, especially in indoor conditions, is a major problem. The authors in (Lehmann et al, 2002) prove that a simple free space model gives very poor results when analyzing such indoor conditions. The free space model overestimates the real measured results. Besides, a disadvantage of the free space model is very low reproducibility and low standard deviation of the measured results comparing to a real situation.

The contributions (Matić & Paunović, 1995; Matić & Paunović, 1997; Matić et al, 2000; Lebl et al, 2017) dealing with the prediction of electromagnetic fields are the direct base which preceded the investigation presented in this paper. These fundamental considerations have included both a theoretical analysis to find an optimal selection procedure for prediction (Matić & Paunović, 1995; Matić & Paunović, 1997) and practical realization on the basis of digital signal processing algorithms (Matić et al, 2000). In the recent past, the contribution (Lebl et al, 2017) included the role of real telecommunication traffic processes in electric field level estimation in the vicinity of base stations. Practical realizations of measurement procedures are presented in (Tušup et al, 2022).

Electric field determination for 5G systems

Frequency selective measurement makes it possible to approximately determine the maximum electromagnetic radiation of base stations when all traffic channels are busy. One possible principle in the case that this method is applied is to measure the electromagnetic field only in channels where emission power is always constant and, for

systems from 2G to 4G, maximal. After this field level is measured, the total radiation is further determined by calculation. Very similar formulas are used for calculation in the case of GSM (2G), UMTS (3G) and LTE (4G) systems (European Committee for Electrotechnical Standardization, 2014). For GSM systems, the following formula is used:

$$E = \sqrt{n_{TRX}} \cdot E_{BCCH} \quad (1)$$

where E_{BCCH} is the electric field level which originates from always active channels on the first carrier (Broadcast Control Channel – *BCCH*) and n_{TRX} is the number of available frequency carriers. Similar formulas for UMTS systems and LTE systems are presented in (European Committee for Electrotechnical Standardization, 2014; RATEL, 2018) where the power coefficient (n_P) is used instead of n_{TRX} for other types of mobile systems instead of GSM. Typical maximum values of coefficients under the square root in equations as (1) are presented in (W-Line, 2021). The formulas in these three emphasized cases imply that power control in traffic channels as a function of mutual distance between a base station and mobile stations is not applied and that all traffic channels are always busy. In such a way, it is achieved that the final result is directed to the safe side: the calculated field is higher than it will be in reality.

The expected forms of the electromagnetic field when 5G systems are applied are shown based on the analysis given in (Franci et al, 2020a; Franci et al, 2020b). Before showing the shape of the signal itself, the basic characteristics of the 5G signal that affect the shape of the signal will be mentioned.

In the time domain, the duration of the basic frame of the 5G signal is 10ms (as is also the case when 4G signals are implemented). This frame is divided to 10 subframes of 1ms duration. Each of these subframes is split to 2^{μ} slots where it is μ=0, 1, 2, 3 or 4. Each slot consists of 14 or, in some cases, 12 Orthogonal Frequency Division Multiplexing (OFDM) symbols. The applied modulation types correspond to those ones at 4G systems: Binary Phase Shift Keying - BPSK, Quadrature Phase Shift Keying – QPSK, Quadrature Amplitude of order 16, 64, 256 – 16QAM, 64QAM, 256QAM.

There are two ranges in the frequency domain dedicated to 5G signals. The first one (Frequency Range 1 – FR1) covers the frequency range 450MHz – 7125MHz and the second one (Frequency Range 2 – FR2) covers the frequency range 24GHz-50GHz. The further analysis will deal with FR1 as in Serbia the frequency range reserved for 5G systems is 3.4-3.8GHz.

The frequency bandwidth intended for one 5G system is 100MHz. This available frequency range is separated to a number of frequency subcarriers whose number depends on the frequency span between the defined subcarriers. This span is directly proportional to the symbol transmission rate in a subframe. That is why it may be expressed as $2^{\mu}\cdot$15kHz. Considering the already emphasized values of μ in the range 0 to 4, the total number of subcarriers would be between $n_{scmax}\approx$6660 (when it is μ=0) and $n_{scmin}\approx$408 (when it is μ=4). The subcarriers are grouped into groups of 12 adjacent ones which form one Resource Block – RB.

It is very important to perform the first electromagnetic field measurements for 5G systems before their operation start-up. In such situations, only a signal in the Synchronization Signal/Physical Broadcast Channel (SS/PBCH) may be expected to exist. This signal is also called the Synchronization Signal Block (SSB). It consists of the Synchronization Signal (SS), the Physical Broadcast Channel (PBCH), and the Physical Broadcast Channel Demodulation Reference Signal (PBCH-DMRS) which is used as a reference signal for decoding the PBCH. This signal takes four symbols in the time domain and n_{scSSB}=240 mutually adjacent subcarriers (or 20 RB) in the frequency domain.

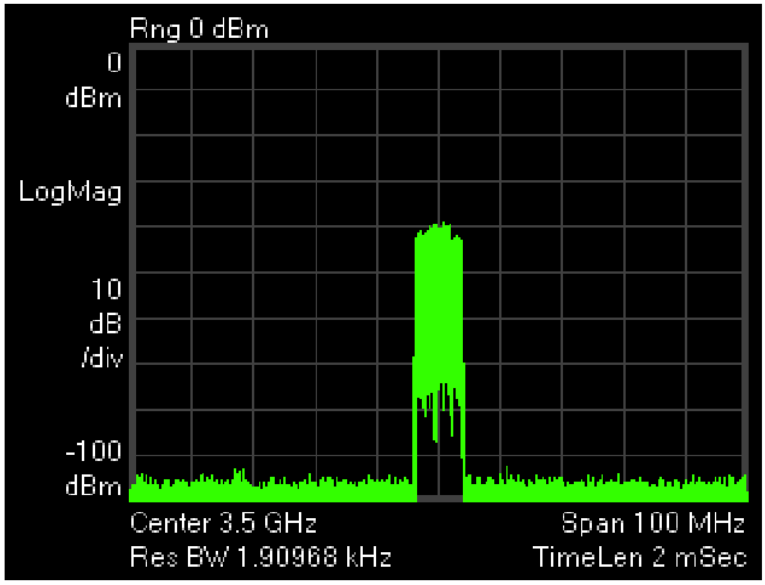

Figure 1 – SSB signal in the frequency domain, i.e. a 5G signal when there is no traffic
Рис. 1 – Сигнал SSB в частотной области, т.е. сигнал 5G при отсутствии трафика
Слика 1 – SSB сигнал у фреквенцијском домену, односно 5G сигнал пре успостављања саобраћаја

The specific shape of the SSB signal in the frequency domain is presented in Figure 1 (Franci et al, 2020b). This is also the shape when there is no traffic because the SSB signal is the only signal which then exists in the 5G subframe. Such a signal is also obtained when electric field intensity is recorded. The total frequency bandwidth where significant frequency components are registered is 7.2MHz (in relation to the whole bandwidth 100MHz for one 5G system). It, further, means that the total frequency span between two adjacent frequency subcarriers is 7.2MHz/240=30kHz or, in other words, it is μ=1. The frequency bandwidth of the SSB signal for other values of μ will be different.

If the value of μ is thus determined, this also determines the total number of frequency subcarriers which are used to calculate the value of the total electric field on the basis of the measured electric field with no traffic.This number is ≈3330, in accordance with the previous considerations. It is necessary first to measure the signal in the frequency band which corresponds to the SSB signal.

Starting from (1), the maximum value of the electric field for 5G systems only on the basis of the measured field caused by the SSB signal in a general case of any value of μ may be expressed as

$$E_{5G} = k_s \cdot \sqrt{\frac{n_{sc\max}}{n_{scSSB} \cdot 2^{\mu}}} \cdot E_{SSB} \tag{2}$$

or, in other words,

$$E_{5G} = k_s \cdot \sqrt{\frac{27.5}{2^{\mu}}} \cdot E_{SSB} \tag{3}$$

In these equations, E_{SSB} is the value of the electric field caused only by the SSB signal and k_s is the coefficient which has to be applied to multiply the obtained field value because traffic channels do not have the same power at the receiving point as the SSB channels. Among all available SSB channels, the one which causes the maximum electric field is selected. The concrete value under the square root in (3) follows from the previous consideration that 240 subcarriers form one SSB signal and the maximum electric field at the place of reception would appear in a very unreal traffic situation that all available $6660/2^{\mu}$ subcarriers are transmitted to only one user. Equations (2) and (3) are based on the analyses and formulas from (Migliore, 2022). A more accurate (but very approximate) value of the number under the square root may be found according to (Malaysian Technical Standards Forum Bhd, 2021).

There is also another important characteristic which has to be emphasized when 5G signals are transmitted: implementation of antennas whose radiation pattern is variable (not fixed). The optimal beamforming for different signals in the 5G subframe is achieved in this way. When the SSB signal is considered, it is transmitted using several radiation beams in fixed, a priori defined directions to allow all users in the area around the base station to detect some of these signals in an adequate way. When traffic channels are the subject of analysis, a radiation beam is separately formed for each user (in a direction towards him) to allow optimal signal detection. The beams for SSB signals are considerably wide to allow for greater space to be covered by one beam. On the contrary, traffic beams are very narrow to decrease interference from other traffic channels at the receiving side as much as possible. This whole analysis is illustrated by Figure 2.

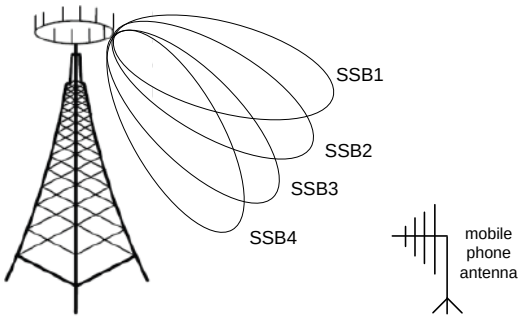

a)

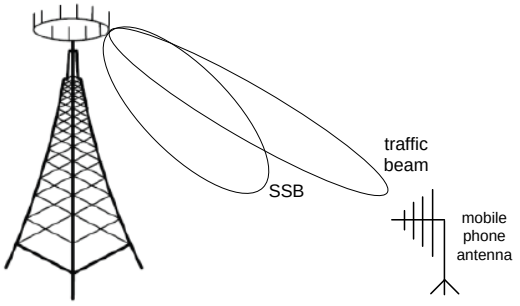

b)

Figure 2 – Beamforming in the case of: a) SSB signals; b) traffic channel compared to SSB signals
Рис. 2 – Формирование пучка излучения в случаях: а) сигналов SSB; б) канала трафика по сравнению с сигналами SSB
Слика 2 – Формирање снопа зрачења у случају: а) SSB сигнала; б) саобраћајног канала у поређењу са SSB сигналом

Figure 2a) presents the radiation pattern for SSB signals which is formed, for example, when a 4-fold beam (SSB1 ... SSB4) is transmitted and when each of these 4 beams is transmitted in a different period of time. The maximum number of SSB beams is 8 for the frequency band 3-6GHz, which is used in Serbia for 5G systems (Migliore, 2022). After that, Figure 2b) presents the relation of two beams: the SSB signal beam and the traffic channel signal beam. As the beam corresponding to the traffic signal is directed directly towards a user, in the case without the applied power control, its level at the receiving side will be higher than the level of the SSB signal. The other important consequence of high directivity of traffic beams is that the electric field level is significantly lower when there is traffic to more than one user and thus distant users have very small influence on the electric field at the place of the considered user. This is the reason why the value of k_s in equations (2) and (3) calculated for some specific user depends primarily on (besides traffic) the antenna radiation pattern for SSB signals, i.e. on the angle between the direction of the maximum SSB signal from a BS and the direction of a BS towards a user. The value of k_s also depends on the ratio of the maximum radiation signals (at 0º of the radiation pattern) for SSB signals and traffic signals. The data about the radiation pattern of active antennas applied for 5G systems are limited or often even not supplied (Migliore, 2022). In such conditions, the antenna characteristics from (Biscontini, 2021), presented in Figure 3, could be incorporated in the procedure of k_s calculation.

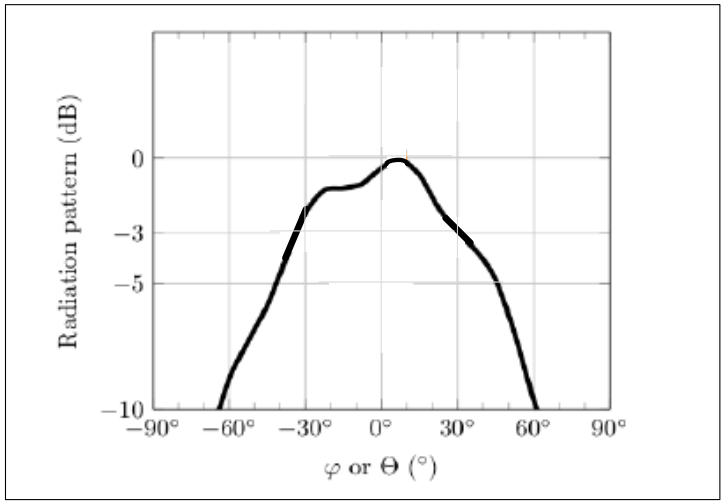

Figure 3 – Example of the radiation pattern of SSB signals (Biscontini, 2021)
Рис. 3 – Пример диаграммы направленности сигналов SSB (Biscontini, 2021)
Слика 3 – Пример дијаграма зрачења SSB сигнала (Biscontini, 2021)

The maximum value of k_s depends on the antenna radiation pattern attenuation at the α_{max} angle ($a_{\alpha max}$) where the SSB signal has the maximum attenuation and the ratio of the traffic signal beam amplitude and the SSB signal beam amplitude (r_{tSSBb}), i.e. their values at the angle 0° of the radiation pattern. Or, in other words,

$$k_s = a_{\alpha \max} \cdot r_{tSSBb} \tag{4}$$

The implemented SSB beams must cover the whole area around a BS to allow all users to receive some of SSB signals. When considering the azimuth (φ), it is 360° and when considering the elevation (θ), it is 180°. This space is in this analysis covered by only four antennas. The beams of these four antennas are directed from the BS tower down at the angle of 45° in relation to the horizontal plane. In such a case, the maximum angle between the highest radiation direction and the user position towards the BS for the nearest SSB signal is $\alpha_{max} \approx 60°$ (OnlineMSchool, 2023). If the radiation pattern such as the one from Figure 3 is applied, the maximum BSS signal attenuation comparing to its peak would be about 10dB ($a_{\alpha max}$=3.16). With the maximum number of 8 beams, this angle would be even lower, but a further calculation will include the worst situation of four antennas.

When dealing with the r_{tSSBb} factor, its estimation is very complex (Adda et al, 2020). The factors which have influence on r_{tSSBb} are reflections, scattering objects around the measurement point, the fact that considered point may be in a Not Line of Sight (NLOS), implemented propagation model, etc. However, the analysis performed in (Adda et al, 2020)] (Figure 7) pointed out that it is $r_{tSSBb} \leq 10$dB, or again $r_{tSSBb} \leq 3.16$. This analysis presented by Figure 7 in (Adda et al, 2020) is limited to free space (Figure 7a) and to the case of free space with added one conducting plane at a significant distance (Figure 7b).

The influence of reflection as a very important factor which increases the electric field should be further modelled. One possibility is to increase the value of r_{tSSBb} by its multiplication with the factor 1+Γ:

$$r_{tSSBb\Gamma} = r_{tSSBb} \cdot (1 + \Gamma) \tag{5}$$

where Γ is the coefficient of surface reflection (W-Line, 2021) and $r_{tSSBb\Gamma}$ is the ratio of the traffic signal beam amplitude to the SSB signal beam amplitude modified by the influence of the reflection coefficient.

The value of Γ is 0.3 in urban surroundings or 0.6 in rural surroundings. Practical importance of the influence of reflection is illustrated in (Conil & Agnani, 2020). Now, taking the value Γ=0.6, the estimated value of the factor ks is ks≤16. Formula (3) may be simplified to:

$$E_{5G} \leq \frac{84.29}{\sqrt{2^{\mu}}} \cdot E_{SSB} \tag{6}$$

Comment about the estimation results reliability on the basis of measurement results

The reliability of formula (6) may be verified on the basis of the results presented in (Agence nationale des fréquences, 2020). The value of the coefficient k_s used to multiply the measured electric field (E_{SSB}) before traffic is established in order to predict the maximum electric field after traffic is established is determined according to the measurement results presented in (Agence nationale des fréquences, 2020) and compared to the corresponding value in (6).

It is emphasized in (Agence nationale des fréquences, 2020) that the applied systems have μ=1, i.e. the frequency gap between carriers is 30 kHz. The value of k_s for such a case in (6) is 59.78. The corresponding values according to the table in the Executive summary of (Agence nationale des fréquences, 2020) are 45 maximum. This means that this paper's estimation is oriented towards the “safe side” i.e. it gives a higher electric field than it is in reality.

Conclusions

The main contribution of this paper is the development of a formula to calculate the maximum electric field for 5G mobile systems. The formula is implementable first of all to predict the field level in the phase before traffic is established. The prediction is based on the measured value of the electric field caused by the SSB signal which is the only signal that exists when there is no traffic. The formula development for 5G systems is based on similar known formulas for other generation systems and it is developed on similar principles. The obtained formula is verified on the basis of the measurement results performed in a highly developed country (Agence nationale des fréquences, 2020; Conil & Agnani, 2020) following a similar procedure as the one presented in this investigation. The analysis is performed in the theoretical sense but it is intended for future practical estimation of measurement results.

References

Adda, S., Aureli, T., D'Elia, S., Franci, D., Grillo, E., Migliore, M.D., Pavoncello, S., Schettino, F. & Suman, R. 2020. A Theoretical and Experimental Investigation on the Measurement of the Electromagnetic Field Level Radiated by 5G Base Station. *IEEE Access*, 8, pp.101448-101463. Available at: https://doi.org/10.1109/ACCESS.2020.2998448.

-Agence nationale des fréquences (ANFR). 2020. *Assessment of the exposure of the general public to 5G electromagnetic waves, Part 2: first measurement results on 5G pilots in the 3,400-3,800 MHz band, First exposure measurement results on 5G 3.4 GHz – 3.8 GHz pilots* [online]. Available at: https://www.anfr.fr/fileadmin/mediatheque/documents/5G/20200410-ANFR-rapport-mesures-pilotes-5G-EN.pdf [Accessed: 20 January 2023].

Bieńkowski, P.P., Cała, P.M. & Zubrzak, B. 2015. Optimization of measurement methods for a multi-freque electromagnetic field from mobile phone base station using broadband EMF meter. *Medycyna Pracy*, 66(5), pp.701-712. Available at: https://doi.org/10.13075/mp.5893.00206.

Biscontini, B. 2021. Recommendation on Base Station Active Antenna System Standards, version 2.0. *NGMN Alliance* [online]. Available at: https://www.ngmn.org/publications/recommendation-on-base-station-active-antenna-system-standards.html [Accessed: 20 January 2023].

Conil, E. & Agnani, J.-B. 2020. Evaluation of exposure induced by a 5G antenna in the 3,4-3,8 GHz band, Future Networks: 5G and beyond. *U.R.S.I. France* [online]. Available at: https://ursifr-2020.sciencesconf.org/306820/document [Accessed: 20 January 2023].

-European Committee for Electrotechnical Standardization. 2014. *European Standard EN 50492: 2008/A1:2014: Basic standard for the in-situ measurement of electromagnetic field strength related to human exposure in the vicinity of base stations, CENELEC*. European Committee for Electrotechnical Standardization.

Franci, D., Coltellaci, S., Grillo, E., Pavoncello, S., Aureli, T., Cintoli, R. & Migliore, M.D. 2020a. Experimental Procedure for Fifth Generation (5G) Electromagnetic Field (EMF) Measurement and Maximum Power Extrapolation for Human Exposure Assessment. *Environments*, 7(3), art.number:22, pp.1-15, Available at: https://doi.org/10.3390/environments7030022.

Franci, D., Coltellaci, S., Grillo, E., Pavoncello, S., Aureli, T., Cintoli, R. & Migliore, M.D. 2020b. An Experimental Investigation on the Impact of Duplexing and Beamforming Techniques in Field Measurements of 5G Signals. *Electronics*, 9(2), art.number:223, pp.1-22. Available at: https://doi.org/10.3390/electronics9020223.

González, F.G. & Infante Moreira, P.S. 2018. Assessment of the real public exposure to base stations over a day from instantaneous measurement. *RIELAC Revista de Ingeniería Electrónica, Automática y Comunicaciones*, 39(2), pp.1-9 [online]. Available at: https://rielac.cujae.edu.cu/index.php/rieac/article/view/594 [Accessed: 20 January 2023].

Hamid, R., Çetintaş, M., Karacadağ, H., Gedik, A., Yoğun, M., Çelik, M. & Fırlarer, A. 2003. Measurement of Electromagnetic Radiation from GSM Base Stations. In: *2003 IEEE International Symposium on Electromagnetic Compatibility, 2003. EMC '03*, Istanbul, Turkey, pp.1211-1214, May 11-16. Available at: https://doi.org/10.1109/ICSMC2.2003.1429136.

Huang, W., Hu, Y., Zhu, J., Cen, Z. & Bao, J. 2022. The Measurement and Evaluation of the Electromagnetic Environment from 5G Base Station. *Detection*, 9(1), pp.1-11. Available at: https://doi.org/10.4236/detection.2022.91001.

Ilić, S., Nešković, A. & Simić, M. 2002. System for automatic electric field level, level and power measurements based on field analyzer PROTEK 3201. In: *10th Telecommunication Forum TELFOR 2002*, Belgrade, November 26-28.

Koprivica, M.T. 2016. *Improving the efficiency of methods for measurement of electric field strength in the vicinity of public mobile system base stations.* Ph.D. thesis. Belgrade, Serbia: University of Belgrade, School of Electrical Engineering (in Serbian) [online]. Available at: https://nardus.mpn.gov.rs/handle/123456789/6140 [Accessed: 20 January 2022].

Kurmaz, C., Yildiz, D. & Karagol, S. 2018. Assessment of short/long term electric field strength measurements for pilot district. *Open Physics*, 16(1), pp.69-74. Available at: https://doi.org/10.1515/phys-2018-0013.

Lebl, A.V., Mileusnić, M., Mitić, D., Matić, V., Pavić, B. & Markov, Ž. 2017. Influence of traffic process characteristics on the electric field in GSM base station cell. In: *International Scientific Conference „Unitech 2017“*, Gabrovo, Bulgaria, pp.II-62-67, November 17-18 [online]. Available at: https://unitech-selectedpapers.tugab.bg/images/papers/2017/s3/s3_p24.pdf [Accessed: 20 January 2023].

Lehmann, H., Eicher, B. & Fritschi, P. 2002. Indoor Measurements of the Electric Field Close to Mobile Phone Base Station. In: *Proceedings of 27th triennial General Assembly of the International Union of Radio Science*, Maastricht, The Netherlands, URSI: paper 2112, pp.1-4 [online]. Available at: http://old.ursi.org/proceedings/procGA02/papers/p2112.pdf [Accessed: 20 January 2023].

-Malaysian Technical Standards Forum Bhd. (MTSFB) 2021. *Technical code: Prediction and measurement of RF EMF exposure from base station, MCMC MTSFB TC G032: 2021*. Cyberjaya, Selangor, Malaysia: Malaysian Technical Standards Forum [online]. Available at: https://www.mcmc.gov.my/skmmgovmy/media/General/registers/MCMC-MTSFB-TC-G032_2021-Prediction-and-Measurement-of-RF-EMF-Exposure-from-Base-Station.pdf [Accessed: 20 January 2023].

Matić, V. & Paunović, Đ. 1995. A choice of the suitable field strength prediction method in Belgrade urban area at 950MHz. In: *39th Conference Etran*, Zlatibor, Serbia, pp.36-39, June 6-9 (in Serbian).

Matić, V. & Paunović, Đ. 1997. A comparison of prediction methods for 900 MHz urban mobile radio propagation. In: *Proceedings of ICICS, 1997 International Conference on Information, Communications and Signal*

Processing. Theme: Trends in Information Systems Engineering and Wireless Multimedia Communications, Singapore, 3, pp.1696-1700, September 12. Available at: https://doi.org/10.1109/ICICS.1997.652284.

Matić, V., Pavić, B. & Tadić, V. 2000. The implementation of digital signal processing for automatic recognition of radio emission type and spectrum occupancy analysis. In: *Proceedings of the 2000 Third IEEE International Caracas Conference on Devices, Circuits and Systems (Cat. No.00TH8474)*, Cancun, Mexico, pp.T55/1-6, March 17. Available at: https://doi.org/10.1109/ICCDCS.2000.869877.

Migliore, M.D. 2022. 5G Field level measurement for human exposure assessment: A lesson for 6G. *IOP Conference Series: Material Science and Engineering ICEMS-BIOMED-2022*, 1254, art.number:012001. Available at: https://doi.org/10.1088/1757-899X/1254/1/012001.

-Ofcom. 2020. *Electromagnetic Field (EMF) measurements near 5G mobile phone base stations - Summary of results, Technical Report*, pp.1-10. London, UK: Ofcom [online]. Available at: https://www.ofcom.org.uk/__data/assets/pdf_file/0015/190005/emf-test-summary.pdf [Accessed: 20 January 2023].

-OnlineMSchool. 2023. calcu. Angle between vectors. *OnlineMSchool* [online]. Available at: https://onlinemschool.com/math/assistance/vector/angl/ [Accessed: 20 January 2023].

-RATEL-The Regulatory Agency for Electronic Communications and Postal Services of the Republic of Serbia. 2018. *An Overview of the Telecom and Postal Services Market in the Republic of Serbia in 2017, Section 6: Public Mobile Telecommunications Networks and Services*. Belgrade: RATEL [online]. Available at: https://www.ratel.rs/uploads/documents/empire_plugin/pregled%20trzista%20eng%20s%20koricama_manji.pdf [Accessed: 20 January 2023].

Şahín, M.E., As, N. & Karan, Y. 2013. Selective Radiation Measurement for Safety Evaluation on Base Station. *Gazi University Journal of Science*, 26(1), pp.73-83 [online]. Available at: https://dergipark.org.tr/en/pub/gujs/issue/7426/97576 [Accessed: 20 January 2023].

-Telecommunication Engineering Centre, New Delhi. 2021. *Test Procedure for Electromagnetic fields from Base Station Antenna No: TEC 13019:2021.* New Delhi, India: Telecommunication Engineering Centre, Division: Radio [online]. Available at: https://dot.gov.in/sites/default/files/Annexure%20to%20letter%20dated%2027-08-2021.pdf?download=1 [Accessed: 20 January 2023].

Tušup, C., Matić, V. & Lebl, A. 2022. Postupak merenja elektromagnetnog polja u okolini stanica mobilne telefonije. In: *Šesti dani elektroinženjera Inženjerske komore Crne Gore*, Podgorica, Montenegro, October 18-19 (in Serbian).

-W-Line Laboratorija. 2021. *Stručna ocena opterećenja životne sredine u lokalnoj zoni bazne stanice mobilne telefonije "Ovča 2" -*

BG142/BGU142/BGL142/BGO142 (in Serbian). Belgrade: W-Line Laboratorija [online]. Available at: https://www.beograd.rs/images/file/0bd5f6fe767f54448fb252c5885eb514_6007050804.pdf [Accessed: 20 January 2023].

Watanabe, S. & Hamada, L. 2017. Measurements of the Electromagnetic Field from a Mobile Phone Base Station. *Journal of the National Institute of Information and Communications Technology* (Special Issue on Calibration and Testing Technologies for Radio Equipment), 63(1), pp.213-231 [online]. Available at: https://www.nict.go.jp/publication/shuppan/kihou-journal/journal-vol63no1/journal-vol63no1-03-04.pdf [Accessed: 20 January 2023].

Оценка максимального электрического поля вблизи базовых станций 5G до ввода в эксплуатацию

Александар В. Лебл[а], *Джурадж* Будимир[б]

[а] АО „ИРИТЕЛ», отделение радиосвязи,
г. Белград, Республика Сербия, **корреспондент**

[б] Вестминстерский университет, г. Лондон, Великобритания

РУБРИКА ГРНТИ: 49.33.29 Сети связи
ВИД СТАТЬИ: оригинальная научная статья

Резюме:

Введение/цель: В данной статье представлена первоначальная разработка процедуры оценки электрического поля вблизи базовых станций 5G.

Методы: Процедура позволяет определять будущий уровень излучения до установления трафика по применяемым антенным системам, на основании измеренных значений уровней электрического поля, вызванных сигналами, образованными блоком сигналов синхронизации. Такой подход дает возможность выполнять необходимые вычисления для сверхточной оценки, даже когда важные параметры и характеристики излучения (такие как диапазон частот между несущими частотами на радиоинтерфейсе) неизвестны. Таким образом, связь с операторами мобильной системы перед измерением значительно упрощается, поскольку операторам необязательно знать технические детали системы.

Результаты: Верификация разработанной формулы для оценки электрического поля произведена путем сравнения вычисленных значений при ее внедрении с практическими результатами, полученными в результате интенсивных измерений на большом количестве базовых станций 5G в высокоразвитой стране. Формула дает пессимистичный результат, т.е. показывает

более высокий уровень электрического поля, чем при всех выполненных измерениях.

Выводы: Благодаря данной оценке операторы мобильных систем могут прогнозировать, будет ли электромагнитное поле вокруг базовых станций при полном введении в эксплуатацию представлять угрозу здоровью человека, с учетом национальных и международных рекомендаций, касающихся уровня излучения.

Ключевые слова: оценка электрического поля 5G, базовая станция, блок сигналов синхронизации, пучок излучения, частотные поднесущие.

Процена максималне јачине електричног поља у близини базне станице 5G технологије пре њеног пуштања у рад

Александар В. Лебл[а], *Ђурађ* Будимир[б]

[а] ИРИТЕЛ а.д., Одељење за радио-комуникације, Београд, Република Србија, **аутор за преписку**

[б] Универзитет Вестминстер, Лондон, Уједињено Краљевство

ОБЛАСТ: телекомуникације
КАТЕГОРИЈА (ТИП) ЧЛАНКА: оригинални научни рад

Сажетак:

Увод/циљ: У раду је приказан почетни развој процедуре за процену јачине електричног поља у близини базне станице 5G технологије.

Методе: Процедура омогућава одређивање будућег нивоа зрачења на основу измереног нивоа електричног поља узрокованог сигналом који формира блок синхронизационих сигнала пре него што се успостави саобраћај преко примењеног антенског система. Могуће је извршити потребне прорачуне ради врло тачне процене, чак и ако неки важни параметри карактеристике зрачења (као што је размак фреквенција између фреквенцијских носилаца на радио-интерфејсу) нису унапред познати. На тај начин је, пре самог мерења, знатно поједностављен процес комуникације са оператором мобилног система јер он не мора познавати детаље техничких података о систему.

Резултати: Изведена формула за процену јачине електричног поља верификована је поређењем њених резултата са практичним резултатима добијеним интензивним мерењима на великом броју базних станица 5G технологије у једној високоразвијеној земљи. Формула даје песимистичан резултат, односно показује виши ниво електричног поља од онога који се добија у свим реализованим мерењима.

Закључак: Ова процена омогућава оператору мобилног система да предвиди да ли би електромагнетно поље у околини базне станице могло да буде опасно за људско здравље када систем ради пуним капацитетом, узимајући у обзир националне и интернационалне препоруке које се односе на ниво зрачења.

Кључне речи: процена електричног поља 5G технологије, базна станица, блок синхронизационих сигнала, саобраћајни сноп зрачења, фреквенцијски подносиоци.

Paper received on / Дата получения работы / Датум пријема чланка: 25.01.2023.
Manuscript corrections submitted on / Дата получения исправленной версии работы / Датум достављања исправки рукописа: 23.03.2023.
Paper accepted for publishing on / Дата окончательного согласования работы / Датум коначног прихватања чланка за објављивање: 25.03.2023.

A more advanced theoretical model of the sphere earth's EM in a foreign homogeneous EM field

Slobodan N. Bjelić[a], *Nenad* A. Marković[b]

[a] University of Priština – Kosovska Mitrovica, Faculty of Technical Sciences, Kosovska Mitrovica, Republic of Serbia,
e-mail: slobodanbjelic49@yahoo.com,
ORCID iD: https://orcid.org/0000-0001-5642-8936

[b] Kosovo and Metohija Academy of Applied Studies,
Department Uroševac – Leposavić, Leposavić, Republic of Serbia,
e-mail: nen.mark74@yahoo.com, **corresponding author**,
ORCID iD: https://orcid.org/0000-0001-6960-1953

DOI: 10.5937/vojtehg71-42923;https://doi.org/10.5937/vojtehg71-42923

FIELD: Theoretical electrical engineering, electromagnetics
ARTICLE TYPE: original scientific paper

Abstract:

Introduction/purpose: The paper describes a more advanced theoretical model of the Earth's EM field based on two-component hypotheses. A defined mathematical model that shows the rotation of the magnetically conducting sphere of Tthe magnetization M in a foreign magnetic field and the components of the magnetic field that may arise due to the rotation of the Earth around its axis. According to the established model, in relation to the reference values of the planet Earth, the values of the components of the other planets in the solar system were calculated and the results were tabulated.

Methods: The solution to the problem highlighted in the title of the paper was determined using the combined, for that purpose, formalized methods of physics and mathematical analysis, in order to develop a new, more advanced mathematical model. For this purpose, the method of analogy was used, related to the application of similar structural forms and systems for researching electromagnetic processes and planetary rotation. The method of analogy was applied for two interrelated reasons. The first one is that all values that characterize the function of any natural system are subject to change, and the second one is that the applied solutions do not determine the conditions of the structure's function in each specific case.

Results: The solutions in the form of original analytical formulas and numerical values arranged in Table 2, referring to the influence of the rotation of the planets and especially the Earth, will be applied to research the effects of the EM field emitted by the Sun towards the planets,

especially the role that the process plays in protecting the planet Earth. The results given in Table 2 are particularly important.

Conclusion: The paper discusses the appearance and effect of the Earth's EM field in a way that is understandable at the current level of scientific development. Scientific findings in science and measurements in geo- and astrophysics indicate the Sun as a possible source of the EM field that extends through interplanetary space and the component of the Earth's magnetic field is only a response to the influence of that source. Natural phenomena and processes on the Earth can be defined in system theory by a model that contains changes in the parameters of the state of the planet.

Key words: advanced model, theory, planets, rotation, magnetism, magnetic field.

Introduction

The division of the Earth's EM field into electric and magnetic field components is relative. Electrostatic loads create a component of electric field strength and in the vicinity of immobile charge carriers there is only an electric field component while a moving carrier creates a magnetic field component (Bjelić & Marković, 2023). The Earth's magnetic field protects life on the Earth from cosmic particles, and a weakening of the field reduces the protection. In astrophysics, the Earth's magnetic field is defined as a physical field created and maintained by the rotation of charged magma in the core (according to the accepted dynamo theory) (Jacobs, 1987).

Nikola Tesla was the first to realize that the Earth is a good electrical conductor and that the upper layers of the atmosphere have an important role because, according to the measurements, they contain a stable conduction line. Based on Tesla's postulate, EM processes inside the Earth and in its outer layers can be viewed through influence as:

- an electrostatic system with a solid sphere and outer layers carrying charges,
- an elementary electrostatic dipole that creates the electric and magnetic components of the EM field,
- an elementary magnetic dipole that creates the electric and magnetic components of the EM field,
- an elementary resonator of the electric component of the EM field, as suggested by Tesla, and
- a planet that rotates under the action of the forces created by the electric and magnetic field components.

A more advanced model of a dielectric sphere in a foreign homogeneous electric field

To obtain a more advanced model of the dielectric sphere in a foreign homogeneous electric field, the starting relation for the potential is important:

$$\varphi_i = \frac{C_{1i}}{r} + C_{2i} + \left(C_{3i} r + C_{4i} / r^2\right) \cos\alpha , \tag{1}$$

$$\varphi_e = \frac{C_{1e}}{r} + C_{2e} + \left(C_{3e} r + C_{4e} / r^2\right) \cos\alpha . \tag{2}$$

The potential $\varphi(r)$ for $r \to \infty$ is $\varphi = \varphi_0 + E_0 r \cos\alpha$. After substitution, we get: $C_{2e} = \varphi_0$, $C_{3e} = E_0$.

For a point charge, the electric field $E = q / 4\pi\varepsilon_0\varepsilon_r r^2$ depends on (r):

$$\varphi_e = -\int E dr = \frac{q}{4\pi\varepsilon_0\varepsilon_r r} = \frac{C_{1e}}{r} . \tag{3}$$

By analogy, C_{1e} / r is a component of the total charge of the sphere. For the total charge of the sphere $q = Q = 0$ in relation φ_e to this constant is equal to $C_{1e} = 0$. After that, the constant is determined C_{4e}:

$$\varphi_e = \varphi_0 + \left(E_0 r + C_{4e} / r^2\right) \cos\alpha . \tag{4}$$

The potential of all points in a spherical dielectric φ_i is a finite value valid only for $C_{1i} = 0$ and $C_{4i} = 0$ (if the $C_{1i} = 0$ component were in the center of the sphere it would be $(C_{1i} / r) \to \infty$. C_{2i} with sufficient accuracy to determine the potential in the field of the outer domain C_{2e} is $C_{2i} = C_{2e} = \varphi_0$. Inside the dielectric is: $\varphi = \varphi_0 + C_{3i} r \cos\alpha$.

The constants C_{4e} and C_{3i} are determined from the boundary conditions. From the equations for φ_e, φ_i for $r = R_1$ which the condition equivalent to the condition $E_{it} = E_{et}$, follows: $C_{3i} R_1 = E_0 R_1 + C_4 / R_1^2$, $C_4 = -E_0 R_1^3$.

C_{4i} and C_{3i} follow from the equality of the normal components of the induction: $D_{1n} = D_{2n}$ and $E_{it} = E_{et}$ at the limit:

$$-\varepsilon_i\left(\frac{\partial\varphi_i}{\partial r}\right)_{r=R_1}=-\varepsilon_e\left(\frac{\partial\varphi_e}{\partial r}\right)_{r=R_1},\ \varepsilon_i(C_{3i})_{r=R_1}=\varepsilon_e\left(E_0-\frac{2C_{4e}}{R_1^3}\right)_{r=R_1}, \tag{5}$$

$$C_{3i}=E_0\frac{3\varepsilon_e}{2\varepsilon_e+\varepsilon_i},\ C_{4i}=C_{4e}=R_1^3E_0\frac{\varepsilon_e-\varepsilon_i}{2\varepsilon_e+\varepsilon_i}, \tag{6}$$

$$\varepsilon_iE_0\frac{3\varepsilon_e}{2\varepsilon_e+\varepsilon_i}=\varepsilon_eE_0\left(1-2\frac{\varepsilon_e-\varepsilon_i}{2\varepsilon_e+\varepsilon_i}\right). \tag{7}$$

The potential in the dielectric from $z=r\cos\alpha$ is:

$$\varphi_i=\varphi_0+E_0r\frac{3\varepsilon_e}{2\varepsilon_e+\varepsilon_i}\cos\alpha=\varphi_0+E_0\frac{3\varepsilon_e}{2\varepsilon_e+\varepsilon_i}z. \tag{8}$$

The strength of the electric field in the dielectric is:

$$E_{zi}=-\frac{\partial\varphi_e}{\partial z}=-E_0\frac{3\varepsilon_e}{2\varepsilon_e+\varepsilon_i}. \tag{9}$$

The strength of the electric field E has the direction of the z axis, does not depend on the coordinate and the field is homogeneous. The potential outside the dielectric is:

$$\varphi_e=\varphi_0+E_0\left[r+\frac{\varepsilon_e-\varepsilon_i}{2\varepsilon_e+\varepsilon_i}\left(R_1^3/r^2\right)\right]\cos\alpha. \tag{10}$$

For the chosen spherical coordinate system, the components of the electric field strength outside the dielectric are:

$$E_{re}=-\frac{\partial\varphi_e}{\partial r}=E_0\left[1-\frac{\varepsilon_e-\varepsilon_i}{2\varepsilon_e+\varepsilon_i}\left(2R_1^3/r^3\right)\right]\cos\alpha. \tag{11}$$

The field strength and potentials of the charged dielectric sphere are calculated according to Gauss's law and the solutions are given in Table 1. The obtained formulas for the sphere are calculated in relation to the parameter α.

On the surface of the sphere for $r=R_1$ is:

$$\begin{aligned}E_{R1e}&=E_0\left(1-2\frac{\varepsilon_e-\varepsilon_i}{2\varepsilon_e+\varepsilon_i}\right)\cos\alpha,\\ E_{\alpha e}&=-\frac{1}{r}\frac{\partial\varphi}{\partial\alpha}=E_0\left(1+\frac{R_1^3}{r^3}\frac{\varepsilon_e-\varepsilon_i}{2\varepsilon_e+\varepsilon_i}\right)\sin\alpha.\end{aligned} \tag{12}$$

Table 1 Electric field strengths on the sphere
Таблица 1 – Напряженность электрического поля в сфере
Табела 1 – Јачине електричног поља у сфери

$\alpha = 0$, Field strength, *N* pole		Equator $\alpha = 90^0$, Field strength		$\alpha = 180^0$, Field strength, *S* pole	
$E_{R1e} = E_0\left(1-2\frac{\varepsilon_e-\varepsilon_i}{2\varepsilon_e+\varepsilon_i}\right)$	$E_\alpha = 0$	$E_{R1e} = 0$	$E_{\alpha e} = E_0\left(1+\frac{\varepsilon_e-\varepsilon_i}{2\varepsilon_e+\varepsilon_i}\right)$	$E_{R1e} = -E_0\left(1-2\frac{\varepsilon_e-\varepsilon_i}{2\varepsilon_e+\varepsilon_i}\right)$	$E_\alpha = 0$

The components E_r at all points on the sphere are greater than the external field components, and the lines D start from free charges, break at the boundary surface and pass through the sphere without interruption. The resulting field is homogeneous, but the field is also affected by the polarization of the bound charges in the dielectric (Đorđević & Olćan 2012).

The resultant field strength in the sphere (inter) is the difference between the strength of the foreign field E_0 and the field E_ω due to the polarization:

$$E_i = E_0 - E_\omega . \tag{13}$$

The potential in the sphere is determined from the component of the foreign field in the sphere $E_0(z)$ for $r \le R_1$, $E_{zi} = -\partial\varphi_e / \partial z$, and the potential of the bound charges if $\varphi_i = 0$. For $z = 0$ and $z = r\cos\alpha$ we get:

$$\varphi_i = -(E_0 - E_\omega) r\cos\alpha . \tag{14}$$

The component $-E_0 r\cos\alpha$ is created by the external field and $E_\omega r\cos\alpha$ is created by the bound charges in the sphere. Part of the potential from the moment of polarization, equivalent to a polarized sphere is $\partial\varphi = \frac{p\cos\alpha}{4\pi\varepsilon_e r^2}$.

The sum of that part and the potential created under the influence of the external field $\varphi_i = \varphi_e + \partial\varphi$ is:

$$\varphi_e = -E_0 r\cos\alpha + \frac{p\cos\alpha}{4\pi\varepsilon_e r^2} . \tag{15}$$

The boundary conditions $r \le R_1$ for strengths E_e and inductions D_e outside the sphere are:

$$E_{it} = E_{et}\,,\ \left(-\frac{1}{r}\frac{\partial\varphi_e}{\partial\alpha}\right)_{r=R_1} = \left(-\frac{1}{r}\frac{\partial\varphi_i}{\partial\alpha}\right)_{r=R_1}, \tag{16}$$

$$-E_0 \sin\alpha + \frac{p\sin\alpha}{4\pi\varepsilon_e R_1^3} = -(E_0 - E_\omega)\sin\alpha\,. \tag{17}$$

From the equation $E_{re} = -\frac{\partial\varphi_e}{\partial r} = E_0\left(1-\frac{2R_1^3}{r^3}\frac{\varepsilon_e-\varepsilon_i}{2\varepsilon_e+\varepsilon_i}\right)\cos\alpha$ and $E_{\alpha e} = -\frac{1}{r}\frac{\partial\varphi}{\partial\alpha} = E_0\left(1+\frac{R_1^3}{r^3}\frac{\varepsilon_e-\varepsilon_i}{2\varepsilon_e+\varepsilon_i}\right)\sin\alpha$ is:

$$E_\omega = \frac{p}{4\pi\varepsilon_e R_1^3}\,. \tag{18}$$

It is also for $r \le R_1$, $D_{in} = D_{en}$, that is for $r = R_1$:

$$\begin{gathered}\varepsilon_e\left(-\frac{\partial\varphi_e}{\partial\alpha}\right)_{r=R_1} = \varepsilon_i\left(\frac{\partial\varphi_i}{\partial\alpha}\right)_{r=R_1}, \\ \varepsilon_e E_0\cos\alpha + \frac{p\cos\alpha}{2\pi R_1^3} = \varepsilon_i(E_0 - E_\omega)\cos\alpha\,.\end{gathered} \tag{19}$$

It follows from equation (18):

$$\varepsilon_e E_0 + 2\varepsilon_e E_\omega = \varepsilon_i E_0 - \varepsilon_i E_\omega\,,\ E_\omega = \frac{\varepsilon_i-\varepsilon_e}{\varepsilon_i+2\varepsilon_e}E_0\,. \tag{20}$$

The vector of the polarization moment of the sphere is:

$$p = 4\pi\varepsilon_e R_1^3 E_\omega = 4\pi\varepsilon_e R_1^3\frac{\varepsilon_i-\varepsilon_e}{\varepsilon_i+2\varepsilon_e}E_0\,. \tag{21}$$

If the surface load density η is uniformly distributed on the surface of the sphere, it is equal to the normal component of the polarization moment of the sphere $\eta = Pn = P\cos\alpha$, where:

$$P = \frac{p}{V_{sf}} = p/\left(\frac{4}{3}\pi R_1^3\right) = 3\varepsilon_e\frac{\varepsilon_i-\varepsilon_e}{\varepsilon_i+2\varepsilon_e}E_0 = 3\varepsilon_e E\omega\,. \tag{22}$$

A model of an electrically conducting sphere in a foreign homogeneous field

At all points of the plane $x0y$ passing through the center, the conductive and electrostatic unloaded sphere has the same potential $\varphi_0 \neq 0$. At a distance $z = r\cos\alpha$ from the sphere that is very small $q = 0$ according to the radius $R_1 = R_{earth}$, it is considered that the sphere has no influence on the EM field (if the total load on the sphere is $q = 0$, the influence of the sphere exists if the point load appears as the sum of the free charges on the sphere $Q \neq 0$).

The potential φ at a distance r is:

$$\varphi = \frac{Q}{4\pi\varepsilon_a r} + \varphi_0 + E_0 r\cos\alpha\,. \tag{23}$$

The first member on the right side is the response of the sphere loaded with $Q \neq 0$, and the increase in potential is $E_0 r\cos\alpha$ due to the influence of the foreign field on the right side $z = r\cos\alpha$ (for $r \to \infty$ the potential is φ_0). The solution of the equation $\varphi = \varphi^M + \varphi^N = (C_1 / r) + C_2 + \left(C_3 r + \left(C_4 / r^2\right)\right)\cos\alpha$ is suitable for points infinitely far from the sphere and can be substituted into the equation for the potential (1) and (2), and then there is a unique solution with 4 constants. After substitution, the constants are:

$$C_1 = Q / 4\pi\cdot\varepsilon_a\,,\ C_2 = \varphi_0\,,\ C_3 = E_0\,,\ C_4\,. \tag{24}$$

C_4 cannot be determined by substitution, because in the equations for the potential (1) and (2) there is no component inversely proportional to r^2, and therefore it is determined from the condition that all points on the boundary surface $r = R_1$ of the sphere have the same potential.

Tangential components at the boundary must be equal to zero. $E_{it} = E_{et} = 0$. Then it is:

$$\varphi = const. = \frac{Q}{4\pi\varepsilon_a R_1} + \varphi_0 + \left[E_0 R_1 + \left(C_4 / R_1^2\right)\right]\cos\alpha\,. \tag{25}$$

When changing the angle α, the right side of the equation is constant if:

$$\left(E_0 R_1 + C_4 / R_1^2\right) = 0\,, \tag{26}$$

where: $C_4 = -E_0 R_1^3$.

Therefore, at all points of the dielectric surrounding the conducting sphere, the potential is equal:

$$\varphi = \frac{Q}{4\pi\varepsilon_a r} + \varphi_0 + E_0\left(R_1 - \frac{R_1^3}{r^2}\right)\cos\alpha\,. \tag{27}$$

For a spherical coordinate system, the two components of the field strength follow from the equations:

$$E_r = -\frac{\partial\varphi}{\partial r},\ E_\alpha = -\frac{1}{r}\frac{\partial\varphi}{\partial\alpha},\ E_\beta = -\frac{1}{r\sin\alpha}\frac{\partial\varphi}{\partial\beta} = 0\,, \tag{28}$$

$$E_r = -\frac{\partial\varphi}{\partial r} = \frac{Q}{4\pi\varepsilon_a r^2} - E_0\left[R_1 + \left(2R_1^3 / r^3\right)\right]\cos\alpha\,, \tag{29}$$

$$E_\alpha = -\frac{1}{r}\frac{\partial\varphi}{\partial\alpha} = E_0\left[1 - \left(R_1^3 / r^3\right)\right]\sin\alpha\,. \tag{30}$$

For $Q = 0$ on the surface $r = R_1$ is $E_r = -3E_0\cos\alpha$. The field strength is for $\alpha = 0$, $E_{R1} = -3E_0$, $E_\alpha = 0$, $\alpha = 180^0$, $E_{R1} = -3E_0$, $E_\alpha = 0$. The E_r components at points on the sphere are three times larger than the components of the foreign field.

At the equator for $\alpha = 90^0$ and $E_{R1} = 0$ is:

$$E_\alpha = E_0\left(1 - R_1^3 / R_1^3\right)\sin\alpha = 0\,. \tag{31}$$

A magnetically conducting sphere in a foreign magnetically homogeneous field

To determine the solution for a magnetic sphere of a radius R_1 in a foreign magnetic field, with given constants inside μ_i and outside μ_e the sphere and boundary conditions, solutions for a dielectric sphere with dielectric constants in a foreign electrostatic field are also used (Dziewonski & Anderson, 1981). In a system of stationary charges and an environment where electrical conductivity is zero, the electrostatic field is a special case of stationary:

a) $rot\vec{E} = 0$, b) $div\vec{D} = \rho_{conv.}$, c) $\vec{D} = \varepsilon_a\vec{E}$. (32)

For $rot\vec{E} = 0$, the electrostatic field is vortex-free. It $rot\vec{E} = rotgrad\varphi = 0$ follows $\vec{E} = -grad\varphi$. So the field is potential because it represents the gradient of the potential function and the sign

(–) indicates that the $\vec{E}$ direction is from a point of greater to a point of lesser potential. If the conduction current density is zero, the magnetic field is:

$$\text{a) } rot\vec{H} = 0\text{, b) } div\vec{B} = 0\text{, c) } \vec{B} = \mu_a\vec{H}. \tag{33}$$

The following equations of magnetostatics are identical to the equations of electrostatics in the areas with $\rho_{conv} = 0$, that is $rot\vec{H} = 0$, $rot\vec{E} = 0$ and are equivalent to the equations $\vec{H} = -grad\varphi_m$ and $\vec{E} = -grad\varphi$.

Boundary conditions on the surface of the magnetic sphere in a foreign magnetic field refer to the equality of the normal components of the magnetic induction and the tangential components of the magnetic field strength in both environments, outside the sphere and inside the sphere (index i for internal space and e for external space).

For a dielectric sphere in a foreign uniform electric field, the boundary condition on the surface is:

$$D_{in} = D_{en},\ E_{it} = E_{et},\ B_{in} = B_{en},\ H_{it} = H_{et}. \tag{34}$$

In the analysis of the influence of the external field $\vec{H}_0$ on the magnetically conducting sphere, the methods of electrostatics $\vec{E} \leftrightarrow \vec{H}$, $\vec{D} \leftrightarrow \vec{B}$, $\vec{P} \leftrightarrow \mu_0\vec{M}$ are used. Polarization $P = dp/dV$ corresponds to the product of the magnetization $M = dm/dV$ and the constant μ_0. A dielectric sphere in a foreign electric field is polarized as a homogeneous medium, and the same thing happens with a conducting magnetic sphere $\mu_a > \mu_0$ in a foreign magnetic field. The strength H_ω of the demagnetization magnetic field in the sphere and the direction opposite to the direction of the foreign field defines the magnetization of the sphere. The equation analogous to the field strength E of the dielectric sphere is the magnetic field strength of the magnetization of the magnetoconducting sphere:

$$E_\omega = \frac{\varepsilon_i - \varepsilon_e}{\varepsilon_i + 2\varepsilon_e}E_0,\ \vec{H}_\omega = \frac{\mu - \mu_0}{2\mu_0 + \mu}. \tag{35}$$

Outside the sphere, the component created by the magnetization of the sphere appears as an elementary current field in the center of the sphere, and the magnetic moment m is the sum of the magnetic moments of all elementary currents in the domain. The magnetization of

the magnetic field in the sphere is obtained similarly to the polarization moment in the dielectric from equation (31):

$$p = 4\pi\varepsilon_e R_1^3 E_\omega = 4\pi\varepsilon_e R_1^3 \frac{\varepsilon_i - \varepsilon_e}{\varepsilon_i + 2\varepsilon_e} E_0 \Leftrightarrow$$
$$\Leftrightarrow \mu_e H_m = 4\pi R_1^3 \mu_e H_\omega = 4\pi R_1^3 \mu_e \frac{\mu_i - \mu_e}{\mu_i + 2\mu_e} E_0 \quad . \tag{36}$$

The product of the magnetization and the constant μ_e are equal to the magnetic moment of the sphere:

$$\mu_e M = \mu_e \frac{dm}{dV} = \frac{\mu_e m}{(4/3)R_1^3} = 3\mu_e \frac{\mu_i - \mu_e}{\mu_i + 2\mu_e} H_0 = 3\mu_e H_\omega . \tag{37}$$

The strength of the magnetic field in the sphere is the difference between the strength of the external H_0 and the field due to the magnetization H_ω and the induction:

$$H = H_0 - H_\omega = \frac{3\mu_e}{\mu_i + 2\mu_e} H_0 , \; B_e = \mu_e H_0 , \tag{38}$$

$$B = \mu_i H = \mu_i \frac{3\mu_e}{\mu_i + 2\mu_e} H_0 = \frac{3\mu_i}{\mu_i + 2\mu_e} B_e . \tag{39}$$

If $\mu_i \to \infty$, $\vec{H}_\omega = H_0$, then $\vec{H} = 0$, $B = 3B_0$. In addition to the speed of light c, in the analysis of EM processes in stationary and/or moving environments, the parameters of those environments are also used.

Basic EM states of the body at rest and in motion (rotation)

In the analysis of the state, one stationary (system 0) is used with a coordinate origin at the point 0, with coordinates in the Cartesian system x, y, z and a time coordinate t and another system connected to a moving medium in relation to the previous one with the a coordinate origin at the point 0_1 and new coordinates in the Cartesian system x_1, y_1, z_1 and the time coordinate t.

If during the time $t = 0$ both coordinate systems coincide and the velocity of the medium in the direction of the axis x is $v(y) \neq 0$ according to the theory of relativity, the Lorentz transformation that connects the space coordinates of both systems and the time t is:

$$x_1 = \frac{x - vt}{\sqrt{1-\beta^2}},\ y_1 = y,\ z_1 = z,\ t_1 = \frac{t - \left(v/c^2\right)x}{\sqrt{1-\beta^2}},\ \beta = v/c. \tag{40}$$

At some point, the stationary carrier with respect to the system 0 has a field strength E and a magnetic induction B. The field strength E is the force acting on a unit static load q in the 0 coordinate system, and the magnetic induction B means the force acting on a unit current element at rest in the stationary 0 system:

$$\vec{E} = \vec{i}E_x + \vec{j}E_y + \vec{k}E_z,\ \vec{B} = \vec{i}B_x + \vec{j}B_y + \vec{k}B_z. \tag{41}$$

The strength of the electric field E_1 and the magnetic induction B_1 that the carrier would have without moving in relation to the system with the beginning 0_1 (the system moving at a speed $v \neq 0$) E_1 represent: the effect of the force acting on a stationary unit load q in the system of coordinates with the beginning at 0_1, and B_1, the effect of the force on the unit element of the current that is at rest in a moving environment (a moving coordinate system with the beginning 0_1):

$$\vec{E}_1 = \vec{i}E_{x1} + \vec{j}E_{y1} + \vec{k}E_{z1},\ \vec{B}_1 = \vec{i}B_{x1} + \vec{j}B_{y1} + \vec{k}B_{z1}. \tag{42}$$

When moving from Maxwell's equations for a stationary medium to the equations of a moving medium, the derivatives $\partial(x,y,z)/\partial t$ (coordinate t) and $\partial(x_1,y_1,z_1)/\partial t_1$ (coordinate t_1) are determined according to equation (40) (Petković, 2016):

$$\frac{\partial}{\partial x} = \alpha\left(\frac{\partial}{\partial x_1} - \frac{v}{c^2}\frac{\partial}{\partial t_1}\right),\ \frac{\partial}{\partial t} = \alpha\left(-v\frac{\partial}{\partial x_1} + \frac{\partial}{\partial t_1}\right),$$

$$\frac{\partial}{\partial x_1} = \alpha\left(\frac{\partial}{\partial x} + \frac{v}{c^2}\frac{\partial}{\partial t}\right),\ \frac{\partial}{\partial t_1} = \alpha\left(v\frac{\partial}{\partial x} + \frac{\partial}{\partial t}\right), \tag{43}$$

$$\frac{\partial}{\partial y_1} = \frac{\partial}{\partial y},\ \frac{\partial}{\partial z_1} = \frac{\partial}{\partial z},\ \alpha = \frac{1}{\sqrt{1-\beta^2}}.$$

By developing the operation rot and joining the terms with the same rots in the first Maxwell's equation, $rot\vec{H} = \vec{J}_{cond} + \partial\vec{D}/\partial t$ it follows that $rot\vec{H}_1 = \vec{J}_{cond_1} + \partial\vec{D}_1/\partial t$. The projections of the vectors onto the coordinates in both systems are:

$$\vec{H}_1 = \vec{i}H_{x1} + \vec{j}H_{y1} + \vec{k}H_{z1},\ H_{x1} = H_x,$$
$$H_{y1} = \alpha\left(H_y + vD_z\right),\ H_{z1} = \alpha\left(H_z - vD_y\right), \tag{44}$$

$$\vec{J}_1 = \vec{i}J_{x1} + \vec{j}J_{y1} + \vec{k}J_{z1},\ J_{x1} = \alpha\left(J_x - v\rho\right),\ J_{z1} = J_z, \tag{45}$$

$$\vec{D}_1 = \vec{i}D_{x1} + \vec{j}D_{y1} + \vec{k}D_{z1},\ D_{x1} = D_x,\ D_{x1} = D_x,$$
$$D_{y1} = \alpha\left[D_y - H_z\left(v/c^2\right)\right],\ D_{z1} = \alpha\left[D_z + H_y\left(v/c^2\right)\right]. \tag{46}$$

A similar transformation of the second Maxwell's equation yields:

$$rot\vec{E} = -\partial\vec{B}/\partial t,\ rot\vec{E}_1 = -\partial\vec{B}_1/\partial t, \tag{47}$$

$$\vec{E}_1 = \vec{i}E_{x1} + \vec{j}E_{y1} + \vec{k}E_{z1},\ E_{x1} = E_x E_{y1} = \alpha\left(E_y - vB_z\right),$$
$$E_{z1} = \alpha\left(E_z + vB_y\right), \tag{48}$$

$$\vec{B}_1 = \vec{i}B_{x1} + \vec{j}B_{y1} + \vec{k}B_{z1},\ B_{x1} = B_x B_{y1} = \alpha\left(B_y + \frac{v}{c^2}E_z\right),$$
$$B_{z1} = \alpha\left(B_z - \frac{v}{c^2}vE_y\right). \tag{49}$$

The third and fourth Maxwell's equations in the coordinate system 0_1 have the forms:

$$div\vec{D}_1 = \rho_1,\ div\vec{B}_1 = 0, \tag{50}$$

and the volume charge density is:

$$\rho_1 = \alpha\left[\rho - \left(v/c^2\right)J_x\right]. \tag{51}$$

In the system 0_1, differentiation is performed by x_1, z_1, y_1. For a stationary medium, the conditions of continuity of the tangential components of strength are fulfilled: E_{t1} and H_{t1} and continuity of the normal components D_{n1} and B_{n1} in the system:

$$0_1 \text{ is: } \vec{M}_1 = \vec{B}_1/\mu_0 - \vec{H}_1,\ \vec{P}_1 = \vec{D}_1 - \varepsilon_0\vec{E}_1, \tag{52}$$

$$0 \text{ is: } \vec{M} = \vec{B}/\mu_0 - \vec{H},\ \vec{P} = \vec{D} - \varepsilon_0\vec{E}. \tag{53}$$

M, M_1 the magnetizations of the medium are the dielectric polarizations P, P_1, in the systems 0 and 0_1:

$$\vec{M}_1 = \vec{i}M_{x1} + \vec{j}M_{y1} + \vec{k}M_{z1},\ \vec{M} = \vec{i}M_x + \vec{j}M_y + \vec{k}M_z\ , \tag{54}$$

$$\vec{P}_1 = \vec{i}P_{x1} + \vec{j}P_{y1} + \vec{k}P_{z1},\ \vec{P} = \vec{i}P_x + \vec{j}P_y + \vec{k}P_z\ . \tag{55}$$

Equations (44), (45) and (46) show the dependence of the magnetization projections on the polarization projections in 0 and 0_1:

$$M_{x1} = M_x\ ,\ M_{y1} = \alpha\left(M_y + vP_z\right),\ M_{z1} = \alpha\left(M_z - vP_y\right), \tag{56}$$

$$P_{x1} = P_x\ ,\ P_{y1} = \alpha\left(P_y - \frac{v}{c^2}P_z\right),\ P_{z1} = \alpha\left(P_z + \frac{v}{c^2}P_y\right). \tag{57}$$

From equations (44) and (45), if there is no magnetic field $B = 0$ and there is an electric field $E \neq 0$, there is both an electric and a magnetic field in the system 0_1. It is also clear that even when there is no electric field in the system 0, $E = 0$, but there is a magnetic one $B \neq 0$, an electric field is created in the system 0_1 in addition to the magnetic one.

The current density in the system 0_1 is produced not only by the conduction current but also by the volume charge density transfer current component $\alpha\rho\cdot\vec{v}$ (convection current density) according to equation (46):

$$\vec{J}_1 = \vec{i}J_{x1} + \vec{j}J_{y1} + \vec{k}J_{z1},\ J_{x1} = \alpha\left(J_x - v\rho\right),\ J_{y1} = J_y\ ,\ J_{z1} = J_z\ . \tag{58}$$

According to equation (47), by moving the current from the system 0 with elementary density J_x parallel to itself in the system 0_1 on the load carrier in the coordinate system starting at 0_1 as part of the current density in the charge density $\rho_1 = \alpha\left(\rho - \frac{v}{c^2}J_x\right)$, a supplementary component appears $\frac{v}{c^2}J_x$.

From Maxwell's basic equation for EM wave propagation $\mu\mu_0\left(\partial H / \partial t\right) = -\partial E / \partial t$ is:

$$\mu\mu_0\frac{\partial x}{\partial t}\partial H = -\partial E \Rightarrow H = \frac{1}{c}\sqrt{\frac{\varepsilon}{\mu}}\cdot E\ ,\ \mu^2H^2 = \frac{\mu\varepsilon}{c^2}\cdot E^2 \Leftrightarrow B^2 = \frac{\mu\varepsilon}{c^2}E^2\ . \tag{59}$$

Due to the movement of the polarized dielectric at the speed v, equations (56) and (57), additional magnetization is created in the

coordinate system 0, and the movement of the magnetized medium at the speed v in system 0 appears as additional polarization.

According to equation (59), for the fields defined in the stationary system 0 and the mobile system 0_1, the following applies:

$$\frac{E_1^2}{c} - B_1^2 c = \frac{E^2}{c} - B^2 c \text{, i.e. } \vec{E}_1 \vec{B}_1 = \vec{E}\vec{B}, \tag{60}$$

$$\frac{H_1^2}{c} - D_1^2 c = \frac{H^2}{c} - D^2 c \text{, i.e. } \vec{D}_1 \vec{H}_1 = \vec{D}H. \tag{61}$$

If the speed of movement of the material medium (conductor/ dielectric/ferromagnetic) is low, according to the speed of light $(v/c)^2 << 1$, the Lorentz transformations change to Galilean ones, i.e. $x_1 = x - vt$, $y_1 = y$, $z_1 = z$, $t_1 = t$. The mathematical relationships between quantities in the systems 0 and 0_1 are:

$$\vec{E}_1 = \vec{E} + \left[\vec{v} \times \vec{B}\right],\ \vec{J}_1 = \vec{J} - \vec{v}\rho,\ \vec{D}_1 = \vec{D} + \frac{\left[\vec{v} \times \vec{H}\right]}{c^2},\ \rho_1 = \rho - \frac{\vec{v}}{c^2}\vec{J},$$

$$\vec{H}_1 = \vec{H} - \left[\vec{v} \times \vec{D}\right],\ \vec{M}_1 = \vec{M} + \left[\vec{v} \times \vec{P}\right],\ \vec{B}_1 = B - \frac{\left[\vec{v} \times \vec{E}\right]}{c^2}, \tag{62}$$

$$\vec{P}_1 = \vec{P} - \frac{\left[\vec{v} \cdot M\right]}{c^2}.$$

Body rotation corresponds to the position of a still body in space in a moving-rotating field created by EM sources by rotation in a time-varying or constant magnetic field. The electric and magnetic components of the field, Figure 1.a,b, can be determined from the magnetic potential vector, i.e. in $\vec{A} = A_r\vec{e}_r + A_\alpha\vec{e}_\alpha + A_\beta\vec{e}_\beta$ the spherical and $\vec{A} = A_x\vec{e}_x + A_y\vec{e}_y + A_z\vec{e}_z$ in the Cartesian systems.

For a body rotating a round the z axis, the possible functions are:

$$f(x,y,z,t) \text{, i.e. } A_z(x - ut, y, z),\ H = H_r(r, \omega \cdot t - \beta). \tag{63}$$

In plane coordinates, rotation is represented by the time-dependent functions:

$$H_x = H_r(r)\cos\omega \cdot t,\ H_y = H_r(r)\sin\omega \cdot t. \tag{64}$$

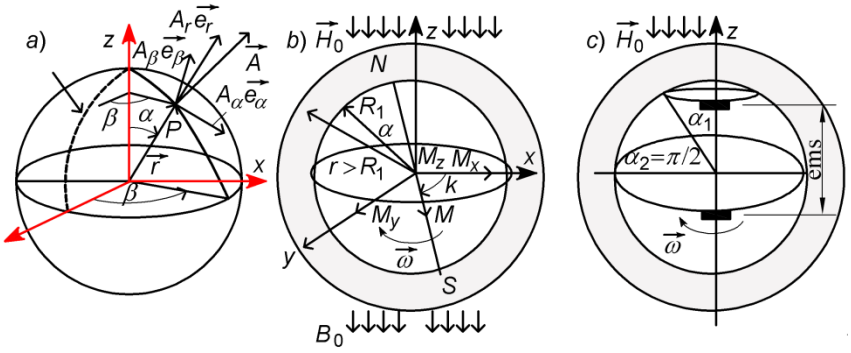

Figure 1 – a) Rotation of the magnetic sphere and the appearance of magnetic vector potential, b) reaction of magnetic and conducting spheres in a constant magnetic field, c) emf due to the rotation of the magnetiec field H_0 (Bjelić, 2021b)

Рис 1 – а) Вращение магнитосферы и возникновение магнитного векторного потенциала, b) реакция магнитосферы и проводящей сферы в постоянном магнитном поле, c) ЭДС вследствие вращения сферы в магнитном поле H_0 (Bjelić, 2021b)

Слика 1 – а) Ротација магнетне сфере и појава магнетног векторског потенцијала, б) реакција магнетне и проводне сфере у сталном магнетном пољу, ц) ЕМС услед ротације сфере у магнетном пољу H_0 (Bjelić, 2021b)

There are several solutions for body rotation in the literature (Davilkovski, Fradkin, Smith, etc.). The EM field in the dielectric layer between the ionosphere and the solid Earth, which rotates together with them in the magnetic field if the magnetic component of the Earth is a response to the EM field of the Sun, is shaped by the parameters in the Earth and the stable parameters of the electrical conductivity of the ionosphere. The elementary layer-ring of the atmosphere, given its dimensions, is treated as a flat channel $-\infty < x < +\infty$ of width $-b < y < +b$ where the velocity of the dielectric in the foreign field $\dot{v}[v(y),0,0]$ is $B[0,0,B(x)]$ (Mihajlović, 1993).

In an isotropic dielectric and magnetic medium, the conductivities of the layer $\hat{\varepsilon}(x)$ and $\tilde{\mu}(x)$, Figure 2, change only in the direction of the axis $-\infty < x < +\infty$ by ε_0. The field strength in the dielectric layer rotating in a foreign unknown magnetic field (the Sun) is determined from the Lorentz force of the field strength $\vec{E}_1 = \vec{F}/q = E + (\vec{v} \times \vec{B})$, stationary in relation to the system at the beginning 0_1 (the system rotates at a speed $\vec{v} \neq 0$), while $\vec{E}$ is stationary in relation to the system 0. From equation (53) follows:

$$\vec{D} = \vec{D}_1 - \varepsilon_0\mu_0\left[\vec{v}\times\vec{H}\right] = \varepsilon_a\vec{E} + \varepsilon_a\left[\vec{v}\times\vec{B}\right] - \varepsilon_0\mu_0\left[\vec{v}\times\vec{H}\right] = \\ = \varepsilon_a\vec{E} + \left(\varepsilon_a - \varepsilon_0 / \mu_r\right)\left[\vec{v}\times\vec{H}\right] \quad . \tag{65}$$

If the dielectric layer of the atmosphere between the ionosphere and the ground surface rotates at a speed of $v \approx 465\,\text{m/s}$, and the speed of light is $c = 3\cdot10^8\,\text{m/s}$, $v^2/c^2 << 1$, by the principle of superposition, Figure 2, the vector $\vec{D}$ is defined by:

$$\vec{D} = \varepsilon_a\vec{E} + \left(\varepsilon_a - \varepsilon_0 / \mu_r\right)\left[\vec{v}\times\vec{B}\right]. \tag{66}$$

The field strength is the gradient of the potential function $\vec{E} = -grad\varphi$, and the induction projections on the axes x and y are:

$$D_x = -\varepsilon_a\frac{\partial\varphi}{\partial x},\; D_y = -\varepsilon_a\frac{\partial\varphi}{\partial y} + \left(\varepsilon_a - \frac{\varepsilon_0}{\mu}\right)\left[\vec{v}\times\vec{B}\right]. \tag{67}$$

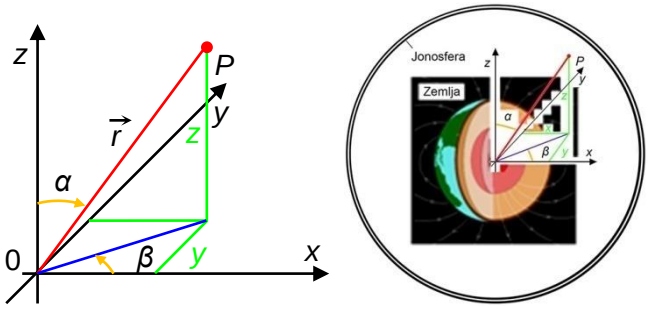

Figure 2 – Spherical coordinate system and the position of the solid Earth and the ionosphere (Bjelić, 2021b)
Рис 2 – Сферическая система координат и положение твердой Земли и ионосферы (Bjelić, 2021b)
Слика 2 – Сферни координатни систем и позиција чврсте Земље и јоносфере (Bjelić, 2021b)

Divergence is the ratio of the output vector D of the surface and the volume covered by the surface according to equation (53):

$$div\vec{D} = div\left\{\varepsilon_a\vec{E} + \left(\varepsilon_a - \frac{\varepsilon_0}{\mu_r}\right)\left[\vec{v}\times\vec{B}\right]\right\} = 0\,. \tag{68}$$

By transforming equation (8) into the operator function of the potential, a more suitable form is obtained:

$$-\varepsilon_a \Delta\varphi - \frac{\partial\varphi}{\partial x}\frac{d\varepsilon_a}{dx} + \left(\varepsilon_a - \frac{\varepsilon_0}{\mu_r}\right) B\frac{dv}{dy} = 0,$$
$$\frac{\partial^2\varphi}{\partial x^2} + \frac{\partial^2\varphi}{\partial y^2} + (ln\,\varepsilon_r)'\frac{\partial\varphi}{\partial x} + \left(1 - \frac{1}{\varepsilon_r \mu_r}\right)\cdot B\frac{dv}{dy} = 0. \quad (69)$$

In a spherical system, the potential gradient is:

$$grad\varphi = \frac{\partial\varphi}{\partial r}\vec{r}_0 + \frac{1}{r}\frac{\partial\varphi}{\partial\alpha}\vec{\alpha}_0 + \frac{1}{r\sin\alpha}\frac{\partial\varphi}{\partial\beta}\vec{\beta}_0,$$
$$E_r = -\frac{\partial\varphi}{\partial r},\ E_\alpha = \frac{1}{r}\frac{\partial\varphi}{\partial\alpha},\ E_\beta = -\frac{1}{r\sin\alpha}\frac{\partial\varphi}{\partial\beta}, \quad (70)$$
$$div\vec{V} = \frac{1}{r}\frac{\partial}{\partial r}\left(r^2 V_r\right) + \frac{1}{r\sin\alpha}\frac{\partial}{\partial\alpha}\left(V_\alpha \sin\alpha\right) + \frac{1}{r\sin\alpha}\frac{\partial V_\beta}{\partial\beta},$$

where $\vec{r}_0$, $\vec{\alpha}_0$, $\vec{\beta}_0$ are the unit vectors of the spherical coordinate system.

The divergence of the field towards the center of the sphere is:

$$div\vec{r} = 3,\ div\varphi(r)\cdot\vec{r} = 3\varphi(r) + r\varphi'(r). \quad (71)$$

Rotation of a magnetic sphere of the magnetization M in a foreign magnetic field

The model of rotation of a conducting sphere in a magnetic field corresponds to the model of rotation of a sphere in a time-varying field. An approximate solution will be determined from the adjusted complex form of the vector potential equation, neglecting wave processes in the domain $R << 2\pi/\omega$:

$$\nabla^2\vec{A} = j\omega\mu_r\mu_0\sigma\hat{A}. \quad (72)$$

The solution of equation (72) has a real and an imaginary component:

$$A_{re} = A_{\beta.re} = \frac{1}{2}(B_0)\left[R + \frac{D}{R^2}\right]\sin\alpha,\ R \geq R_1 = a, \quad (73)$$

$$A_{im} = A_{\beta.im} = \frac{C}{\xi}\left[\frac{\sin\xi}{\xi} - \cos\xi\right]\sin\alpha,\ R \leq R_1 = a, \quad (74)$$

$$\xi = R\sqrt{-js},\ s = \omega\mu_r\mu_0\sigma,\ R = a,\ \xi = a\sqrt{-j\omega\mu_r\mu_0}. \quad (75)$$

The integration constants are:

$$D = a^2 \frac{2(\mu_r + 1)(\sin\xi - \xi\cos\xi) - \xi^2 \sin\xi}{(\mu_r - 1)(\sin\xi - \xi\cos\xi) + \xi^2 \sin\xi}, \tag{76}$$

$$C_1 = \frac{B_0}{2} \frac{a\xi^2}{\sin\xi - \xi\cos\xi}\left(1 + \frac{D}{a^3}\right). \tag{77}$$

For an out-of-sphere domain $R > a$ they are:

$$B_R = B_0\left(1 + \frac{D}{R^3}\right)\cos\alpha,\ B_\alpha = -B_0\left(1 - \frac{1}{2}\frac{D}{R^3}\right)\sin\alpha. \tag{78}$$

In the outer domain, the field is similar to the field of a homogeneously magnetized sphere, or a sphere that is introduced into a homogeneous variable field without eddy currents. At equivalent magnetic permeability is:

$$\mu_{r.re} = \mu'_{r.re} - j\mu''_{r.re} = 2\mu_r \frac{tg\xi - \xi}{\xi^2 tg\xi - (tg\xi - \xi)}. \tag{79}$$

By expanding the tangent in a degree order with the limitation to only two terms of the order (allowed for frequencies), we get:

$$\begin{aligned} &\text{Low frequency } \omega \le 1/\ \mu_r\mu_0\sigma\cdot a^2,\ \mu_{r,re} = \mu_r\left(1 - 0{,}1\omega\mu_r\mu_0\sigma\cdot a^2\right), \\ &\text{High frequencies } |tg\xi| \cong 1,\ \mu_{r,re} = 2\mu_r / a\sqrt{j\omega\mu_r\mu_0}\ . \end{aligned} \tag{80}$$

The magnetization M of a stationary sphere, $\mu_i / \mu_e = \mu_r$ in a constant field $\vec{H}_0$ is determined from equation (37):

$$\mu_e M = 3\mu_e \frac{\mu_i - \mu_e}{\mu_i + 2\mu_e} H_0,\ M = 3\mu_e \frac{\mu_r - 1}{\mu_r + 2} H_0. \tag{81}$$

With a shift $\mu_{r.} = \mu_{r.re}$ in the harmonic field, equation (37), $\tilde{m}$ is equal to:

$$\begin{aligned} \tilde{m} = V_{sf}\tilde{M} = \frac{4}{3}\pi a^2\tilde{M} = 4\pi a^2\tilde{H}_0 \frac{\mu_{r.re} - 1}{\mu_{r.re} + 2} = \tilde{H}_0 K\angle -k, \\ \tilde{K} = 4\pi a^2 \frac{\mu_{r.re} - 1}{\mu_{r.re} + 2}\angle -k, \end{aligned} \tag{82}$$

where K is the modulus m for $H_0 = B_0 / \mu_0$, k (phase attitude) of the moment with respect to the external field H_0.

Electromotive force (emf) can be generated by induction during the rotation of a conductive sphere with a magnetization vector $M = Mz$ of the radius a and the angular velocity ω around the z axis in an external magnetic field of induction B_0. Maxwell formulated the emf $e = -d\phi / dt$ of induction where ϕ is covered by a contour for which the direction of the circuit is the same as the direction of the emf $e > 0$ according to the positive direction of the flux $\phi > 0$ in the system where the work W performed is conditioned by the effect of non-Coulomb forces f for the transfer of a unit charge q, $e = W / q$. The work during the transfer of a unit charge achieved by the effect of non-Coulomb forces of EM induction is the integral $\vec{E}^{ind} = f / q$ of the field strength along a closed contour $\vec{l}$:

$$e = \oint_{\ell} E^{ind} d\ell = -\frac{d}{dt} \int_S \vec{B} d\vec{S} . \tag{83}$$

In Faraday's equation, $e = -dN / dt$, N is the number of magnetic lines intersected by the contour and one line corresponds to the unit flux. For some orientation of the flux line cutting speed (or B), the emf on the part $d\vec{l}$ of the contour $\vec{l}$ is $de = \left(\vec{v} \times \vec{B}\right) d\vec{\ell}$. Maxwell's and Faraday's formulas are equivalent - the general Maxwell's equation.

The gradient vanishes on closed-loop integration. If part of the contour is determined by the line ab emf induced in it is:

$$e = \oint \left(-\nabla\varphi - \partial\vec{A} / \partial t + \vec{v} \times \vec{B}\right) d\vec{\ell} , \; e = \int_a^b \left(-\partial\vec{A} / \partial t + \vec{v} \times \vec{B}\right) d\vec{\ell} . \tag{84}$$

Due to the symmetry of the sphere towards the plane of the equator, Figure 1.c, from the point corresponding to the position of the N pole, $\alpha_1 = 0$ where one hole is at the position of the equator and the other hole is at $\alpha_2 = \pi / 2$, emf is determined between the circles at those corners. For $\partial\phi / \partial t = \partial A / \partial t = 0$ remains only the component $\vec{v} \times \vec{B} = \omega a B_R e_\alpha$, $d\ell = -a d\alpha e_\alpha$ where:

$$E_r = -\frac{\partial\varphi}{\partial r} , \; E_\alpha = \frac{1}{r}\frac{\partial\varphi}{\partial\alpha} , \; E_\beta = -\frac{1}{r \sin\alpha}\frac{\partial\varphi}{\partial\beta} , \tag{85}$$

$$div\vec{V} = \frac{1}{r}\frac{\partial}{\partial r}\left(r^2 V_r\right) + \frac{1}{r \sin\alpha}\frac{\partial}{\partial\alpha}\left(V_\alpha \sin\alpha\right) + \frac{1}{r \sin\alpha}\frac{\partial V_\beta}{\partial\beta} , \tag{86}$$

$$e = \int \left(\vec{v} \times \vec{B}\right) d\vec{\ell} = \int_{\alpha 2 = \pi/2}^{\alpha 1} \omega \left[\cdot a \sin\alpha \cdot B_R \left(-a d\alpha\right)\right]. \quad (87)$$

For $R \le a$ it is $B = B_z = 2\mu_0 M / 3$. For $R = a$ you get:

$$B_R = B_z = 2\mu_0 M(\cos\alpha) / 3. \quad (88)$$

The induced emf is:

$$e = \left(\omega \cdot a^2 2\mu_0 M / 3\right) \int_{\alpha 1}^{\alpha 2} \sin\alpha \cos\alpha \cdot d\alpha = \left(\omega a^2 \mu_0 M / 3\right)\left(1 - \sin^2\alpha_1\right). \quad (89)$$

Equation (89) shows which quantities determine $v \times B$ depending on the speed of rotation in space.

Components of the magnetic field that can arise due to the rotation of the planets and the Earth

During the rotation of an electrostatically neutral body (rotor), higher densities of free charges in the area can excite the magnetic field in a similar way to be created by the currents flowing through the rotor, Figure 1.a.

The consequence of the rotation of the body is the creation of a weak magnetic field, and this phenomenon can be used to explain the appearance of the components of the Earth's magnetic field. If the number n of free electrons passing through the unit volume of the conductive part, e is the charge of the electrons, u the resultant chaotic speed of the electrons due to the effect of the field (thermal effects are small due to the small number of collisions of oscillating atoms), the current I through the surface s is:

$$I = Js = dQ / dt = nedV / dt = nesdl / dt = nesv, \quad (90)$$

$$J = I / s \Leftrightarrow I = Js = nev_0 (u / c)^2 s, \quad (91)$$

where n is the volume density of free charges, s the cross-section of the rotor body, v_0 the speed of the rotor, u the speed of the chaotic movement of free charges, and c the speed of light.

Bio-Savar, Ampere and the law of EM induction were created empirically. It was later concluded that these laws can be obtained from Coulomb's law, if the corrections derived from the special theory of relativity (Bjelić, 2019), are applied to the charge interaction forces. Already known physical phenomena can also be considered in two projections and are the result of facts that were not known before. Ampere's law allows the interaction of a conductor with a current to be

determined. If the current elements I_1dl_1 and I_2dl_2 are normal to the radius of the sector, $r_{1,2}$ Figure 3.b, the forces of interaction between them are equal.

The assumption is that the positive charge elements dl_1 and dl_2 are also stationary, while the negative charge elements have velocities v_1 and v_2 corresponding to the currents I_1 and I_2. The EM force, Figure 3.b, is determined by Coulomb's law with the application of the theory of relativity (Bjelić, 2019).

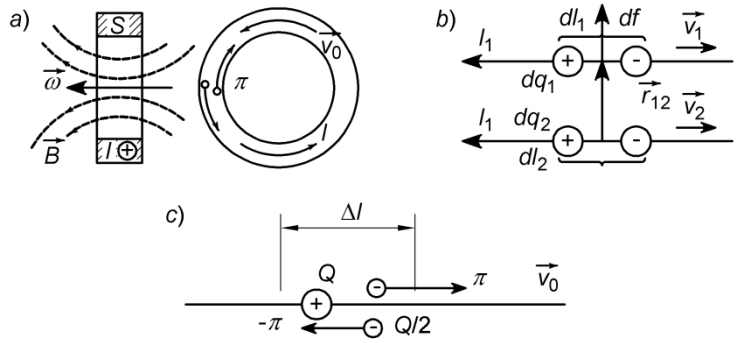

Figure 3 – a) Generation of a magnetic field during rotation, b) EM effect of the current elements I_1dl_1 and I_2dl_2, c) The movement of a neutral conductor along its axis at the speed of that chaotic movement v_0 (Bjelić, 2021b)

Рис 3 – а) Создание магнитного поля при вращении, b) ЭМ воздействие элементов тока I_1dl_1 и I_2dl_2, с) движение нейтрального проводника вдоль своей оси со скоростью хаотического движения v_0 (Bjelić, 2021b)

Слика 3 – а) Стварање магнетног поља при ротацији, б) ЕМ ефекат струјних елемената I_1dl_1 и I_2dl_2, ц) кретање неутралног проводника дуж своје осе брзином тог хаотичног кретања v_0 (Bjelić, 2021b)

If the requirements of the theory of relativity are taken into account, the forces acting between the charges of the elements dl_1 and dl_2 are:

$$df = -\frac{\mu_0}{4\pi}\frac{I_1dl_1I_2dl_2}{r_{1,2}^2}, \tag{92}$$

$$df = df_0\left(1-\frac{v_1v_2}{c^2}\right)\left[1-\left(\frac{v_2}{c}\right)\right]^{-1/2}, \tag{93}$$

where the force df_0 is determined by Coulomb's law:

$$df_0 = -\frac{1}{4\pi\varepsilon_0}\frac{dq_1 dq_2}{r_{1,2}^2}\,. \tag{94}$$

Index (1) refers to the rate of charging of a positive or negative element dl_1, while index (2) refers to the rate of charging, also of a positive or negative element dl_2.

The force acting from the positive charge of the element dl_2 to the positive charge dl_1 is:

$$df_{++} = df_0\left(1-\frac{v_1^+ v_2^+}{c^2}\right)\left[1-\left(\frac{v_2^+}{c}\right)^2\right]^{-1/2} = df_0\,, \tag{95}$$

$$v_1^+ = v_2^+ = 0\,,\ df_{-+} = -df_0\,, \tag{96}$$

$$df_{+-} = df_0\left[1-\left(\frac{v_2^-}{c^2}\right)^2\right]^{-1/2}\,, \tag{97}$$

$$df_{--} = df_0\left(1-\frac{v_1^- v_2^-}{c^2}\right)\left[1-\left(\frac{v_2^-}{c}\right)^2\right]^{-1/2}\,. \tag{98}$$

In equations (95) to (98), the index $(+)$ refers to the action on the element dl_1 and the index $(-)$ to the action on the element dl_2.

Adding equations (95) to (98) and omitting the index gives:

$$df = -df_0\frac{v_1 v_2}{c^2}\left[1-\left(\frac{v_2}{c}\right)^2\right]. \tag{99}$$

By expanding the series in middle brackets, the higher-order line terms v/c of equation (99) become:

$$df = -df_0\frac{v_1 v_2}{c^2}\left[1-\left(\frac{v_2}{c}\right)^2+.....\right]. \tag{100}$$

If in equation (100) the calculation is limited only to the first term of the series (one), then:

$$df = -df_0 \frac{v_1 v_2}{c^2}. \tag{101}$$

If it is known that $\mu_0 \varepsilon_0 c^2 = 1$, then:

$$I_1 dl_1 = dq_1 / dt \cdot dl_1 = v_1 dq_1,\ I_2 dl_2 = dq_2 / dt \cdot dl_2 = v_2 dq_2. \tag{102}$$

According to equations (92) and (102), the interaction forces of the two current elements are equal. When deriving Ampere's law from Coulomb's law, corrections according to the theory of relativity must be taken into account. In equation (100), the higher order terms are discarded because they are very small. If the v^2 relative speed corresponding to the permissible current density, the correction is:

$$\frac{1}{2}\left(\frac{v_2}{c^2}\right)^2 \approx 10^{-23}. \tag{103}$$

The correction deviates from the measurement, although the laws of Bio-Savar, Ampere and EM induction do not raise doubts about their accuracy. In the numerical sequence of equation (100), the first term is the charge rate squared. It is a correction of the force or magnetic field created by the conductor, which depends on the speed of orderly and chaotic movement of charges whose order of magnitude is much higher than the speed of orderly movement. A neutral conductor with no current is observed, which moves along its axis at the speed v_0, Figure 3.c.

The assumption is that positive charges are stationary in relation to the conducting part, and negative charges are in chaotic motion and equally probable in all directions. The average speed v of that chaotic movement is determined by the Fermi energy and is $v \approx 10^6$ m/s, i.e. significantly exceeds the rate of charging at the permitted current density. The unprincipled assumption is that: the first half of the negative charges move in the direction v_0 and the second half in the opposite direction $-v_0$, Figure 3.a. The movement of charges creates current. For a stationary conductive body, the current as the sum of all charges, Figure 3.c, is equal to zero. The result will not change even when the conductive body is moved because all charges, positive and negative, get the same additional speed Figure 3.a. The situation is different if the sum of velocities is calculated according to the theory of relativity (Bjelić, 2019). The speed of negative charges is determined in relation to the conductive part, which then represents a moving coordinate system. For a stationary observer, the charge rates will be equal to:

positive $v_+ = v_0^-$, (104)

negative moving in the direction of v_0:

$$v_-^{(1)} = \frac{v_0 + u}{1 + \left(v_0 u / c^2\right)} \approx \left(v_0 + u\right)\left(1 - \frac{v_0 u}{c^2}\right), \tag{105}$$

negative if it moves opposite to v_0:

$$v_-^{(2)} = \frac{v_0 - u}{1 - \frac{v_0 u}{c^2}} \approx \left(v_0 - u\right)\left(1 + \frac{v_0 u}{c^2}\right). \tag{106}$$

The total current of all charges can then be determined:

$$I = Q \cdot v, \tag{107}$$

where Q is the charge per unit length (in contrast to equation (102)) for the conductor.

The current created by positive charge is:

$$I_+ = Q \cdot v. \tag{108}$$

The currents created by negative charging are:

$$I_-^{(1)} = -\frac{1}{2} Q\left(v_0 + u\right)\left(1 - \frac{v_0 u}{c^2}\right), \tag{109}$$

$$I_-^{(2)} = -\frac{1}{2} Q\left(v_0 - u\right)\left(1 + \frac{v_0 u}{c^2}\right). \tag{110}$$

Adding equations (109) and (110) gives the total current:

$$I = Q \cdot v_0 \left(u / c\right)^2. \tag{111}$$

$Q = nes$ is determined from the volume charge density n and the cross-sectional area of the conductor s. At the same time, equation (111) takes a form that agrees with equation (91):

$$I = nes \cdot v_0 \left(\frac{u}{c}\right)^2. \tag{112}$$

The effect of moving the neutral conductor along the axis is similar to the effect of the current-carrying conductor. The conductive part can be spaced several times and the current I will not change. It is a consequence of the chaotic movement of charges, because the speed of movement in equation (112) is included in the term with the square. An

example estimate is the current for an aluminum rotor: $n = 10^{28}\,1/\text{m}^3$, $e = 1.6 \cdot 10^{-19}\,\text{C}$, $s = 0.5 \cdot 10^{-2}\,\text{m}^2$, $v_0 = 10\,\text{m/s}$, $u = 10^6\,\text{m/s}$, $c = 3 \cdot 10^8$ m/s, $I \approx 10^3\,\text{A}$.

From equation (112), the charge density n and the speed of chaotic movement should be known to estimate the current.

In this example, these values are taken for pure metal. Some impurities can reduce the value n by a higher order of magnitude. Experimental confirmation of formula (112) requires a preliminary analysis of the rotor material to determine n and u. However, there is indirect confirmation of currents and fields generated by cosmic bodies (Bjelić, 2021a; Dziewonski & Anderson, 1981). If equation (112) is applied to analyze the magnetic field of a homogeneous rotating sphere, the total current is:

$$I = \frac{1}{12}\frac{nD^3}{T} e \left(\frac{u_2}{c}\right)^2 . \tag{113}$$

The strength of the magnetic field at its poles is approximately:

$$H = I / D , \tag{114}$$

and for magnetic induction is:

$$B = \mu_0 \grave{\mu} \cdot H = \mu_0 \grave{\mu} \cdot I / D \text{, i.e. } B = \frac{1}{12}\frac{nD^2}{T} e \left(\frac{u_2}{c}\right)^2 \mu_0 \grave{\mu} . \tag{115}$$

Equation (115) can also be obtained from equation (111) $I = e \cdot v_0 (u / c)^2$ (if e is the electron charge) and then the relation is derived from equation (112):

$$B = \left[\frac{1}{12} e \left(\frac{u_2}{c}\right)^2 \mu_0 \cdot \mu\right]\grave{} \Big|_{=A} \frac{1}{T}\frac{\left(nD^3\right)_{=m}}{D} = A\frac{m}{TD} , \; B = A\frac{m}{TD} , \tag{116}$$

where $\grave{\mu}$ is relative magnetic conductivity, m is the mass, $D = 2r$ is the body diameter, T is the period of rotation around the axis, A is the constant.

In equation (116), the charge density n is proportional to the mass density $n \approx m / D^3$, and the discharge rate depends on the Fermi energy and is included in the constant A. If the formula for the Earth's magnetic field is written, then it is:

$$B_z = A\frac{m_z}{T_z D_z}. \tag{117}$$

When equation (116) is divided by equation (117) we get:

$$B = \frac{\dot{m}}{\dot{T}\dot{D}} B_z. \tag{118}$$

If the Earth's magnetic field is at the pole $B_z = 0.5 \cdot 10^{-4}$ T, then the magnetic field of an arbitrary cosmic body is:

$$B = 0.5\frac{\dot{m}}{\dot{T}\dot{D}} 10^{-4} \text{T}. \tag{119}$$

Table 2 includes a limited number of objects and allows an assessment of the degree of agreement between computational and experimental data for some space objects. Asterisks mean that the parameters are taken in relative values (to Earth). It is not known at what distance from the object the measurements were made, at the pole or at the equator, while the calculated data refer to the pole on the surface of the object.

Table 2 – Comparison of computational and experimental data of some space bodies
Таблица 2 – Сравнение расчетных и экспериментальных данных некоторых небесных тел
Табела 2 – Поређење рачунских и експерименталних података неких свемирских тела

Object	$\dot{m}$	$\dot{D}$	$\dot{T}$	$\dot{B}$	Calculated value B 10^{-4} T	Measure value B 10^{-4} T
Earth	1	1	1	1	1	1
Mercury	0.05	0.38	58	$2.3 \cdot 10^{-3}$	$1.2 \cdot 10^{-3}$	10^{-3}
Venus	0.81	0.95	243	$3.5 \cdot 10^{-3}$	$1.7 \cdot 10^{-3}$	$0.15 \cdot 10^{-3}$
Jupiter	318	11.2	0.4	72	36	4.5
Saturn	95	9.5	0.45	20	10	0.6
Sun	$33 \cdot 10^4$	10^9	25	120	60	(10-100)
White dwarfs	10^6	1.0	1.0	10^6	$0.5 \cdot 10^6$	10^5
Neutron stars	10^3	10^{-3}	10^{-5}	10^{11}	$0.5 \cdot 10^{11}$	10^{12}

To date, magnetic fields have been measured for thousands of cosmic bodies. Their analysis would allow formula (118) to be evaluated more fully. The approximate coincidence of the calculated data with the experimental data is not considered accidental (Petković, 2016; Prodanović, 2006).

Conclusion

The obtained formulas can predict the order of magnitude of magnetic fields for known cosmic bodies, whose parameters such as masses, diameters and periods of rotation around the axis-differ by tens of thousands of times.

However, these formulas cannot explain many characteristics of magnetic fields, related to various, perhaps still unknown reasons.

The formulas and the results obtained in the paper indicate a possible common origin of the source of the magnetic field on the Earth (the Sun), and their accuracy can only be confirmed by cosmic research, experiment or computer simulation.

References

Bjelić, S. 2019. *Algorithms for diagnostics of disturbance in the electrical network and protection against them*. Belgrade, Serbia: Balkan Scientific Center of the Russian Academy of Natural Sciences. ISBN: 978-86-6042-018-5.

Bjelić, S.N. 2021a. *Atmospheric and commutation overvoltages in electrical distribution networks*. Chișinău, Moldova: Generis Publishing. ISBN: 978-1-63002-486-5 [online]. Available at: http://generis-publishing.com/book.php?title=atmospheric-and-commutation-overvoltages-in-electrical-distribution-networks [Accessed: 20 October 2022].

Bjelić, S.N. 2021b. *Alternative theoretical models of the Earth's electromagnetic field*. Niš, Serbia: Control P. ISBN: 978-86-900399-2-0.

Bjelić, S. & Marković, N. 2023. An alternative theoretical model of the Earth's EM field based on two-component field hypotheses. *Vojnotehnički glasnik/Military Technical Courier*, 71(1), pp. 42-65 (in English). Available at: https://doi.org/10.5937/vojtehg71-41987.

Dziewonski, A.M. & Anderson, D.L. 1981. Preliminary reference Earth model. *Physics of the Earth and Planetary Interiors*, 25(4), pp. 297-356. https://doi.org/10.1016/0031-9201(81)90046-7.

Đorđević, A. & Olćan, D. 2012. *Ispitivanje elektromagnetske kompatibilnosti* (in Serbian). Belgrade: Akademska misao. ISBN: 978-86-7466-444-5.

Jacobs, J.A. 1987. Chapter Four The Earth's Magnetic Field. In: Jacobs, J.A (Eds.) *International Geophysics (Book series),* 37, pp. 191-296. Cambridge, Massachusetts: Academic Press. Available at: https://doi.org/10.1016/S0074-6142(08)60712-3.

Mihajlović, J.S. 1993. *Spectral analysis of secular variations and magnetic storms at the Grock Geomagnetic Observatory*. Master's thesis. Belgrade: Universty of Belgrade - Faculty of Mining and Geology (in Serbian).

Petković, D.M. 2016. *Elektromagnetna zračenja, Sveska III, Elektromagnetizam*. Niš, Serbia: University of Niš – Faculty of Occupational Safety. ISBN: 978-86-6093-015-8 [online]. Available at: https://www.znrfak.ni.ac.rs/serbian/010-STUDIJE/OAS-4-1/II%20GODINA/PREDMETI/203-ELEKTROTEHNIKA/ET%20-%20Literatura/ELEKTROMAGNETIZAM.pdf (in Serbian) [Accessed: 15 February 2023].

Prodanović, G. 2006. Matematical analysis of geomagnetic field. *Vojnotehnički glasnik/Military Technical Courier*, 54(1), pp. 88-96 (in Serbian). Available at: https://doi.org/10.5937/vojtehg0601088P.

Прогрессивная теоретическая модель ЭМ поля земной сферы Земли в чужом однородном ЭМ поле

Слободан Н. Белич[а], *Ненад* А. Маркович[б]

[а] Приштинский университет - Косовска Митровица,
Факультет технических наук, Косовска Митровица, Республика Сербия

[б] Косовско-Метохиийская академия профессиональных исследований,
отделение Урошевац – Лепосавич,
г. Лепосавич, Республика Сербия, **корреспондент**

РУБРИКА ГРНТИ: 37.15.00 Геомагнетизм и высокие слои атмосферы
ВИД СТАТЬИ: оригинальная научная статья

Резюме:

Введение/цель: В данной статье описывается прогрессивная теоретическая модель электромагнитного поля Земли, основанная на двухкомпонентных гипотезах. В статье определены математическая модель, показывающая вращение магнитосферы М в чужом магнитном поле и компоненты магнитного поля, которые могут возникнуть вследствие вращения Земли вокруг своей оси. По установленной модели по отношению к эталонным значениям планеты Земля были рассчитаны значения компонентов других планет Солнечной системы. Результаты расчетов представлены в виде таблиц.

Методы: Решение проблемы, обозначенное в заголовке статьи, найдено с помощью комбинированных для этой цели формализованных методов физического и математического анализа с целью разработки новой, прогрессивной математической модели. Для этого использовался метод аналогии, связанный с применением сходных структурных форм и систем для исследования электромагнитных процессов и вращения планет. Метод аналогии применялся по двум взаимосвязанным причинам. Первая заключается в том, что все величины, характеризующие функцию любой естественной системы, подвержены изменению, а вторая − в том, что

применяемые решения не определяют условия функционирования структуры для каждого отдельного случая.

Результаты: Решения в виде оригинальных аналитических формул и многочисленных значений, упорядоченных в Таблице 2, относящихся к влиянию вращения планет, в частности Земли, будут применены для исследования воздействия электромагнитного поля, излучаемого Солнцем по отношению к другим планетам. Это особенно важно в изучении роли, которую этот процесс играет в защите планеты Земля. В Таблице 2 приведены особо важные результаты.

Выводы: В статье обсуждаются возникновение и влияние электромагнитного поля Земли в доступной форме для понимания на современном уровне развития науки. Научные исследования и измерения в геофизике и астрофизике указывают на Солнце как на возможный источник ЭМ поля, распространяющийся через межпланетное пространство, а составляющая магнитного поля Земли является лишь откликом на влияние этого источника. Природные явления и процессы на Земле могут быть представлены в теории систем моделью, содержащей изменения параметров состояния планеты.

Ключевые слова: усовершенствованная модель, теория, планеты, вращение, магнетизм, магнитное поле.

Напреднији теоријски модел ЕМ поља сфере Земље у страном хомогеном ЕМ пољу

Слободан Н. Бјелић[а], *Ненад* А. Марковић[б]

[а] Универзитет у Приштини са седиштем у Косовској Митровици,
Факултет техничких наука, Република Србија
[б] Академија струковних студија косовско метохијска,
Одсек Урошевац – Лепосавић,
Лепосавић, Република Србија, **аутор за преписку**

ОБЛАСТ: теоријска електротехника, електромагнетика
КАТЕГОРИЈА (ТИП) ЧЛАНКА: оригинални научни рад

Сажетак:

Увод/циљ: У раду је описан напреднији теоријски модел ЕМ поља Земље заснован на хипотезама о две компоненте. Дефинисан је математички модел који приказује ротацију магнетнопроводне сфере магнетизације М у страном магнетном пољу и компоненте магнетног поља које могу настати услед ротације Земље око своје осе. Према успостављеном моделу, у односу на референтне вредности планете Земље израчунате су вредности компоненти осталих планета у Сунчевом систему, а резултати су приказани табеларно.

Методе: Решење проблема, дефинисано у наслову рада, одређено је помоћу комбинованих, за ту намену формализованих метода физике и математичке анализе, а ради развоја новог напреднијег математичког модела. У ту сврху коришћен је и метод аналогије који се односио на примену сличних структурних форми и система за истраживање електромагнетних процеса и ротације планета. Метода аналогије примењена је због два узајамно повезана разлога. Први је да су све вредности које карактеришу функцију било ког природног система подложне променама, а други да примењивана решења не одређују услове функције структуре у сваком конкретном случају.

Резултати: Решења у виду оригиналних аналитичких формула и бројне вредности наведене у табели 2, референтне у односу на утицај ротације планета а посебно Земље, биће примењена за истраживање утицаја ефеката ЕМ поља које емитује Сунце према планетама нарочито за улогу коју процес има за заштиту Земље. Посебно су важни резултати приказани у табели 2.

Закључак: У раду су размотрени појава и дејство ЕМ поља Земље на начин разумљив садашњем нивоу развоја науке. Научна сазнања и мерења у геофизици и астрофизици наговештавају да је Сунце могући извор ЕМ поља које се простире кроз интерпланетарни простор, а да је компонента магнетног поља Земље само одзив на утицај тог извора. Природни феномени и процеси на Земљи могу се дефинисати у теорији система моделом који садржи промене параметара стања на планети.

Кључне речи: напреднији модел, теорија, планете, ротација, магнетизам, магнетно поље.

Paper received on / Дата получения работы / Датум пријема чланка: 17.02.2023.
Manuscript corrections submitted on / Дата получения исправленной версии работы / Датум достављања исправки рукописа: 25.03.2023.
Paper accepted for publishing on / Дата окончательного согласования работы / Датум коначног прихватања чланка за објављивање: 27.03.2023.

Analysis of impact toughness and the critical stress intensity factor K_{Ic} in ferrite-austenite welded joints with different heat input

Aleksandar G. Bukvić[a], *Dalibor* P. Petrović[b], *Igor* Z. Radisavljević[c], *Saša* S. Dimitrić[d]

[a] University of Defense in Belgrade, Military Academy, Belgrade, Republic of Serbia,
e-mail: a_bukvic@yahoo.com, **corresponding author**,
ORCID iD: https://orcid.org/0000-0002-3025-8446

[b] University of Defense in Belgrade, Military Academy, Belgrade, Republic of Serbia,
e-mail: dalibor.petrovic140@gmail.com,
ORCID iD: https://orcid.org/0000-0001-6092-5695

[c] Ministry of Defense of the Republic of Serbia, Military Technical Institute, Belgrade, Republic of Serbia,
e-mail: radisavljevicigorbg@gmail.com,
ORCID iD: https://orcid.org/0000-0002-8523-0993

[d] University of Defense in Belgrade, Military Academy, Belgrade, Republic of Serbia,
e-mail: sasa.dimitric@mod.gov.rs,
ORCID iD: https://orcid.org/0000-0003-3547-7047

DOI: 10.5937/vojtehg71-42358; https://doi.org/10.5937/vojtehg71-42358

FIELD: mechanical engineering, mechanical materials, fracture mechanics
ARTICLE TYPE: original scientific paper

Abstract:

Introduction/purpose: Constructions always have several critical points that can be sources of possible defects. All these critical places must be taken into account in safety assessment where the most unfavorable exploitation factors are considered and the local safety of a joint is assessed. Today, joints of various compositions are becoming more frequent in metal constructions. Due to the requirements of economy and ecology, welded joints of microalloyed ferritic steels with high-alloyed austenitic steels are increasingly encountered during the construction of power plants, chemical facilities, etc. Tests of such welded joints have been performed on tanks for oil derivatives, where parts of the tank shell are made of microalloyed ferritic steel and the roof structure is made of high-alloyed austenitic steel.

Methods: In the paper, an experimental analysis of crack propagation in an austenitic-ferritic welded joint was performed. The welding was performed by the MIG welding process with two different heat inputs, and the same filler material MIG 18/8/6 was used. Two types of welded plates were tested.

the characteristics of the base, filler and auxiliary materials and welding technologies are given. Notched test specimens with an initiated crack-type fracture were made in order to determine the impact properties and fracture mechanics parameters.

The results: The research carried out within this study aimed to compare the obtained results of the impact toughness and fracture toughness at flat deformation in a ferrite-austenitic welded joint. An evaluation of the results obtained during the testing of the experimental plates welded with different amounts of heat input is also given.

Conclusion: These test results established the dependence of the geometry of a propagating crack and the stress conditions for further crack propagation. It is possible to determine the values of the parameters that describe the behavior of the material, both in linear-elastic and in elasto-plastic fracture mechanics.

Key words: ferrite-austenitic welded joint, impact toughness, critical stress intensity factor K_{Ic}.

Introduction

Impact toughness tests are important when considering a material's tendency to brittle fracture. Impact tests are performed in order to determine total energy (impact toughness) as well as energy of crack creation and growth in critical parts of welded joints (Rabbolini et al, 2015; Bukvić, 2012).

Efforts are constantly made to study the causes of material fatigue and to mitigate its consequences. Material failure caused by fatigue is the most common form of failure in practice. Such fractures occur at stress values that are lower than the tensile strength even in low-strength plastic materials (Bukvić, 2012; Rabbolini et al, 2015). A large number of structure fractures which occur during exploitation at lower than permissible stress levels indicate the risk of brittle fracture (Bukvić, 2012; Rabbolini et al, 2015).

When studying fatigue of materials using fracture mechanics, it is assumed that there is an initial crack or that the period of its formation is short or negligible. Determining the working life of a structure is reduced to predicting the time of crack growth. The process of material fatigue under variable loading can be divided into three phases (Zerbst et al, 2015), as in Figure 1:

1. *crack formation* (threshold value below which a fatigue crack has no conditions for growth);

2. *crack propagation up to a critical value* (area of application of the Paris equation); and

3. unstable fracture of the final part of the section (ΔK_c at which a fracture occurs).

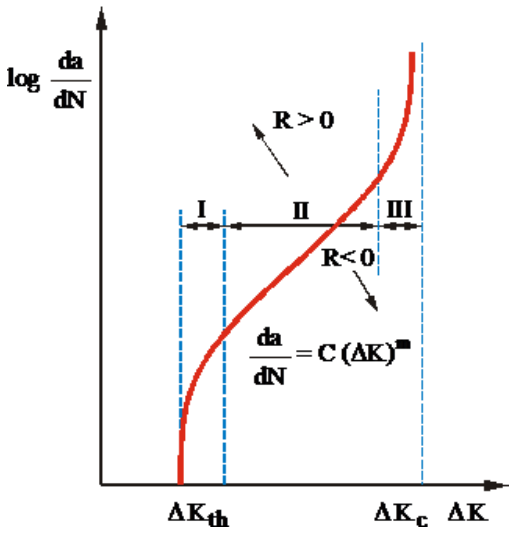

Figure 1 – Typical appearance of the fatigue crack growth curve as a function of ΔK
Рис. 1 – Типичный вид кривой роста усталостной трещины в функции от ΔK
Слика 1 – Типичан изглед криве раста заморне прслине у функцији од ΔK

Fatigue occurs as a result of plastic deformation during the stages of crack formation and growth. Until the final failure of the material, fatigue spreads in the form of plastic failure of the material, although this plasticity, of a completely local nature, is limited only to the process zone. The fatigue effect is a cumulative action of microscopically limited events which can add up to several million in a single fatigue process. Therefore, it is difficult to predict in advance the service life of a structural element that has begun to break and is permanently loaded with a variable load (Zerbst et al, 2015).

The fracture toughness test at flat deformation K_{Ic} was carried out in order to determine the critical factor of stress intensity, K_{Ic}, i.e. the evaluation of the behavior of the components of a welded joint, weld metal and the HAZ in the presence of a crack-type defect as the most dangerous of all defects in structural materials, especially welded joints (Bukvić, 2012; Zerbst et al, 2015).

Chemical and mechanical characteristics of materials and welding technology

Base materials

Two base materials were used for welding: microalloyed steel S500NL1, under the commercial name NIOMOL 490K with a thickness of 16 mm (marked with M) and high-alloyed steel X6CrNiMoTi 17 12 2 according to EN 10088 (Č.4574 according to SRPS EN 10088-1) with a thickness of 12 mm (marked with V) (Bukvić, 2012). Table 1 shows the chemical compositions and Table 2 shows the mechanical properties of the base materials.

Table 1 – Chemical compositions of the base materials (Bukvić, 2012)
Таблица 1 – Химический состав основных материалов (Bukvić, 2012)
Табела 1 – Хемијски састав основних материјала (Bukvić, 2012)

	C	Si	Mn	P	S	Cr	Ni	Cu	Al	Mo	Ti	V	Nb
M	0.10	0.38	0.64	0.014	0.02	0.76	0.10	–	–	0.33	–	0.02	–
V	0.04	0.35	1.73	0.031	0.004	17.9	11.6	0.18	0.061	2.16	0.38	0.079	0.016

Table 2 – Mechanical properties of the base materials (Bukvić, 2012)
Таблица 2 – Механические свойства основных материалов (Bukvić, 2012)
Табела 2 – Механичке особине основних материјала (Bukvić, 2012)

Base materials	Yield stress $R_{0,2}$ [MPa]	Tensile strength R_m [MPa]	Elongation A [%]	Contraction Z [%]
M	497	584	20	65
V	321	596	37	53

Filler material

Welding was performed using filler material MIG 18/8/6, produced in Železarne ACRONI, Jesenice, Slovenia (Bukvić, 2022; Jesenice Ironworks, 2005). Table 3 shows the chemical compositions and Table 4 shows the mechanical properties of the welding wire.

The filler material MIG 18/8/6 was selected based on recommendations from the literature (Jovicic, 2007; Bukvić et al, 2022) and in accordance with the results obtained from the Schaeffler diagram (Bukvić, 2012; Bukvić et al 2022). The result from the Schaeffler diagram is shown in Figure 2.

Table 3 – Chemical compositions of the filler materials (Bukvić, 2022; Jesenice Ironworks, 2005)
Таблица 3 – Химические составы дополнительных материалов (Bukvić, 2022; Jesenice Ironworks, 2005)
Табела 3 – Хемијски састави додатних материјала (Bukvić, 2022; Jesenice Ironworks, 2005)

	C	Si	Mn	Cr	Ni
MIG 18/8/6	0,08	<1.0	7	18.5	9

Table 4 – Mechanical properties of the pure weld metal filler material (Bukvić, 2022; Jesenice Ironworks, 2005)
Таблица 4 – Механические свойства присадочного материала из чистого металла сварного шва (Bukvić, 2022; Jesenice Ironworks, 2005)
Табела 4 – Механичке особине чистог метал шава додатног материјала (Bukvić, 2022; Jesenice Ironworks, 2005)

	R_e, [N/mm^2]	R_m, [N/mm^2]	A_5, [%]	KV,[J]
MIG 18/8/6	> 380	560 do 660	35	> 40 (pri 20 ^{0}C)

The choice of a filler material is directly related to the need for the desired chemical composition. Then the composition of the filler material corresponds to the chemical composition of one of the base materials or the average chemical composition. For bonding high-alloy steel with some other less alloyed or unalloyed steel, a high-alloy filler material should be used, as shown by the position of the filler metal in Figure 2 of the Schaeffler diagram (Bukvić et al, 2022).

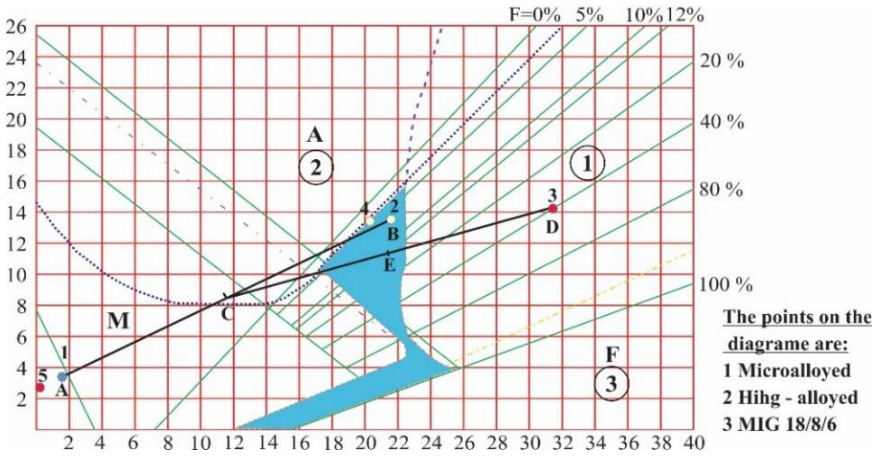

Figure 2 – Positions of base and filler materials in the Schaeffler diagram
Рис. 2 – Положение основных и дополнительных материалов на диаграмме Шеффлера
Слика 2 – Положај основних и додатних материјала у Шефлеровом дијаграму

Welding technology

The plates of the base materials are welded by the electric arc semi-automatic MIG/MAG process. A MIG/MAG welding device KEMPACT 3000+ FastMig 400 was use for welding. Two different heat inputs were applied, as shown in Tables 5 and 6. Two welded experimental plates were formed: with a maximum heat input of 8.88 [kJ/cm], plate number 1, and with a minimum heat input of 6.87 [kJ/cm], plate number 2 (Bukvić, 2012; Bukvić et al 2022).

Table 5 – Average amount of heat input during the welding of plate number 1 (Bukvić, 2012)
Таблица 5 – Среднее количество подводимого тепла при сварке пластины № 1 (Bukvić, 2012)
Табела 5 – Просечан унос количине топлоте при заваривању плоче број 1 (Bukvić, 2012)

Plate and wire designation	Welding		Average strength electricity [A]	Average voltage [V]	Average amount of heat input [kJ/cm]
	Mean time [min.]	Medium speed [cm/min]			
Plate number 1	2.22	24.2	214	26.37	8.88

Table 6 – Average input of heat during the welding of plate number 2 (Bukvić, 2012)
Таблица 6 – Среднее количество подводимого тепла при сварке пластины № 2 (Bukvić, 2012)
Табела 6 – Просечан унос количине топлоте при заваривању плоче број 2 (Bukvić, 2012)

Plate and wire designation	Welding		Average strength electricity [A]	Average voltage [V]	Average amount of heat input [kJ/cm]
	Mean time [min.]	Medium speed [cm/min]			
Plate number 2	2.19	34.15	243	30.47	6.87

The shielding gas flow was 12 l/min. A mixture of Ar and 2% O_2 gases was used as a protective atmosphere during welding (Smiljanić, 2006; Messer Tehnogas, 2008).

The welding was performed using the multi-pass advance welding technique. For each welded plate, the number of passes during welding was six and it was determined by the speed of welding, different voltage and strength of current, i.e. different amount of heat input during welding. Each plate of the base material was preheated, and the intermediate temperature was maintained by heating with a flame from a mixture of oxygen and acetylene. With each welded plate, the root passage is first welded from the inside of the groove. After that, the filling passages were welded. The

resulting welded plates were cooled in still air (Bukvić, 2012; Bukvić et al, 2022).

The welded joints were visually inspected and subjected to radiographic ventilation with γ-rays. No defects such as cracks, lack of penetration, sticking, etc. were detected.

The welded plates were machined to the same thickness of 12 mm (Bukvić, 2012; Bukvić et al, 2022).

From the obtained welded plates number 1 and 2 of the ferritic-austenitic welded joint, test specimens were cut in accordance with the standards for testing impact toughness and for determining fracture toughness at flat deformation K_{Ic}.

Test of impact toughness on an instrumented Charpy pendulum

The test of impact force on notched test specimens can provide an explanation about the behavior of a material around the crack tip, starting from the assumption that the test specimen material is sufficiently homogeneous under a plane state of stress (Miletić et al, 2020; Paris & Erdogen, 1963). Determining the energy required for fracture under established test conditions is most often used for regular control of the quality and homogeneity of a material, as well as for its processing quality control. With this test procedure, the tendency to increase brittleness during exploitation (aging) can be determined. The impact tests of the test specimens were performed in accordance with ASTM E23-95 Standard (Miletić et al, 2020; Paris & Erdogen, 1963), on the test specimens of the dimensions and appearance as in Figure 3 and in order to determine the total impact energy (Miletić et al, 2020; Paris & Erdogen, 1963).

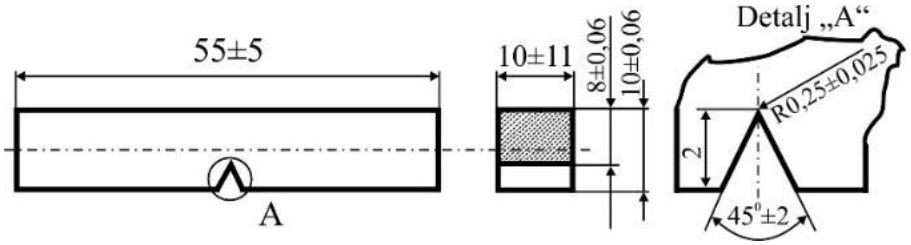

Figure 3 – Standard impact test specimen
Рис. 3 – Стандартный образец для испытания на удар
Слика 3 – Стандардна епрувета за испитивање ударне жилавости

The notch position in relation to the welded joint is defined by ISO 9016:2022 Standard (ISO, 2022). The notch is made by milling so that the state of the material does not change during processing.

In bending impact load testing, fracture energy is determined as an integral quantity. The fracture energy determined in this way does not give the possibility of separating the resistance of the material related to the formation, i.e. the propagation of the crack. The impact force and time were continuously recorded during the test on an instrumented pendulum. This is how the force-time diagram was obtained. From it, it is possible to calculate the total energy E_{uk}, required for the fracture of a specimen using the formula (Miletić et al, 2020; Paris & Erdogen, 1963):

$$E_{uk} = \int_0^{t_1} F(t) \cdot v(t) \cdot dt \quad (1)$$

where: *F(t)* – force; *v (t)* – change in the speed of the pendulum during the break; and *t* – duration of fracture.

In order to evaluate the behavior of the material under impact load, it is necessary to know which part of the energy is used for the formation of the crack, and which part for the propagation of the crack. The procedure for determining the energy of crack growth through the "fatigue crack" was used. The part of the energy required to form an E_{inic} crack is calculated by the formula (Miletić et al, 2020; Paris & Erdogen, 1963):

$$E_{inic} = E_{uk} - E_{lom} \quad (2)$$

The energy of formation and the energy of crack growth are determined by this method on one specimen (unlike other procedures), which gives higher accuracy (Miletić et al, 2020; Paris & Erdogen, 1963).

Impact toughness test results on an instrumented Charpy pendulum

The impact energy was determined on an instrumented Charpy pendulum with an oscilloscope whose impact load range is 150/300 J. Standard Charpy V-notch test specimens were used during the test, as in Figure 3, and the energies were calculated by formulas (1) and (2).

Results of testing the toughness of the base material

At the very beginning, before welding, from the plate of microalloyed steel NIOMOL 490K, the test specimens were cut normal to the direction of rolling of the plate and marked with a U mark with a notch normal to the rolling direction. After that, test specimens were cut from the same plates

in the rolling direction and marked with a P, with a notch parallel to the rolling direction. The cut test specimens were tested for impact toughness. The test was performed at room temperature. The obtained results are shown in Table 7 and Figure 4.

Table 7 – Fracture energy of the test specimens made of a microalloyed steel base material
Таблица 7 – Энергия разрушения испытуемых образцов, изготовленных из микролегированной стали
Табела 7 – Енергија лома епрувета из основног материјала микролегираног челика

Material	Test specimen label	Notch place	Impact energy, E_u [J]		Crack formation energy, E_{inic} [J]		Propagation energy, E_{lom}[J]	
			By test specimen	Average value	By test specimen	Average value	By test specimen	Average value
Microalloyed steel NIOMOL 490 K	P–1	Transverse to the rolling direction	279.2	265.9	73.7	78.1	205.5	201.1
	P–2		252.6		82.5		196.7	
	U–1	Normal to the rolling direction	253.4	252.1	78.2	77.1	175.2	175
	U–2		250.8		76.1		174.7	

As it can be seen from Table 7 and from the diagram in Figure 4, the total impact energies of microalloyed steel do not differ significantly depending on where the notch is placed in relation to the plate rolling direction. The total energy is slightly higher when the notch is transverse to the rolling direction and ranges from 252.6 J to 279.2 J. When the notch is placed normally to the rolling direction, the total energy is slightly lower and has a value of 250.8 J to 253.4 J.

Table 7 and the diagrams in Figure 4 show that the energy of crack formation does not depend significantly on the position of the notch. It ranges from 78.1 J when the notch is transverse to the rolling direction to 77.1 J when the notch is normal to the rolling direction. It is observed that the crack propagation energy depends on the position of the notch. It ranges from 201.1 J when the notch is transverse to the rolling direction to 175 J when the notch is normal to the rolling direction.

The properties of high-alloy austenitic steel were not investigated, because it is known from the literature (Sedmak A. et al, 2022) that austenitic steels have good toughness at low temperatures. On pressure vessels (Golubović et al, 2018), structural changes in the base material and the HAZ were neither expected nor revealed by the examination.

Diagrams $F-\tau$ and $E_u-\tau$

The specimen P-2 *The specimen U-1*

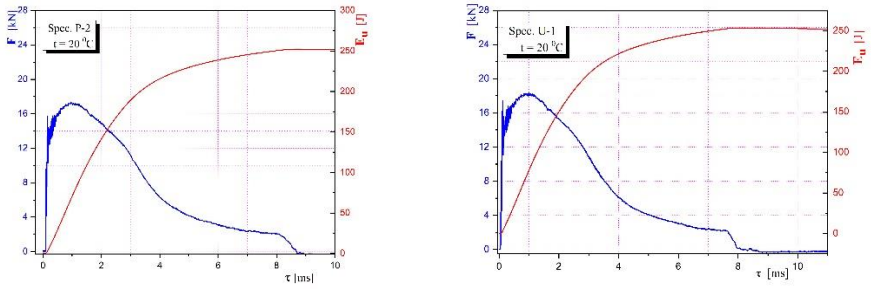

Figure 4 – Diagrams obtained from the impact tests of the microalloyed steel test specimens
Рис. 4 – Диаграммы, полученные в результате испытаний образцов из микролегированной стали на ударную вязкость
Слика 4 – Дијаграми добијени ударним испитивањима епрувета од микролегираног челика

Results of the impact tests on the test specimens with a notch in the filler metal

During the test, standard Charpy test specimens with a V notch in the filler metal were used, as in Figure 3. Two test specimens were cut from the welded experimental plates number 1 and 2, and the test was performed at room temperature. The obtained results are shown in Table 8 and Figure 5.

Table 8 – Fracture energy of the test specimens with a notch in the filler metal
Таблица 8 – Энергия разрушения испытуемых образцов с надрезом в металле шва
Табела 8 – Енергија лома епрувета са зарезом у метал шаву

Plate no.	Test specimen label	Impact energy, E_u [J]		Formation energy, E_{inic} [J]		Propagation energy, E_{lom}[J]	
		By test specimen	Average value	By test specimen	By test specimen	Average value	By test specimen
1	1.1	126	130.5	49.8	55	76.2	75.5
	1.2	135.1		60.2		74.9	
2	2.1	134.9	135.3	52.2	58.5	82.7	76.8
	2.2	135.8		64.7		71.1	

As it can be seen from Table 8 and from the diagram in Figure 5, the difference in total impact energies for all test specimens is not large. The total impact energy is the highest in the test specimen from plate number

2 and it ranges from 134.9 J to 135.8 J. Negligibly lower total impact energy was achieved in the test specimen from plate number 1 - from 126 J to 135.1 J. Obviously, a different amount of heat input during welding did not affect the total toughness energy when the notch is located in the filler metal zone.

Diagrams $F-\tau$ and $E_u-\tau$

The specimen 1.1 *The specimen 2.1*

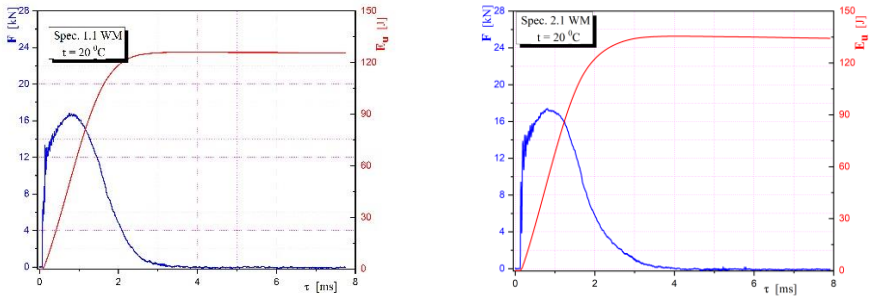

Figure 5 – Diagrams of the impact tests of the test specimens from experimental plates 1 and 2 with a notch in the filler metal
Рис. 5 – Диаграммы ударных испытаний образцов - опытных пластин № 1 и 2 с надрезом в металле шва
Слика 5 – Дијаграми ударних испитивања епрувата из експерименталних плоча број 1 и 2 са зарезом у метал шаву

Plate 2 has a slightly higher crack formation energy of 58.5 J, and the lower crack formation energy of the test specimen from plate number 1 is 55 J. The difference is not significant.

Plate number 2 has a higher crack propagation energy of 76.8 J and the test specimens from plate number 1 have a lower crack propagation energy of 75.5 J. The difference is negligible.

Results of the impact tests on the test specimens with a notch in the HAZ

During the test, standard Charpy test specimens were used, where a V notch was placed in the HAZ towards the microalloyed steel, as in Figure 3. Two test specimens were cut from experimental plates 1 and 2. The obtained results are shown in Table 9 and Figure 6.

In Table 9 and in the diagram of Figure 6, the total impact energies are slightly higher than the impact energies obtained from the test specimens with a notch in the filler metal in Table 8. In the test specimen from plate 1, the total

energy is from 190.5 J to 218.1 J, while it is from 189.5 J to 216.3 J in the test specimen from plate 2.

Table 9 – Fracture energy of the notched test specimens in the HAZ towards the microalloyed steel
Таблица 9 – Энергия разрушения испытуемых образцов с надрезами в ЗТВ по отношению к микролегированной стали
Табела 9 – Енергија лома епрувета са зарезом у ЗУТ ка микролегираном челику

Plate no.	Test specimen label	Impact energy, E_u [J]		Formation energy, E_{inic} [J]		Propagation energy, E_{lom}[J]	
		By test specimen	Average value	By test specimen	By test specimen	Average value	By test specimen
1	1.3	218.1	204.3	68.5	63.5	149.3	140.8
	1.4	190.5		58.2		132.3	
2	2.3	189.5	202.9	61.1	67.8	128.4	135.1
	2.4	216.3		74.6		141.7	

Diagrams $F-\tau$ and $E_u-\tau$
The specimen 1.3 *The specimen 2.3*

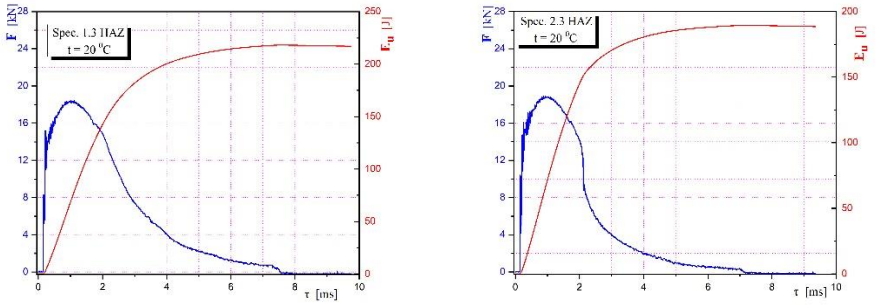

Figure 6 – Diagrams of the impact tests of the test specimens with a notch in the HAZ
Рис. 6 – Диаграммы ударных испытаний образцов с надрезом в ЗТВ
Слика 6 – Дијаграми ударних испитивања епрувета са зарезом у ЗУТ

The crack formation energy is of very uniform values. The test specimens from plate 2 have a higher crack formation energy of 67.8 J while the test specimens from plate 1 have a slightly lower crack formation energy of 63.5 J.

Crack propagation energy does not differ from plate to plate. The test specimens from experimental plate 1 have a higher crack propagation energy of 140.8 J and the test specimens from experimental plate 2 have a slightly lower crack propagation energy of 135.1 J.

Determining the fracture toughness during flat deformation K_{Ic}

Examining test specimens with a crack shows the local behavior of the material around the crack tip, starting from the assumption that the material around the crack is sufficiently homogeneous, which means that the results of the local behavior can be treated globally, i.e. they can be directly transferred to an appropriate construction. The influence of the heterogeneity of a structure and the mechanical properties of a welded joint is primarily reflected in the position of the fatigue crack tip and the characteristics of the area through which the fracture propagates (Bukvić, 2012; Zerbst et al, 2015; Kumar et al, 2016).

The test of fracture toughness during flat deformation K_{Ic} was carried out in order to determine the critical stress intensity factor K_{Ic}, i.e. the evaluation of the behavior of the components of the welded joint, weld metal and the HAZ in the presence of a crack-type defect as the most dangerous of all defects in structural materials, especially welded joints (Bukvić, 2012; Zerbst et al, 2015; Kumar et al, 2016). The test was performed at room temperature.

Two groups of test specimens were tested depending on the location of the fatigue crack tip, namely:

- Group I - test specimens with the fatigue crack tip in the filler metal,
- Group II - test specimens with the fatigue crack tip in the HAZ towards microalloyed steel.

Three-point bending test specimens (SEB) were used to determine K_{Ic}, the geometry of which is defined by ASTM E399 Standard and given in Figure 7.

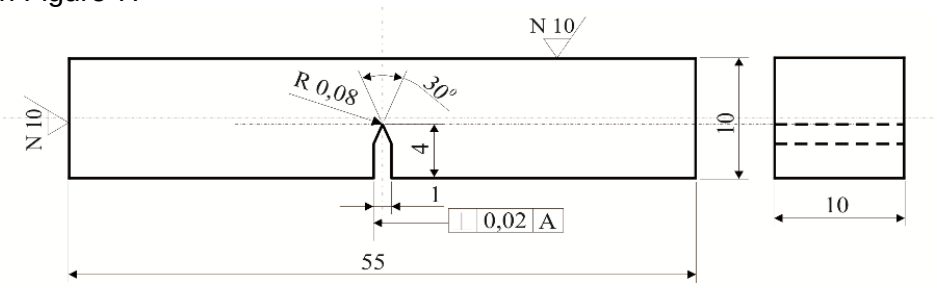

Figure 7 – Specimen for fracture mechanics testing
Рис. 7 – Образец для испытаний на механику разрушения
Слика 7 – Епрувета за испитивање механике лома

As defined by ASTM E399 Standard, i.e. BS 7448 Part 1, the first step was to prepare a test specimen, i.e. to form a fatigue crack. The fatigue crack on the fractured test specimen marked 1.5 under c is shown in Figure 8. Approximately 50% of the final length of the fatigue crack was produced at the maximum fatigue force $F_{max} = 0.4 \cdot F_L$. In this case, the minimum force was $F_{min} = 0.1 \cdot F_{max}$. The fatigue crack was formed on an AMSLER high-frequency pulsator". The condition of flat state of deformation is not satisfied according to ASTM E399:

$$B \geq 2.5 \cdot \left(\frac{K_{Ic}}{R_{p0.2}}\right)^2 \tag{3}$$

In that case, instead of applying linear-elastic fracture mechanics (LEML) defined by ASTM E399 Standard, elasto-plastic fracture mechanics (EPML) defined by ASTM E813, ASTM E1152, ASTM E1820-18 and BS 7448 Part 1 and 2 Standards was applied. the purpose of using elasto-plastic fracture mechanics is to determine the value of the critical stress intensity factor K_{Ic} indirectly via the critical J-integral J_{Ic}, i.e. to monitor the crack growth under the conditions of pronounced plasticity. The behavior of the elasto-plastic material, which also includes the components of the welded joint, during a stable crack growth can be described by the *J-Δa* diagram, where *Δa* is crack growth (Bukvić, 2012; Zerbst et al, 2015; Kumar et al, 2016).

Based on the obtained data, a *J-Δa* curve is constructed, on which a regression line is constructed according to ASTM E1152. The critical J-integral J_{Ic} is obtained from the obtained regression line. Knowing the values of the critical J_{Ic} integral, one can calculate the value of the critical stress intensity factor or the fracture toughness at flat deformation K_{Ic}, using dependence (4) ASTM E399:

$$K_{Ic} = \sqrt{\frac{J_{Ic} \cdot E}{1-\nu^2}} \tag{4}$$

where: *E* – modulus of elasticity and *v* – Poisson's ratio.

The critical value of the stress intensity factor K_{Ic} was determined using the method of one test specimen with successive loading and unloading (Bukvić, 2012; Zerbst et al, 2015; Kumar et al, 2016).

Based on the data collected from a tensile machine (force transducer and COD transducer), the diagrams of force *F*–Crack Mouth Opening Displacement *δ* (CMOD–Crack Mouth Opening Displacement) were constructed.

These diagrams are the basis for determining the critical value of the J-integral J_{Ic}. However, in order to determine the length of the crack ***Δa***, it is necessary to measure the length of the original fatigue crack a_Z (Bukvić, 2012; Zerbst et al, 2015; Kumar et al, 2016).

Determination of K_{Ic} in the test specimens with a notch in the filler metal

The results of measuring the length of the fatigue crack are given in Table 10 while the diagrams *F-δ* and *J-Δa* for the test specimens with a notch in the filler metal are given in Figures 8 and 9.

Table 10 – Fatigue crack lengths of the specimens with a notch in the filler metal

Таблица 10 – Длина усталостной трещины образца с надрезом в металле шва

Табела 10 – Дужине заморне прслине епрувета са зарезом у метал шаву

Plate no.	Test specimen label	Fatigue crack length, a_Z[mm]					Average value, a_{ZSR}[mm]
		a_{z1}	a_{z2}	a_{z3}	a_{z4}	a_{z5}	
1	1.5	2.85	2.93	3.34	3.67	3.26	3.21
2	2.5	2.42	2.90	2.65	2.92	2.92	2.762

The calculated values of the critical stress intensity factor, K_{Ic}, are given in Table 11 for the test specimens with a notch in the filler metal. In the calculation for fracture toughness at flat deformation K_{Ic}, a single value for the modulus of elasticity at room temperature of 210 GPa was used.

The fracture toughness values K_{Ic} of the specimens with a notch in the filler metal range from 125.1 MPa $m^{1/2}$ to 130.5 MPa $m^{1/2}$. The values do not differ significantly, because it is the same filler material, regardless of the difference in the amount of heat input during welding.

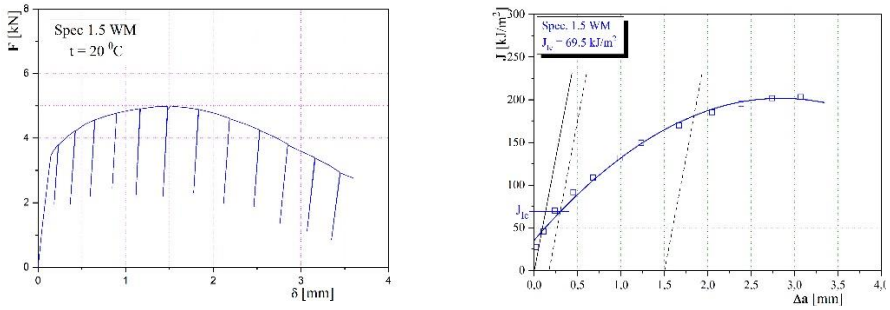

a) b)

c)

Figure 8 – (a) F–δ diagram, (b) J–Δa diagram and (c) a broken test specimen 1.5 with a notch in the filler metal

Рис. 8 – Диаграммы F–δ (a), J–Δa (b) и (c) разрушенный образец 1,5 с надрезом в металле шва

Слика 8 – (а) дијаграми F-δ , (b) J-Δa и (c)преломљена епрувета 1,5 са зарезом у метал шаву

Table 11 – K_{Ic} values of the specimens with a notch in the filler metal

Таблица 11 – Значения образцов K_{Ic} с надрезом в металле шва

Табела 11 – Вредности K_{Ic} епрувета са зарезом у метал шаву

Plate no.	Test specimen label	Critical J–integral, J_{Ic} [kJ/m^2]	Critical stress intensity factor, K_{Ic} [MPa m$^{1/2}$]	Critical crack length, a_C [mm]
1	1.5	69.5	125.1	93.4
2	2.5	75.6	130.5	100.9

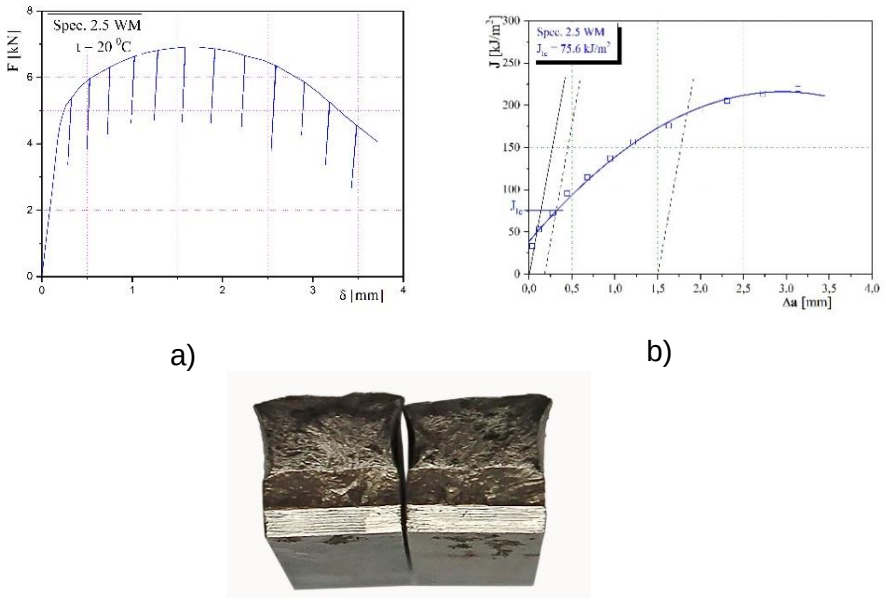

Figure 9 – (a) F–δ diagram, (b)J–Δa diagram and (c) a broken test specimen 2.5 with a notch in the filler metal
Рис. 9 – Диаграммы F–δ (a), F–δ (b) и (c) в разрушенных образцах 2.5 с надрезом в металле шва
Слика 9 – (а) дијаграми F-δ, (b) F-δ и (c)преломљена епрувета 2,5 са зарезом у метал шаву

Determination of K_{Ic} in the test specimens with a notch in the HAZ

The results of measuring the fatigue crack length in the test specimens with a notch in the HAZ towards microalloyed steel are given in Table 12 and in the *F-δ* and *J-Δa* diagrams in Figures 10 and 11.

Table 12 – Fatigue crack lengths of the notched test specimens in the HAZ at room temperature
Таблица 12 – Длины усталостных трещин на испытуемых образцах с надрезами в ЗТВ при комнатной температуре
Табела 12 – Дужине заморне прслине епрувета са зарезом у ЗУТ на собној температури

Plate no.	Test specimen label	Fatigue crack length, a_Z [mm]					Average value, a_{ZSR} [mm]
		a_{z1}	a_{z2}	a_{z3}	a_{z4}	a_{z5}	
1	1.6	3.46	3.47	3.28	2.41	2.34	2.99
2	2.6	2.17	3.56	3.19	3.43	3.31	3.13

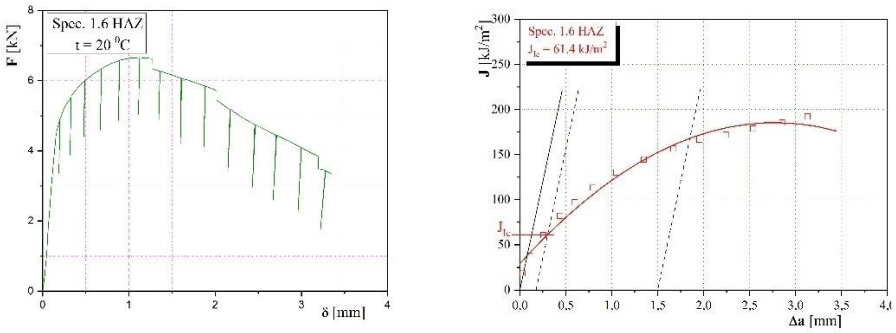

a) b)

c)

Figure 10 – (a) F - δ diagram, (b) J - Δa diagram and (c) a broken test specimen 1.6 with a notch in the HAZ towards the microalloyed base material

Рис. 10 –(a) диаграмма F - δ, (b) J - Δa и (c) разрушенный испытуемый образец 1.6 с надрезом в ЗТВ со стороны микролегированного основного материала

Слика 10 – (a) дијаграми F-δ , (b) J-Δa и (c)преломљена епрувета 1,6 са зарезом у ЗУТ са стране микролегираног основног материјала

Table 13 – Fatigue crack lengths of the notched test specimens in the HAZ

Таблица 13 – Длины усталостных трещин на испытуемых образцах с надрезами в ЗТВ
Табела 13 – Дужине заморне прслине епрувета са зарезом у ЗУТ

Plate no.	Test specimen label	Critical J–integral, J_{Ic} [kJ/m^2]	Critical stress intensity factor, K_{Ic} [MPa m$^{1/2}$]	Critical crack length, a_C [mm]
1	1.6	61.4	117.6	82.5
2	2.6	69.5	125.1	92.7

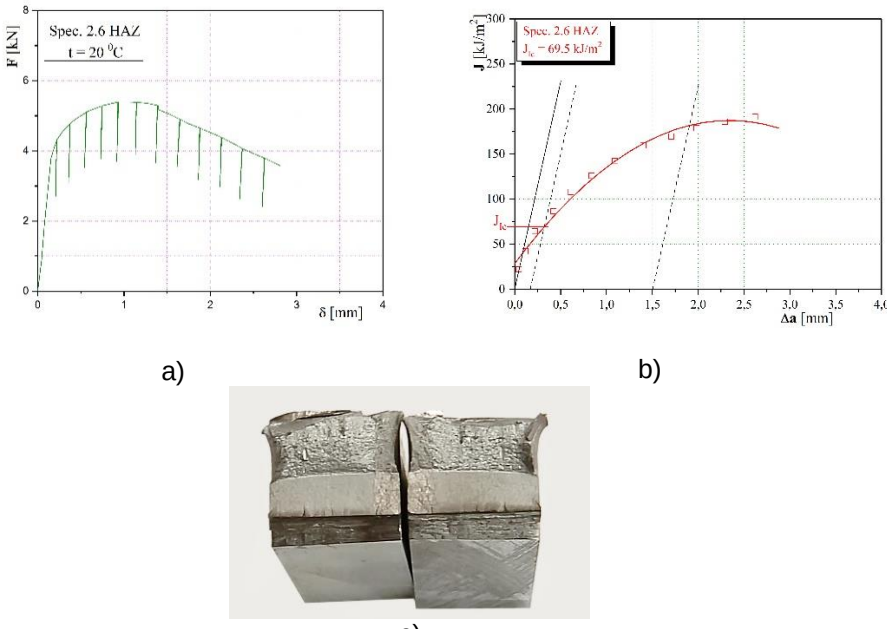

Figure 11 – (a) F - δ diagram, (b) J - Δa diagram and (c) a broken test specimen 2.6 with a notch in the HAZ towards the microalloyed base material
Рис. 11 –(а) диаграмма F - δ, (b) J - Δa и (c) разрушенный испытуемый образец 2.6 с с надрезом в ЗТВ со стороны микролегированного основного материала
Слика 11 – (а) дијаграми F-δ, (b) J-Δa и (c)преломљена епрувета 2,6 са зарезом у ЗУТ са стране микролегираног челика

The obtained values of fracture toughness K_{Ic} of the test specimens with a notch in the HAZ towards microalloyed steel, shown in Table 13, range from 117.6 MPa $m^{1/2}$ to 125.1 MPa $m^{1/2}$. The values do not differ significantly, which means that a different amount of heat input during welding had no effect.

Analysis of the results

In practice, different base and filler materials are used for welding in order to optimise constructions. The economy of construction is not the only reason for such use of materials. For example, storage tanks for liquid petroleum products are made of different materials. This paper deals with base materials with different chemical compositions and filler materials that have similar characteristics to one of base materials, i.e. to austenitic high-alloy steel. In such cases, different microstructures can be expected

to appear in welded joints. All this makes it difficult to predict the behaviour of such joints in use.

Welding with the filler material MIG 18/8/6 yielded two welded experimental plates, marked 1 and 2, where different amounts of heat input were used.

Experimental plates 1 and 2 were welded with the highest and lowest allowed amount of heat input. It is noted that the difference in heat input is about 30%. The obtained values of the quantity of input heat represent, in this case, the limit values for the chosen welding procedure and the filler material.

According to the Schaeffler diagram (Figure 2), it is possible to use the filler material MIG 18/8/6 during welding because the result of this bonding is in the safe area.

In testing microalloyed steel toughness at room temperature, it was observed that high values of total energy were obtained regardless of the direction in which either the test specimens or the notches were cut (transverse or normal to the rolling direction). The total impact energy is 5.3% lower for the test specimens cut transversely to the rolling direction and with their notch normal to the rolling direction. From the obtained results, the energies of crack propagation are higher than the energies of formation, which indicates the fact that the examined material is ductile.

The total impact energy obtained by testing the test specimens with a notch in the metal seam from experimental plates 1 and 2 shows that the highest achieved total energy is for the test specimens from plate 2, and a total energy lower by 3% was obtained for the test specimens from plate 1. In the tested cases, the ductile component is greater than the brittle one, so it can be concluded that experimental plates 1 and 2 with a notch in the metal seam behaved as ductile at room temperature.

The comparison of the obtained impact toughness values for the test specimens with a notch in the HAZ towards microalloyed steel from plates 1 and 2 shows that the values are high and slightly lower than the toughness values in the microalloyed steel test specimens. This decrease in toughness is due to the growth of grains in the HAZ and the appearance of bainite in the structure. In all tested samples, the energy of propagation is higher than the energy of formation. This leads to the conclusion that the test specimens were ductile at room temperature.

Observing the obtained values of the critical stress intensity factor K_{Ic} for the test specimens with a notch in the metal seam, one can notice that different amounts of heat input during welding did not give significant differences in the values of K_{Ic}.

The obtained critical crack lengths are adequate to the obtained K_{Ic} values, so the highest value is for plate 2, and a slightly smaller one for plate 1. It can be concluded, based on the values of the critical crack lengths and fatigue crack lengths for the test specimens with a notch in the metal seam, that the best characteristics in the presence of a crack-type defect will be shown by plate 2 followed closely by plate 1.

Observing the obtained values of the critical stress intensity factor K_{Ic} for the test specimens with a notch in the HAZ towards microalloyed steel leads to the conclusion that plate 2 has the highest values while plate 1 has a lower value by 6%.

The obtained critical crack lengths are adequate to the obtained K_{Ic} values, so the highest value is obtained by plate 2 while plate 1 has a lower value by 11%.

Conclusions

Based on the test results, the following conclusions can be drawn:

1. The resistance of microalloyed steel to crack formation and growth is uniform regardless of whether test specimens are cut in the rolling direction of the experimental plates or cut normal to the rolling direction of the plates;
2. The obtained impact energies from the test specimens with a notch in the metal seam are lower than the impact energies from the test specimens with a notch in the HAZ by about 35%;
3. Different amount of heat input during welding with the same filler material does not give a difference in the obtained impact energy;
4. A higher value of the critical stress intensity factor K_{Ic} was obtained for the test specimens with a notch in the metal seam compared to the test specimens with a notch in the HAZ;
5. The critical length of the cracks is smaller in the test specimens with a notch in the HAZ by about 10%; and
6. If a construction made of the materials used in this study is exposed to a stress lower than the yield stress and if there is a crack in their welded joint smaller than the critical one, there is no risk of fracture.

References

-ASTM International. 1989. *ASTM E813 (1989) Standard Test Method for J_{Ic} a Measure of Fracture Toughness.* West Conshohocken, PA, USA: ASTM International.

-ASTM International. 2017. *ASTM E399-90 (1997) Standard Test Method for Plane-Strain Fracture Toughness of Metallic Materials.* Available at: https://doi.org/10.1520/E0399-90R97.

-ASTM International. 2019. *ASTM E1820-18 Standard Test Method for Measurement of Fracture Toughness.* Available at: https://doi.org/10.1520/E1820-18.

-ASTM International. 2021. *ASTM E1152-95 Test Method for Determining J-R Curves (Withdrawn 1997)* [online]. Available at: https://www.astm.org/standards/e1152 [Accessed: 20 January 2023].

-British Standards Institution (BSI). 2023. *Multi-part Document BS 7448- Fracture mechanics toughness tests.* London, UK: The British Standards Institution (BSI). Available at: https://doi.org/10.3403/BS7448.

Bukvić, A. 2012. *Research of the influence of additional materials on the behavior of ferritic austenitic welded joints*. Ph.D. thesis. Belgrade: University of Belgrade - Faculty of Mechanical Engineering (in Serbian).

Bukvić, A., Petrović, D., Radisavljević, I. & Dimitrić, S. 2022. Influence of heat input on the tensile properties of austenitic-ferritic welded joints. *Vojnotehnički glasnik/Military Technical Courier*, 70(2), pp.409-432. Available at: https://doi.org/10.5937/vojtehg70-36252.

Golubović, T., Sedmak, A., Spasojević-Brkić, V., Kirin, S. & Veg, E. 2018. Welded joints as critical regions in pressure vessels - case study of vinyl-chloride monomer storage tank. *Hemijska industrija*, 72(4), pp.177-182. Avaliable at: https://doi.org/10.2298/HEMIND171009006G.

-ISO. 2022. *ISO 9016:2022 Destructive tests on welds in metallic materials - Impact tests - Test specimen location, notch orientation and examination* [online]. Available at: https://www.iso.org/standard/81122.html [Accessed: 20 January 2023].

-Jesenice Ironworks. 2022. *Additional welding materials, catalog*. Jesenice Ironworks.

Jovičić, R. 2007. *Analysis of the effect of cracks on the integrity of ferritic-austenitic welded joints*. Ph.D. thesis. Belgrade: University of Belgrade - Faculty of Mechanical Engineering (in Serbian).

Kumar, Y., Venugopal, S., Sasikala, G., Albert, S.K. & Bhaduri, A.K. 2016. Study of creep crack growth in a modified 9Cr–1Mo steel weld metal and heat affected zone. *Materials Science and Engineering: A*, 655, pp.300-309. Available at: https://doi.org/10.1016/j.msea.2015.12.053.

-Messer Tehnogas. 2008. *Technical documentation: Shielding gases in welding*. Belgrade, Serbia: Messer Tehnogas AD (in Serbian).

Miletić, I., Ilić, A., Nikolić, R.R., Ulewicz, R. Ivanović, L . & Sczygiol, N. 2020. Analysis of Selected Properties of Welded Joints of the HSLA Steels. *Materials*, 13(6), art.ID:1301. Available at: https://doi.org/10.3390/ma13061301.

Paris, P. & Erdogen, F. 1963. A Critical Analysis of Cracks Propagation Laws. *Journal of Basic Engineering*, 85(4), pp.528-533. Available at: https://doi.org/10.1115/1.3656900.

Rabbolini, S., Beretta, S., Foletti, S. & Riva, A. 2015. Short crack propagation in LCF regime at room and high temperature in Q & T rotor steels. *International Journal of Fatigue*, 75, pp.10-18. Available at: https://doi.org/10.1016/j.ijfatigue.2015.01.009.

Sedmak, A., Arsić, M., Milovanović, N., Opačić, M. & Đorđević, B. 2022. Structural Integrity Analysis of a Kaplan Turbine Cover. *Procedia Structural Integrity*, 37, pp.263-268. Available at: https://doi.org/10.1016/j.prostr.2022.01.083.

Smiljanić, M. 2006. Zaštitni gasovi u zavarivanju. In: *DUZS Seminar*, pp.36-43, July 2006. (in Serbian).

Zerbst, U., Klinger, C. & Clegg, R 2015. Fracture mechanics as a tool in failure analysis - Prospects and limitations. *Engineering Failure Analysis*, 55, pp.376-410. Available at: https://doi.org/10.1016/j.engfailanal.2015.07.001

Анализ ударной вязкости и критического коэффициента интенсивности напряжений K_{ic} в ферритно-аустенитных сварных соединениях с различным подводом тепла

Александар Г. Буквич[а], **корреспондент**, *Далибор* П. Петрович[а], *Игор* З. Радисавлевич[б], *Саша* С. Димитрич[а]

[а] Университет обороны в г. Белград, Военная академия, г. Белград, Республика Сербия

[б] Министерство обороны Республики Сербия, Военно-технический институт, г. Белград, Республика Сербия

РУБРИКА ГРНТИ: 81.35.39 Сварные металлоконструкции, 81.35.13 Технология и оборудование сварочного производства

ВИД СТАТЬИ: оригинальная научная статья

Резюме:

Введение/цель: В любой конструкции всегда имеется несколько критических точек, которые могут оказаться источниками образования дефектов. Все эти критические места однозначно должны приниматься во внимание при оценке безопасности, которая нацелена на выявление наиболее неблагоприятных факторов эксплуатации и оценку локальной безопасности соединений. Сегодня в металлоконструкциях все чаще встречаются соединения различного состава. В связи с требованиями энергоэффективности и экологии при строительстве электростанций, химических объектов и пр. сварные соединения микролегированных ферритных сталей с высоколегированными аустенитными сталями встречаются все чаще. Испытания таких сварных соединений проводились на резервуарах для нефтепродуктов, части корпуса которого изготовлены из микролегированной ферритной стали, а конструкция крыши − из высоколегированной аустенитной стали.

Методы: В данной статье представлены результаты экспериментального анализа распространения трещины в аустенитно-ферритном сварном соединении. Сварка выполнялась методом MIG с двумя различными тепловыми подводами, причем

использовался один и тот же присадочный материал MIG 18/8/6. Были испытаны два типа сварных пластин. В статье описаны характеристики основных, дополнительных и расходных материалов, а также технологии сварки. Для определения ударных свойств и параметров механики разрушения были изготовлены испытательные образцы с надрезами и начавшимся разрушением по типу трещины.

Результаты: Целью данного исследования являлось сравнение полученных результатов ударной вязкости, вязкости разрушения и деформации в плоскости феррито-аустенитного сварных соединений. Также в статье приведена оценка результатов, полученных при испытании экспериментальных пластин, свариваемых с различным количеством подводимого тепла.

Выводы: По результатам испытаний выявлена зависимость геометрии расширения трещины от условиий напряжения. Таким образом можно определить значения параметров, описывающих поведение материала, как при линейно-упругой, так и при упруго-пластической механике разрушения.

Ключевые слова: ферритно-аустенитное сварное соединение, ударная вязкость, критический коэффициент интенсивности напряжений K_{Ic}.

Анализа ударне жилавости и критичног фактора интензитета напона K_{Ic} код феритно-аустенитних заварених спојева различитим уносом топлоте

Александар Г. Буквић[а], **аутор за преписку**, *Далибор* П. Петровић[а], *Игор* З. Радисављевић[б], *Саша* С. Димитрић[а]

[а] Универзитет одбране у Београду, Војна академија, Београд, Република Србија

[б] Министарство одбране Републике Србије, Војнотехнички институт, Београд, Република Србија

ОБЛАСТ: машинство, машински материјали
ВРСТА ЧЛАНКА: оригинални научни рад

Сажетак:

Увод/циљ: Критична места конструкција извор су могућих дефеката, па се морају узети у обзир при процени сигурности, где ће се сагледати најнеповољнији експлоатациони фактори и проценити локална сигурност споја. Данас је све учесталија примена разнородних спојева у металним конструкцијама. Због економичности и екологије, при изградњи енергетских, хемијских или неких других постројења све чешће се срећу заварени спојеви микролегираних феритних челика са високолегираним аустенитним челицима. Одговарајућа испитивања вршена су на

резервоарима за нафтне деривате, који се израђују од делова оплате од микролегираног феритног челика и кровне конструкције од високолегираног аустенитног челика.

Методе: У раду је извршена експериментална анализа ширења прслине код феритно-аустенитног завареног споја. Заваривање је изведено МИГ поступком заваривања са два различита уноса количине топлоте, а коришћен је исти додатни материјал МИГ 18/8/6. Испитиване су две врсте заварених плоча. Наведене су карактеристике основних, додатних и помоћних материјала и технологија заваривања. Израђене су епрувете са зарезом са иницираном грешком типа прслине ради одређивања ударних својстава и параметара механике лома.

Резултати: Спроведена истраживања имала су за циљ да упореде добијене резултате ударне жилавости и жилавости лома при равној деформацији код феритно-аустенитног завареног споја. Дата је и оцена добијених резултата при испитивању експерименталних плоча које су заварене различитим уносом количине топлоте.

Закључак: Резултати испитивања јесу успостављање зависности геометрије покретне прслине и услова напрезања за даље ширење прслине. Омогућено је одређивање износа параметара који описују понашање материјала, како у линеарно-еластичној, тако и у еластично-пластичној механици лома.

Кључне речи: феритно-аустенитни заварени спој, ударна жилавост, критични фактор интензитета напона K_{Ic}.

Paper received on / Дата получения работы / Датум пријема чланка: 23.01.2023.
Manuscript corrections submitted on / Дата получения исправленной версии работы / Датум достављања исправки рукописа: 23.03.2023.
Paper accepted for publishing on / Дата окончательного согласования работы / Датум коначног прихватања чланка за објављивање: 25.03.2023.

Modeling and simulation of hydraulic buffering valve for power-shift transmission

Momir M. Drakulić[a], *Aleksandar* S. Đurić[b], *Luka* M. Ponorac[c], *Abdeselem* B. Benmeddah[d], *Sreten* R. Perić[e]

[a] University of Defence in Belgrade, Military Academy, Department for Military Mechanical Engineering, Belgrade, Republic of Serbia, e-mail: drakulic.momir@gmail.com, **corresponding author**, ORCID iD: https://orcid.org/0000-0002-8367-7281

[b] University of Defence in Belgrade, Military Academy, Department for Military Mechanical Engineering, Belgrade, Republic of Serbia, e-mail: aleksandar.djrc@gmail.com, ORCID iD: https://orcid.org/0000-0002-2165-528X

[c] AMSS Motor Vehicle Centre, ADR Laboratory, Belgrade, Republic of Serbia, e-mail: luka.ponorac@cmv.rs, ORCID iD: https://orcid.org/0000-0003-2315-8743

[d] University of Defence in Belgrade, Military Academy, Department for Military Mechanical Engineering, Belgrade, Republic of Serbia, e-mail: benabde1993@gmail.com, ORCID iD: https://orcid.org/0000-0001-6696-3422

[e] University of Defence in Belgrade, Military Academy, Department for Military Mechanical Engineering, Belgrade, Republic of Serbia, e-mail: sretenperic@yahoo.com, ORCID iD: https://orcid.org/0000-0002-7270-5187

DOI: 10.5937/vojtehg71-43175; https://doi.org/10.5937/vojtehg71-43175

FIELD: mechanical engineering
ARTICLE TYPE: original scientific paper

Abstract:

Introduction/purpose: The hydraulic buffering valve has the greatest influence on the dynamic characteristics of power-shift transmission. The hydraulic buffering valve is a transmission element that controls increase in pressure in friction assemblies during the gear shifting process. By choosing the optimal control of pressure increase during shifting, reduction of dynamic loads in gear transmissions and thermal loads in friction assemblies is achieved.

Methods: The paper analyzes the principle of one of hydraulic buffering valve solutions as well as the influence of certain parameters on the control of pressure increase. After the analysis of the working principle of the hydraulic buffering valve, a simulation model was developed in the MATLAB/Simulink software package.

Results: The results obtained using the simulation model were compared with the experimental results of the selected pressure modulator solution. The selected hydraulic buffering valve was developed as part of the development of a device for power-shift transmission. The simulation results showed a satisfactory match with the experimental results.

Conclusion: The developed simulation model enables a relatively easy and quick change of the parameters of the hydraulic buffering valve as well as a possibility of a faster and better understanding of the influence of individual parameters on pressure increase during the gear shifting process.

Key words: power-shift transmission, pressure control valve, simulation.

Introduction

Gear shifting in the transmission of a motor vehicle is a process in which power parameters are changed in order to adapt the vehicle to road conditions (Balau et al, 2011). The way the transmission management system is implemented significantly affects the traction and dynamic characteristics of the vehicle, which is particularly pronounced in tracked vehicles where the transmission management system, in addition to gear shift, also ensures the turning of the vehicle. Increasing demands for high-performance tracked vehicles in terms of mobility have imposed the need to improve their subsystems, primarily the engine and the gearbox.

The improvement of the gearbox is of particular importance because, depending on its performance, the traction and maneuvering characteristics of the vehicle can be significantly increased or decreased, and the steering system has a special place in this (Grkić et al, 2009). The hydraulic buffering valve is one of the most important elements of the power-shift transmission system. The quality of the transition process of gear shifting depends on its characteristics, which directly affects the traction and maneuvering characteristics of the vehicle (Meng et al, 2015).

Working principle of the hydraulic buffering valve

Figure 1 shows the hydraulic buffering valve which consists of a regulator piston (a), an accumulator piston (b), springs (c) and (i), an orifice (d) and (f), and a non-return valve (e). The channel (g) is connected to the valve for gear selection, and the channel (h) to the corresponding friction clutch assembly. Figure 1 shows the position of the elements at the time of the beginning of the pressure modulation process. From that moment, the modulation of the pressure p_1 in the channel (h), and therefore in the cylinder of the friction clutch assembly, takes place in accordance with the

movement of the piston (b) and the stiffness of the springs (c) and (i). The pressure modulation process will be completed when the piston (b) rests on the piston outlet (a), after which the nominal pressure is established in the cylinder of the friction clutch assembly (Jian et al, 2018).

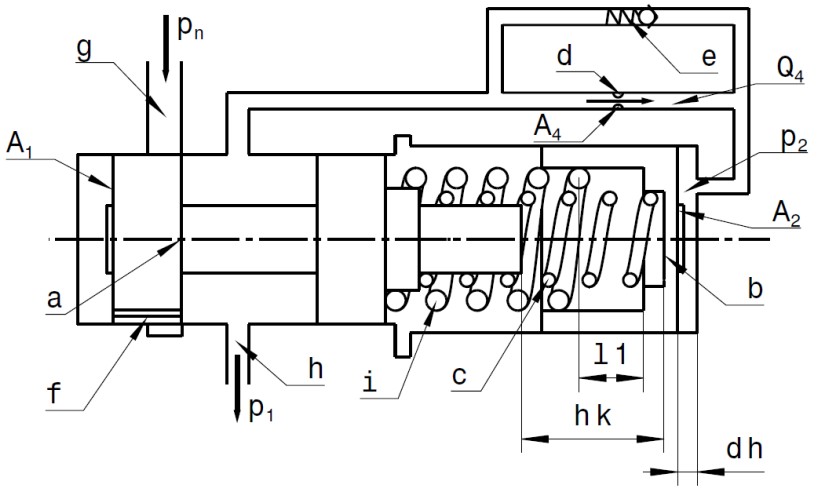

Figure 1 – Positions of the hydraulic buffering valve elements at the beginning of the pressure modulation process
Рис. 1 – Положение деталей модулятора давления в начале процесса модуляции давления
Слика 1 – Положај елемената модулатора притиска на почетку процеса модулације притиска

The orifice (f) in Figure 1 determines the movement speed of the piston (a), and the orifice (d) determines the pressure change in the process of pressure modulation. The non-return valve (e) is intended to assist in the process of turning off the friction clutch assembly, to help discharge the volume of the accumulator (b) faster and to prepare the pressure modulator for reactivation.

The character of the pressure change in the modulation process depends primarily on the design parameters of the hydraulic buffering valve elements (front surfaces of the regulator piston (a) A_1 and the accumulator piston (b) A_2, the stiffness of the spring (c) C_1 and the spring (9) C_2 and their preloads, the piston stroke accumulator dh and the orifice (d)).

The general character of the pressure change in the friction assemblies during gear shifting is shown in Figure 2 (Baogang et al, 2019).

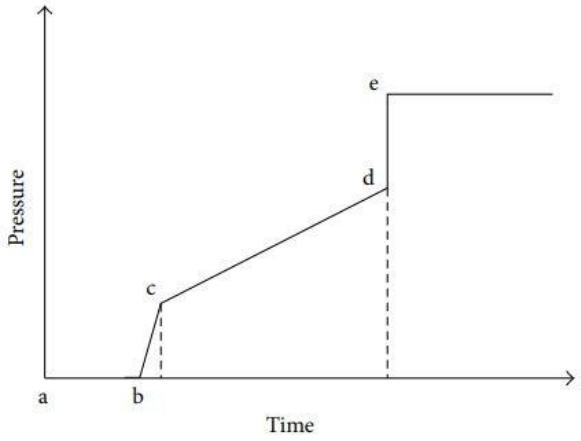

Figure 2 – Pressure change in the process of pressure modulation
Рис. 2 – Изменение давления в процессе модуляции давления
Слика 2 – Карактер промене притиска у процесу његове модулације

Phase a-b – represents the filling of the volume of the pipeline and the initial volume of the clutch cylinder with the motionless piston of the friction assembly.

Phase b-c – represents the filling of the volume of the clutch cylinder, followed by the movement of the piston of the friction assembly from the initial to the end position, when the pressure increases due to the compression of the spring in the friction clutch assembly.

Phase c-d – represents the process of pressure modulation in the clutch cylinder of the friction clutch assembly followed by the slippage of its elements. The pressure modulation process takes place in accordance with the movement of the accumulator piston (b) and the stiffness of the springs (c) and (i). This phase has the greatest impact on the quality of the gear shifting process (Walker et al, 2011). The duration of the gear shift depends on the character of the phase c-d, as well as the increase of the friction moment and the dynamic loads of the elements.

Phase d-e – indicates the establishment of the nominal pressure, after the completion of the pressure modulation process, which is equal to the working pressure (Liu et al, 2014).

Mathematical model of the hydraulic buffering valve

The initial pressure in the process of engaging the friction clutch assembly, the final pressure and the character of the pressure change during the pressure modulation have a direct impact on the performance

of the hydraulic buffering valve. The transient process, the pressure modulation process, is described by a simplified mathematical model (Živanović, 1991). Friction and inertial forces are neglected in the calculation, the working fluid is incompressible and the hydraulic pipeline is absolutely rigid. Taking into account the equilibrium condition of the piston (a) and the piston (b), as well as the continuity equation, the following system of differential equations can be written:

$$\begin{aligned} Q_4 dt &= A_2 dh \\ A_1 dp_1 &= c dh \end{aligned} \tag{1}$$

where:

A_1 and A_2 – surfaces of the pistons (a) and (b),
c – spring stiffness (d) and (i),
dh – elemental displacement of the piston (b),
dp_1 – pressure increase in the channel (h) which corresponds to the displacement of the piston (b), and
Q_4 – flow through the orifice (d), determined by the equation:

$$Q_4 = C_{d4} A_4 \sqrt{\frac{2}{\rho}(p_1 - p_2)} \tag{2}$$

where:

C_{d4} – flow coefficient through the orifice (d),
A_4 – orifice surface (d), and
p_2 – pressure in the accumulator chamber (b).

If substitution is introduced into the equation:

$$\xi = C_{d4} A_4 \sqrt{\frac{2}{\rho}} \tag{3}$$

where ξ represents the flow through the orifice at a pressure difference of 1 bar, then:

$$Q_4 = \xi \sqrt{(p_1 - p_2)} \tag{4}$$

If expression (4) is included in the first differential equation of system (1) and dh is replaced from the second equation (1), we get:

$$c\xi \sqrt{p_1 - p_2} dt = A_1 A_2 dp_1 \tag{5}$$

From the balance of the piston (b) of the accumulator, the equation can be written:

$$p_2 = \frac{F_o}{A_2} \tag{6}$$

where:
F_o – the force of the springs (c) and (i) of the accumulator (b) in an arbitrary position.

The spring force Fo can also be expressed through the pressure p_1, setting the equilibrium condition for the piston (a).

$$F_o = p_1 A_1 \tag{7}$$

Putting the value of Fo in expression (6) and then in expression (5) we get:

$$c\xi\sqrt{p_1 - p_1\frac{A_1}{A_2}}\,dt = A_1 A_2 dp_1 \tag{8}$$

and that is:

$$\mathrm{dt} = \frac{\mathrm{A_1 A_2}}{\mathrm{c\xi}\sqrt{\mathrm{p_1 - p_1\frac{A_1}{A_2}}}}\mathrm{dp_1} \tag{9}$$

In order to determine the total duration of the modulation process t_{mod} with the specified hydraulic buffering valve, equation (9) will be integrated. The limits of the integral for the left side of the differential equation are from 0 to t_{mod}, and for the right side from p_{10} to p_{1mod}, where:
t_{mod} – duration of the pressure modulation process,
p_{10} – pressure at the beginning of the modulation process, and
p_{1mod} – pressure at the end of the modulation process.

The pressure value p_{10} corresponds to the rightmost position of the accumulator piston (b), while the pressure value p_{1mod} corresponds to the pressure at the end of the pressure modulation process, that is:

$$\mathrm{p_{10}} = \frac{\mathrm{F_{0mod}}}{\mathrm{A_1}}; \quad \mathrm{p_{1mod}} = \frac{\mathrm{F_{omod} + c_1 \cdot h_k + c_2 \cdot (h_k - l_1)}}{\mathrm{A_1}} \tag{10}$$

where:
F_{omod} – the force of the spring (c) of the accumulator (b) at the beginning of the pressure modulation and
l_1 – distance between the springs (c) and (i) in the accumulator (b).

Integrating equation (9) with replacement and introducing the specified limits of the integral for the first stage gives the duration of the pressure modulation process:

$$\mathrm{t}_{mod} = \frac{\mathrm{A_1 A_2}}{c\xi}\frac{2}{\sqrt{1 - \frac{\mathrm{A_1}}{\mathrm{A_2}}}}\left(\sqrt{\mathrm{p_{1mod}}} - \sqrt{\mathrm{p_{10}}}\right) \tag{11}$$

in which:

$$c = c_1 + c_2 \tag{12}$$

where:

c_1 – spring stiffness (c) and

c_2 – spring stiffness (i).

In order to obtain the dependence of the pressure change during the modulation process, differential equation (9) will be integrated in the limits for the left side from 0 to t and the limits for the right side from p_{10} to p_1, where t and p_1 are current variables and the result will be:

$$t = \frac{A_1 A_2}{c\xi} \frac{2}{\sqrt{1-\frac{A_1}{A_2}}} \left(\sqrt{p_1} - \sqrt{\frac{F_{omod}}{A_1}} \right) \tag{13}$$

and that is:

$$p_1 = \frac{F_{oo}}{A_1} + \frac{\left(\frac{c\xi t}{2}\right)^2 \left(\frac{A_2}{A_1}-1\right) + c\xi t \sqrt{F_{omod} {A_2}^3 \left(\frac{A_2}{A_1}-1\right)}}{A_1 {A_2}^3} \tag{14}$$

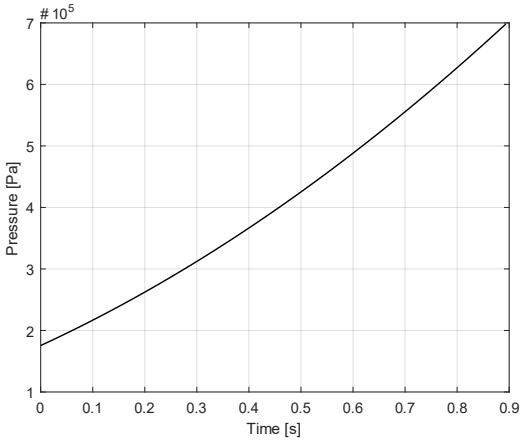

Figure 3 – Dependence of pressure increase on time during the pressure modulation process

Рис. 3 – Повышение давления в зависимости от времени процесса модуляции давления

Слика 3 – Зависност приraштаја притиска од времена у току процеса његове модулације

Equation 14 represents the pressure change in the friction clutch assembly during the process of pressure modulation with the described hydraulic buffering valve. Figure 3 shows the dependence of the pressure fit on time during the pressure modulation process obtained by solving equation 14.

Simulation model of the hydraulic buffering valve in MATLAB/Simulink

The simulink module developed in the MATLAB environment enables modeling, simulation and analysis of various dynamic systems. It supports linear and nonlinear systems modeled in both continuous and discrete time (Grkić et al, 2011).

Modeling in simulink uses a graphical environment, as well as „click-and-drag" mouse operations for block drawing. Simulink contains a large library of generators of input excitations, displays of output variables as well as linear and non-linear components of the system (Raikwar et al, 2015). By means of block diagrams from the library, a simulation model of the pressure modulator shown in Figure 4 was developed.

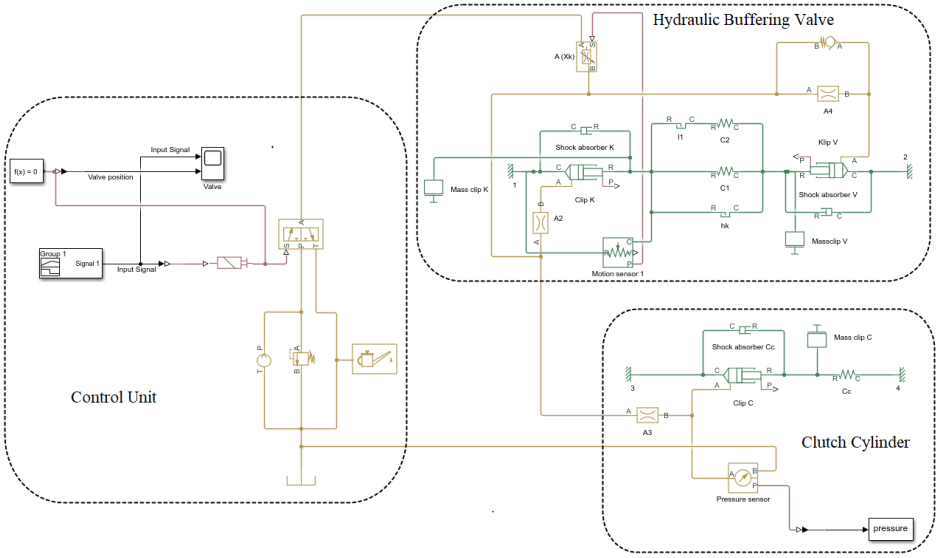

Figure 4 – Simulation model of the hydraulic buffering valve
Рис. 4 – Имитационная модель гидравлического модулятора давления
Слика 4 – Симулациони модел модулатора притиска

The simulation model consists of three parts. The first unit is the part for managing the system and consists of a hydraulic pump, a hydraulic distributor, a safety valve and components that manage the aforementioned. The second unit is represented by the hydraulic buffering valve, while the third unit is represented by the piston model of the friction clutch assembly that is activated in the process of pressure modulation. The results obtained through simulation are shown in Figure 5.

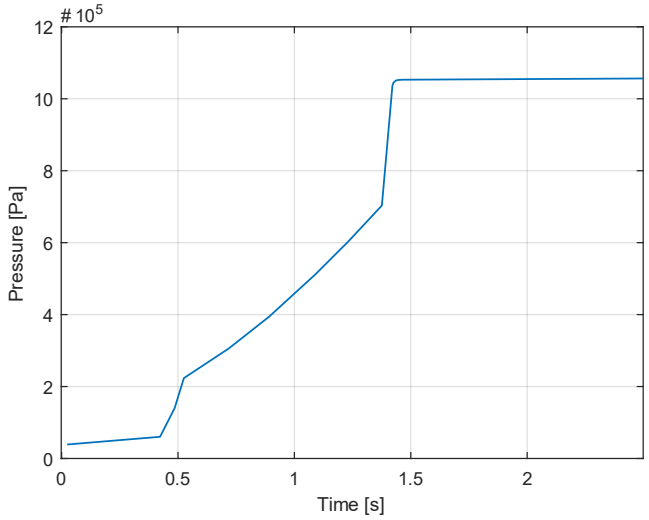

Figure 5 – Simulation results in MATLAB/Simulink
Рис. 5 – Результаты моделирования в MATLAB/Simulink
Слика 5 – Резултат добијен симулацијом у MATLAB/Simulik

The parameters used for the simulation as well as for solving equation (14) are shown in Table 1.

Table 1 – Parameters of the hydraulic buffering valve
Таблица 1 – Параметры гидравлического модулятора давления
Табела 1 – Параметри модулатора притиска

Fluid density	830	kg/m^3
Surface area of the piston (A_1)	4.9	cm^2
Surface area of the piston (A_2)	7.1	cm^2
Surface area of the orifice (A_4)	0.0113	cm^2
Discharge Coefficient (C_{d4})	0.7	
Stiffness of the spring (c)	4.21	N/mm
Pre-tightening force of the spring (c)	38	N
Stiffness of the spring (i)	10.8	N/mm
Pre-tightening force of the spring (i)	0	N
Distance between springs (c) and the piston (b) (l_1)	4.5	mm
Distance between the piston (a) and (b) (h_k)	23.5	mm
Force at the beginning of modulation (F_{omod})	86	N

Experimental research and simulation model validation

Experimental studies of the operation of the hydraulic buffering valve were carried out as part of the study of the possibility of applying a power-shift transmission.

The entire experimental research was carried out in laboratory conditions, through two stages and several test blocks with a larger number of experiments, on a real gearbox.

The results of the experimental test of the hydraulic buffering valve are shown in Figure 6 (Živanović, 1991).

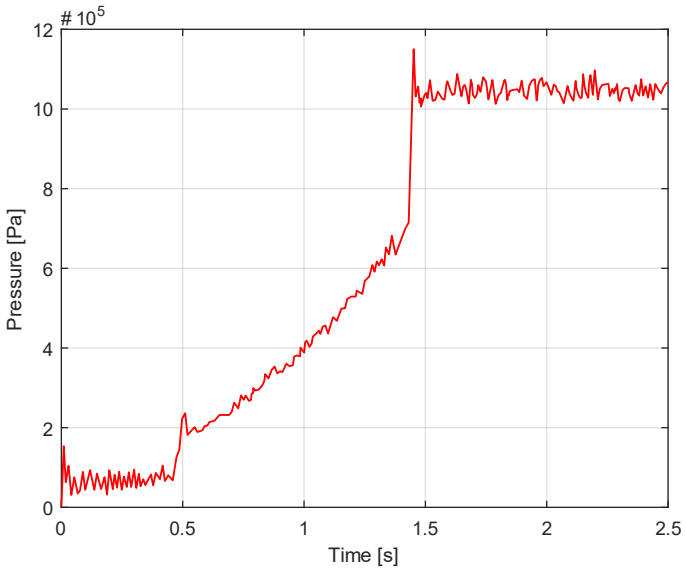

Figure 6 – Results of the experimental test
Рис. 6 – Результаты экспериментального испытания
Слика 6 – Резултати експерименталног испитивања

After the experimental tests, the obtained results were compared with the results obtained by solving equation 14 and by simulating the operation of the hydraulic buffering valve in the MATLAB/Simulink software package. Figure 7 shows the comparative results.

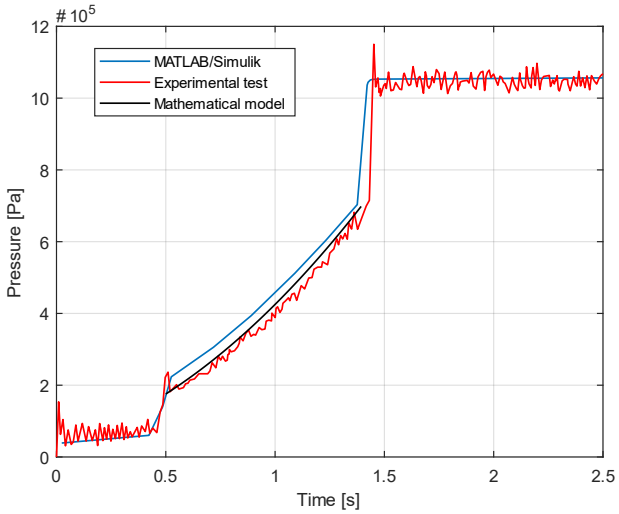

Figure 7 – Comparative presentation of the results obtained
Рис. 7 – Сравнительный обзор полученных результатов
Слика 7 – Упоредни приказ добијених резултата

Figures 8, 9, and 10 show the comparative results obtained by changing certain design parameters of the hydraulic buffering valve.

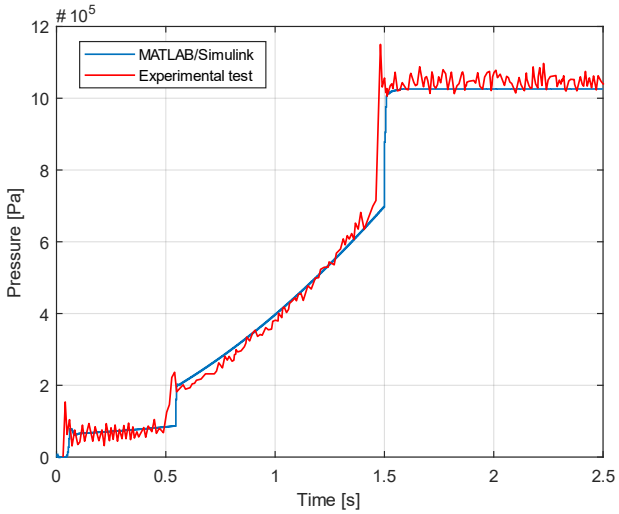

Figure 8 – Comparative presentation of the obtained results - T1
Рис. 8 – Сравнительный обзор полученных результатов – T1
Слика 8 – Упоредни приказ добијених резултата – T1

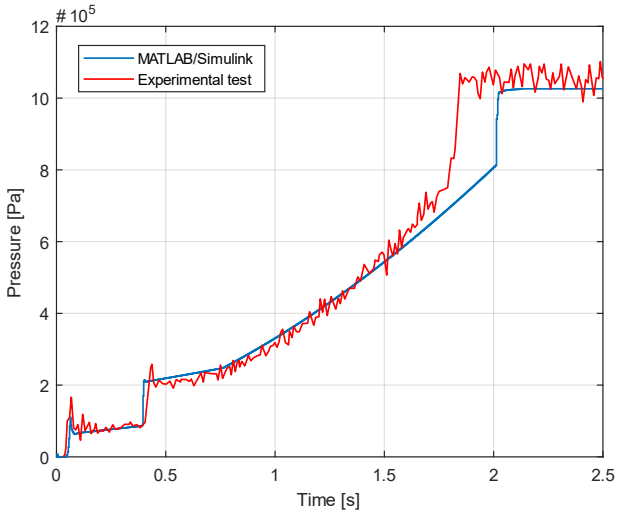

Figure 9 – Comparative presentation of the obtained results – T2
Рис. 9 – Сравнительный обзор полученных результатов – T2
Слика 9 – Упоредни приказ добијених резултата – T2

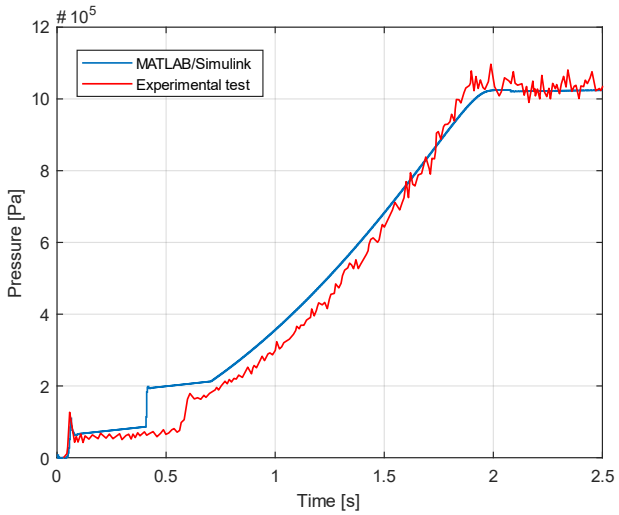

Figure 10 – Comparative presentation of the obtained results – T3
Рис. 10 – Сравнительный обзор полученных результатов – T3
Слика 10 – Упоредни приказ добијених резултата – T3

The values of the design parameters with which the results obtained are shown in Figures 8, 9 and 10 are shown in Table 2.

Table 2 – Hydraulic buffering valve parameters for T1, T2 and T3 results
Таблица 2 – Параметры гидравлического модулятора давления по результатам T1, T2 и T3
Табела 2 – Параметри модулатора притиска за резултате T1, T2 и T3

	T1	**T2**	**T3**	
Surface area of the orifice (A_4)	0.0079	0.0050	0.0095	cm^2
Stiffness of the spring (c)	5.8	5.8	5.8	N/mm
Pre-tightening force of the spring (c)	72	70	22	N
Stiffness of the spring (i)	14.5	31.5	0	N/mm
Distance between the springs (c) and the piston (b) (l_1)	8.5	5.9	0	mm
Distance between the piston (a) and (b) (hk)	25	23.5	23.5	mm

The analysis of the obtained results shows that the results obtained by simulation sufficiently match the results obtained by experimental measurements. The deviations of the results obtained through simulation from the results obtained experimentally are the consequence of the impossibility of completely accurate determination of the actual values of the design parameters of the hydraulic buffering valve and the friction clutch assembly. The values of the parameters with which the hydraulic buffering valve process was simulated are nominal values and, as it is known, can vary within certain limits (Meng et al, 2016).

When the influence of each of the displayed parameters and the facts presented are taken into account, the matching of the results obtained by simulation and experimental results can be considered completely satisfactory, as well as that the simulation model can be used for further research in terms of investigating the influence of the most important parameters on the pressure modulation process as well as development of a simulation model of power-shift transmission.

Investigating the influence of certain parameters on the pressure modulation process

After the accuracy of the developed hydraulic buffering valve MATLAB/Simulink model being confirmed, the operation of the hydraulic buffering valve can be simulated with a level of certainty at different values of particular parameters that have a significant impact on the pressure modulation process.

The paper analyzed the effects of the following parameters: preload force Fo in the spring (c), stiffness of the spring (c) and the spring (i), distance between the pistons (a) and (b), distance between the piston (b) and the spring (i) and the orifice (d) size.

The results of these simulations are shown in Figures 11, 12, 13, 14, 15, and 16 (Wang et al, 2017).

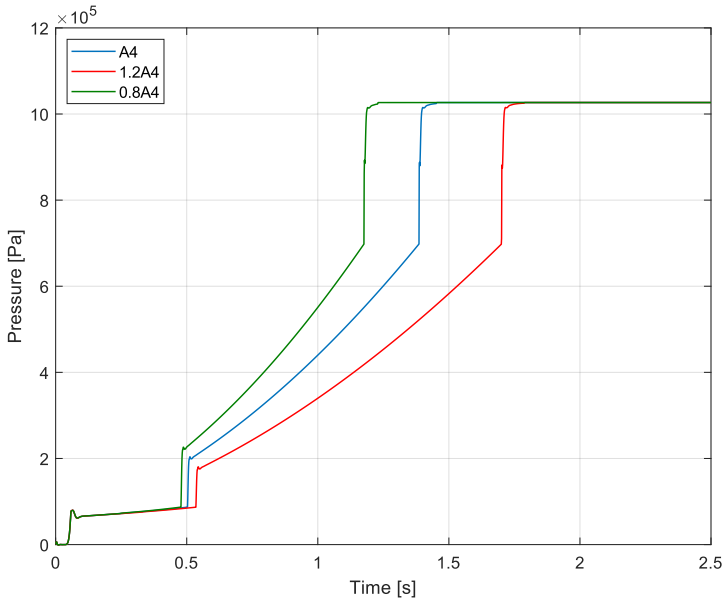

Figure 11 – Influence of the A_4 orifice surface (d) on the pressure modulation process
Рис. 11 – Влияние поверхности отверстия A_4 (d) на процесс модуляции давления
Слика 11 – Утицај површине A_4 прогушнице (d) на процес модулације притиска

The size of the orifice (d) is of particular importance in the pressure modulation process, as its reduction ensures a smaller increase in pressure in the pressure modulation process and increases the total duration of the pressure modulation process.

With an increase in the size of the orifice (d), there is a greater increase in pressure in the modulation process and the duration of the pressure modulation process is reduced.

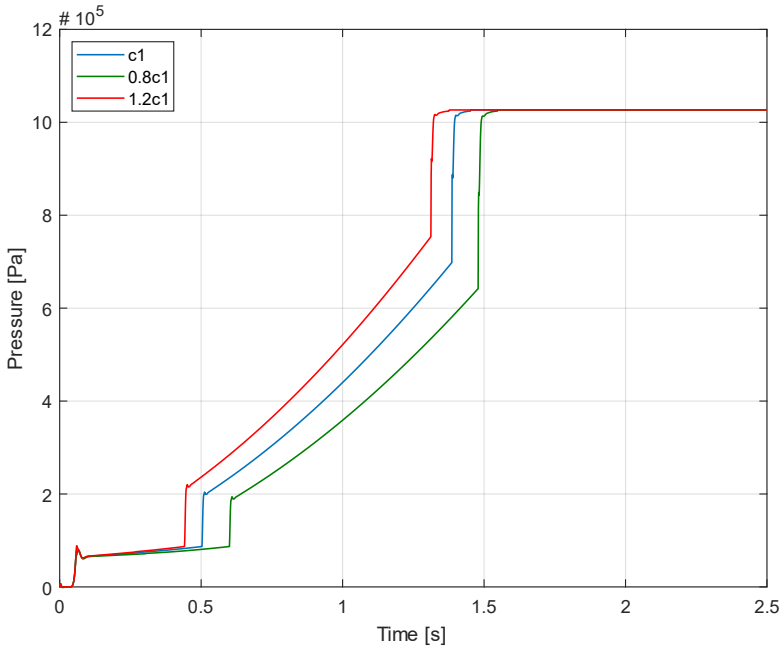

Figure 12 – The influence of the stiffness of the c_1 spring (c) on the pressure modulation process

Рис. 12 – Влияние жесткости пружины c_1 (c) на процесс модуляции давления

Слика 12 – Утицај крутости c_1 опруге (c) на процес модулације притиска

Changing the stiffness of the c_1 spring (c) leads to the increase in the pressure intensity and the pressure modulation time change.

As the stiffness increases, the time of the pressure modulation process decreases.

Also, with an increase in spring stiffness, there is also an increase in pressure at the end of the pressure modulation process (Ren et al, 2014).

The effect of changing the stiffness of the c_2 spring (i) is identical to the effect of changing the stiffness of the c_1 spring (c).

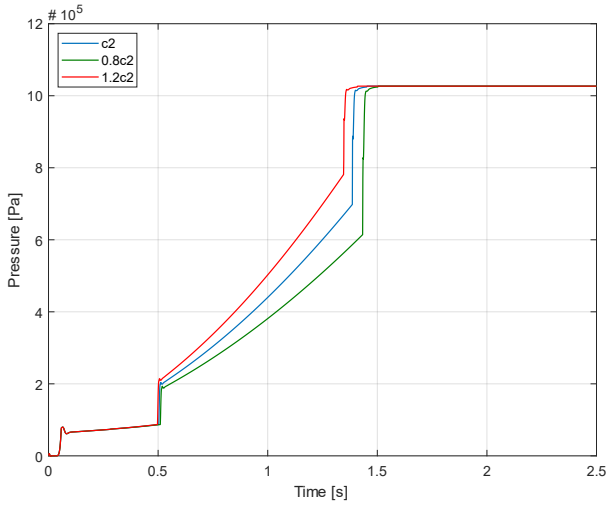

Figure 13 – Influence of the stiffness of the c_2 spring (i) on the pressure modulation process
Рис. 13 – Влияние жесткости пружины c_2 (i) на процесс модуляции давления
Слика 13 – Утицај крутости c_2 опруге (i) на процес модулације притиска

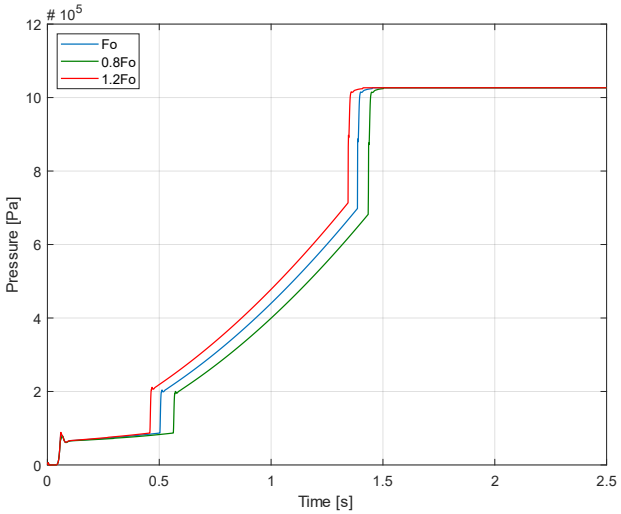

Figure 14 – Influence of the preload force Fo of the spring (c) on the process of pressure modulation
Рис. 14 – Влияние усилия преднатяга Fo пружины (c) на процесс модуляции давления
Слика 14 – Утицај силе преднапрезања Fo опруге (c) на процес модулације притиска

Changing the pre-tightening force Fo in the spring (c) changes the regularity of the increase in pressure in the executive cylinder.

Its increase reduces the time required to move the piston of the friction scope to the end position and increases the initial pressure in the process of pressure modulation in the friction clutch assembly, which can lead to the appearance of shock engagement of the friction clutch assembly.

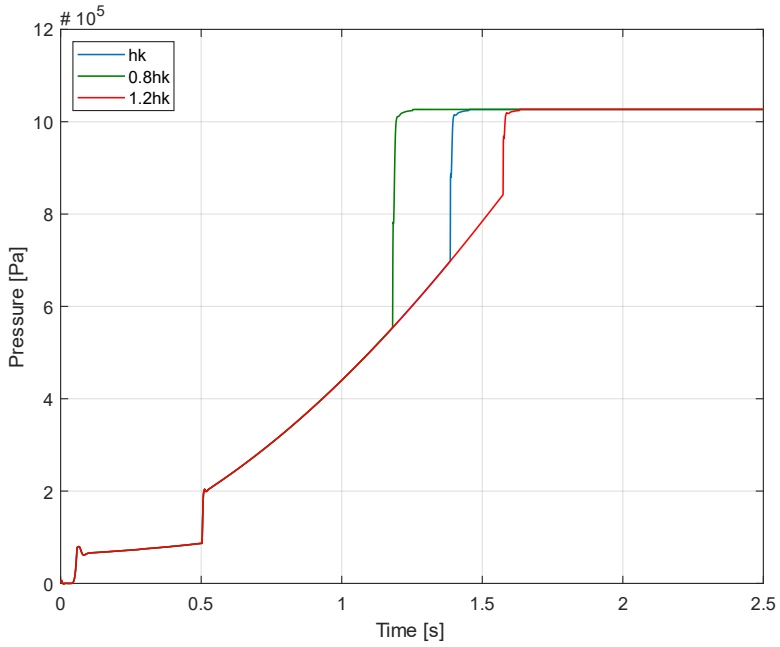

Figure 15 – Influence of the distance between the piston (a) and the piston (b) on the pressure modulation process

Рис. 15 – Влияние расстояния между поршнем (a) и поршнем (b) на процесс модуляции давления

Слика 15 – Утицај растојања између клипа (a) и клипа (b) на процес модулације притиска

Changing the distance between the pistons (a) and (b) can affect the magnitude of the pressure and the duration of the pressure modulation process.

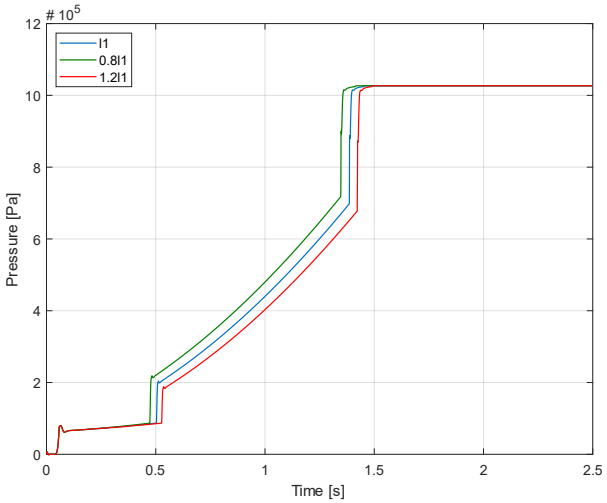

Figure 16 – Influence of the distance between the piston (b) and the spring (i) on the pressure modulation process
Рис. 16 – Влияние расстояния между поршнем (b) и пружиной (i) на процесс модуляции давления
Слика 16 – Утицај растојања између клипа (b) и опруге (i) на процес модулације притиска

Changing the distance between the accumulator piston (b) and the spring (i) can adjust the moment when this spring will come into effect. The pressure modulation takes place first in accordance with the stiffness of the spring (c) and then in accordance with the stiffness of both springs.

Conclusion

A simulation model of the hydraulic buffering valve was developed in the MATLAB/Simulink software package, and the influence of the most important parameters of the pressure modulator on the pressure modulation process was analyzed. The results of the simulation of the operation of the pressure modulator sufficiently match the results obtained by experimental measurements in laboratory conditions. After the comparison of the obtained results, it was determined that the results obtained using the simulink model are within 10% of the relative error compared to the experimental test. The simulation model enables an easy change of parameters. The deviation of the obtained results in relation to the experimental tests can be explained by a large number of variables that affect the process of pressure modulation. Also, certain parameters

are variable during the experiment measurement, such as the temperature and viscosity of the fluid. Larger number of simulations of the system operation can be performed in a shorter period of time, in order to observe the behavior of the system and choose the optimal values of the most important parameters.

It is concluded that the developed simulink model met the set requirements, and as such it can be used to evaluate the operation of the hydraulic buffering valve for power-shift transmission. It can be used for both calculation and design. The developed simulink model can be implemented in the simulation model of the transmission, which will represent the simulation model of the powershift transmission during the gear change.

References

Balau, A.-E., Caruntu, C.-F. & Lazar, C. 2011. Simulation and control of an electro-hydraulic actuated clutch. *Mechanical Systems and Signal Processing,* 25(6), pp.1911-1922. Available at: https://doi.org/10.1016/j.ymssp.2011.01.009.

Baogang, L., Dongye, S., Minghui, H., Xingyu, Z., Junlong, L. & Dongyang, W. 2019. Coordinated control of gear shifting process with multiple clutches for power-shift transmission. *Mechanism and Machine Theory*, 140, pp.274-291. Available at: https://doi.org/10.1016/j.mechmachtheory.2019.06.009.

Grkić, A.R., Duboka, Č.V. & Krsmanović, M.M. 2011. Modeling of the process of gear shifting in planetary gear trains of motor vehicle. *Vojnotehnički glasnik/Military Technical Courier,* 59(2), pp.41-59 (in Serbian). Available at: https://doi.org/10.5937/vojtehg1102041G.

Grkić, A., Duboka, Č. & Muždeka, S. 2009. Simulation model of multiple plate friction clutches and brakes. *Vojnotehnički glasnik/Military Technical Courier,* 57(1), pp.65-80 (in Serbian). Available at: https://doi.org/10.5937/vojtehg0901065G.

Jian, H., Wei, W., Li, H. & Yan, Q. 2018. Optimization of a pressure control valve for high power automatic transmission considering stability. *Mechanical Systems and Signal Processing,* 101, pp.182-196. Available at: https://doi.org/10.1016/j.ymssp.2017.08.018.

Liu, Y., Qin, D., Jiang, H. & Zhang, Y. 2014. Shift control strategy and experimental validation for dry dual clutch transmissions. *Mechanism and Machine Theory*, 75, pp.41-53. Available at: https://doi.org/10.1016/j.mechmachtheory.2014.01.013.

Meng, F., Chen, H., Zhang, T. & Zhu, X. 2015. Clutch fill control of an automatic transmission for heavy-duty vehicle applications. *Mechanical Systems and Signal Processing*, 64-65, pp.16-28. Available at: https://doi.org/10.1016/j.ymssp.2015.02.026.

Meng, F., Shi, P., Karimi, H.R. & Zhang, H. 2016. Optimal design of an electro-hydraulic valve for heavy-duty vehicle clutch actuator with certain constraints. *Mechanical Systems and Signal Processing*, 68-69, pp.491-503. Available at: https://doi.org/10.1016/j.ymssp.2015.06.025.

Raikwar, S., Tewari, V.K., Mukhopadhyay, S., Verma, C.R.B. & Sreenivasulu Rao, M. 2015. Simulation of components of a power shuttle transmission system for an agricultural tractor. *Computers and Electronics in Agriculture*, 114, pp.114-124. Available at: https://doi.org/10.1016/j.compag.2015.03.006.

Ren, F., Liu, X., Chen, J., Zeng, P., Liu, B. & Wang, Q. 2014. Dynamic Characteristics Analysis of power shift control valve. *Advances in Mechanical Engineering*, 2014, at.ID:824853, pp.1-7. Available at: https://doi.org/10.1155/2014/824853.

Walker, P.D., Zhang, N. & Tamba, R. 2011. Control of gear shifts in dual clutch transmission powertrains. *Mechanical Systems and Signal Processing*, 25(6), pp.1923-1936. Available at: https://doi.org/10.1016/j.ymssp.2010.08.018.

Wang, F., Wang, Y., Han, J.-h. & Jao, Y. 2017. Experimental and simulated studies on hydraulic buffering valve for ZF-4WG308 power-shift transmission. *Journal of Central South University*, 24, pp.1801-1807. Available at: https://doi.org/10.1007/s11771-017-3588-4.

Živanović, Ž. 1991. *Research of theoretical model and device for optimum power-shift in transmission of motor vehicle*. Ph. D. thesis. Belgrade, Serbia: University of Belgrade, Faculty of Mechanical Engineering (in Serbian).

Имитационное моделирование работы модулятора давления в коробках передач без разрыва потока мощности

Момир М. Дракулич[а], **корреспондент,** *Александр* С. Джурич[а], *Лука* М. Понорак[б], *Абдеселем* Б. Бенмеддах[а], *Сретен* Р. Перич[а]

[а] Университет обороны в г. Белград, Военная академия, кафедра военного машиностроения, г. Белград, Республика Сербия

[б] Центр автотранспортных средств AMSS, лаборатория ADR, г. Белград, Республика Сербия

РУБРИКА ГРНТИ: 55.43.00 Автомобилестроение
ВИД СТАТЬИ: оригинальная научная статья

Резюме:

Введение/цель: Модулятор давления оказывает наибольшее воздействие на динамические характеристики трансмиссии с переключением передач, не прерывая поток мощности. Модулятор давления — запчасть коробки передач, контролирующая повышение давления в узлах трения в процессе переключения передач. За счет выбора оптимального управления повышением давления при изменении уровня передачи достигается снижение

динамических нагрузок в зубчатых передачах и тепловых нагрузок в узлах трения.

Методы: В данной статье анализируется принцип работы одного из решений моделятора давления, а также влияние некоторых параметров на управление повышением давления при переключении передач. После анализа принципа работы модулятора давления была разработана имитационная модель в пакете программного обеспечения MATLAB/Simulink.

Результаты: В статье также проведен сравнительный анализ результатов, полученных с помощью имитационной модели, и результатов испытаний выбранного модулятора давления. Результаты моделирования показали удовлетворительное совпадение с экспериментальными результатами. Установлено предельное отклонение в размере 10%.

Выводы: Разработанная имитационная модель обеспечивает относительно простое и быстрое изменение параметров модулятора давления, а также способствует более быстрому и лучшему пониманию, как те или иные параметры влияют на повышение давления в процессе переключения передач.

Ключевые слова: переключение передач без разрыва потока мощности, модулятор давления, моделирование.

Моделирање и симулација рада модулатора притиска код мењачких преносника са променом степена преноса без прекида тока снаге

Момир М. Дракулић[а], **аутор за преписку**, *Александар* С. Ђурић[а], *Лука* М. Понорац[б], *Абдеселем* Б. Бенмеддах[а], *Сретен* Р. Перић[а]

[а] Универзитет одбране у Београду, Војна академија, Катедра војномашинског инжењерства, Београд, Република Србија

[б] АМСС Центар за испитивање возила, АДР лабораторија, Београд, Република Србија

ОБЛАСТ: машинство
КАТЕГОРИЈА (ТИП) ЧЛАНКА: оригинални научни рад

Сажетак:

Увод/циљ: Модулатор притиска има највећи утицај на динамичке карактеристике мењачких преносника са променом степена преноса без прекида тока снаге. Представља елемент мењачког преносника који контролише повећање притиска у фрикционим склоповима током процеса промене степена преноса. Избором оптималне контроле прираштаја притиска при промени степена преноса постиже се смањење динамичких оптерећења у зупчастим преносницима и термичких оптерећења у фрикционим склоповима.

Drakulić, M. et al, Modeling and simulation of hydraulic buffering valve for power-shift transmission, pp.417-438

Методе: Анализиран је принцип једног од решења моделатора притиска, као и утицај појединих параметара на контролу прираштаја притиска у току промене степена преноса. Након анализе принципа рада модулатора притиска, развијен је симулациони модел у софтверском пакету MATLAB/Simulink.

Резултати: Резултати добијени коришћењем симулационог модела упоређени су са експерименталним резултатима изабраног модулатора притиска. Резултати симулације су показали задовољавајуће поклапање са експерименталним резултатима, у границама до 10% одступања од експерименталних резултата.

Закључак: Развијени симулациони модел омогућава релативно лаку и брзу промену параметара модулатора притиска, као и могућност бржег и бољег разумевања утицаја појединих параметара на повећање притиска током процеса промене степена преноса.

Кључне речи: промена степена преноса без прекида тока снаге, модулатор притиска, симулација.

Paper received on / Дата получения работы / Датум пријема чланка: 02.01.2023.
Manuscript corrections submitted on / Дата получения исправленной версии работы / Датум достављања исправки рукописа: 25.03.2023.
Paper accepted for publishing on / Дата окончательного согласования работы / Датум коначног прихватања чланка за објављивање: 27.03.2023.

ПРЕГЛЕДНИ РАДОВИ

ОБЗОРНЫЕ СТАТЬИ

REVIEW PAPERS

Supersymmetry

Nicola Fabiano

University of Belgrade, "Vinča" Institute of Nuclear Sciences - National Institute of the Republic of Serbia, Belgrade, Republic of Serbia,
e-mail: nicola.fabiano@gmail.com,
ORCID iD: https://orcid.org/0000-0003-1645-2071

DOI: 10.5937/vojtehg71-40268;https://doi.org/10.5937/vojtehg71-40268

FIELD: physics

ARTICLE TYPE: review paper

Abstract:

Introduction/purpose: Supersymmetry is a symmetry of the Lagrangian that goes beyond Lie groups. It allows the exchange of bosons and fermions. The most important model is the Minimal Supersymmetric Standard Model, or MSSM.

Methods: Supercharge algebra, superfields, Grassmann numbers, Berezin integral.

Results: Supersymmetric transformations are global, they do not depend on spacetime coordinates. In the case of Supergravity, they are local.

Conclusion: Supersymmetric models, and MSSM in particular, could describe more physics and more particles beyond the Standard Model.

Key words: supersymmetry, minimal supersymmetric standard sodel.

Supersymmetry

Supersymmetry – or SUSY for short – is a symmetry that interchanges bosons with fermions (Gervais & Sakita, 1971; Volkov & Akulov, 1972, 1973, 1974; Ramond, 1971). It is one of the best candidates for physics beyond the Standard Model, with the so–called Minimal Supersymmetric Standard Model, MSSM for short (Fayet, 1975, 1976, 1977; Fayet & Ferrara, 1977). In this extension to the Standard Model, each particle has its corresponding *superpartner* with same mass and other quantum numbers, but with different spin by one half. For instance, the electron has a selectron, a bosonic superpartner, while photon, Z and gluon have fermionic superpartners called photino, zino and gluino respectively. Names are as-

signed in following manner: bosonic superpartners gain the s- prefix, while fermionic superpartners gain the -ino suffix.

As we easily distinguish between bosons and fermions at current energies, this symmetry has to be spontaneously broken. After supersymmetry breaking superpartners masses may differ.

Supersymmetry algebra

A supersymmetric transformation brings a scalar to a fermion and viceversa. The generator Q_α of the transformation, known as the supercharge, brings from the boson field ϕ to the Weyl spinor ψ_α.

In order to describe supersymmetry transformation it is better to operate with Weyl spinors rather than Dirac ones, and to change usual notation a bit. Weyl spinors $\psi_{L,R}$ transform under Lorentz group as

$$\psi_{L,R}(x) \to \psi'_{L,R}(x') = \Lambda_{L,R}\psi_{L,R}(x) \ , \tag{1}$$

where the transformations $\Lambda_{L,R}$ are given by

$$\Lambda_{L,R} = \exp\left(\frac{1}{2}\vec{\sigma}\cdot(\vec{\omega} \mp i\vec{\nu})\right) \ , \tag{2}$$

$\vec{\sigma}$ being the three Pauli matrices

$$\sigma_1 = \begin{pmatrix} 0 & 1 \\ 1 & 0 \end{pmatrix}, \ \sigma_2 = \begin{pmatrix} 0 & -i \\ i & 0 \end{pmatrix}, \ \sigma_3 = \begin{pmatrix} 1 & 0 \\ 0 & -1 \end{pmatrix} \ , \tag{3}$$

$\vec{\omega}$ the three real rotational parameters, and $\vec{\nu}$ the three real boost parameters. The transformations Λ_L and Λ_R are related by

$$\Lambda_L^{-1} = \Lambda_R^\dagger \ . \tag{4}$$

The four component Dirac spinor Ψ is written as follows:

$$\Psi = \begin{pmatrix} \psi_L \\ \psi_R \end{pmatrix} \ , \tag{5}$$

equivalent to

$$\Psi = \begin{pmatrix} \psi_\alpha \\ \overline{\chi}^{\dot{\alpha}} \end{pmatrix} \ . \tag{6}$$

Often, it is found that Weyl spinors are written starting from Dirac spinors in the following way, as projections, see for instance (Fabiano, 2021):

$$\psi_{L,R} = \frac{1}{2}(1 \pm \gamma_5)\psi \ . \tag{7}$$

In this formalism we have the Weyl representation of the Dirac matrices

$$\gamma^\mu = \begin{pmatrix} 0 & \sigma^\mu \\ \overline{\sigma}^\mu & 0 \end{pmatrix} \ , \tag{8}$$

where $\sigma^\mu = (\mathbb{1}, \sigma^i) = (\sigma^\mu)_{\alpha\beta}$ and $\overline{\sigma}^\mu = (\mathbb{1}, -\sigma^i) = (\overline{\sigma}^\mu)^{\dot{\alpha}\beta} = (\sigma^\mu)^{\beta\dot{\alpha}}$. The matrices σ^μ and $\overline{\sigma}^\mu$ mix dotted and undotted indices, that is left and right spinor indices. The dot in the notation is similar to the covariant and contravariant – or upper and lower indices in general and special relativity. We always contract an upper with a lower index, and we have the additional rule that only dotted or undotted indices can be contracted together, not mixed dotted–undotted.

The generator Q_α transforms as a Weyl spinor, that means

$$[J^{\mu\nu}, Q_\alpha] = -i(\sigma^{\mu\nu})_\alpha^{\ \beta} Q_\beta \ , \tag{9}$$

where $J^{\mu\nu}$ is the generator of Lorentz group, while

$$\sigma^{\mu\nu} \equiv \frac{1}{4}(\sigma^\mu \overline{\sigma}^\nu - \sigma^\nu \overline{\sigma}^\mu) \ , \text{ and } \overline{\sigma}^{\mu\nu} \equiv \frac{1}{4}(\overline{\sigma}^\mu \sigma^\nu - \overline{\sigma}^\nu \sigma^\mu) \ . \tag{10}$$

Q_α is independent from spacetime coordinates, then

$$[P^\mu, Q_\alpha] = 0 \ . \tag{11}$$

Denoting the conjugate of Q_α as $\overline{Q}_{\dot{\alpha}}$ we have

$$[J^{\mu\nu}, \overline{Q}^{\dot{\alpha}}] = -i(\overline{\sigma}^{\mu\nu})_{\ \dot{\beta}}^{\dot{\alpha}} \overline{Q}^{\dot{\beta}} \ . \tag{12}$$

The conjugation of spinors works as follows:

$$(\psi^\alpha)^* = \overline{\psi}^{\dot{\alpha}}, \ \text{ and } \ (\psi_\alpha)^* = \overline{\psi}_{\dot{\alpha}} \ . \tag{13}$$

The supersymmetry algebra is given by the anticommutator

$$\{Q_\alpha, \overline{Q}_{\dot{\beta}}\} = 2(\sigma^\mu)_\alpha^{\ \dot{\beta}} P_\mu \ . \tag{14}$$

How to justify (14)? By inspection, the rhs of the expression should carry indices α and $\dot{\beta}$. The simplest object that carries those two indices is σ^μ,

which also carries a Lorentz index. The latter has to be contracted with a vector index, that is P_μ, the generator of translations. The factor of 2 is for normalisation.

By the same line of reasoning we should have $\{Q_\alpha, Q^\beta\} = c_1(\sigma^{\mu\nu})_\alpha^{\ \beta} J_{\mu\nu} + c_2\delta_\alpha^{\ \beta}$, where c_1 and c_2 are constants. Commuting with P^λ results that $c_1 = 0$. Since we have that $Q_\alpha = \epsilon_{\alpha\beta}Q^\beta$ where $\epsilon_{01} = 1$, we obtain $\{Q_\alpha, Q_\beta\} = c_2\epsilon_{\alpha\beta}$, but because lhs is symmetric in α and β we deduce that $c_2 = 0$. The complete supersymmetry algebra is therefore given by relations:

$$\{Q_\alpha, \overline{Q}_{\dot\beta}\} = 2(\sigma^\mu)_\alpha^{\ \dot\beta} P_\mu \tag{15}$$

$$\{Q_\alpha, Q_\beta\} = 0 \tag{16}$$

$$\{\overline{Q}_{\dot\alpha}, \overline{Q}_{\dot\beta}\} = 0 \tag{17}$$

$$[Q_\alpha, J_{\mu\nu}] = \frac{1}{2}(\sigma^\mu)_\alpha^{\ \beta} Q_\beta \tag{18}$$

$$[\overline{Q}_{\dot\alpha}, J_{\mu\nu}] = -\frac{1}{2}\overline{Q}_{\dot\beta}(\overline{\sigma}_{\mu\nu})_{\dot\alpha}^{\ \dot\beta} \tag{19}$$

$$[Q_\alpha, P_\mu] = 0 \tag{20}$$

$$[\overline{Q}_{\dot\alpha}, P_\mu] = 0\ . \tag{21}$$

There is an immediate physical result coming from eq. (14): when contracted with $(\overline{\sigma})^{\dot\beta\alpha}$ one has

$$4P^\nu = (\overline{\sigma})^{\dot\beta\alpha}\{Q_\alpha, \overline{Q}_{\dot\beta}\}\ . \tag{22}$$

The first component P^0 is the Hamiltonian, so

$$4\mathcal{H} = \sum_\alpha \{Q_\alpha, \overline{Q}_{\dot\beta}\} = \sum_\alpha \{Q_\alpha, Q_\alpha^\dagger\} = \sum_\alpha (Q_\alpha Q_\alpha^\dagger + Q_\alpha^\dagger Q_\alpha)\ , \tag{23}$$

because the conjugate of Q_α is $\overline{Q}_{\dot\beta}$. It is clear that $\mathcal{H}$ is non negative definite (the value 0 is admitted), so in supersymmetric theory any physical state $|S\rangle$ has a non negative energy:

$$\langle S\,|\mathcal{H}|\,S\rangle = \frac{1}{2}\sum_\alpha \sum_{S'} \left|\langle S'\left|Q_\alpha^2\right|\,S\rangle\right|^2 \geq 0\ . \tag{24}$$

Superspace and superfields

From the relation (14), that could be also written as

$$\{Q_\alpha, Q_\alpha^\dagger\} = 2(\sigma^\mu)_{\alpha\alpha} P_\mu \ , \tag{25}$$

we could construct a so–called *superspace*, an abstract space with both bosonic and fermionic coordinates. The fermionic coordinates should be constructed with the aid of *Grassmann numbers* (Grassmann, 1844). Those are anticommuting numbers θ_i that commute with ordinary numbers x:

$$\theta_i \theta_j = -\theta_j \theta_i \ , \text{ and } \theta_i x = x \theta_i \ . \tag{26}$$

It is clear that

$$(\theta_i)^2 = 0 \text{ because } \theta_i \theta_i = -\theta_i \theta_i \ , \tag{27}$$

and therefore any function defined on Grassmann numbers has at most a constant and a linear term: $f(\theta) = a + b\theta$, where a, b are ordinary numbers. It is also easy to find out that a product of two Grassmann numbers, that is $\theta_i \theta_j$, obeys to Bose–Fermi statistics.

The integral over Grassmann functions is called *Berezin integral* (Berezin, 1966). It is a sort of integral over fermionic variables, and can be determined by asking basic properties of ordinal integration like linearity

$$\int \mathrm{d}\theta \ [a f(\theta) + b g(\theta)] = a \int \mathrm{d}\theta \ f(\theta) + b \int \mathrm{d}\theta \ g(\theta) \tag{28}$$

translational invariance

$$\int d\theta f(\theta + \theta') = \int d\theta f(\theta) \ , \tag{29}$$

and partial integration formula

$$\int \mathrm{d}\theta \ \left[\frac{\partial}{\partial \theta} f(\theta) \right] = 0 \ . \tag{30}$$

Starting from formula (29), and the fact that any function of Grassmann numbers is linear one finds out that

$$\int d\theta(a + b\theta + b\theta') = \int d\theta(a + b\theta) \ , \tag{31}$$

$$a \int d\theta + b \int d\theta\theta + b\theta' \int d\theta = a \int d\theta + b \int d\theta\theta \ , \tag{32}$$

providing the result

$$\int d\theta = 0 \ . \tag{33}$$

This leads to very simple integration rules:

$$\int \mathrm{d}\theta \ 1 = 0 \ , \tag{34}$$

and

$$\int \mathrm{d}\theta \ \theta = 1 \ , \tag{35}$$

the latter formula is a matter of convention for normalisation, used originally by Berezin.

Formally, the polynomials constructed by n Grassmann variables $\theta_1, \ldots, \theta_n$, form the Grassmann algebra G_n. The Grassmann algebra uses the wedge product as multiplication, being anticommutative and associative, which is similar to the more familiar cross product of two vectors. The Berezin integral on G_n is defined as a linear functional having the following properties:

$$\int_{G_n} d\theta\theta_1, \ldots, \theta_n = 1 \ , \tag{36}$$

and

$$\int_{G_n} d\theta \frac{\partial f}{\partial \theta_i} = 0, i = 1 \ldots n \ ; \tag{37}$$

it could be shown that Berezin integral is the only possible functional with the above mentioned properties.

The superspace is formed from bosonic and fermionic coordinates, $\{x^\mu, \theta^\alpha, \overline{\theta}^{\dot{\beta}}\}$. Here θ^α is a two component left handed Weyl spinor $(\theta^{(0)}, \theta^{(1)})$, $\overline{\theta}^{\dot{\beta}}$ a two component right handed Weyl spinor $(\overline{\theta}^{(0)}, \overline{\theta}^{(1)})$. We have a total of 4 bosonic dimensions and 4 Grassmann dimensions. This combination of ordinary coordinates x^μ and one couple of Weyl spinors $\{\theta^\alpha, \overline{\theta}^{\dot{\beta}}\}$ is called $N = 1$ supersymmetric space.

The basic relation (14) for supersymmetry generators shows that the application of two consecutive transformations leads to P^μ, a translation in ordinary bosonic space. So we expect that operators Q_α and $\overline{Q}_{\dot\beta}$ generate a translation in superspace, respectively in θ^α and $\overline{\theta}^{\dot\beta}$ Grassmann coordinates. The supercharges are explicitly represented by

$$Q_\alpha = \frac{\partial}{\partial\theta^\alpha} - i(\sigma^\mu)_{\alpha\dot\alpha}\overline{\theta}^{\dot\alpha}\partial_\mu \tag{38}$$

and

$$\overline{Q}_{\dot\beta} = -\frac{\partial}{\partial\overline{\theta}^{\dot\beta}} + i\theta^\beta(\sigma^\mu)_{\beta\dot\beta}\partial_\mu \ . \tag{39}$$

These expressions satisfy the anticommutation relation (14). Notice that the "naive" guess $Q_\alpha = \partial/\partial\theta^\alpha$ and $\overline{Q}_{\dot\beta} = -\partial/\partial\overline{\theta}^{\dot\beta}$ would give 0 in the anticommutator, thus not satisfying (14).

A *superfield* is a function defined on superspace: $\Phi(x^\mu, \theta^\alpha, \overline{\theta}^{\dot\beta})$. An infinitesimal supersymmetric transformation acts on Φ in the following manner

$$\Phi' - \Phi = \delta\Phi = i(\xi^\alpha Q_\alpha + \overline{\xi}_{\dot\alpha}\overline{Q}^{\dot\alpha})\Phi \ , \tag{40}$$

where ξ and $\overline{\xi}$ are Grassmann variables. Looking at the explicit form of the supersymmetric generators in eqs. (38)–(39), we could define also another set of independent generators:

$$D_\alpha = \frac{\partial}{\partial\theta^\alpha} + i(\sigma^\mu)_{\alpha\dot\alpha}\overline{\theta}^{\dot\alpha}\partial_\mu \tag{41}$$

and

$$\overline{D}_{\dot\beta} = -\frac{\partial}{\partial\overline{\theta}^{\dot\beta}} - i\theta^\beta(\sigma^\mu)_{\beta\dot\beta}\partial_\mu \ . \tag{42}$$

The D set is "orthogonal" to the Q set: in fact D_α and $\overline{D}_{\dot\beta}$ anticommute with Q_α and $\overline{Q}_{\dot\beta}$. So if we impose the condition $\overline{D}_{\dot\beta}\Phi = 0$ because of (40) also $\overline{D}_{\dot\beta}\Phi' = 0$ holds true. Such superfields are called *chiral superfields*. An analogy in the ordinary $\mathbb{R}^2$ space is the following: find a function $f(x,y)$ such that $[x(\partial/\partial y) - y(\partial/\partial x)]\, f(x,y) = 0$. Defining $r \equiv (x^2+y^2)^{1/2}$ any $f(r)$ will satisfy this condition.

Now if we call $y^\mu = (x^\mu + i\theta^\alpha(\sigma^\mu)_{\alpha\dot{\alpha}}\overline{\theta}^{\dot{\alpha}})$, which is a bosonic variable as x^μ and $\theta\theta'$ are such, the application of $\overline{D}_{\dot{\beta}}$ gives

$$\begin{gathered}\overline{D}_{\dot{\beta}}y^\mu = \left[-\frac{\partial}{\partial\overline{\theta}^{\dot{\beta}}} - i\theta^\beta(\sigma^\nu)_{\beta\dot{\beta}}\partial_\nu\right](x^\mu + i\theta^\alpha(\sigma^\mu)_{\alpha\dot{\alpha}}\overline{\theta}^{\dot{\alpha}}) = \\ -\frac{\partial}{\partial\overline{\theta}^{\dot{\beta}}}x^\mu - i\frac{\partial}{\partial\overline{\theta}^{\dot{\beta}}}\left[\theta^\alpha(\sigma^\mu)_{\alpha\dot{\alpha}}\overline{\theta}^{\dot{\alpha}}\right] - i\theta^\beta(\sigma^\nu)_{\beta\dot{\beta}}\partial_\nu x^\mu + \\ \theta^\beta(\sigma^\nu)_{\beta\dot{\beta}}\partial_\nu\theta^\alpha(\sigma^\mu)_{\alpha\dot{\alpha}}\overline{\theta}^{\dot{\alpha}} = \\ 0 + i\theta^\alpha(\sigma^\mu)_{\alpha\dot{\beta}} - i\theta^\beta(\sigma^\mu)_{\beta\dot{\beta}} + 0 = 0\ . \end{gathered} \tag{43}$$

A chiral superfield depends only on a two component spinor beyond the bosonic coordinate, $\Phi(y,\theta)$. Because of that and of Grassmann numbers properties we can form an object with at most two powers of θ, that is $\theta\theta$. Upper powers of θ vanish, so for a chiral superfield we have

$$\Phi(y,\theta) = \phi(y) + \sqrt{2}\theta\psi(y) + \theta\theta F(y)\ , \tag{44}$$

where ϕ and F are complex scalar fields, ψ a Weyl spinor. Expanding with Taylor (44) around x we obtain

$$\begin{gathered}\Phi(y,\theta) = \phi(x) + \sqrt{2}\theta\psi(x) + \theta\theta F(y) + \\ i\theta\sigma^\mu\overline{\theta}\partial_\mu\phi(x) - \frac{1}{2}\theta\sigma^\mu\overline{\theta}\theta\sigma^\nu\overline{\theta}\partial_\mu\partial_\nu\phi(x) + \sqrt{2}\theta i\theta\sigma^\mu\overline{\theta}\partial_\mu\psi(x)\ . \end{gathered} \tag{45}$$

The conjugate of a chiral superfield, $\overline{\Phi}$, will satisfy the relation

$$D_\alpha\overline{\Phi} = 0\ , \tag{46}$$

and is called *antichiral superfield*.

The most general Lagrangian with two derivatives constructed from chiral superfields Φ_i is written as

$$\mathcal{L} = K(\Phi_i,\overline{\Phi}_j)\big|_{\theta^2\overline{\theta}^2} + W(\Phi_i)|_{\theta^2} + \overline{W}(\overline{\Phi}_i)\big|_{\overline{\theta}^2}\ , \tag{47}$$

where the subscripts denote the coefficients in power expansion of θ and $\overline{\theta}$. K is a real function, the *Kähler potential* (Kähler, 1933), W is a holomorphic function, the *superpotential*. We have the relations of integration over

Grassmann coordinates

$$\int \mathrm{d}^2\theta\, \mathrm{d}^2\overline{\theta}\; K \equiv K|_{\theta^2\overline{\theta}^2} \tag{48}$$

and

$$\int \mathrm{d}^2\theta\; W \equiv W|_{\theta^2} \ . \tag{49}$$

The Lagrangian (47) is renormalisable if and only if K is quadratic and W is at most a cubic function.

A standard example of a supersymmetric model is the Wess–Zumino model (Wess & Zumino, 1974), the first known supersymmetric interacting model. It is defined as

$$K = \overline{\Phi}\Phi \ , \quad W = \frac{m^2}{2}\Phi^2 + \frac{\lambda}{3}\Phi^3 \ , \tag{50}$$

where parameters m and λ are real. Plugging in the expansion of the superfield (45) we have

$$\mathcal{L} = \int \mathrm{d}^2\theta\, \mathrm{d}^2\overline{\theta}\; \overline{\Phi}\Phi + \int \mathrm{d}^2\theta\; \left(\frac{m^2}{2}\Phi^2 + \frac{\lambda}{3}\Phi^3\right) + \int \mathrm{d}^2\overline{\theta}\; \left(\frac{m^2}{2}\overline{\Phi}^2 + \frac{\lambda}{3}\overline{\Phi}^3\right) \ , \tag{51}$$

obtaining

$$\mathcal{L} = \overline{F}F + m\phi F + \lambda\phi^2 F - \frac{m}{2}\psi\psi - \lambda\phi\psi\psi + m\overline{\phi F} + \lambda\overline{\phi}^2\overline{F} - \frac{m}{2}\overline{\psi\psi} - \lambda\overline{\phi\psi\psi} + \text{ derivative terms acting on } \phi \text{ and } \psi \ . \tag{52}$$

The F field can be eliminated from equation of motion which reads

$$\frac{\partial\mathcal{L}}{\partial F} - \partial_\mu \frac{\partial\mathcal{L}}{\partial(\partial^\mu F)} = 0 = \frac{\partial\mathcal{L}}{\partial F} = \overline{F} + m\phi + \lambda\phi^2 \ . \tag{53}$$

So we obtain two equations

$$F = -m\overline{\phi} - \lambda\overline{\phi}^2 \ , \quad \overline{F} = -m\phi - \lambda\phi^2 \ . \tag{54}$$

Substituting this expressions for F and $\overline{F}$ into eq. (52) we eventually obtain

$$\mathcal{L} = -\partial_\mu\phi\partial^\mu\overline{\phi} + i\overline{\psi}\sigma^\mu\partial_\mu\psi - \frac{m}{2}(\psi^2 + \overline{\psi}^2) - \lambda\phi\psi^2 - \lambda\overline{\phi\psi}^2 -$$

$$|m\phi - \lambda\phi^2|^2 \ . \tag{55}$$

This is the Lagrange for ϕ^4 theory of a massive complex scalar coupled with Yukawa interactions to a massive two component Weyl spinor ψ. As we have already discussed, a consequence of supersymmetry is that the scalar and spinor masses are equal.

Supersymmetry transformations we have seen are global. When they are combined with general relativity and become local, we have *supergravity* or SUGRA for short (Kähler, 1933; Volkov & Soroka, 1973; Gol'fand & Likhtman, 1971; Nath & Arnowitt, 1975; Gol'fand & Likhtman, 1989). This theory has become less popular after meeting various shortcomings, among others having an unrealistically large cosmological constant and gauge anomalies (Fabiano, 2022).

There are many existing supersymmetric theories. In particle physics, the MSSM has been extensively searched for, in particular at Cern with the Large Hadron Collider - LHC - for years, without even a hint of new observed phenomena. The lack of experimental evidence, united to the absence of indications for a new energy scale beyond the electroweak model to search for, have ruled out some supersymmetric extensions to the Standard Model, and, albeit supersymmetry has not been completely excluded as a theory, those facts are responsible for the decline towards the interest in the subject.

References

Berezin, F.A. 1966. *The Method of Second Quantization, 1st edition*. New York, London: Academic press. ISBN-13: 978-0120894505.

Fabiano, N. 2022. Anomalies in quantum field theories. *Vojnotehnički glasnik/Military Technical Courier*, 71(1), pp.100-112. Available at: https://doi.org/10.5937/vojtehg71-38164.

Fabiano, N. 2021. Quantum electrodynamics divergencies. *Vojnotehnički glasnik/Military Technical Courier*, 69(3), pp.656-675. Available at: https://doi.org/10.5937/vojtehg69-30366.

Fayet, P. 1975. Supergauge invariant extension of the Higgs mechanism and a model for the electron and its neutrino. *Nuclear Physics B*, 90, pp.104-124. Available at: https://doi.org/10.1016/0550-3213(75)90636-7.

Fayet, P. 1977. Spontaneously broken supersymmetric theories of weak, electromagnetic and strong interactions. *Physics Letters B*, 69(4), pp.489-494. Available at: https://doi.org/10.1016/0370-2693(77)90852-8.

Fayet, P. 1976. Supersymmetry and weak, electromagnetic and strong interactions. *Physics Letters B* Volume 64, Issue 2, Pages 159-162. Available at: https://doi.org/10.1016/0370-2693(76)90319-1.

Fayet, P. & Ferrara, S. 1977. Supersymmetry. *Physics Reports*, 32(5), pp.249-334. Available at: https://doi.org/10.1016/0370-1573(77)90066-7.

Gervais, J.-L. & Sakita, B. 1971. Field theory interpretation of supergauges in dual models. *Nuclear Physics B*, 34(2), pp.632-639. Available at: https://doi.org/10.1016/0550-3213(71)90351-8.

Gol'fand, Yu.A. & Likhtman, E.P. 1971. Extension of the algebra of the Poincare group generators and violation of P invariance. *JETP Letters*, 13(8), pp.452-455 (in Russian) [online]. Available at: http://jetpletters.ru/ps/717/article_11110.shtml [Accessed: 20 September 2022]. (In the original: Гольфанд Ю.А. и Лихтман Е.П. 1971. Расширение алгебры генераторов группы Пуанкаре и нарушение Р-инвариантности. *Письма в ЖЭТФ*, 13(8), стр.452-455 [онлайн]. Доступно на: http://jetpletters.ru/ps/717/article_11110.shtml [Дата обращения: 20 Сентябрь 2022].)

Gol'fand, Yu.A. & Likhtman, E.P. 1989. Extension of the algebra of Poincaré group generators and violation of p invariance. In: Salam, A. & Sezgin, E. (Eds.) *Supergravities in Diverse Dimensions Commentary and Reprints (In 2 Volumes)*. Singapore: World Scientific. Available at: https://doi.org/10.1142/9789814542340_0001.

Grassmann, H. 1844. *Die Lineale Ausdehnungslehre – Ein neuer Zweig der Mathematik* (in German). Leipzig: Verlag von Otto Wigand [online]. Available at: https://gdz.sub.uni-goettingen.de/id/PPN534901565 [Accessed: 20 September 2022].

Kähler, E. 1933. Über eine bemerkenswerte Hermitesche Metrik. *Abh.Math.Semin.Univ.Hambg.*, 9, pp.173-186. Available at: https://doi.org/10.1007/BF02940642.

Nath, P. & Arnowitt, R. 1975. Generalized super-gauge symmetry as a new framework for unified gauge theories. *Physics Letters B*, 56(2), pp.177-180. Available at: https://doi.org/10.1016/0370-2693(75)90297-X.

Ramond, P. 1971. Dual Theory for Free Fermions. *Physical Review D*, 3(10), pp.2415-2418. Available at: https://doi.org/10.1103/PhysRevD.3.2415.

Volkov, D.V. & Akulov, V.P. 1972. Possible Universal Neutrino Interaction. *JETP Letters*, 16(11), pp.438-440 [online]. Available at: http://jetpletters.ru/ps/1766/article_26864.shtml [Accessed: 20 September 2022].

Volkov, D.V. & Akulov, V.P. 1973. Is the neutrino a goldstone particle? *Physics Letters B*, 46(1), pp.109-110. Available at: https://doi.org/10.1016/0370-2693(73)90490-5.

Volkov, D.V. & Akulov, V.P. 1974. Goldstone fields with a spin one half. *Teor. Mat. Fiz.*, 18(1), pp.39-50 (in Russian).

Volkov, D.V. & Soroka, V.A. 1973. Higgs effect for Goldstone particles with spin 1/2. *JETP Letters*, 18(8), pp.529-532 [online]. Available at: http://jetpletters.ru/ps/1568/article_24038.shtml [Accessed: 20 September 2022].

Wess, J. & Zumino, B. 1974. Supergauge transformations in four dimensions. *Nuclear Physics B*, 70(1), pp.39-50. Available at: https://doi.org/10.1016/0550-3213(74)90355-1.

Суперсимметрия

Никола Фабиано

Белградский университет, Институт ядерных исследований «Винча» − Институт государственного значения для Республики Сербия, г. Белград, Республика Сербия

РУБРИКА ГРНТИ: 29.05.03 Математические методы теоретической физики,
29.05.23 Релятивистская квантовая теория. Квантовая теория поля
29.05.33 Электромагнитное взаимодействие

ВИД СТАТЬИ: обзорная статья

Резюме:

Введение/цель: Суперсимметрия — это симметрия лагранжиана, выходящая за пределы Группы Ли. Это позволяет обмениваться бозонами и фермионами. Большинство важной моделью является минимальная суперсимметричная стандартная модель или MSSM.

Методы: Алгебра суперзарядов, суперполя, числа Грассмана, интеграл Березина.

Результаты: Суперсимметричные преобразования глобальны, они не зависят от координат пространства-времени. В случае Супергравитации они локальны.

Выводы: Суперсимметричные модели и, в частности, MSSM могли бы описывать больше физики. и больше частиц за пределами Стандартной модели.

Ключевые слова: суперсимметрия, минимальная суперсимметричная стандартная модель.

Суперсиметрија

Никола Фабиано

Универзитет у Београду, Институт за нуклеарне науке ”Винча”-Институт од националног значаја за Републику Србију,
Београд, Република Србија

ОБЛАСТ: физика
КАТЕГОРИЈА (ТИП) ЧЛАНКА: прегледни рад

Сажетак:

Увод/циљ: Суперсиметрија је симетрија Лагранжиана која у опису симетрија иде даље од Лијевих група. Суперсиметрија омогућава размену бозона и фермиона. Најважнији модел је минимални суперсиметрични стандардни модел, или MSSM.

Методе: Алгебра супернабоја, суперполја, Грасманови бројеви, интеграл Березина.

Резултати: Суперсиметричне трансформације су глобалне, не зависе од просторно-временских координата. У случају супергравитације, оне су локалне.

Закључак: Суперсиметрични модели, а посебно MSSM, могли би унапредити опис физике честица у односу на стандардни модел.

Кључне речи: суперсиметрија, минимални суперсиметрични стандардни модел.

Paper received on / Дата получения работы / Датум пријема чланка: 13.09.2022. Manuscript corrections submitted on / Дата получения исправленной версии работы / Датум достављања исправки рукописа: 25. 03. 2023.
Paper accepted for publishing on / Дата окончательного согласования работы / Датум коначног прихватања чланка за објављивање: 27. 03. 2023.

Numerical methods and their application in dynamics of structures

Rade R. Vasiljević

Faculty of Technical Academic Studies, Belgrade, Republic of Serbia,
e-mail: r.r.vasiljevic@gmail.com,
ORCID iD: https://orcid.org/0000-0003-0458-8545

DOI: 10.5937/vojtehg71-42781; https://doi.org/10.5937/vojtehg71-42781

FIELD: mathematics, computer sciences, mechanics, mechanical engineering
ARTICLE TYPE: review paper

Abstract:

Introduction/purpose: The aim of this paper is to analyse the numerical methods for solving differential equations of dynamic equilibrium in technical problems.

Methods: The paper gives an overview of the following numerical methods: the method of central difference, the method of linear acceleration, the Newmark method, and the Wilson θ method.

Results: Various problems in applying numerical methods in dynamics of structures have been solved.

Conclusion: It has been shown that the application of numerical methods has a fundamental importance in dynamics of structures.

Key words: numerical methods, method of central difference, method of linear acceleration, Newmark method, Wilson θ method.

Introduction

Numerical methods have played a very significant role in the development of technical sciences. Today, these methods, above all, have great importance and wide application in engineering (e.g. in mechanical and civil engineering). They represent one approach to solving problems in higher mathematics with the help of computers. The main advantage of numerical methods is that the solution can be obtained even in cases where it is not possible to obtain an analytical solution. Numerical methods provide solutions that are always approximations, but mostly accurate enough from the aspect of engineering accuracy.

Numerical methods are processed in numerous papers and books, see (Hoffman, 2001; Rao, 2001; Wilson, 2001; Bathe, 2014; Subbaraj & Dokainish, 1989; Newmark, 1959; Noh & Bathe, 2019; Jin et al, 2004; Liu et al, 2018). Wilson in the ref. (2001) investigated dynamics of structures using numerical integration. The paper of Liu et al. (2018) gives an

improvement of the Wilson-θ and Newmark-β methods for quasi-periodic solutions of nonlinear dynamical systems.

Various problems are solved by numerical methods (e.g. solving large systems of linear equations, solving systems of nonlinear equations, solving all types of partial differential equations, solving eigenvalues and eigenvectors, etc.).

In this paper, the emphasis is placed on applying numerical methods in dynamics of structures. Using numerical methods, it is possible to obtain the dynamic response of a structure excited due to various influences. Depending on the specific problem, excitation can be given in the form of mathematical functions or deterministic (very complex problems). Dynamic responses of structures include the following dynamic parameters: dynamic internal forces, dynamic strains, modal parameters, dynamic displacements, dynamic velocities, dynamic accelerations, and others. Problems from dynamics of structures have been solved by numerical methods in numerous papers, e.g. (Wu, 2008; Bamer et al, 2021; Esen, 2017; Tapia Andrade & Torres Berni, 2021).

Numerical methods

Many numerical methods for analysis, simulation and design of engineering processes and systems are described in (Hofman, 2001; Rao, 2001).

Equations of oscillation of a dynamic system in a closed form can only be solved in the case of linear systems and under the action of simpler forms of load which can be formulated analytically. For more complex loads which are defined as a discrete function (e.g. moving load, seismic load, and others), it is necessary to use numerical methods even in the analysis of simpler linear systems. The inclusion of nonlinearity is achieved by numerical approximation. Numerical solutions, in principle, are based on iterative methods. The most famous iterative method is Runge-Kutta.

To determine the dynamic response of a structure excited by various influences, it is necessary to solve a system of differential equations:

$$\left[\mathbf{M}\right]\left\{\ddot{\mathbf{U}}\right\}+\left[\mathbf{C}\right]\left\{\dot{\mathbf{U}}\right\}+\left[\mathbf{K}\right]\left\{\mathbf{U}\right\}=\left\{\mathbf{P(t)}\right\}. \qquad (1)$$

In Eq. (1), the notations [**M**], [**C**] and [**K**] are the matrices of consistent mass, damping and stiffness of the system. The notations {**Ü**}, {$\dot{\mathbf{U}}$} and {**U**} are the acceleration, velocity and displacement vectors of the system. The notation {**P(t)**} represents the vector of external forces in the nodes of the system. For more information on structural dynamics, see (Dhatt & Touzot, 1984; Wilson, 2001; Clough & Penzien, 2015).

There are various methods for numerically determining dynamic responses of structures. In this paper, the emphasis is placed on direct integral numerical methods. To solve the problem of a dynamic response of structures, the following four direct integral methods will be presented:

- method of central difference,
- method of linear acceleration,
- Newmark method, and
- Wilson θ method.

The first two methods are explicit while the second two methods are implicit. Explicit methods generally require a small time step Δt, but their solution does not require a relatively long time. On the other hand, implicit methods allow a relatively large time step Δt, but their solution requires a much longer time. It is important to choose the appropriate time step Δt. It affects the stability and accuracy of the solution, but also the total calculation time. Too large a step can lead to inaccurate results and an unstable response of the structure. On the other hand, too small a step can result in an unnecessarily long time to solve the problem.

Method of central difference

The central differential method is used in systems with fast and short-term oscillations and impulse loads. It is based on the approximation of differential expressions by difference. It is conditionally stable. It is excellent for small Δt, while it is unstable for large Δt. In order to obtain results of satisfactory accuracy, the time interval must be chosen so that it is small enough, i.e. $\Delta t<T_n/\pi$ (e.g. $\Delta t=0.1T_n$), where T_n is the oscillation period of the structure that coincides with the largest oscillation mode. More details on this method are given in (Jin et al, 2004; Wilson, 2001). The main steps of the central difference method are shown in Algorithm 1:

Algorithm 1 - Method of central difference

1: $\ddot{u}_0 = \dfrac{p_o - c\dot{u}_o - ku}{m}$

2: Select Δt

3: $u_{-1} = u_0 - \Delta t\dot{u}_0 + \dfrac{(\Delta t)^2}{2}\ddot{u}_0$

4: $k = \dfrac{m}{(\Delta t)^2} + \dfrac{c}{2\Delta t}$

5: $a = \frac{m}{(\Delta t)^2} + \frac{c}{2\Delta t}$

6: $b = k - \frac{2m}{(\Delta t)^2}$

7: $\hat{p}_i = p_i - au_{i-1} - bu_i$

8: $u_{i+1} = u_i + \Delta u_i,\ \dot{u}_{i+1} = \dot{u}_i + \Delta\dot{u}_i,\ \ddot{u}_{i+1} = \ddot{u}_i + \Delta\ddot{u}_i$

Method of linear acceleration

The linear acceleration method is one of the most well-known step-by-step integration methods. This method gives excellent results with relatively little effort in computation. Its main characteristics are: the acceleration changes linearly during the interval, the damping and stiffness coefficients of the system remain constant during the time interval, the accuracy of the method depends on the size of the selected time step, and sudden changes of the stiffness and damping function must be taken into account. It is very good for small Δ*t*, while it is unstable for large Δ*t*. A detailed description of this method is given in (Bathe, 2014; Wilson, 2001). The procedure of the linear acceleration method is shown in the form of Algorithm 2:

Algorithm 2 - Method of linear acceleration

1: $\ddot{u}_0 = \frac{p_o - c\dot{u}_o - ku}{m}$

2: Select Δt

3: $\Delta\hat{p}_i = \Delta p_i + a\dot{u}_i + b\ddot{u}_i$

4: $\hat{k} = k + \frac{4m}{\Delta t^2} + \frac{2c}{\Delta t}$

5: $\Delta u_i = \frac{\Delta\hat{p}_i}{k}$

6: $\Delta\dot{u}_i = \frac{2}{\Delta t}\Delta u_i - 2\dot{u}_i$

7: $\Delta\ddot{u}_i = \frac{4}{(\Delta t)^2}(\Delta u_i - \Delta t\dot{u}_i) - 2\ddot{u}_i$

8: $u_{i+1} = u_i + \Delta u_i,\ \dot{u}_{i+1} = \dot{u}_i + \Delta\dot{u}_i,\ \ddot{u}_{i+1} = \ddot{u}_i + \Delta\ddot{u}_i$

Newmark method

The Newmark method of direct integrations is a special case of the linear acceleration method. It is the most well-known implicit method for solving the dynamic equilibrium equation, which involves the choice of two parameters. It is used in systems with fast and short-term oscillations. Newmark established this method in 1959 (Newmark, 1959). In this method, the parameters β and γ are introduced, defining the change of acceleration over a time interval, the stability and accuracy of the method. The method is unconditionally stable. The time step Δt is chosen more for accuracy than for stability, if the condition $\gamma \geq 0.5$ and $\beta \geq 0.25(\gamma+05)^2$. The negative characteristic of this method is reflected in the numerical extension of the period. It is described in more detail in (Bathe, 2014; Newmark, 1959; Jin et al, 2004; Liu et al, 2018; Wilson, 2001; Anahory Simoes et al, 2023; Karimi et al, 2018; Hassan, 2019). Solving system oscillation equations using the Newmark method by direct integration is shown by Algorithm 3.

Algorithm 3 - Newmark method

1: $\ddot{u}_0 = \dfrac{p_o - c\dot{u}_o - ku}{m}$

2: Select Δt

3: $\hat{k} = k + \dfrac{m}{\beta(\Delta t)^2} + \dfrac{\gamma c}{\beta \Delta t}$

4: $a = \dfrac{m}{\beta \Delta t} + \dfrac{\gamma c}{\beta}$

5: $b = \dfrac{m}{2\beta} + \Delta t\left(\dfrac{\gamma}{2\beta} - 1\right)c$

6: $\Delta\hat{p}_i = \Delta p_i + a\dot{u}_i + b\ddot{u}_i$

7: $\Delta u_i = \dfrac{\Delta\hat{p}_i}{k}$

8: $\Delta\dot{u}_i = \dfrac{\gamma}{\beta \Delta t}\Delta u_i - \dfrac{\gamma}{\beta}\dot{u}_i + \Delta t\left(\dfrac{\gamma}{2\beta} - 1\right)\ddot{u}_i$

9: $\Delta\ddot{u}_i = \dfrac{1}{\beta(\Delta t)^2}\Delta u_i - \dfrac{1}{\Delta t \beta}\dot{u}_i - \dfrac{1}{2\beta}\ddot{u}_i$

10: $u_{i+1} = u_i + \Delta u_i,\ \dot{u}_{i+1} = \dot{u}_i + \Delta\dot{u}_i,\ \ddot{u}_{i+1} = \ddot{u}_i + \Delta\ddot{u}_i$

Wilson θ method

The Wilson θ method is applied to slowly oscillating systems. The time interval is defined by the condition $0 \leq T \leq \theta \cdot \Delta t$. The accuracy of the method depends on lengthening the period and decreasing the amplitude. The method is unconditionally stable if the extended time step meets the condition $\theta \geq 1.37$ (customary: $\theta = 1.4$). In this case, there is a very slight extension of the period and a slight decrease of the amplitude. It is used in systems with slow oscillations. The negative characteristics of this method are the extension of the period and damping. It is described in detail, see (Liu et al, 2018; Wilson, 2001; Mohammadzadeh et al, 2017). In this paper, the Wilson θ method is briefly described in Algorithm 4.

Algorithm 4 - Wilson θ method

1: $m\ddot{u}_0 = p_o - c\dot{u}_o - ku$

2: Select Δt i θ

3: $k = k + \dfrac{6m}{\theta(\Delta t)^2} + \dfrac{3c}{\theta \Delta t}$

4: $\Delta\hat{p}_i = p_{i+1} + (p_{i+2} - p_{i+1})(\theta - 1) - p_i$

5: $\overline{\Delta\hat{p}_i} = \hat{p}_i + m\left(\dfrac{6}{\theta\Delta t}\dot{u}_i + 3\ddot{u}_i\right) + C\left(3\dot{u}_i + \dfrac{\theta\Delta t}{2}\ddot{u}_i\right)$

6: $\bar{k}\hat{u}_i = \overline{\Delta\hat{p}_i}$

7: $\Delta\hat{\ddot{u}}_i = \dfrac{6}{\theta^2\Delta t^2}\Delta\hat{u}_i - \dfrac{6}{\theta\Delta t}\dot{u}_i - \dfrac{\theta\Delta t}{2}\ddot{u}_i$

8: $\Delta\ddot{u}_i = \dfrac{\Delta\hat{\ddot{u}}_i}{\theta\Delta t}$

9: $\Delta\dot{u}_i = \ddot{u}_i\Delta t - 2\dot{u}_i$

10: $\Delta u_i = \dot{u}_i\Delta t + \dfrac{1}{2}\ddot{u}_i\Delta t^2 + \dfrac{1}{6}\Delta\ddot{u}_i\Delta t^2$

11: $u_{i+1} = u_i + \Delta u_i,\ \dot{u}_{i+1} = \dot{u}_i + \Delta\dot{u}_i,$
$m\ddot{u}_{i+1} = p_{i+1} + C\dot{u}_{i+1} - Ku_{i+1}$

Examples of codes in structural dynamics

There are several programming environments designed to perform complex mathematical operations. On the one hand, programming is done in different programming languages (e.g. Fortran, C, C++, C#, Java, and others). On the other hand, ready-made software packages (e.g. Mathematica, Matlab, Mathcad, and others) can be used. The author of

this paper selected Wolfram Mathematica for solving the problem of dynamic behaviour of complex structures. Mathematica is a software package that shapes a fully integrated computing and communication environment. It is based on symbolic problem solving. It handles both complex analytical expressions and purely numerical values equally well. For more detail on Mathematica, see (Wolfram, 2003).

In the continuation of this paper, some examples of the numerical determination of dynamic parameters of real structures are illustrated, using programs written in the Mathematica software package. The author compiled and solved all the examples. The examples are given in order, from simple problems to complex ones.

Example problem 1

The sketch and the discrete model of the single-degree system (SDOF) of a bridge crane are shown in Figure 1.

Given: m=4485 kg, L=9.2 m, l=4.6 m, I=0.00264 m^4, E=2.1·10^{11} N/m^2, t_0 = 0 s, y_0=-0.06 m, y'$_0$=0 m/s, and T=2 s.

Find: Response of free undamped oscillations of the crane's main girder.

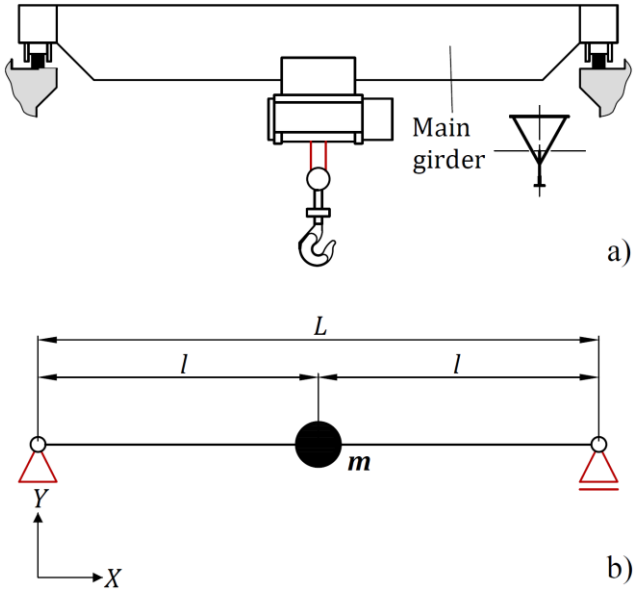

Figure 1 – a) Sketch of the bridge crane, b) Model with the concentrated mass of the bridge crane

Рис. 1 – а) Эскиз мостового крана, б) Модель мостового крана с сосредоточенными нагрузками

Слика 1 – а) Скица мосне дизалице, б) модел са концентрисаном масом мосне дизалице

Solution:

The computer code "RV-program_1" for solving free undamped oscillations of the main girder of the bridge crane was written in the program package (language) Mathematica based on the Newmark method.

```
(*Input data*)
P[t_]:=0
m=4485;k=7.32×10^6;t0=0;q={-0.06};dq={0};T=2;
(*Initialisation*)
ddq=LinearSolve[m,P[t0]-k.q];
Print["t=",t0,",q=",q,",dq=",dq,",ddq=",ddq]
Dt=0.01;
ut={t0};u={q};du={dq};ddu={ddq};
(*Loops*)
Do[DP=P[t+Dt]-P[t];
DPhat=DP+m.(4 dq/Dt+2 ddq);
khat=k+4 m/dt^2;
Dq=LinearSolve[khat,DPhat];
dDq=2 Dq/Dt-2 qd;
ddDq=4(Dq-Dt dq-dt^2 ddq/2)/Dt^2;
q=q+Dq;
dq=dq+dDq;
ddq=ddq+ddDq;
ut=Append[ut,t];u=Append[u,q];
du=Append[du,dq];ddu=Append[ddu,ddq];
(*Print["t=",t,",q=",q,",dq=",dq,",ddq=",ddq]*),{t,t0+Dt,T,Dt}]
Print["Total node:",n=Length[u]]
Print["ut=",ut,",u=",u]
(*Plot *)
ListPlot[{Table[{ut[[i]],u[[i]]},{i,n}]},PlotStyle>{Thickness[0.005],{Blue}}},
Frame>True,FrameLabel>{"t(s)","qdin(m)"},GridLines>Automatic,
Joined->True]
```

The displacement diagram of free undamped oscillations of the crane main girder is shown in Figure 2.

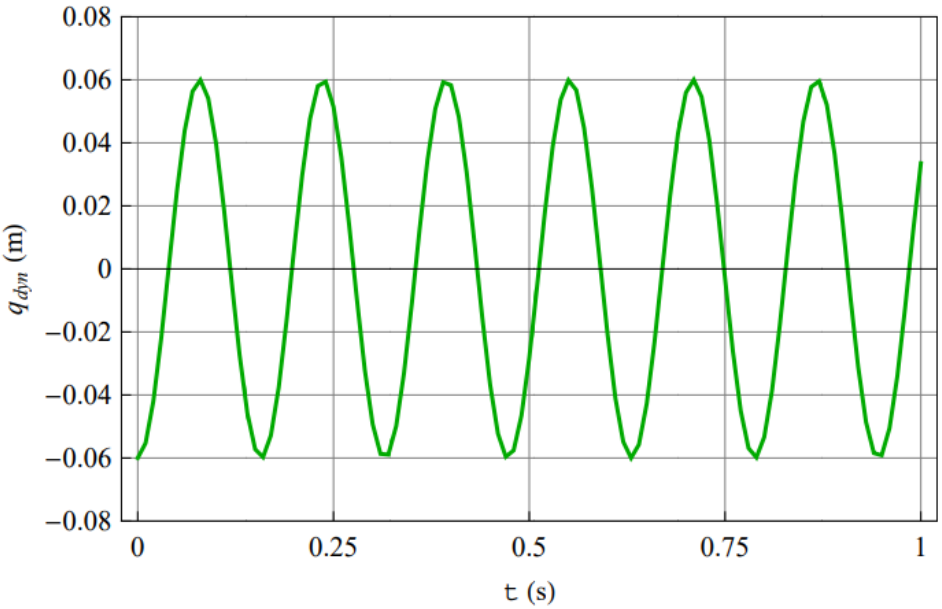

Figure 2 – Response – displacement of the middle of the bridge

Рис. 2 – Ответ - смещение середины моста

Слика 2 – Одговор – померање средине моста

Example problem 2

The sketch of the physical representation and the discrete model of the two-degree of freedom (2-DOF') system of a twin winch bridge crane are shown in Figure 3.

Given: m_1=10000 kg, m_2=10000 kg, L=16 m, a=3 m, c=9 m, I=0.00065 m^4, E=2.1·10^{11} N/m^2, t_0=0 s, y_{10}=-0.0453 m, y_{20}= -0.0582 m, y'_{10}=0 m/s, y'_{20}=0 m/s, and T=2 s.

Find: Eigenfrequencies and the response of free undamped oscillations of the crane main girder.

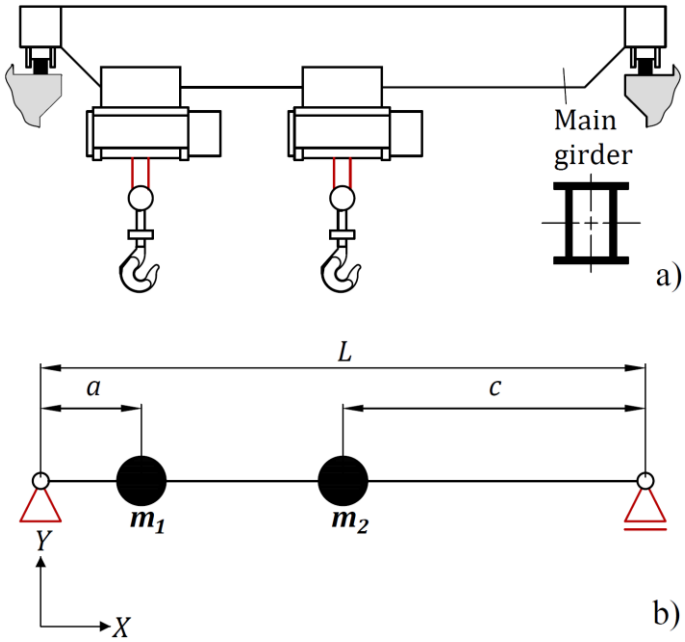

Figure 3 – a) Sketch of a bridge crane with two winches, b) Model with the concentrated masses of the carrying structure of the bridge crane
Рис. 3 – а) Эскиз мостового крана с двумя лебедками, б) Модель с сосредоточенными нагрузками несущей конструкции мостового крана
Слика 3 – а) Скица мосне дизалице са два витла, б) модел са концентрисаним масама носеће конструкције мосне дизалице

Solution:

The code "RV-program_2" for calculating the frequencies and periods of oscillations and for determining free damped oscillations of the main girder of a bridge crane with two winches was written in the Mathematica program package based on the Wilson θ method.

```
(*Input data 1*)
P[t_]:={0,0}
M={{10000,0},{0,10000}};C={{0,0},{0,0}};K=10^6{{3.64,-1.16667},
{-1.16667,1.12346}};
(*I - Frequencies and periods oscillation*)
ev=Sort[Eigenvalues[{K,M}]];
w=Sqrt[{ev}];w= w[[1]];n=2;
f=Table[w[[i]]/(2*\[Pi]),{i,n}];
T=Table[(2*\[Pi])/w[[i]],{i,n}];
Print["cfreq=",w,",cfreq=",f,",period=",T]
```

```
      (*II - Response - displacements, speeds and accelerations*)
      (*Input data 2*)
t0=0;q={-0.0453,-0.0582};q'10={0,0};T=2;
      (*Initialisation*)
ddq=LinearSolve[M,P[t0]-K.q];
Print["t=",t0,",q=",q,",dq=",dq,",ddq=",ddq]
Dt =0.01;θ=1.4;Dτ=θ Dt;
ut={t0};u={q};du={dq};ddu={ddq};
      (*Loops*)
Do[DP=P[t+Dt]+(P[t+2 Dt]−P[t+Dt])(θ−1)−P[t];
DPhat=DP+M.(6 dq/Dτ+3 ddq)+C.(3 dq+Dτ ddq/2);Khat=K+6 M/Dτ^2+3 C/Dτ;
Dq=LinearSolve[Khat,DPhat];
Dddq=(6 Dq/Dτ^2−6 dq/Dτ−3 ddq)/θ;
dDq=ddq Dt+Dddq Dt/2;
Dq=dq Dt+ddq Dt^2/2+Dddq Dt^2/6;
q=q+Dq;
dq=dq+Ddq;
ddq=LinearSolve[M,P[t]−C.dq−K.q];
ut=Append[ut,t];u=Append[u,q];
du=Append[du,dq];ddu=Append[ddu,ddq];
(*Print["t=",t,",q=",q,",dq=",dq,",ddq=",ddq]*),{t,t0+Dt,T,Dt}]
Print["Total node:",n=Length[u]]
Print["ut=",ut,",u=",u]
u1=u[[All,1]];u2=u[[All,2]];du1=du[[All,1]];du2=du[[All,2]];ddu1=ddu[[All,1]];
ddu2=ddu[[All,2]];
      (*Plot*)
ListPlot[{Table[{ut[[i]],u1[[i]]},{i,n}],Table[{ut[[i]],u2[[i]]},{i,n}]},
PlotStyle->{{Thickness[0.005],Darker[Green]},{Dashed,Darker[Blue]}},
Frame->True,FrameLabel->{"t(s)","qdin(m)"},GridLines->Automatic,
Joined->True]
```

First, natural oscillation frequencies and oscillation periods of the crane main girder carrier were obtained: *f*=(1.30, 3.20) Hz; *T*=(0.77, 0.31) s.

The results of the execution of the program in the form of a diagram of the functions of the free undamped displacement of the crane's main girder, at the locations of the trolleys, are shown in Figure 4.

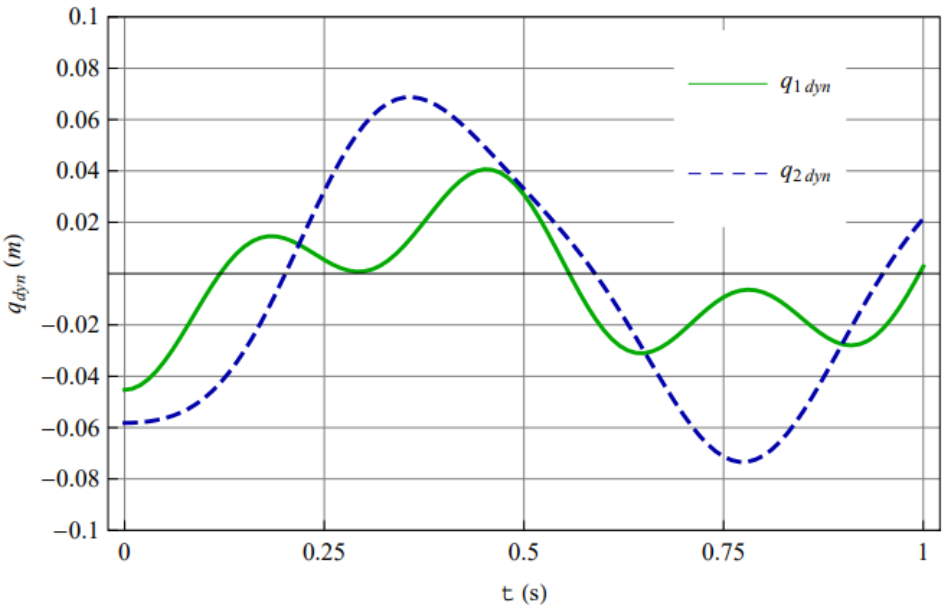

Figure 4 – Response - displacements in the locations of the trolley

Рис. 4 – Ответ - смещения в местах расположения тележки

Слика 4 – Одговор – померања на местима колица

Example problem 3

The physical representation and the discrete model with the single degree of freedom (SDOF') of the steel water tank are shown in Figure 5.

Given: m=15000 kg, k=18·10^6 N/m, c=20000 Ns/m; H=8 m, t_0 =0 s, T=1 s, and $P(t)$ – (see Figure 6).

Find: Determine the response of the vertical carrying column of the tank due to the action of the impact force $P(t)$.

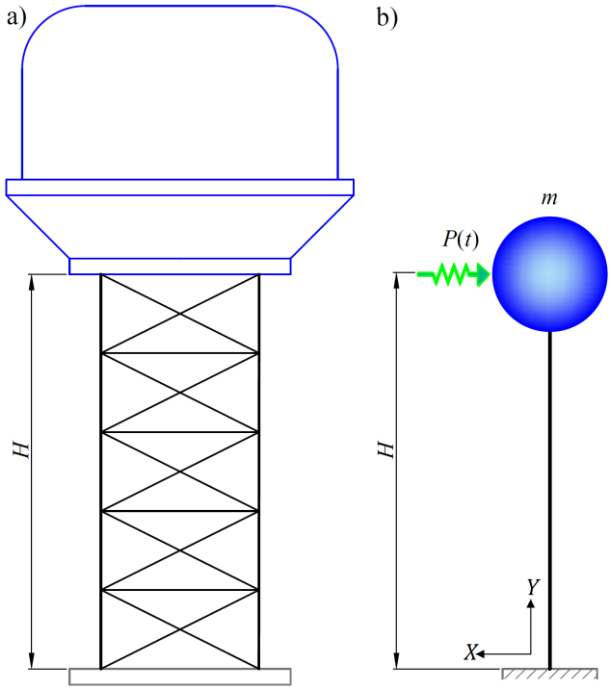

Figure 5 – a) Sketch of a steel water tank, b) Discrete model of a steel water tank - SDOF
Рис. 5 – а) Эскиз стального резервуара для воды, б) Дискретная модель стального резервуара для воды - SDOF
Слика 5 – а) Скица челичног воденог резервоара, б) дискретни модел челичног воденог резервоара – SDOF

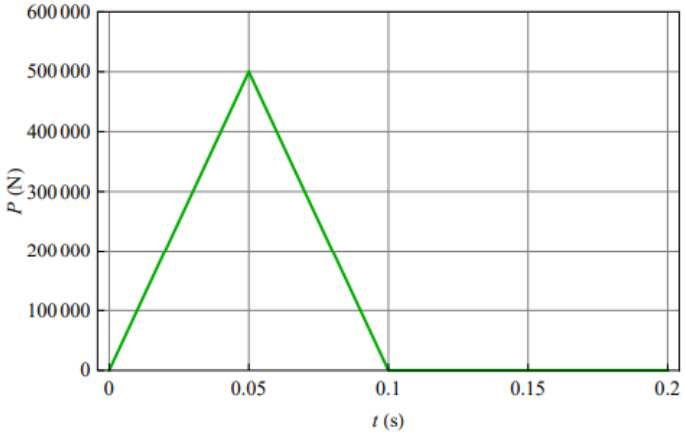

Figure 6 – Diagram of the change of the impact load in time
Рис. 6 – График изменения ударной нагрузки во времени
Слика 6 – Дијаграм промене ударног оптерећења у времену

Solution:

The code "RV-program_3" for solving the problem of oscillations of the vertical column of the tank excited by the impact force was written in the Mathematica programming language based on the Newmark method.

```
(*Input data*)
P[t_]:=If[t<=0.05,5×10^5t/0.05,If[t<=0.1,0.15×10^5/0.05-5×10^5 t/0.05,0]]
m=15000;c=20000;k=18×10^6;t0=0;q={0};dq={0};T=0.5;
(*Initialisation*)
ddq=LinearSolve[m,P[t0]-k.q];
Print["t=",t0,",q=",q,",dq=",dq,",ddq=",ddq]
Dt=0.01;
ut={t0};u={q};du={dq};ddu={ddq};
(*Loops*)
Do[DP=P[t+Dt]-P[t];
DPhat=DP+m.(4 dq/Dt+2 ddq);
khat=k+4 m/Dt^2;
Dq=LinearSolve[khat,DPhat];
Ddq=2 Dq/Dt-2 qd;
Dddq=4(Dq-Dt dq-Dt^2 ddq/2)/Dt^2;
q=q+Dq;
dq=dq+Ddq;
ddq=ddq+Dddq;
ut=Append[ut,t];u=Append[u,q];du=Append[du,dq];ddu=
Append[ddu,ddq];
(*Print["t=",t,",q=",q,",dq=",dq,",ddq=",ddq]*),{t,t0+Dt,T,Dt}]
Print["Total node:",n=Length[u]]
Print["ut=",ut,",u=",u]
(*Plot*)
ListPlot[{Table[{ut[[i]],u[[i]]},{i,n}]},PlotStyle>{Thickness[0.005],{Blue}}},Fra
me->True,FrameLabel->{"t(s)","qdin(m)"},GridLines->Automatic,Joined->
True]
```

The results in the form of a displacement diagram at the place of the concentrated mass are shown in Figure 7.

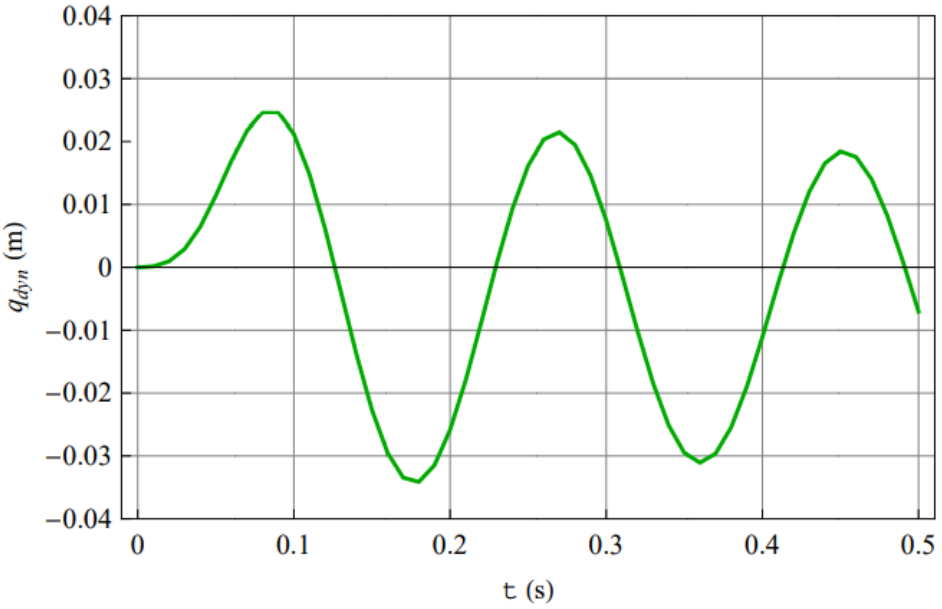

Figure 7 – Response - displacement at the tank place

Рис. 7 – Ответ - смещения в месте резервуара

Слика 7 – Одговор – померање на месту резервоара

Example problem 4

The physical description and the finite element model of the eight degree of freedom (8-DOF') overhead crane system are shown in Figure 8.

Given: m=8000 kg*; L*=16 m, *l*=2 m, *A*=0.0174 m^2, *I*=0.001723 m^4, *E*=2.1·10^{11} N/m^2, *ρ* =7850 kg/m^3*; t_0*=0 s, and *T*=10 s.

Find: Determine the response of the main girder of the bridge crane excited by the moving of the trolley.

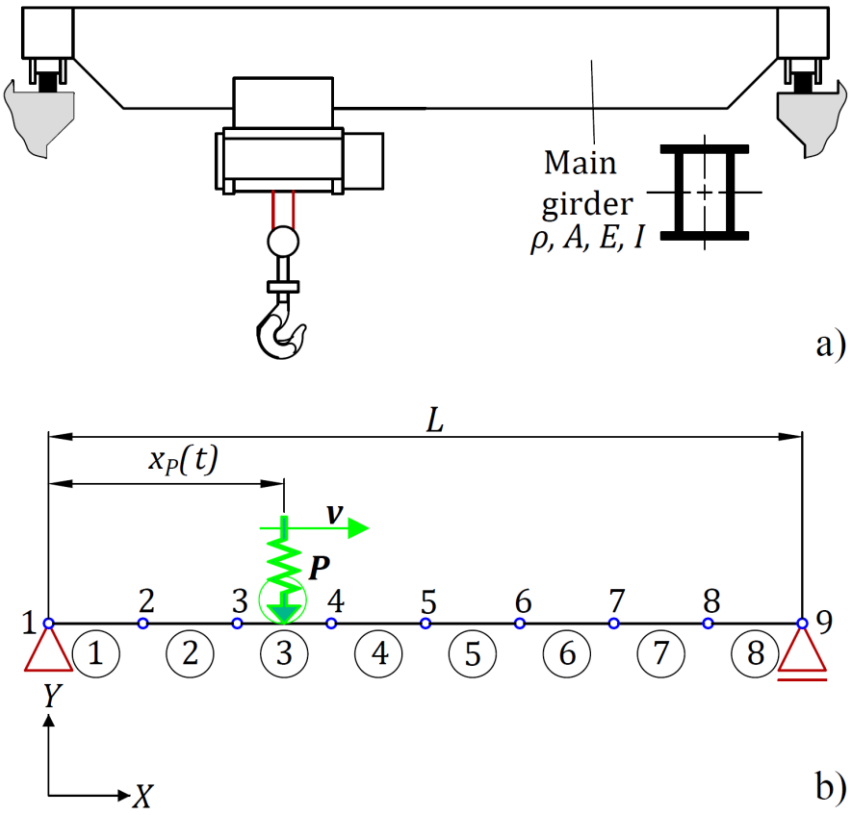

Figure 8 – a) Sketch of a bridge crane, b) Finite element model with the moving load of a bridge crane
Рис. 8 – а) Эскиз мостового крана, б) Конечно-элементная модель мостового крана с перемещением груза
Слика 8 – а) Скица мосне дизалице, б) завршноелементни модел са помичним оптерећењем мосне дизалице

Solution:

The code "RV-program_4" for solving the problem of the moving load of the bridge crane was programmed in the Mathematica programming language based on the Newmark method. Due to the scope of the program, a 6-step procedure is provided:

(i) Calculation of the stiffness [**K**] and inertia [**M**] matrices of the finite element model of the bridge crane;
(ii) Calculation of the eigenfrequencies of the FE model of the considered crane, using the algebraic equation $\det(K-\omega^2 M)=0$;
(iii) Calculation of the global position of the moving load $x_p(t)$ in relation to the left end position of the main girder in the time step;

(iv) Dividing the total time domain T into n steps so that the corresponding time interval Δt is obtained;
(v) Calculation of the external force vector {**P**(**t**)} as a function of time t of the finite element model of the bridge crane; and
(vi) Solving equation (1) for the finite element model of the bridge crane for each time step n (n takes values from 1 to p).

In equation (1), the influence of structural damping is excluded. The code was programmed in Mathematica software based on the Newmark numerical method (Bathe, 2014).

The result in the form of a diagram of the displacement of node 5 of the main girder of the bridge crane during the moving of the trolley from the end left position to the middle of the bridge is shown in Figure 9.

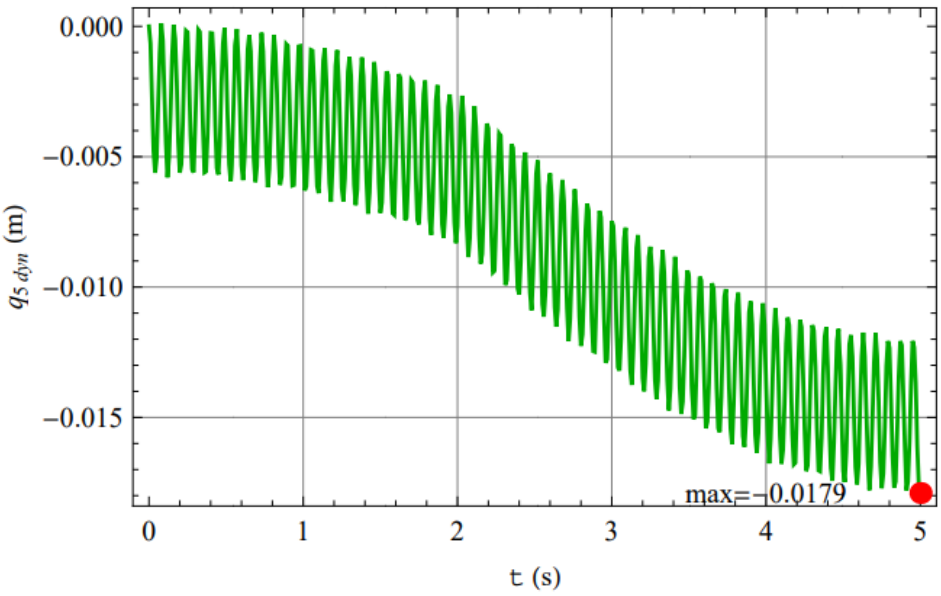

Figure 9 – Response – displacement, node 5 - q_{5dyn}
Рис. 9 – Ответ - смещение, узел 5 - $q_{5дин}$
Слика 9 – Одзив – померање, чвор 5-q_{5din}

Examples of problems in references

The dynamics of carrying structures of portal cranes using the Newmark numerical method was solved in papers (Vasiljević et al, 2016; Vasiljevic, 2020).

Conclusion

In this paper, four numerical methods with their algorithms and examples of their application in structural dynamics are briefly described. Critical comments were made on the possibilities of applying numerical methods in dynamics of structures.

Through some examples of real mechanical constructions, it is shown how to choose the size of the time step. The emphasis in practical examples is placed on the Newmark method and the Wilson θ method.

The importance of the paper is reflected in the importance of making regular decisions on choosing the most adequate numerical method in a specific situation. The paper can be useful to engineers-designers and researchers who deal with the problems of structural dynamics.

References

Anahory Simoes, A., Ferraro, S.J., Marrero, J.C. & Martín de Diego, D. 2023. A nonholonomic Newmark method. *Journal of Computational and Applied Mathematics*, 421, art.number:114873. Available at: https://doi.org/10.1016/j.cam.2022.114873.

Bamer, F., Shirafkan, N., Cao, X., Oueslati, A., Stoffel, G., Saxcé, M. & Markert, B. 2021. A Newmark space-time formulation in structural dynamics. *Computational Mechanics*, 67, pp.1331-1348. Available at: https://doi.org/10.1007/s00466-021-01989-4.

Bathe, K.-J. 2014. *Finite Element Procedures, 2nd edition.* New Jersey: Prentice-Hall. ISBN: 978-0-9790049-0-2.

Clough, R.W. & Penzien, J. 2015. *Dynamics of Structures, 2nd edition.* Berkeley, CA, USA: Computers & Structures, Inc. ISBN: 978-0923907518.

Dhatt, G. & Touzot, G.1984. *The Finite Element Method Displayed, 1st edition.* Norwich: John Wiley & Sons. ISBN: 978-0471901105.

Esen, I. 2017. A Modified FEM for Transverse and Lateral Vibration Analysis of Thin Beams Under a Mass Moving with a Variable Acceleration. *Latin American Journal of Solids and Structures*, 14(3), pp.485-511. Available at: https://doi.org/10.1590/1679-78253180.

Hassan, W.M. 2019. Numerical error assessment in nonlinear dynamic analysis of structures. *HBRC Journal*, 15(1), pp.1-31. Available at: https://doi.org/10.1080/16874048.2019.1619257.

Hoffman, J.D. 2001. *Numerical methods for Engineers and Scientists, 2nd edition.* New York, NY, USA: Marcel Dekker. ISBN: 0-8247-0443-6.

Jin, X, Ma, Q. & Li, S. 2004. Comparison of four numerical methods for calculating seismic dynamic response of sdof system. In: *13th World Conference on Earthquake Engineering*, Vancouver, B.C., Canada, Paper No. 2889, August 1-6 [online]. Available at: http://www.iitk.ac.in/nicee/wcee/article/13_2889.pdf [Accessed: 10 February 2023].

Karimi, Y., Rashahmadi, S. & Hasanzadeh, R. 2018. The Effects of Newmark Method Parameters on Errors in Dynamic Extended Finite Element Method Using Response Surface Method. *International Journal of Engineering*, 31(1), pp.50-57 [online]. Available at: https://www.ije.ir/article_73091.html [Accessed: 10 February 2023].

Liu, G., Lv, Z.R. & Chen, Y.M. 2018. Improving Wilson-θ and Newmark-β Methods for Quasi-Periodic Solutions of Nonlinear Dynamical Systems. *Journal of Applied Mathematics and Physics*, 6(8), pp.1625-1635. Available at: https://doi.org/10.4236/jamp.2018.68138.

Mohammadzadeh, S., Ghassemieh, M. & Park, Y. 2017. Structure-dependent improved Wilson-θ method with higher order of accuracy and controllable amplitude decay. *Applied Mathematical Modelling*, 52, pp.417-436. Available at: https://doi.org/10.1016/j.apm.2017.07.058.

Newmark, N.M. 1959. A Method of Computation for Structural Dynamics. *Journal of the Engineering Mechanics Division*, 85(3), pp.67-94. Available at: https://doi.org/10.1061/JMCEA3.0000098.

Noh, G. & Bathe, K.J. 2019. For direct time integrations: A comparison of the Newmark and ρ∞-Bathe schemes. *Computers & Structures*, 225, art.number:106079, pp.1-12. Available at: https://doi.org/10.1016/j.compstruc.2019.05.015.

Rao, S.S. 2001. *Applied Numerical Methods for Engineers and Scientists, 1st edition.* Hoboken, NJ, USA: Prentice Hall. ISBN: 978-0130894809.

Subbaraj, K. & Dokainish, M.A. 1989. A survey of direct time integration methods in computational structural dynamics − Part II. Implicit methods. *Computers & Structures*, 32(6), pp.1387-1401. Available at: https://doi.org/10.1016/0045-7949(89)90315-5.

Tapia Andrade, A. & Torres Berni, W. 2021. Evaluation of the dynamic properties of a 2D-frame (MDOF) in a shake table. *Ingenius*, 26, pp.49-62. Available at: https://doi.org/10.17163/ings.n26.2021.05.

Vasiljevic, R. 2020. Transverse and longitudinal vibrations of a frame structure due to a moving trolley and the hoisted object using moving finite element. *Journal of Theoretical and Applied Mechanics*, 58(4), pp.825-839. Available at: https://doi.org/10.15632/jtam-pl/126755.

Vasiljević, R., Gašić, M. & Savković, M. 2016. Parameters Influencing the Dynamic Behaviour of the Carrying Structure of a Type H Portal Crane. *Strojniški Vestnik/Journal of Mechanical Engineering*, 62(10), pp.591-602. Available at: https://doi.org/10.5545/sv-jme.2016.3553.

Wilson, E.I. 2001. *Three-Dimensional Static and Dynamic Analysis of Structures, 3rd edition.* Berkeley, CA, USA: Computers and Structures Inc. ISBN: 978-0-923907-00-9.

Wolfram, S. 2003. *The Mathematica Book, 5th edition.* Champaign, IL, USA: Wolfram Media. ISBN: 978-1–57955–022–3.

Wu, J.-J. 2008. Transverse and longitudinal vibrations of a frame structure due to a moving trolley and the hoisted object using moving finite element. *International Journal of Mechanical Sciences*, 50(4), pp.613-625. Available at: https://doi.org/10.1016/j.ijmecsci.2008.02.001.

Численные методы и их применение в динамике структур

Раде Р. Васильевич

Факультет технических академических исследований,
г. Белград, Республика Сербия

РУБРИКА ГРНТИ: 27.41.41 Алгоритмы решения задач вычислительной и дискретной математики,
30.15.27 Колебания механических систем,
30.03.19 Математические методы механики,
55.01.77 Методы исследования и моделирования. Математические и кибернетические методы
ВИД СТАТЬИ: обзорная статья

Резюме:

Введение/цель: Целью данной статьи является анализ численных методов решения дифференциальных уравнений динамического равновесия в технических задачах.

Методы: В статье приведен обзор численных методов: метод центральных разностей, метод линейного ускорения, метод Ньюмарка и θ - метод Вильсона.

Результаты: Решены различные задачи применения численных методов в динамике сооружений.

Выводы: Результаты исследования показали, что применение численных методов имеет ключевое значение в динамике сооружений.

Ключевые слова: численные методы, метод центральных разностей, метод линейного ускорения, метод Ньюмарка, θ - метод Вильсона.

Нумеричке методе и њихова примена у динамици конструкција

Раде Р. Васиљевић

Висока техничка школа академских студија, Београд, Република Србија

ОБЛАСТ: математика, рачунарске науке, механика, машинство
КАТЕГОРИЈА (ТИП) ЧЛАНКА: прегледни рад

Сажетак:

Увод/циљ: У раду су анализиране нумеричке методе решавања диференцијалних једначина динамичке равнотеже у техничким проблемима.

Методе: Представљене су нумеричке методе: метода централних диференција, метода линеарног убрзања, Њумаркова метода и Вилсонова θ-метода.

Резултати: Решени су различити проблеми који се јављају при примени нумеричких метода у динамици конструкција.

Закључак: Показано је да примена нумеричких метода има фундаменталан значај у динамици конструкција.

Кључне речи: нумеричке методе, метода централних диференција, метода линеарног убрзања, Њумаркова метода, Вилсонова θ-метода.

Paper received on / Дата получения работы / Датум пријема чланка: 14.02.2023.
Manuscript corrections submitted on / Дата получения исправленной версии работы / Датум достављања исправки рукописа: 26.03.2023.
Paper accepted for publishing on / Дата окончательного согласования работы / Датум коначног прихватања чланка за објављивање: 27.03.2023.

Руски *Mig-31 Foxhound* са ракетом *Vympel R-37M*[1]

Русија нема стално стационирану јединицу ловаца пресретача *Mig-31 Foxhound* близу украјинских граница. То није необично, јер је донедавно био незамислив сценарио у којем би у рату у Украјини могла бити потребна летелица са тако специфичном улогом – пресретање великог домета. То се сада драматично променило, а *Mig-31* има важну, али још увек недовољно познату улогу у сукобу у Украјини. Ови ловци су тренутно распоређени у две базе ближе Украјини како би учествовали у борбама. У тој улози сада им се придружују и вишенаменски ловци *Su-35S Flanker*.

Ловац пресретач MiG-31BM

Првобитни MiG-31, познат у НАТО-у као Foxhound-A, развијен је током хладног рата и био је намењен заштити објеката од стратешког значаја у Совјетском Савезу од напада крстарећим ракетама које су лансирали бомбардери и подморнице. Пошто најкраћи пут од (и до) вероватног противника – Сједињених Држава пролази кроз огромна пространства на

[1] The War Zone, November 10, 2022

северу Русије, где је мрежа аеродрома веома ретка, MiG-31 је морао да има велики домет. То је, пак, значило да се ради о великом авиону; његова максимална маса је 46 тона. Потреба за брзим одговором на претњу од пројектила резултирала је захтевом за максималном брзином од 2,8 маха (или 2,35 маха у режиму крстарења).

Да би могао истовремено да се супротстави већем броју циљева који лете и високо и веома ниско, MiG-31 је добио пасивни електронски скенирајући радар RP-31 Zaslon, што је било први пут да један ловац користи ову врсту технологије. Тешка ракета ваздух-ваздух Vympel R-33 (AA-9A Amos), са дометом од 110 км, и дериват R-33S (AA-9B), са нуклеарном бојевом главом, развијени су специјално за MiG-31. Четири такве ракете носе се у тандем паровима испод трупа.

Ракета ваздух-ваздух R-33 на пресретачу MiG-31BM

Почевши од 2008. године, фабрика „Сокол" у Нижњем Новгороду надоградила је преостале пресретаче на стандард MiG-31BM (Foxhound-C), са изузетком неколико авиона који још чекају на надоградњу у пуку базираном у Јелизову, на полуострву Камчатка. MiG-31BM има радар Zaslon-AM са претпостављеним дометом претраживања до 240 км, против мете величине ловца, двоструко дуже од оригиналног Zaslona. Оружје *MiG-31BM* је допуњено са четири тешке ракете ваздух-ваздух *R-73 M* са дометом од 200 км. Унапређени ловац такође може да носи четири ракете средњег домета *R-77-1 (AA-12 Adder*) или четири борбене ракете за блиску борбу *R-73 (AA-11 Archer*) које су замениле застареле *R-40 и R-60M*.

Ракету ваздух-ваздух *Vympel R-37M,* или *AA-13 Axehead*, први пут је лансирао ловац *MiG-31* 2011. године и убрзо је ушла у пуну производњу у фабрици „Корпорација тактичких ракета" у Корољову. Прва оперативна

јединица која је добила ове ракете био је 712. ловачки авијацијски пук у Канску, у Централном војном округу, почетком 2018. године.

Производња ракете ваздух-ваздух R-37M

Ракета *R-37M*, тешка 510 кг, по величини је слична *R-33* (489 кг), али захваљујући двоструком импулсном ракетном мотору на чврсто гориво и оптимизованом профилу лета, постиже скоро дупло већи домет. Лети до циља на уздигнутој путањи, коју контролише инерцијални навигациони систем са радио-корекцијом средњег курса, и користи активни радарски трагач са двоструким dual X- и Ku опсегом за свој напад у терминалној фази.

Foxhound у Украјини

Летелица MiG-31 је првобитно пројектована да брани простране границе Совјетског Савеза од надолазећих непријатељских бомбардера са нуклеарним оружјем – америчких B-52, B-1 и FB-111 Aardvarks. Оптимизован да брзо обара бомбардере ракетама дугог домета, MiG-31 нема велике маневарске способности. Посада има слабу видљивост због чега је у неповољном положају у борби са непријатељским ловцима унутар визуелног домета. С друге стране, био је заслепљујуће брз; наследио је максималну брзину од 3 маха од претходног пресретача MiG-25 Foxbat са радаром са фазном решетком Zaslon N007 који је подржан инфрацрвеним сензором кратког домета, а којим би могао да открије нисколетеће бомбардере и крстареће ракете. Даталинкови су омогућили посади пресретача *Foxhound* и земаљским јединицама противваздухопловне одбране да „виде" једни друге кроз сензоре, размењујући податке о навођењу пројектила.

Модернизовани модел *MiG-31BM* опремљен је моћнијим радаром *Zaslon-M* са максималним дометом детекције до 400 км за веће ваздушне циљеве (авиони попут *E-3* или *E7 AWACS*) и способношћу гађања шест циљева истовремено. То омогућава пилоту да искористи већи домет побољшаних пројектила *R-37M*.

Модернизована варијанта *MiG-31BSM* има сонду за допуњавање горива путем летећих танкера која повећава потенцијални домет пресретача и перископ кокпита са задње стране. Тело пресретача је израђено од материјала отпорнијег на топлоту, која омогућава континуирано надзвучно крстарење брзином од 2,4 маха (при тој брзини, надолазећи молекули ваздуха производе веома велико трење). Такође, пресретач поседује и нови рачунар *Baget-55-06* са вишенаменским мониторима и новим опцијама за напад на земаљске и поморске циљеве.

Ваздушно-космичке снаге Русије (ВКС) и руска ратна морнарица имају између 110 и 120 пресретача *MiG-31*. Они су додељени 790. ловачком авијацијском пуку (ИАП) у Кхотилову који покрива Москву, 98. самосталном композитном авијацијском пуку (ОСАП) у Мончегорску, који покрива стратешку базу Северне флоте у Мурманску, 712 ИАП-у у Канску и 764 ИАП-у у месту Бољшоје Савино, који су одговорни за централну Русију, као и 317. ОСАП-у у Јелизову и 22. ИАП-у у Централној Угловаји, који штите базе Пацифичке флоте на Камчатки и Владивостоку,

Русија користи стратешки ударни авион *MiG-31,* чија је примарна улога пресретање, који је додељен далекометној авијацији. Ови авиони, са хиперсоничним балистичким пројектилима *Kinzhal*, наводно су коришћени против украјинских циљева у специјалној војној операцији у марту и априлу. Од тада Русија тврди да није поново користила *Kinzhal.*

Што се тиче пресретача *Foxhound,* највећи изазов представља покушај уништавања ваздушних циљева на веома великим удаљеностима, јер постоји проблем исправне идентификације, а затим и одређивања врсте ракете за напад. Такође је тешко, на удаљености од 200 или више километара, одредити који су авиони који се виде на радару пријатељски, а који непријатељски, нарочито у динамичној ситуацији и ако лет пројектила ка циљу траје неколико минута. На интернету су се појавиле (не)проверене информације да је један број руских авиона, нарочито ловаца-бомбардера *Su-34* и *Su-35* уништен пријатељском ватром због проблема са функционисањем или правилном интерпретацијом система „свој-туђи". Није потврђено да су ове информације тачне, али и ако јесу: да ли су те авионе оборили ловци пресретачи са великих даљина или противваздухопловни ракетни системи ПВО.

За пресретаче *MiG-31,* који су стационирани на северу Русије, изнад Арктика, Сибира или Пацифика, ратно тактичко окружење је једноставно: све што се налази у ваздушном простору је непријатељ.

Ситуација у Украјини је слична за Русе: све што лети дубоко унутар Украјине је украјински војни авион. Руски авиони не лете тако далеко на запад, а цивилни ваздушни саобраћај изнад Украјине је обустављен од

фебруара 2022. године. Сада ловци *MiG-31BM,* наоружани ракетама *R-37M,* покривају велики део југоисточне Украјине.

Русија је пре неколико месеци распоредила четири пресретача *MiG-31BM* у ваздухопловној бази Белбек на Криму. Познато је да су ротирани ловци из Хотиловског и Канског пука, али је могуће да су укључени и ловци из других јединица.

Министарство одбране Русије је у неколико наврата објавило обарање украјинских авиона пресретачима *MiG-31*. На пример, према саопштењу од 7. јула 2022. године, *MiG-31BM* је оборио украјински јуришни авион *Su-25 Frogfoot* изнад Миколајевске области.

У видео-снимку који је приказала Звезда ТВ (повезана са Министарством одбране Русије), 27. октобра 2022. године, пилот који се представио као Александар и стоји испред авиона *MiG-31BM*, изјавио је да је оборио украјински *Su-24 Fencer* „ракетом дугог домета". Тачан тип пројектила није прецизиран. На истом снимку приказан је *MiG-31BM „24 Red*", регистрације РФ-90888, са 712. ИАП-а у Канску из Централног војног округа. Видело се како полеће из Белбека, наоружан са три ракете *R-37M* и две *R-77-1,* а затим слеће са истим комплетом оружја.

Смештена у предграђу Севастопоља, авио-база Белбек је сада главно средиште за руске борбене авионе који су ангажовани против Украјине. У међувремену, у Белбеку је стално базиран 38. ИАП са борбеним ловцима *Su-27SM* и *Su-27SM3* и неколико двоседа *Su-30M2* за обуку. Сада је, поред тога, Русија у исту базу распоредила и *MiG-31BM*, као и вишенаменске ловце *Su-35S* и *Su-30SM.* У бази се, такође, налазе различити транспортни авиони и хеликоптери.

Иако ракете *R-37M* тамо нису примећене, ловци *Su-35S* и *Su-30SM* такође полећу из ваздухопловне базе Ворољеж, уобичајеног места где се налазио 47. бомбардерски авијацијски пук са ударним авионима *Su-34 Fullback*. Руски *Фленкери* који се налазе на том аеродрому распоређени су са руског Далеког истока, а дејствовали су из Барановича у Белорусији на почетку рата, пре него што су пребачени у Ворољеж.

Ракета ваздух-ваздух R-37M

За разлику од ракета R-33 и R-33S, које су биле намењене искључиво за пресретач MiG-31 и нису је користили други авиони, нова ракета R-37M је „универзална". Она је интегрисана са ловцима Su-30SM, Su-35S, и Su-57 *Felon*; наводно је у току интеграција са авионом MiG-35S *Fulcrum*.. На Међународном ваздухопловном и космичком салону (МАКС) близу Москве, 2019. године, ракета *R-37M* је приказана заједно са *Su-35S,* а на изложби АРМИЈА-2020 приказана је и уз *MiG-35S*.

Ракета *R-37M (AA-13 Axehead-B*) има убрзање и до 6 маха (мало ловаца лети много брже од 2 маха) и може да гађа спорије мете на удаљености до невероватних 400 км. Свака ракета је дуга 4 м и тежи 598 кг.

Вођење таквог оружја је такође захтевно*; R-37M* се ослања на инерцијалну навигацију, побољшану корекцијама које се преносе од лансирног ловца док лети у луку ка мети како би се повећао домет. Тек када се приближи кругу од око 29 км, његов унутрашњи двопојасни радарски трагач може наћи циљ за прецизније навођење у терминалној фази.

До сада су највише страдали нисколетећи украјински авиони *Su-25 Frogfoot* и *Su-24 Fencer*. Авиони *Su-25* имају мању максималну брзину, око маховог броја 0,79, што значи да су им могућности бекства знатно ограничене, док *Su-24* имају већу брзину, око једног маха на малим висинама и 1,6 маха на великим висинама, па би можда имали прилику да бржим маневрима избегну ракету, али се ти авиони користе, углавном, за лет на малим висинама због избегавања откривања од стране руских летећих радара *A-50,* што их ставља у исту позицију као и бомбардере *Su-25*.

С друге стране, мала маневарска пераја ракете *R-37* указују на могуће ниже маневарске особине ракете, што значи да би била мање ефикасна када би била лансирана против ловца који би летео већом брзином и на већим висинама.

Ракете *R-37M* се до сада нису производиле у већем броју, јер су се у Русији израђивале углавном ракете *R-77-1* које, такође, имају велики домет, иако упола мањи од ракета *R-37M*. Сада је ситуација ипак промењена, па у наоружање стиже све већи број тих далекометних ракета.

На друштвеним мрежама су се појавиле информације да је Русија употребила свој најновији ловац бомбардер *Su-57* који је оборио украјински ловац-пресретач *Su-27* близу ваздухопловне базе код Белбека, са даљине од 217 км.

Телевизија Звезда је, 1. новембра 2022. године, приказала још један снимак из Белбека, на којем други пилот, такође под именом Александар, објашњава како је оборио украјинску летелицу далекометном ракетом, али не помиње тип ракете. Овога пута у позадини се налазио ловац *Su-35S* наоружан са две ракете *R-37M,* постављене у тандему између мотора, две ракете *R-77-1* испод усисника ваздуха, два R-73 испод крила и једна противрадарска ракета *Kh-31PM* испод крила.

Према недавном извештају истраживачког центра Краљевског института уједињених служби (РУСИ), *MiG-31BM* и *Su-35S* обично обезбеђују покривеност осам додељених зона у оперативном подручју, са по пар ловаца за сваку. Међутим, с обзиром на то да у ваздушном простору нема доступних танкера за допуњавање горива, ови ловци су ограничени на борбене ваздушне патроле у трајању од око два сата; оваква врста ротације захтева око 96 летова дневно, ако се рачунају само дневни сати.

Ипак, РУСИ напомиње да су се „ове патроле показале веома ефикасним против украјинских јуришних авиона и ловаца, при чему су ракете ваздух-ваздух великог домета *R-37M* на ловцима *MiG-31BM* посебно проблематичне по украјинску авијацију". У извештајима се додаје да су

ловци ВКС током октобра лансирали до шест ракета *R-37M* дневно и да се избегавање ове ракете показало посебно тешким због „екстремно велике брзине оружја, у комбинацији са веома великим ефективним дометом и трагачем дизајнираним за гађање циљева на малим висинама".

Одбрамбене мере

Са ракетом R-37M на располагању, руски ловци *MiG-31BM* и *Su-35S* сада могу да гађају украјинске авионе са веома велике удаљености, не улазећи ни у једну од области у којима делује украјинска противваздухопловна одбрана.

Su-35S наоружан ракетом R-37M

Да би се супротставила претњи, Украјини су преко потребни противваздухопловни системи веома великог домета, при чему су ракете земља-ваздух (SAM) најочигледније решење. Ипак, ракете највећег домета доступне Украјини део су система *S-300P (SA-10 Grumble*) совјетског дизајна који је био у употреби на почетку рата. Од тада је постепено смањиван број таквих система на располагању Украјини, а вероватно ће остати мета високог приоритета руских средстава за сузбијање одбране.

Међутим, чак и постојећи *S-300P* не може да обезбеди дуготрајну противваздхопловну одбрану са својом ракетом *5V55R* – главним типом који је доступан Украјини – који има максимални домет од 90 км. Једна батерија *S-300PMU,* коју је Словачка обезбедила почетком рата, нешто је способнија.

У међувремену, *S-300V1 (SA-12 Gladiator/Giant),* систем који се заснива на *S-300P*, нуди побољшану покретљивост по земљи и способност против балистичких пројектила. Може да испали ракету *9M83 (SA-12A*

Vučković, D., SAVREMENO NAORUŽANJE I VOJNA OPREMA / MODERN WEAPONS AND MILITARY EQUIPMENT, pp.473-488

Gladiator), максималног домета од око 90 км, док *9M82 (SA-12B Giant*)) може да гађа циљеве на удаљености до 100 км.

Верзија *SA-12A S-300V1* била је доступна Украјини у ограниченом броју, а преостали примерци су вероватно предвиђени за одбрану од напада балистичким пројектилима.

Украјински систем S-300V1

Поновљени позиви Кијева за снажнијом копненом противваздухопловном одбраном дали су резултате, укључујући системе који су много напреднији од украјинских ракета земља-ваздух из совјетске ере. Међутим, наоружање које је до сада испоручено, или обећано, првенствено је оптимизовано за тачкасту одбрану критичних инсталација (I*RIS-T SLM, MIM-23 HAWK, NASAMS, Aspide, u Crotale NG*), или се ради о системима противваздухопловне одбране мањег домета, од којих су неки пројектовани за садејство са копненим снагама (*Strela-10M, Stormer HVM*).

Систем већег домета који би потенцијално могао да угрози руске ловце на већим даљинама јесте *Patriot*. Он је однедавно укључен на листу система противваздухопловне одбране који би могли помоћи Украјини у борби против Русије.

Поред своје способности гађања циљева на већим даљинама, систем *Patriot* би, такође, обезбедио даљу заштиту од напада балистичких пројектила од којих ће један део представљати и иранске ракете земља-земља.

Лансирање америчке ПВО ракете Patriot PAC-3

Чак и ако би Украјина добила системе ПВО дугог домета, нови лансери би вероватно били намењени за одбрану приоритетних циљева, као што су критична инфраструктура и велики градови.

Без обзира на то, свака врста ракета земља-ваздух која може ефикасно да угрози ваздушне циљеве на већим даљинама помоћи ће Украјини. Ипак, чак и са прилично скромном копненом ПВО мрежом, Украјина је успела да нанесе велике губитке ВКС и истера руске авионе из значајних области свог ваздушног простора. У областима где руски ударни авиони и јуришни хеликоптери дејствују принуђени су да примене мање ефикасне тактике на ниском нивоу, док су ловци попут *MiG-31BM* и *Su-35S* ограничени на патролирање на великим висинама.

Пре или касније, Украјина ће набавити западне авионе, вероватно приступачне тактичке ловце, као што су *F-16* или шведски *JAS 39 Gripen*.

Ови авиони ће бити у домету пројектила и радара *MiG-31BM*, али би требало да имају много боље сензоре и противмере за откривање надолазећих *R-37* и њихово избегавање док су још у „зони бекства". Размак домета ће такође бити много мањи за млазне авионе наоружане ракетама дугог домета *Meteor* или *AIM-120* (од 96 до 200 км) од садашњих украјинских авиона *Su-27* и *MiG-29* са *R-27* (од 40 до 80 км), а *MiG-31* има велики радарски одраз. То би могло натерати *MiG-31* да лансира ракете са веће удаљености, што значи да би вероватноћа поготка била мања.

Додуше, тешко је проценити да ли је руска употреба ловаца у ваздушним бојевима ван визуелног домета у Украјини применљива ван контекста украјинско-руског ваздушног рата, где су авиони једне стране у значајном техничком заостатку у односу на другу страну. Ипак, успешна употреба руских авиона сугерише да би они могли бити још ефикаснији

уколико би имали приступ танкерима за допуњавање горива и још бољу координацију са својим летећим радарима.

Могло би се рећи да за Украјину не постоји начин да се суочи са претњом руских пресретача као што су *MiG-31BM* који делују ван визуелног домета. Њена једина могућност тренутно лежи у нападу на аеродроме са којих узлећу руски авиони, што је изгледа већ урађено са значајним успехом на Криму.

Драган М. Вучковић (*Dragan* M. Vučković),
e-mail: draganvuckovic64@gmail.com,
ORCID iD: https://orcid.org/0000-0003-1620-5601

Футуристичка минобацачка купола[2]

Америчке специјалне снаге које се боре против милитаната ISIS на Блиском истоку недавно су објавиле фотографије испаљивања мина из напредног заштитног минобацачког система *XM905 (Advanced Mortar Protection System, или AMPS*) у Сирији.

Компјутерски асистиран минобацач *XM905* калибра 120 мм, са куполом, посебно је развијен да пружи додатни слој одбране у истуреним оперативним базама. Комплетан систем изгледа као у некој видео-игрици, попут *Call Of Duty: Modern Warfare или Command & Conquer*.

Комбинована оперативна група за специјалне операције – *Levant (CSOJTF-L*) објавила је на Твитеру фотографије за које је речено да су снимљене у ватреној бази у региону Ал Шадади у источној Сирији. Године 2021. *CSOJTF-L* је укључио Заједничку оперативну групу за специјалне операције – Операцију *Inherent Resolve (SOJTF-OIR*) и сада обезбеђује главни штаб који надгледа коалиционе снаге за специјалне операције предвођене САД које се боре против ИСИС-а у Сирији, Ираку, Либану и Египту. Системи су распоређени у америчким истуреним базама у Сирији од 2018, године.

„Коалиционе снаге испаљују 120 мм осветљавајуће мине користећи систем *XM905*." Осветљавајуће мине се могу користити за откривање непријатељских формација, за сигнализацију или обележавање циљева.

Овај систем се налази у употреби још од 2011. године и састоји се од минобацача 120 мм *XM905,* постављеног на електричну куполу која се окреће у радијусу од 360 степени. Оруђе се налази на широкој куполи која је стабилизована на три стопала.

За разлику од класичних минобацача, *XM905* има противтрзајни механизам који умањује трзај приликом испаљења и притом повећава прецизност, док изгледом више подсећа на мању хаубицу. Оруђе је изведено од израелског минобацача *Recoil Mortar System 6-Light* (*RMS6-L*)

[2] The War Zone, February 21, 2023

који је монтиран и на одређене варијанте америчких оклопних возила точкаша *Stryker*.

Напредни минобацачки заштитни систем XM905

Припадник америчких специјалних снага пуни минобацач осветљавајућом мином 120 мм, док се у позадини види ефекат осветљавања претходне мине

Комплетан систем XM905

Поред осветљавајућих мина, минобацач испаљује мине са експлозивним пуњењем за напад на непријатељске снаге, као и мине за стварање димних завеса или за означавање непријатеља. Минобацачки систем користи и мине са сателитским или ласерским навођењем. Мине са ласерским навођењем могу се употребљавати и за напад на покретне циљеве.

Овај минобацачки систем опремљен је напредним нишанским системом *Enhanced Mortar Targeting System (EMTAS*) који омогућава аутоматску паљбу на било које координате које зада нишанџија. Систем окреће куполу за 180 степени за само 12 секунди.

Систем AMPS обезбеђује додатну ватрену моћ, али и друге опције, као што је осветљавање бојишта у околини америчких истурених база у Сирији.

Драган М. Вучковић (*Dragan* M. Vučković),
e-mail: draganvuckovic64@gmail.com,
ORCID iD: https://orcid.org/0000-0003-1620-5601

Русија користи вођене бомбе у Украјини[3]

Олупина пронађена у Украјини доказ је да је дошло до употребе планирајуће бомбе *Grom*, што је, чини се, први пут од почетка рата у Украјини.

На снимку се види већи део планирајуће бомбе *Grom*, руског оружја ваздух-земља, као и пар искачућих крила која јој омогућују напад на циљ са већих даљина. Изгледа да су ове бомбе са и без погона. На основу фотографије могло би се закључити да се ради о верзији са погоном, експортној верзији *Grom-E1.*

Ову планирајућу бомбу производи *Tactical Missiles Corporation (KTRV*). Дизајн пројекта проистиче од ракете ваздух-земља типа *Kh-38M* коју је произвела иста корпорација.

Пројектил *Kh-38* има четири крилца везана за тело и репни део на крају. Компанија је додала искачућа крила и делимично променила дизајн да би добила пројектил *Grom*. Ради се о модулу који садржи дуга склапајућа крила која су причвршћена на тело пројектила. Другим речима, ради се о адаптираном пројектилу *Kh-38M* који је пројектован тако да, захваљујући склопивим крилима, постигне већу даљину.

Још се не знају тачне перформансе и техничке карактеристике пројектила, као ни када је почела оперативна употреба, али се претпоставља да се ради о периоду после 2010. године. Постоје варијанте овог пројектила, објављени су и детаљи, али у форми брошура, тако да још увек није могуће сазнати прецизне податке.

[3] The War Zone, March 15, 2023

Пројектил ваздух-земља Kh-38

До сада су обелодањене две верзије пројектила *Grom –Grom-E1* и *Grom-E2*. Обе верзија су намењене за извоз, а претпоставља се да су испитивања завршена током 2019. године.

Grom-E1 је пројектил погоњен ракетним мотором и заснован на телу авионске бомбе *OFAB-500U*. Његова маса је око 700 кг, а пречник око 30 цм. Ракета је дуга око 7 м са распоном крила од око 3,5 м.

Часопис *Janes* наводи да је *Grom-E1* наоружан бојевом главом са високоексплозивним пуњењем, масе од око 350 кг и ударним упаљачем. Такође, извештава да се погонски део састоји од бустера и ракетног мотора који ракети омогућава лет до 130 км.

Руски медији су раније тврдили да ракета може летети на даљину до 150 км, али то вероватно зависи од висине, брзине и путање авиона који је лансира.

Претпоставља се да је ракета навођена путем инерцијалне навигације са сателитским корекцијама, што би значило да нема активни трагач. То значи да се ракета може лансирати само на фиксне мете, што, међутим, не искључује могућност додавања полуактивног ласерског, инфрацрвеног или радарског трагача.

Пројектил *Grom-E2,* руске ознаке 9-А2-7759, заснован је на телу бомбе *KAB-500OD*. Часопис *Janes* наводи да се ради о планирајућој бомби, али не износиникакве детаље. Ова планирајућа бомба нема погонски део који се, у овом случају, замењује додатном високоексплозивном бојевом главом. Претпоставља се да је укупна маса бојеве главе око 450 кг, али је и даљина гађања циљева знатно смањена у односу на ракетну верзију.

Конфигурација пројектила Grom са склапајућим крилима.

Путања ракете Grom након лансирања из авиона

Планирајућа бомба Grom-E2

Пројектиле *Grom E-1/E-2* у свом интерном спремишту носи ловац-бомбардер *Su-57 Felon*. Други руски авиони, као што су *MiG-29, MiG-35, Su-34 и Su-35,* такође могу носити овакво оружје.

Сада је могуће доказати да Русија већ користи овакво оружје у својој специјалној војној операцији у Украјини. Могуће је да је тајно започела и серијску производњу породице пројектила *Grom,* као што је то урадила и са другим пројектилима као што је *Izdelie 305 LMUR*. Међутим, због уведених санкција питање је да ли Русија има могућност серијске производње оваквог оружја или се ради о употреби једног броја пројектила који је раније произведен и намењен извозу.

Оваква врста пројектила била би изузетно корисна руским снагама, јер још нису успеле да остваре ваздушну надмоћ над територијом Украјине, па је њихово ратно ваздухопловство константно под ризиком обарања приликом ваздушних мисија.

Драган М. Вучковић (*Dragan* M. Vučković),
e-mail: draganvuckovic64@gmail.com,
ORCID iD: https://orcid.org/0000-0003-1620-5601

ПОЗИВ И УПУТСТВО АУТОРИМА
ПРИГЛАШЕНИЕ И ИНСТРУКЦИЯ ДЛЯ АВТОРОВ РАБОТ
CALL FOR PAPERS AND INSTRUCTIONS FOR AUTHORS

ПОЗИВ И УПУТСТВО АУТОРИМА О НАЧИНУ ПРИПРЕМЕ ЧЛАНКА

Упутство ауторима о начину припреме чланка за објављивање у *Војнотехничком гласнику* урађено је на основу Правилника о категоризацији и рангирању научних часописа Министарства просвете, науке и технолошког развоја Републике Србије ("Службени гласник РС", број 159/20). Примена овог Правилника првенствено служи унапређењу квалитета домаћих часописа и њиховог потпунијег укључивања у међународни систем размене научних информација.

Војнотехнички гласник / Vojnotehnički glasnik / Military Technical Courier (втг.мо.упр.срб, www.vtg.mod.gov.rs, ISSN 0042-8469 – штампано издање, e-ISSN 2217-4753 – online, UDC 623+355/359, DOI: 10.5937/VojnotehnickiGlasnik; https://doi.org/10.5937/VojnotehnickiGlasnik), јесте рецензирани научни часопис.

Власници часописа су Министарство одбране Републике Србије и Војска Србије. Издавач и финансијер часописа је Универзитет одбране у Београду (Војна академија).

Програмска оријентација часописа заснива се на годишњој категоризацији часописа, коју врши надлежно државно министарство у одређеним областима, као и на његовом индексирању у међународним индексним базама.

Часопис обухвата научне, односно стручне области у оквиру образовно-научног поља **природно-математичких наука**, као и у оквиру образовно-научног поља **техничко-технолошких наука**, а нарочито области **одбрамбених наука и технологија**. Објављује теоријска и практична достигнућа која доприносе усавршавању свих припадника српске, регионалне и међународне академске заједнице, а посебно припадника војски и министарстава одбране. Публикује радове са уравнотеженим извештавањем о аналитичким, експерименталним и примењеним истраживањима, као и нумеричким симулацијама, обухватајући различите дисциплине. Објављени материјали су високог квалитета и релевантности, написани на начин који их чини доступним широкој читалачкој публици. Сви радови који извештавају о оригиналним теоријским и/или практично оријентисаним истраживањима или проширеним верзијама већ објављених радова са конференција су добродошли. Радови за објављивање одабиру се двоструко слепим поступком рецензије како би се осигурала оригиналност, релевантност и читљивост. Притом циљ није само да се квалитет објављених радова одржи високим већ и да се обезбеди правовремени, темељни и уравнотежени поступак рецензије.

Уређивачка политика *Војнотехничког гласника* заснива се на препорукама Одбора за етичност у издаваштву (COPE Core Practices) и заједничким принципима транспарентности и најбоље праксе у издаваштву COPE, DOAJ, OASPA и WAME, као и на најбољим прихваћеним праксама у научном издаваштву. *Војнотехнички гласник* је члан COPE (Committee on Publication Ethics) од 2. маја 2018. године и члан OASPA (Open Access Scholarly Publishers Association) од од 27. новембра 2015. године.

Министарство просвете, науке и технолошког развоја Републике Србије утврдило је дана 25. 10. 2022. године категоризацију *Војнотехничког гласника*, за 2022. годину:

– на листи часописа за рачунарске науке:
категорија врхунски часопис националног значаја **(M51)**,
– на листи часописа за електронику, телекомуникације и информационе технологије:
категорија врхунски часопис националног значаја **(M51)**,
– на листи часописа за машинство:
категорија врхунски часопис националног значаја **(M51)**,
– на листи часописа за материјале и хемијске технологије:
категорија врхунски часопис националног значаја **(M51)**.

Усвојене листе домаћих часописа за 2022. годину могу се видети на сајту *Војнотехничког гласника*, страница *Категоризација часописа*.

Детаљније информације могу се пронаћи и на сајту Министарства просвете, науке и технолошког развоја Републике Србије.

Подаци о категоризацији могу се пратити и на сајту КОБСОН-а (Конзорцијум библиотека Србије за обједињену набавку).

Категоризација часописа извршена је према Правилнику о категоризацији и рангирању научних часописа Министарства просвете, науке и технолошког развоја Републике Србије ("Службени гласник РС", број 159/20).

Часопис се прати у контексту Српског цитатног индекса – СЦиндекс (база података домаћих научних часописа), Научно-информационог система Redalyc и Руског индекса научног цитирања (РИНЦ). Подвргнут је сталном вредновању (мониторингу) у зависности од утицајности (импакта) у самим базама. Детаљи о индексирању могу се видети на сајту *Војнотехничког гласника*, страница *Индексирање часописа*.

Војнотехнички гласник омогућава и примењује Creative Commons (CC BY) одредбе о ауторским правима. Детаљи о ауторским правима могу се видети на сајту часописа, страница *Ауторска права и политика самоархивирања*.

Радови се предају путем онлајн система за електронско уређивање АСИСТЕНТ, који је развио Центар за евалуацију у образовању и науци (ЦЕОН).

Приступ и регистрација за сервис врше се на сајту www.vtg.mod.gov.rs, преко странице *АСИСТЕНТ* или *СЦИНДЕКС*, односно директно на линку aseestant.ceon.rs/index.php/vtg.

Детаљно упутство о регистрацији и пријави за сервис налази се на сајту www.vtg.mod.gov.rs, страница *Упутство за АСИСТЕНТ*.

Потребно је да се сви аутори који подносе рукопис за објављивање у *Војнотехничком гласнику* региструју у регистар ORCID (Open Researcher and Contributor ID), према упутству на страници сајта *Регистрација за добијање ORCID идентификационе шифре*.

Војнотехнички гласник објављује чланке на енглеском језику (arial, величина слова 11 pt, проред Single).

Поступак припреме, писања и уређивања чланка треба да буде у сагласности са *Изјавом о етичком поступању* (http://www.vtg.mod.gov.rs/izjava-o-etickom-postupanju.html).

Чланак треба да садржи сажетак са кључним речима, увод (мотивацију за рад), разраду (адекватан преглед репрезентативности рада у његовој области, јасну изјаву о новини у представљеном истраживању, одговарајућу теоријску позадину, један или више примера за демонстрирање и дискусију о представљеним

идејама), закључак и литературу (без нумерације наслова и поднаслова). Обим чланка треба да буде до једног ауторског табака (16 страница формата А4 са проредом Single), а највише 24 странице.

Чланак треба да буде написан на обрасцу за писање чланка, који се у електронској форми може преузети са сајта на страници *Образац за писање чланка*.

Наслов

Наслов треба да одражава тему чланка. У интересу је часописа и аутора да се користе речи прикладне за индексирање и претраживање. Ако таквих речи нема у наслову, пожељно је да се придода и поднаслов.

Текући наслов

Текући наслов се исписује са стране сваке странице чланка ради лакше идентификације, посебно копија чланака у електронском облику. Садржи презиме и иницијал имена аутора (ако аутора има више, преостали се означавају са „et al.“ или „и др.“), наслове рада и часописа и колацију (година, волумен, свеска, почетна и завршна страница). Наслови часописа и чланка могу се дати у скраћеном облику.

Име аутора

Наводи се пуно име и презиме (свих) аутора. Веома је пожељно да се наведу и средња слова аутора. Имена и презимена домаћих аутора увек се исписују у оригиналном облику (са српским дијакритичким знаковима), независно од језика на којем је написан рад.

Назив установе аутора (афилијација)

Наводи се пун (званични) назив и седиште установе у којој је аутор запослен, а евентуално и назив установе у којој је аутор обавио истраживање. У сложеним организацијама наводи се укупна хијерархија (нпр. Универзитет одбране у Београду, Војна академија, Катедра природно-математичких наука). Бар једна организација у хијерархији мора бити правно лице. Ако аутора има више, а неки потичу из исте установе, мора се, посебним ознакама или на други начин, назначити из које од наведених установа потиче сваки од наведених аутора. Афилијација се исписује непосредно након имена аутора. Функција и звање аутора се не наводе.

Контакт подаци

Адреса или е-адреса свих аутора даје се поред имена и презимена аутора.

Категорија (тип) чланка

Категоризација чланака обавеза је уредништва и од посебне је важности. Категорију чланка могу предлагати рецензенти и чланови уредништва, односно уредници рубрика, али одговорност за категоризацију сноси искључиво главни уредник.

Чланци у *Војнотехничком гласнику* класификују се на научне и стручне чланке.

Научни чланак је:

– оригиналан научни рад (рад у којем се износе претходно необјављени резултати сопствених истраживања научним методом);

– прегледни рад (рад који садржи оригиналан, детаљан и критички приказ истраживачког проблема или подручја у којем је аутор остварио одређени допринос, видљив на основу аутоцитата);

– кратко или претходно саопштење (оригинални научни рад пуног формата, али мањег обима или прелиминарног карактера);

– научна критика, односно полемика (расправа на одређену научну тему, заснована искључиво на научној аргументацији) и осврти.

Изузетно, у неким областима, научни рад у часопису може имати облик монографске студије, као и критичког издања научне грађе (историјско-архивске, лексикографске, библиографске, прегледа података и сл.), дотад непознате или недовољно приступачне за научна истраживања.

Радови класификовани као научни морају имати бар две позитивне рецензије.

Ако се у часопису објављују и прилози ваннаучног карактера, научни чланци треба да буду груписани и јасно издвојени у првом делу свеске.

Стручни чланак је:

– стручни рад (прилог у којем се нуде искуства корисна за унапређење професионалне праксе, али која нису нужно заснована на научном методу);

– информативни прилог (уводник, коментар и сл.);

– приказ (књиге, рачунарског програма, случаја, научног догађаја, и сл).

Пожељно је да обим кратких саопштења буде 4 до 7 страница, научних чланака и студија случаја 10 до 14 страница, док прегледни радови могу бити и дужи. Број страница није строго ограничен и, уз одговарајуће образложење, пријављени чланци такође могу бити дужи или краћи.

Ако су радови који су претходно објављени на конференцији проширени, уредници ће проверити да ли је додато довољно новог материјала који испуњава стандарде часописа и квалификује поднесак за поступак рецензије. Додати материјал не сме бити претходно објављен. Нови резултати нису нужно потребни, али су пожељни. Међутим, поднесак треба да садржи проширене кључне идеје, примере, разраде, итд., који су претходно били садржани у поднеску са конференције.

Језик рада

Језик рада треба да буде енглески.

Текст мора бити језички и стилски дотеран, систематизован, без скраћеница (осим стандардних). Све физичке величине морају бити изражене у Међународном систему мерних јединица – SI. Редослед образаца (формула) означава се редним бројевима, са десне стране у округлим заградама.

Сажетак

Сажетак јесте кратак информативан приказ садржаја чланка који читаоцу омогућава да брзо и тачно оцени његову релевантност. У интересу је уредништава и аутора да сажетак садржи термине који се често користе за индексирање и претрагу чланака. Саставни делови сажетка су увод/циљ истраживања, методи, резултати и закључак. Сажетак треба да има од 100 до 250 речи и треба да се налази између заглавља (наслов, имена аутора и др.) и кључних речи, након којих следи текст чланка.

Кључне речи

Кључне речи су термини или фразе које адекватно представљају садржај чланка за потребе индексирања и претраживања. Треба их додељивати ослањајући се на неки међународни извор (попис, речник или тезаурус) који је најшире прихваћен или унутар дате научне области. За нпр. науку уопште, то је листа кључних речи Web of Science. Број кључних речи не може бити већи од 10, а у

интересу је уредништва и аутора да учесталост њихове употребе буде што већа. У чланку се пишу непосредно након сажетка.

Систем АСИСТЕНТ у ту сврху користи специјалну алатку KWASS: аутоматско екстраховање кључних речи из дисциплинарних тезауруса/речника по избору и рутине за њихов одабир, тј. прихватање односно одбацивање од стране аутора и/или уредника.

Датум прихватања чланка

Датум када је уредништво примило чланак, датум када је уредништво коначно прихватило чланак за објављивање, као и датуми када су у међувремену достављене евентуалне исправке рукописа наводе се хронолошким редоследом, на сталном месту, по правилу на крају чланка.

Захвалница

Назив и број пројекта, односно назив програма у оквиру којег је чланак настао, као и назив институције која је финансирала пројекат или програм, наводи се у посебној напомени на сталном месту, по правилу при дну прве стране чланка.

Претходне верзије рада

Ако је чланак у претходној верзији био изложен на скупу у виду усменог саопштења (под истим или сличним насловом), податак о томе треба да буде наведен у посебној напомени, по правилу при дну прве стране чланка. Рад који је већ објављен у неком часопису не може се објавити у *Војнотехничком гласнику* (прештампати), ни под сличним насловом и измењеном облику.

Табеларни и графички прикази

Пожељно је да наслови свих приказа, а по могућству и текстуални садржај, буду дати двојезично, на језику рада и на енглеском језику.

Табеле се пишу на исти начин као и текст, а означавају се редним бројевима са горње стране. Фотографије и цртежи треба да буду јасни, прегледни и погодни за репродукцију. Цртеже треба радити у програму word или corel. Фотографије и цртеже треба поставити на жељено место у тексту.

За слике и графиконе не сме се користити снимак са екрана рачунара програма за прикупљање података. У самом тексту чланка препоручује се употреба слика и графикона непосредно из програма за анализу података (као што су Excel, Matlab, Origin, SigmaPlot и други).

Навођење (цитирање) у тексту

Начин позивања на изворе у оквиру чланка мора бити једнообразан.

Војнотехнички гласник за референцирање (цитирање и навођење литературе) примењује Харвардски систем референци, односно Харвардски приручник за стил (Harvard Referencing System, Harvard Style Manual). У самом тексту, у обичним заградама, на месту на којем се врши позивање, односно цитирање литературе набројане на крају чланка, обавезно у обичној загради написати презиме цитираног аутора, годину издања публикације из које цитирате и, евентуално, број страница. Нпр. (Petrović, 2012, pp.10–12).

Детаљно упутство о начину цитирања, са примерима, дато је на страници сајта *Упутство за Харвардски приручник за стил*. Потребно је да се позивање на литературу у тексту уради у складу са поменутим упутством.

Систем АСИСТЕНТ у сврху контроле навођења (цитирања) у тексту користи специјалну алатку CiteMatcher: откривање изостављених цитата у тексту рада и у попису референци.

Напомене (фусноте)

Напомене се дају при дну стране на којој се налази текст на који се односе. Могу садржати мање важне детаље, допунска објашњења, назнаке о коришћеним изворима (на пример, научној грађи, приручницима), али не могу бити замена за цитирану литературу.

Листа референци (литература)

Цитирана литература обухвата, по правилу, библиографске изворе (чланке, монографије и сл.) и даје се искључиво у засебном одељку чланка, у виду листе референци. Референце се не преводе на језик рада и набрајају се у посебном одељку на крају чланка.

Војнотехнички гласник, као начин исписа литературе, примењује Харвардски систем референци, односно Харвардски приручник за стил (Harvard Referencing System, Harvard Style Manual).

Литература се обавезно пише на латиничном писму и набраја по абецедном редоследу, наводећи најпре презимена аутора, без нумерације.

Детаљно упутство о начину пописа референци, са примерима, дато је на страници сајта *Упутство за Харвардски приручник за стил*. Потребно је да се попис литературе на крају чланка уради у складу са поменутим упутством.

Нестандардно, непотпуно или недоследно навођење литературе у системима вредновања часописа сматра се довољним разлогом за оспоравање научног статуса часописа.

Систем АСИСТЕНТ у сврху контроле правилног исписа листе референци користи специјалну алатку RefFormatter: контрола обликовања референци у складу са Харвардским приручником за стил.

Изјава о ауторству

Поред чланка доставља се *Изјава о ауторству* у којој аутори наводе свој појединачни допринос у изради чланка. Такође, у тој изјави потврђују да су чланак урадили у складу са *Позивом и упутством ауторима* и *Изјавом о етичком поступању часописа*.

Сви радови подлежу стручној рецензији.

Списак рецензената *Војнотехничког гласника* може се видети на страници сајта *Списак рецензената*. Процес рецензирања објашњен је на страници сајта *Рецензентски поступак*.

Уредништво

Адреса редакције:
Војнотехнички гласник
Вељка Лукића Курјака 33
11042 Београд
e-mail: vojnotehnicki.glasnik@mod.gov.rs.
тел: војни 40-260 (011/3603-260), 066/8700-123

ПРИГЛАШЕНИЕ И ИНСТРУКЦИЯ ДЛЯ АВТОРОВ О ПОРЯДКЕ ПОДГОТОВКИ СТАТЬИ

Инструкция для авторов о порядке подготовки статьи к опубликованию в журнале *«Военно-технический вестник»* разработана согласно Регламенту о категоризации и ранжировании научных журналов Министерства образования, науки и технологического развития Республики Сербия («Службени гласник РС», № 159/20). Применение этого Регламента способствует повышению качества отечественных журналов и их более полному вовлечению в международную систему обмена научной информацией.

Военно-технический вестник (**Vojnotehnički glasnik / Military Technical Courier**), втг.мо.упр.срб, www.vtg.mod.gov.rs/index-ru.html, ISSN 0042-8469 – печатное издание, e-ISSN 2217-4753 – online, UDK 623+355/359, DOI: 10.5937/VojnotehnickiGlasnik; https://doi.org/10.5937/VojnotehnickiGlasnik, является рецензируемым научным журналом.

Собственники журнала: Министерство обороны и Вооруженые силы Республики Србия.

Издатель журнала: Университет обороны в г. Белград (Военная академия).

Программная ориентация журнала основана на ежегодной категоризации журнала, которая производится соответствующим отраслевым министерством, в зависимости от области исследований, а также на его индексировании в международных наукометрических базах данных.

Журнал охватывает научные и профессиональные сферы в рамках учебно-научной области **естественно-математических наук**, а также в рамках учебно-научной области **технико-технологических наук**, особенно в области **оборонных наук и технологии**. В журнале публикуются теоретические и практические достижения, которые способствуют повышению квалификации представителей сербского, регионального и международного академического сообщества, особенно служащих Министерств Обороны и Вооружённых сил. В журнале публикуются статьи со соответствующими обзорами об аналитических, экспериментальных и прикладных исследованиях, а также о численном моделировании, охватывая различные дисциплины. Публикуемые материалы отличаются высоким качеством и актуальностью. Они написаны научным, но понятным и доступным для широкого круга читателей языком. Приветствуются все статьи, сообщающие об оригинальных теоретических и/или практических исследованиях и/или расширенные версии ранее опубликованных статей, представленных на конференциях. Статьи для публикации отбираются путем двойного слепого рецензирования, которое гарантирует оригинальность, актуальность и удобочитаемость. Цель состоит не только в поддержании высокого качества публикуемых статей, но и в обеспечении своевременного, тщательного и соответствующего процесса рецензирования.

Редакционная политика журнала *«Военно-технический вестник»* основана на рекомендациях Комитета по этике научных публикаций (COPE Core Practices), общих принципах прозрачности и лучшей практике издательской деятельности COPE, DOAJ, OASPA и WAME, а также на лучшей практике научно-издательской деятельности. Журнал *«Военно-технический вестник»* является членом COPE (Комитет по этике научных публикаций) со 2 мая 2018 года и членом OASPA (Ассоциация научных издателей открытого доступа) с 27 ноября 2015 года.

Министерством образования, науки и технологического развития Республики Сербия утверждена 25 октября 2022 г. категоризация журнала *«Военно-технический вестник»* за 2022 год:

– **Область компьютерные науки:**
ведущий журнал государственного значения **(M51)**,
– **Область электроники, телекоммуникаций и информационных технологий:**
ведущий журнал государственного значения **(M51)**,
– **Область машиностроения:**
ведущий журнал государственного значения **(M51)**,
– **Область материалов и химической технологии:**
ведущий журнал государственного значения **(M51)**.

С информацией относительно категоризации за 2022 год можно ознакомиться на странице сайта *«Военно-технического вестника» Категоризация Вестника*.

Более подробную информацию можно найти на сайте Министерства образования, науки и технологического развития Республики Сербия.

С информацией о категоризации можно ознакомиться и на сайте КОБСОН (Консорциум библиотек Республики Сербия по вопросам объединения закупок).

Категоризация Вестника проведена согласно Регламенту о категоризации и ранжировании научных журналов Министерства образования, науки и технологического развития Республики Сербия («Службени гласник РС», № 159/20)

Журнал соответствует стандартам Сербского индекса научного цитирования (СЦИндекс/SCIndeks) - наукометрической базы данных научных журналов Республики Сербия, Научно-информационного система Redalyc, а также Российского индекса научного цитирования (РИНЦ). Журнал постоянно подвергается мониторингу и оценивается количественными наукометрическими показателями отражающими его научную ценность.

С информацией об индексировании можно ознакомиться на странице сайта журнала *Индексирование Вестника*.

«Военно-технический вестник» обеспечивает читателям возможность открытого доступа, в соответствии с положениями об авторских правах, утверждёнными Creative Commons (CC BY). С инструкцией об авторских правах можно ознакомиться на странице *Авторские права и политика самоархивирования*, перейдя по ссылке http://www.vtg.mod.gov.rs/index-ru.html.

Рукописи статей направляются в редакцию журнала с использованием online системы ASSISTANT, запущенной Центром поддержи развития образования и науки (ЦПРОН). Регистрация в системе и оформление прав доступа выполняется по адресу http://www.vtg.mod.gov.rs/index-ru.html, через страницу *ASSISTANT* или *СЦИНДЕКС* (aseestant.ceon.rs/index.php/vtg). С инструкцией по регистрации и правам доступа можно ознакомиться по адресу http://www.vtg.mod.gov.rs/index-ru.html, на странице *Инструкция по ASSISTANT*.

Все авторы, предоставляющие свои рукописи для публикации в редакцию журнала *«Военно-технический вестник»* должны пройти предварительную регистрацию в реестре ORCID (Open Researcher and Contributor ID). Эта процедура осуществляется в соответствии с инструкцией, размещенной на странице сайта *Регистрация в реестре ORCID для присвоения идентификационного кода*.

«Военно-технический вестник» публикует статьи на английском языке (Arial, шрифт 11 pt, пробел Single). Процесс подготовки, написания и редактирования статьи

должен осуществляться в соответствии с принципами *Этического кодекса* (http://www.vtg.mod.gov.rs/etichyeskiy-kodyeks.html). Статья должна содержать резюме с ключевыми словами, введение (цель исследования), основную часть (соответствующий обзор представительного исследования в данной области, четкое изложение научной новизны в представленном исследовании, соответствующую теоретическую основу, один или несколько примеров для демонстрирования и обсуждения представленных тезисов), заключение и список литературы (без нумерации заголовков и подзаголовков). Объем статьи не должен превышать один авторский лист (16 страниц формата А4 с одинарным интервалом, максимум до 24 страниц, включая ссылки и приложения). Статья должна быть набрана на компьютере с использованием специально подготовленного редакцией макета, который можно скачать на странице сайта *Правила и образец составления статьи*.

Заголовок

Заголовок должен отражать тему статьи. В интересах журнала и автора необходимо использовать слова и словосочетания, удобные для индексации и поиска. Если такие слова не содержатся в заголовке, то желательно их добавить в подзаголовок.

Текущий заголовок

Текущий заголовок пишется в титуле каждой страницы статьи с целью упрощения процесса идентификации, в первую очередь копий статьей в электронном виде. Заголовок содержит в себе фамилию и инициал имени автора (в случае если авторов несколько, остальные обозначаются с «et al.» или «и др.»), название работы и журнала (год, том, выпуск, начальная и заключительная страница). Заголовок статьи и название журнала могут быть приведены в сокращенном виде.

ФИО автора

Приводятся полная фамилия и полное имя (всех) авторов. Желательно, чтобы были указаны инициалы отчеств авторов. Фамилия и имя авторов из Республики Сербия всегда пишутся в оригинальном виде (с сербскими диакритическими знаками), независимо от языка, на котором написана работа.

Наименование учреждения автора (аффилиация)

Приводится полное (официальное) наименование и местонахождение учреждения, в котором работает автор, а также наименование учреждения, в котором автор провёл исследование. В случае организаций со сложной структурой приводится их иерархическая соподчинённость (напр. Военная академия, кафедра военных электронных систем, г. Белград). По крайней мере, одна из организаций в иерархии должна иметь статус юридического лица. В случае если указано несколько авторов, и если некоторые из них работают в одном учреждении, нужно отдельными обозначениями или каким-либо другим способом указать в каком из приведённых учреждений работает каждый из авторов. Аффилиация пишется непосредственно после ФИО автора. Должность и специальность по диплому не указываются.

Контактные данные

Электронный адрес автора указываются рядом с его именем на первой страницы статьи.

Категория (тип) статьи

Категоризация статьей является обязанностью редакции и имеет особое значение. Категорию статьи могут предлагать рецензенты и члены редакции, т.е.

редакторы рубрик, но ответственность за категоризацию несет исключительно главный редактор. Статьи в журнале распределяются по следующим категориям:

Научные статьи:

– оригинальная научная статья (работа, в которой приводятся ранее неопубликованные результаты собственных исследований, полученных научным методом);

– обзорная статья (работа, содержащая оригинальный, детальный и критический обзор исследуемой проблемы или области, в который автор внёс определённый вклад, видимый на основе автоцитат);

– краткое сообщение (оригинальная научная работа полного формата, но меньшего объёма или имеющая предварительный характер);

– научная критическая статья (дискуссия-полемика на определённую научную тему, основанная исключительно на научной аргументации) и научный комментарий.

Однако, в некоторых областях знаний научная работа в журнале может иметь форму монографического исследования, а также критического обсуждения научного материала (историко-архивного, лексикографического, библиографического, обзора данных и т.п.) – до сих пор неизвестного или недостаточно доступного для научных исследований. Работы, классифицированные в качестве научных, должны иметь, по меньшей мере, две положительные рецензии. В случае если в журнале объявляются и приложения, не имеющие научный характер, научные статьи должны быть сгруппированы и четко выделены в первой части номера.

Профессиональные статьи:

– профессиональная работа (приложения, в которых предлагаются опыты, полезные для совершенствования профессиональной практики, но которые не должны в обязательном порядке быть обоснованы на научном методе);

– информативное приложение (передовая статья, комментарий и т.п.);

– обзор (книги, компьютерной программы, случая, научного события и т.п.).

Объем кратких сообщений составляет 4-7 страниц, исследовательские статьи и тематические исследования с проблемно-ситуационным анализом − 10-14 страниц, однако объем обзорных статей может быть больше. Ограничения по количеству страниц не являются строгими, следовательно при соответствующем обосновании предоставленные работы могут быть длиннее или короче. В случае подачи расширенных версий ранее опубликованных докладов, представленных на конференции, редакция проверит было ли добавлено достаточно новых материалов для того, чтобы статья соответствовала стандартам журнала и условиям рецензирования. Добавленный материал должен быть новым, неопубликованным ранее. Новые результаты приветствуются, но не являются обязательным условием; однако ключевые тезисы, примеры, разработки и пр. должны быть более подробно представлены в статье по сравнению с первичным докладом на конфереции.

Язык работы

Статья должна быть написана на английском языке. Текст должен быть в лингвистическом и стилистическом смысле упорядочен, систематизирован, без сокращений (за исключением стандартных). Все физические величины должны соответствовать Международной системе единиц измерения – СИ. Очередность формул обозначается порядковыми номерами, проставляемыми с правой стороны в круглых скобках.

Резюме

Резюме является кратким информативным обзором содержания статьи, обеспечивающим читателю быстроту и точность оценки её релевантности. В интересах редакции и авторов, чтобы резюме содержало термины, часто используемые для индексирования и поиска статьей. Составными частями резюме являются введение/цель исследования, методы, результаты и выводы. В резюме должно быть от 100 до 250 слов, и оно должно находится между титулами (заголовок, ФИО авторов и др.) и ключевыми словами, за которыми следует текст статьи.

Ключевые слова

Ключевыми словами являются термины или фразы, адекватно представляющие содержание статьи, необходимые для индексирования и поиска. Ключевые слова необходимо выбирать, опираясь при этом на какой-либо международный источник (регистр, словарь, тезаурус), наиболее используемый внутри данной научной области. Число ключевых слов не может превышать 10. В интересах редакции и авторов, чтобы частота их встречи в статье была как можно большей. В статье они пишутся непосредственно после резюме.

Программа ASSISTANT предоставляет возможность использования сервиса KWASS, автоматически фиксирующего ключевые слова из источников/словарей по выбору автора/редактора.

Дата получения статьи

Дата, когда редакция получила статью; дата, когда редакция окончательно приняла статью к публикации; а также дата, когда были предоставлены необходимые исправления рукописи, приводятся в хронологическом порядке, как правило, в конце статьи.

Выражение благодарности

Наименование и номер проекта, т.е. название программы благодаря которой статья возникла, совместно с наименованием учреждения, которое финансировало проект или программу, приводятся в отдельном примечании, как правило, внизу первой страницы статьи.

Предыдущие версии работы

В случае если статья в предыдущей версии была изложена устно (под одинаковым или похожим названием, например, в виде доклада на научной конференции), сведения об этом должны быть указаны в отдельном примечании, как правило, внизу первой страницы статьи. Работа, которая уже была опубликована в каком-либо из журналов, не может быть напечатана в *«Военно-техническом вестнике»* ни под похожим названием, ни в изменённом виде.

Нумерация и название таблиц и графиков

Желательно, чтобы нумерация и название таблиц и графиков были исполнены на двух языках (на языке оригинала и на английском). Таблицы подписываются таким же способом как и текст и обозначаются порядковым номером с верхней стороны. Фотографии и рисунки должны быть понятны, наглядны и удобны для репродукции. Рисунки необходимо делать в программах Word или Corel. Фотографии и рисунки надо поставить на желаемое место в тексте. Для создания изображений и графиков использование функции снимка с экрана (скриншота) не допускается. В самом тексте статьи рекомендуется применение изображений и графиков, обработанных такими компьютерными программами, как: Excel, Matlab, Origin, SigmaPlot и др.

Ссылки (цитирование) в тексте

Оформление ссылок на источники в рамках статьи должно быть однообразным. *«Военно-технический вестник»* для оформления ссылок, цитат и списка использованной литературы применяет Гарвардскую систему (Harvard Referencing System, Harvard Style Manual). В тексте в скобках приводится фамилия цитируемого автора (или фамилия первого автора, если авторов несколько), год издания и по необходимости номер страницы. Например: (Petrović, 2010, pp.10-20). Рекомендации о способе цитирования размещены на странице сайта *Инструкция по использованию Гарвардского стиля*. При оформлении ссылок, цитат и списка использованной литературы необходимо придерживаться установленных норм. Программа ASSISTANT предоставляет при цитировании возможность использования сервиса CiteMatcher, фиксирующего пропущенные цитаты в работе и в списке литературы.

Примечания (сноски)

Примечания (сноски) к тексту указываются внизу страницы, к которой они относятся. Примечания могут содержать менее важные детали, дополнительные объяснения, указания об использованных источниках (напр. научном материале, справочниках), но не могут быть заменой процедуры цитирования литературы.

Литература (референции)

Цитированной литературой охватываются, как правило, такие библиографические источники как статьи, монографии и т.п. Вся используемая литература в виде референций размещается в отдельном разделе статьи. Названия литературных источников не переводятся на язык работы. *«Военно-технический вестник»* для оформления списка использованной литературы применяет Гарвардскую систему (Harvard Style Manual). В списке литературы источники указываются в алфавитном порядке фамилий авторов или редакторов. Рекомендации о способе цитирования размещены на странице сайта *Инструкция по использованию Гарвардского стиля*. При оформлении списка использованной литературы необходимо придерживаться установленных норм. При оформлении списка литературы программа ASSISTANT предоставляет возможность использования сервиса RefFormatter, осуществляющего контроль оформления списка литературы в соответствии со стандартами Гарвардского стиля. Нестандартное, неполное и непоследовательное приведение литературы в системах оценки журнала считается достаточной причиной для оспаривания научного статуса журнала.

Авторское заявление

Авторское заявление предоставляется вместе со статьей, в нем авторы заявляют о своем личном вкладе в написание статьи. В заявлении авторы подтверждают, что статья написана в соответствии с *Приглашением и инструкциями для авторов*, а также с *Кодексом профессиональной этики журнала*.

Все рукописи статей подлежат профессиональному рецензированию.

Список рецензентов журнала *«Военно-технический вестник»* размещён на странице сайта *Список рецензентов*. Процесс рецензирования описан в разделе *Правила рецензирования*.

Редакция

Почтовый адрес редакции:

«Војнотехнички гласник»
ул. Велька Лукича Куряка 33, 11042 Белград, Республика Сербия
e-mail: vojnotehnicki.glasnik@mod.gov.rs,
тел: +381 11 3603 260, +381 66 8700 123

CALL FOR PAPERS AND ARTICLE FORMATTING INSTRUCTIONS

The instructions to authors about the article preparation for publication in the *Military Technical Courier* are based on the Regulations on categorization and ranking of scientific journals of the Ministry of Education, Science and Technological Development of the Republic of Serbia (Official Gazette of the Republic of Serbia, No 159/20). This Regulations aims at improving the quality of national journals and raising the level of their compliance with the international system of scientific information exchange.

The Military Technical Courier / Vojnotehnički glasnik (www.vtg.mod.gov.rs/index-e.html, втг.мо.упр.срб, ISSN 0042-8469 – print issue, e-ISSN 2217-4753 – online, UDC 623+355/359, DOI: 10.5937/VojnotehnickiGlasnik; https://doi.org/10.5937/VojnotehnickiGlasnik), is an peer-reviewed scientific journal.

The owners of the journal are the Ministry of Defence of the Republic of Serbia and the Serbian Armed Forces. The publisher and financier of the *Military Technical Courier* is the University of Defence in Belgrade (Military Academy).

The program of the journal is based on the annual classification of journals performed by a relevant Ministry as well as on its indexing in international indexing databases.

The journal covers scientific and professional fields within the educational-scientific field of **Natural-Mathematical Sciences**, as well as within the educational-scientific field of **Technical-Technological Sciences**, and especially the field of **defense sciences and technologies**. It publishes theoretical and practical achievements leading to professional development of all members of Serbian, regional and international academic communities as well as members of the military and ministries of defence in particular. It publishes papers with balanced coverage of analytical, experimental, and applied research as well as numerical simulations from various disciplines. The material published is of high quality and relevance, written in a manner that makes it accessible to a wider readership. The journal welcomes papers reporting original theoretical and/or practice-oriented research as well as extended versions of already published conference papers. Manuscripts for publication are selected through a double-blind peer-review process to validate their originality, relevance, and readability. This being so, the objective is not only to keep the quality of published papers high but also to provide a timely, thorough, and balanced review process.

The editorial policy of the *Military Technical Courier* is based on the COPE Core Practices, common COPE, DOAJ, OASPA and WAME Principles of Transparency and Best Practice in Scholarly Publishing as well as on the best accepted practices in scientific publishing. The Military Technical Courier has been a COPE (Committee on Publication Ethics) member since 2nd May 2018 and a member of OASPA (Open Access Scholarly Publishers Association) since 27th November 2015.

The Ministry of Education, Science and Technological Development of the Republic of Serbia classified the *Military Technical Courier* for the year 2022, on October 25, 2022

- **on the list of periodicals for computer sciences,**
  category: reputed national journal **(M51)**,
- **on the list of periodicals for electronics, telecommunications and IT,**
  category: reputed national journal **(M51)**,
- **on the list of periodicals for mechanical engineering,**
  category: reputed national journal **(M51)**,
- **on the list of periodicals for materials and chemical technology,**
  category: reputed national journal **(M51)**.

The approved lists of national periodicals for the year 2022 can be viewed on the website of the *Military Technical Courier*, page *Journal categorization*.

More detailed information can be found on the website of the Ministry of Education, Science and Technological Development of the Republic of Serbia.

The information on the categorization can be also found on the website of KOBSON (Consortium of Libraries of Serbia for Unified Acquisition).

The periodical is categorized in compliance with the Regulations on categorization and ranking of scientific journals of the Ministry of Education, Science and Technological Development of the Republic of Serbia (Official Gazette of the Republic of Serbia, No 159/20). More detailed information can be found on the website of the Ministry of Education, Science and Technological Development.

The journal is in the Serbian Citation Index – SCIndex (data base of national scientific journals), in the Scientific Information System Redalyc, and in the Russian Index of Science Citation/Российский индекс научного цитирования (RINC/РИНЦ) and is constantly monitored depending on the impact within the bases themselves. More detailed information can be viewed on the website of the *Military Technical Courier*, page *Journal indexing*.

Military Technical Courier enables open access and applies the Creative Commons Attribution (CC BY) licence provisions on copyright. The copyright details can be found on the *Copyright notice and Self-archiving policy* page of the journal's website.

Manuscripts are submitted online, through the electronic editing system ASSISTANT, developed by the Center for Evaluation in Education and Science – CEON.

The access and the registration are through the *Military Technical Courier* site http://www.vtg.mod.gov.rs/index-e.html, on the page *ASSISTANT* or the page *SCINDEKS* or directly through the link (aseestant.ceon.rs/index.php/vtg).

The detailed instructions about the registration for the service are on the website http://www.vtg.mod.gov.rs/index-e.html, on the page *Instructions for ASSISTANT*.

All authors submitting a manuscript for publishing in the *Military Technical Courier* should register for an ORCID ID following the instructions on the web page *Registration for an ORCID identifier*.

The *Military Technical Courier* publishes articles in English, using Arial and a font size of 11pt with Single Spacing.

The procedures of article preparation, writing and editing should be in accordance with the *Publication ethics statement* (http://www.vtg.mod.gov.rs/publication-ethics-statement.html).

The article should contain an abstract with keywords, introduction (motivation for the work), body (adequate overview of the representative work in the field, a clear statement of the novelty in the presented research, suitable theoretical background, one or more examples to demonstrate and discuss the presented ideas), conclusion, and references (without heading and subheading enumeration). The article length should not normally exceed 16 pages of the A4 paper format with single spacing, up to a maximum of 24 pages with references and supplementary material included.

The article should be formatted following the instructions in the Article Form which can be downloaded from website page *Article form*.

Title

The title should be informative. It is in both Journal's and author's best interest to use terms suitable for indexing and word search. If there are no such terms in the title, the author is strongly advised to add a subtitle.

Letterhead title

The letterhead title is given at a top of each page for easier identification of article copies in an electronic form in particular. It contains the author's surname and first name initial (for multiple authors add "et al"), article title, journal title and collation (year, volume, issue, first and last page). The journal and article titles can be given in a shortened form.

Author's name

Full name(s) of author(s) should be used. It is advisable to give the middle initial. Names are given in their original form (with diacritic signs if in Serbian).

Author's affiliation

The full official name and seat of the author's affiliation is given, possibly with the name of the institution where the research was carried out. For organizations with complex structures, give the whole hierarchy (for example, University of Defence in Belgrade, Military Academy, Department for Military Electronic Systems). At least one organization in the hierarchy must be a legal entity. When some of multiple authors have the same affiliation, it must be clearly stated, by special signs or in other way, which department exactly they are affiliated with. The affiliation follows the author's name. The function and title are not given.

Contact details

The postal addresses or the e-mail addresses of the authors are given in the first page.

Type of articles

Classification of articles is a duty of the editorial staff and is of special importance. Referees and the members of the editorial staff, or section editors, can propose a category, but the editor-in-chief has the sole responsibility for their classification.

Journal articles are classified as follows:

Scientific articles:

– Original scientific papers (giving the previously unpublished results of the author's own research based on scientific methods);

– Review papers (giving an original, detailed and critical view of a research problem or an area to which the author has made a contribution demonstrated by self-citation);

– Short communications or Preliminary communications (original scientific full papers but shorter or of a preliminary character);

– Scientific commentaries or discussions (discussions on a particular scientific topic, based exclusively on scientific argumentation) and opinion pieces.

Exceptionally, in particular areas, a scientific paper in the Journal can be in a form of a monograph or a critical edition of scientific data (historical, archival, lexicographic, bibliographic, data survey, etc.) which were unknown or hardly accessible for scientific research.

Papers classified as scientific must have at least two positive reviews.

If the journal contains non-scientific contributions as well, the section with scientific papers should be clearly denoted in the first part of the Journal.

Professional articles:

– Professional papers (contributions offering experience useful for improvement of professional practice but not necessarily based on scientific methods);

– Informative contributions (editorial, commentary, etc.);

– Reviews (of a book, software, case study, scientific event, etc.)

Short communications are usually 4-7 pages long, research articles and case studies 10-14 pages, while reviews can be longer. Page number limits are not strict and, with appropriate reasoning, submitted manuscripts can also be longer or shorter. If extended versions of previously published conference papers are submitted, Editors will check if sufficient new material has been added to meet the journal standards and to qualify such manuscripts for the review process. The added material must not have been previously published. New results are desired but not necessarily required; however, submissions should contain expansions of key ideas, examples, elaborations, etc. of conference papers.

Language

The language of the article should be in English. The grammar and style of the article should be of good quality. The systematized text should be without abbreviations (except standard ones). All measurements must be in SI units. The sequence of formulae is denoted in Arabic numerals in parentheses on the right-hand side.

Abstract and summary

An abstract is a concise informative presentation of the article content for fast and accurate evaluation of its relevance. It contains the terms often used for indexing and article search. A 100- to 250-word abstract has the following parts: introduction/purpose of the research, methods, results and conclusion.

Keywords

Keywords are terms or phrases showing adequately the article content for indexing and search purposes. They should be allocated heaving in mind widely accepted international sources (index, dictionary or thesaurus), such as the Web of Science keyword list for science in general. The higher their usage frequency is, the better. Up to 10 keywords immediately follow the abstract and the summary, in respective languages. For this purpose, the ASSISTANT system uses a special tool KWASS for the automatic extraction of key words from disciplinary thesauruses/dictionaries by choice and the routine for their selection, i.e. acceptance or rejection by author and/or editor.

Article acceptance date

The date of the reception of the article, the dates of submitted corrections in the manuscript (optional) and the date when the Editorial Board accepted the article for publication are all given in a chronological order at the end of the article.

Acknowledgements

The name and the number of the project or programme within which the article was realised is given in a separate note at the bottom of the first page together with the name of the institution which financially supported the project or programme.

Article preliminary version

If an article preliminary version has appeared previously at a meeting in a form of an oral presentation (under the same or similar title), this should be stated in a separate note at the bottom of the first page. An article published previously cannot be published in the *Military Technical Courier* even under a similar title or in a changed form.

Tables and illustrations

All the captions should be in the original language as well as in English, together with the texts in illustrations if possible. Tables are typed in the same style as the text and

are denoted by Arabic numerals at the top. Photographs and drawings, placed appropriately in the text, should be clear, precise and suitable for reproduction. Drawings should be created in Word or Corel.

For figures and graphs, proper data plot is recommended i.e. using a data analysis program such as Excel, Matlab, Origin, SigmaPlot, etc. It is not recommended to use a screen capture of a data acquisition program as a figure or a graph.

Citation in the text

Citation in the text must be uniform. The *Military Technical Courier* applies the Harvard Referencing System given in the Harvard Style Manual. When citing sources within your paper, i.e. for in-text references of the works listed at the end of the paper, place the year of publication of the work in parentheses and optionally the number of the page(s) after the author's name, e.g. (Petrovic, 2012, pp.10-12). A detailed guide on citing, with examples, can be found on *Military Technical Courier* website on the page *Instructions for Harvard Style Manual*. In-text citations should follow its guidelines. For checking in-text citations, the ASSISTANT system uses a special tool CiteMatcher to find out quotes left out within papers and in reference lists.

Footnotes

Footnotes are given at the bottom of the page with the text they refer to. They can contain less relevant details, additional explanations or used sources (e.g. scientific material, manuals). They cannot replace the cited literature.

Reference list (Literature)

The cited literature encompasses bibliographic sources such as articles and monographs and is given in a separate section in a form of a reference list. References are not translated to the language of the article.

In compiling the reference list and bibliography, the *Military Technical Courier* applies the Harvard System – Harvard Style Manual. All bibliography items should be listed alphabetically by author's name, without numeration. A detailed guide for listing references, with examples, can be found on *Military Technical Courier* website on the page *Instructions for Harvard Style Manual*. Reference lists at the end of papers should follow its guidelines. In journal evaluation systems, non-standard, insufficient or inconsequent citation is considered to be a sufficient cause for denying the scientific status to a journal.

Authorship Statement

The Authorship statement, submitted together with the paper, states authors' individual contributions to the creation of the paper. In this statement, the authors also confirm that they followed the guidelines given in *the Call for papers* and the *Publication ethics and malpractice statement of the journal*.

All articles are peer reviewed.

The list of referees of the *Military Technical Courier* can be viewed at website page *List of referees*. The article review process is described on the *Peer Review Process* page of the website.

Editorial Team

Address of the Editorial Office:
Vojnotehnički glasnik / Military Technical Courier
Veljka Lukića Kurjaka 33
11042 Belgrade, Republic of Serbia
e-mail: vojnotehnicki.glasnik@mod.gov.rs, tel.: +381 11 3603 260, +381 66 8700 123

Ликовно-графички уредник
Марија Марић, e-mail: marija.maric@mod.gov.rs

Лектор
Добрила Милетић, e-mail: miletic.dobrila@gmail.com

Превод на енглески
Јасна Вишњић, e-mail: jasnavisnjic@yahoo.com

Превод на руски
Др *Карина* Авагјан, e-mail: karinka2576@mail.ru

CIP – Каталогизација у публикацији
Народна библиотека Србије, Београд

623+355/359

ВОЈНОТЕХНИЧКИ гласник : научни часопис Министарства одбране и Војске Србије = Военно-технический вестник : научный журнал Министерства обороны и Вооружённых сил Республики Сербия = Military Technical Courier : scientific Journal of the Ministry of Defence and the Serbian Armed Forces / главни и одговорни уредник Драган Памучар. - Год. 1, бр. 1 (1. јан. 1953)- . - Београд : Универзитет одбране у Београду, Војна академија, 1953- (Београд : Војна штампарија). - 23 cm

Тромесечно. - Текст на срп., рус. и енгл. језику. - Друго издање на другом медијуму: Vojnotehnički glasnik (Online) = ISSN 2217-4753
ISSN 0042-8469 = Војнотехнички гласник
COBISS.SR-ID 4423938

Цена: 600,00 динара

Тираж: 100 примерака

На основу мишљења Министарства за науку, технологију и развој Републике Србије, број 413-00-1201/2001-01 од 12. 9. 2001. године, часопис „Војнотехнички гласник“ је публикација од посебног интереса за науку.

УДК: Народна библиотека Србије, Београд

Адреса редакције: Војнотехнички гласник,
Вељка Лукића Курјака 33, 11042 Београд

http://www.vtg.mod.gov.rs
http://aseestant.ceon.rs/index.php/vtg/issue/current
http://scindeks.nb.rs/journaldetails.aspx?issn=0042-8469
https://www.redalyc.org/revista.oa?id=6617
http://elibrary.ru/title_about.asp?id=53280
https://doaj.org/toc/2217-4753

Војнотехнички гласник је лиценциран код EBSCO Publishing-a.
Комплетан текст *Војнотехничког гласника* доступан је у базама података EBSCO Publishing-a.

e-mail: vojnotehnicki.glasnik@mod.gov.rs
Twitter: @MilTechCourier

Претплата на штампано издање: e-mail: vojnotehnicki.glasnik@mod.gov.rs; тел. 066/87-00-123.

Часопис излази тромесечно.

Први штампани број *Војнотехничког гласника* објављен је 1. 1. 1953. године.

Прво електронско издање *Војнотехничког гласника* на Интернету објављено је 1. 1. 2011. године.

Штампа: Војна штампарија – Београд, Ресавска 40б, e-mail: vojna.stamparija@mod.gov.rs

Художественный редактор
Мария Марич, e-mail: marija.maric@mod.gov.rs

Корректор
Добрила Милетич, e-mail: miletic.dobrila@gmail.com

Перевод на английский язык
Ясна Вишнич, e-mail: jasnavisnjic@yahoo.com

Перевод на русский язык
Д.филол.н. *Карина* Кареновна Авагян, e-mail: karinka2576@mail.ru

CIP – Каталогизация в публикации
Национальная библиотека Сербии, г. Белград

623+355/359

ВОЈНОТЕХНИЧКИ гласник : научни часопис Министарства одбране и Војске Србије = Военно-технический вестник : научный журнал Министерства обороны и Вооружённых сил Республики Сербия = Military Technical Courier : scientific Journal of the Ministry of Defence and the Serbian Armed Forces / главни и одговорни уредник Драган Памучар. - Год. 1, бр. 1 (1. јан. 1953)- . - Београд : Универзитет одбране у Београду, Војна академија, 1953- (Београд : Војна штампарија). - 23 cm

Тромесечно. - Текст на срп., рус. и енгл. језику. - Друго издање на другом медијуму: Vojnotehnički glasnik (Online) = ISSN 2217-4753
ISSN 0042-8469 = Војнотехнички гласник
COBISS.SR-ID 4423938

Цена: 600,00 динаров

Тираж: 100 экземпляров

На основании решения Министерства науки и технологий Республики Сербия, № 413-00-1201/2001-01 от 12. 9. 2001 года, журнал «Военно-технический вестник» объявлен изданием, имеющим особое значение для науки.

УДК: Национальная библиотека Сербии, г. Белград

Адрес редакции: Војнотехнички гласник,
Ул. Велька Лукича Куряка 33, 11042 Белград, Республика Сербия

http://www.vtg.mod.gov.rs
http://aseestant.ceon.rs/index.php/vtg/issue/current
http://scindeks.nb.rs/journaldetails.aspx?issn=0042-8469
https://www.redalyc.org/revista.oa?id=6617
http://elibrary.ru/title_about.asp?id=53280
https://doaj.org/toc/2217-4753

«Военно-технический вестник» включен в систему EBSCO. Полный текст журнала «Военно-технический вестник» можно найти в базах данных EBSCO Publishing.

e-mail: vojnotehnicki.glasnik@mod.gov.rs
Twitter: @MilTechCourier

Подписка на печатную версию журнала: e-mail: vojnotehnicki.glasnik@mod.gov.rs; тел. +381 66 87 00 123.

Журнал выпускается ежеквартально.

Первый номер журнала «Военно-технический вестник» выпущен 1.1.1953 года.

Первая электронная версия журнала размещена на интернет странице 1.1.2011 года.

Типография: Војна штампарија – Белград, Ресавска 40б, e-mail: vojna.stamparija@mod.gov.rs

Graphic design editor
Marija Marić, e-mail: marija.maric@mod.gov.rs

Proofreader
Dobrila Miletić, e-mail: miletic.dobrila@gmail.com

English translation and polishing
Jasna Višnjić, e-mail: jasnavisnjic@yahoo.com

Russian translation and polishing
Dr. *Karina* Avagyan, e-mail: karinka2576@mail.ru

CIP – Catalogisation in the publication
National Library of Serbia, Belgrade

623+355/359

ВОЈНОТЕХНИЧКИ гласник : научни часопис Министарства одбране и Војске Србије = Военно-технический вестник : научный журнал Министерства обороны и Вооружённых сил Республики Сербия = Military Technical Courier : scientific Journal of the Ministry of Defence and the Serbian Armed Forces / главни и одговорни уредник Драган Памучар. - Год. 1, бр. 1 (1. јан. 1953)- . - Београд : Универзитет одбране у Београду, Војна академија, 1953- (Београд : Војна штампарија). - 23 cm

Тромесечно. - Текст на срп., рус. и енгл. језику. - Друго издање на другом медијуму: Vojnotehnički glasnik (Online) = ISSN 2217-4753
ISSN 0042-8469 = Војнотехнички гласник
COBISS.SR-ID 4423938

Price: 600.00 RSD

Printed in 100 copies

According to the Opinion of the Ministry of Science and Technological Development No 413-00-1201/2001-01 of 12th September 2001, the *Military Technical Courier* is a publication of special interest for science.

UDC: National Library of Serbia, Belgrade

Address: Vojnotehnički glasnik/Military Technical Courier,
Veljka Lukića Kurjaka 33, 11042 Belgrade, Republic of Serbia

http://www.vtg.mod.gov.rs/index-e.html
http://aseestant.ceon.rs/index.php/vtg/issue/current
http://scindeks.nb.rs/journaldetails.aspx?issn=0042-8469
https://www.redalyc.org/revista.oa?id=6617
http://elibrary.ru/title_about.asp?id=53280
https://doaj.org/toc/2217-4753

Military Technical Courier has entered into an electronic licensing relationship with EBSCO Publishing. The full text of *Military Technical Courier* can be found on EBSCO Publishing's databases.

e-mail: vojnotehnicki.glasnik@mod.gov.rs
Twitter: @MilTechCourier

Subscription to print edition: e-mail: vojnotehnicki.glasnik@mod.gov.rs; Tel. +381 66 87 00 123.

The journal is published quarterly.

The first printed issue of the *Military Technical Courier* appeared on 1st January 1953.
The first electronic edition of the *Military Technical Courier* on the Internet appeared on 1st January 2011.

Printed by Vojna štamparija – Belgrade, Resavska 40b, e-mail: vojna.stamparija@mod.gov.rs


ВТГ
ОД 1953.
ГОДИНА


VTC
OD 1953.
GODINA


ВТЕ
С 1953 г.
ЛЕТ


MTC
SINCE 1953
YEARS